

بِسْمِ اللَّهِ الرَّحْمَنِ الرَّحِيمِ

Flow in a Corrugated Walls with EMHD



By

MADHIA RASHID

**Department of Mathematics
Quaid-i-Azam University
Islamabad, Pakistan
2021**

Flow in a Corrugated Walls with EMHD



By

MADHIA RASHID

Supervised By

PROF. DR. SOHAIL NADEEM

Department of Mathematics
Quaid-i-Azam University
Islamabad, Pakistan
2021

Flow in a Corrugated Walls with EMHD



By

MADHIA RASHID

A THESIS SUBMITTED IN THE PARTIAL FULFILLMENT OF THE REQUIREMENT FOR
THE DEGREE OF
DOCTOR OF PHILOSOPHY
IN
MATHEMATICS

Supervised By

PROF. DR. SOHAIL NADEEM

Department of Mathematics
Quaid-i-Azam University
Islamabad, Pakistan
2021

Author's Declaration

I, **Madhia Rashid**, hereby state that my PhD thesis titled **Flow in a Corrugated Walls with EMHD** is my own work and has not been submitted previously by me for taking any degree from the Quaid-I-Azam University Islamabad, Pakistan or anywhere else in the country/world.

At any time if my statement is found to be incorrect even after my graduate the university has the right to withdraw my PhD degree.



Name of Student: **Madhia Rashid**

Date: **04-Jan-2021**

Plagiarism Undertaking

I solemnly declare that research work presented in the thesis titled “ **Flow in a Corrugated Walls with EMHD**” is solely my research work with no significant contribution from any other person. Small contribution/help wherever taken has been duly acknowledged and that complete thesis has been written by me.

I understand the zero tolerance policy of the HEC and **Quaid-i-Azam University** towards plagiarism. Therefore, I as an Author of the above titled thesis declare that no portion of my thesis has been plagiarized and any material used as reference is properly referred/cited.

I undertake that if I am found guilty of any formal plagiarism in the above titled thesis even afterward of PhD degree, the University reserves the rights to withdraw/revoke my PhD degree and that HEC and the University has the right to publish my name on the HEC/University Website on which names of students are placed who submitted plagiarized thesis.



Student/Author Signature

Name: **Madhia Rashid**

Flow in a Corrugated Walls with EMHD


By

Madhia Rashid


CERTIFICATE

A THESIS SUBMITTED IN THE PARTIAL FULFILLMENT OF THE
REQUIREMENTS FOR THE DEGREE OF THE
DOCTOR OF PHILOSOPHY IN MATHEMATICS

We accept this thesis as conforming to the required standard

1. 


Prof. Dr. Sohail Nadeem
(Chairman)

2. 

Prof. Dr. Sohail Nadeem
(Supervisor)

3. 

Dr. Rahmat Ellahi
(External Examiner)

4. 

Dr. Noreen Sher Akbar
(External Examiner)

Department of Mathematics International
Islamic University H-10 Islamabad.

Department of Basic Humanities, CE&ME,
(NUST) Peshawar Road Rawalpindi.

Department of Mathematics
Quaid-I-Azam University
Islamabad, Pakistan
2021

Certificate of Approval

This is to certify that the research work presented in this thesis entitled **Flow in a Corrugated Walls with EMHD** was conducted by **Ms. Madhia Rashid** under the kind supervision of **Prof. Dr. Sohail Nadeem**. No part of this thesis has been submitted anywhere else for any other degree. This thesis is submitted to the Department of Mathematics, Quaid-i-Azam University, Islamabad in partial fulfillment of the requirements for the degree of Doctor of Philosophy in field of Mathematics from Department of Mathematics, Quaid-i-Azam University Islamabad, Pakistan.

Student Name: **Madhia Rashid**

Signature: 


External committee:

a) **External Examiner 1:**

Name: **Dr. Rahmat Ellahi**

Designation: Associate Professor

Office Address: Department of Mathematics International Islamic University H-10 Islamabad.

Signature: 

b) **External Examiner 2:**

Name: **Dr. Noreen Sher Akbar**

Designation: Associate Professor

Office Address: Department of Basic Humanities, CE&ME, (NUST) Peshawar Road Rawalpindi.

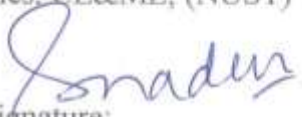
Signature: 

c) **Internal Examiner**

Name: **Prof. Dr. Sohail Nadeem**

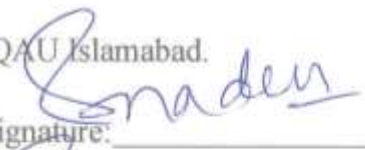
Designation: Professor

Office Address: Department of Mathematics, QAU Islamabad.

Signature: 

Supervisor Name:

Prof. Dr. Sohail Nadeem

Signature: 

Name of Dean/ HOD

Prof. Dr. Sohail Nadeem

Signature: 

This thesis is dedicated to

my beloved parents

*for their endless love, devotions and belief in me
for achieving success in life.*

And to

my caring Husband

*for his countless prayers, lots of love and
measureless support to accomplish hard goals of
my life.*

*In the Name of Allah,
The Most Gracious, The Most Merciful.*

Acknowledgement

“The will of God will never take you where Grace of God will not protect”

*Although it is just my name mentioned on the cover, many people have contributed to this research in their own way and for that I want to give them special thanks. My first and foremost gratitude and thanks go to **Almighty Allah** for making me enable to proceed in this dissertation successfully. Sure, all praise is for HIM who created us as best of HIS creations and grant us strength, health, knowledge, ability and opportunity to achieve our goals. I also express my sincere gratitude to **Holy Prophet Hazrat Muhammad S.A.W.** for guide us to right path by HIS teachings of patience, motivation and immense knowledge.*

*No research is possible without infrastructure and requisite materials and resource. At the very outset, I express my deepest thanks to **Quaid-I-Azam University** for all the academic support to complete my degree as a PhD student.*

*I owe my gratitude to my esteemed supervisor **Prof. Dr. Sohail Nadeem** for providing me this great opportunity to do my doctoral programmed under his guidance and to learn from his research expertise. His support and advice helped me in all the time of research and writing of this thesis.*

*Similar, profound gratitude goes to **Prof. Dr. Muhammad Yousaf Malik, Prof. Dr. M. Ayub, Prof. Dr. Taswar Hayat and Dr. Masood Khan** for their valuable support during my student carrier.*

*I wish to express my heartiest thanks and gratitude to my parents **Mr. and Mrs. Rashid Khan**, the ones who can never ever be thanked enough for the overwhelming love, kindness and care they bestow upon me. They supported me financially as well as morally and without their proper*

guidance it would not been possible for me to complete my higher education. I also owe my gratitude to my siblings **Prof. Sadaf, Lubna, Uzma, Maryam, Aimen and Kashan Ali** for being there for me. I would not be who am I today without you all.

Special mention goes to my dear husband **Dr. Junaid Azam** for his guidance, support and encouragement during this work. The journey of Ph.D was just like climbing a high peak step by step. His presence taught me to get through the hardship and frustration. He helped me keep things in perspective. I am indebted to him for giving me this feeling of fulfillment in life.

Completing this work would have been more difficult without a support and friendship. I have great pleasure in acknowledging my gratitude to my colleagues and fellow research scholars at QAU. My profound thanks and best wishes go to my friends **Ms. Sadia Rashid and Ms. Komal Ansar**. I wish them all the luck in completion of their PhD degrees soon. I also want to take a moment to thank my senior **Dr. Hina Sadaf, Dr. Iqra Shahzadi, Dr. Nuzhat and Dr. M. Noor** for their help and suggestions.

I also owe great level of appreciation to office staff of mathematics Department for their correct guidance.

Finally, my heart felt regard goes to my father in law and mother in law **Mr. and Mrs. Muhammad Azam Khan** for their love and moral support.

I thank the Almighty for giving me the strength and patience to work through all these years so that today I can stand proudly with my head held high.

Finally, I would like to express thanks to those who have been helpful and well-wishers for me throughout my life and my educational carrier.

For those who are reading this, I am also thank you too for taking the time to read this work. I hope that this work can be as informational as possible to you. Enjoy reading!

Madhia Rashid

04-01-2021

Contents

Nomenclature	5
1 Introduction	8
2 Electromagnetohydrodynamic flow in microchannel by velocity slip and temperature jump through a porous medium under corrugated wall	16
2.1 Mathematical development	17
2.2 Perturbation analysis	19
2.3 Solution of the problem	21
2.4 Volume flow rate	26
2.5 Graphical consequence	26
2.5.1 Effect of wall roughness on contour distributions of velocity and temperature	27
2.5.2 Effect of wall roughness on velocity	29
2.5.3 Effect of wall roughness on temperature	32
2.6 Conclusions	34
3 Significance of knudsen number and corrugation on EMHD flow under metallic nanoparticles impact	36
3.1 Mathematical model	36
3.2 Solution of technique	40
3.2.1 Zeroth order classification	40
3.2.2 First order classification	41
3.2.3 Second order classification	41

3.3	Heat transfer rate	45
3.4	Volume Flow rate	46
3.4.1	Mean velocity	46
3.5	Thermophysical properties	47
3.6	Graphical consequence	47
3.6.1	Effect of wall roughness on 3D velocity and contour distributions	47
3.6.2	Effect of wall roughness on velocity	53
3.6.3	Effect of wall roughness on temperature	58
3.7	Tables Description	61
3.8	Conclusions	63
4	EMHD flow of Couple stress nanofluid inside a vertical corrugated wavy walls	64
4.1	Mathematical model	64
4.2	Solution by Perturbation method	68
4.2.1	Zero Order classification	68
4.2.2	First Order classification	69
4.2.3	Second Order classification	69
4.2.4	Solution of second order classification	72
4.2.5	Volume flow rate	74
4.2.6	Mean velocity	75
4.3	Thermophysical properties of water and silver	75
4.4	Graphical consequence	76
4.5	Graphs	78
4.6	Conclusions	85
5	Impacts of heat generation and heat flow on Al_2O_3-Cu/water hybrid nanofluid in microchannel under corrugated walls through porous medium	86
5.1	Problem formulation	87
5.2	Solution of Problem	89
5.2.1	Zero Order classification	91

5.2.2	First Order classification	91
5.2.3	Second Order classification	92
5.2.4	Solution of first order	93
5.2.5	Solution of second order	94
5.2.6	Volume flow rate	96
5.2.7	Mean velocity	97
5.2.8	Heat transfer rate	97
5.3	Thermophysical properties	98
5.4	Graphical consequence	99
5.4.1	Tables Description	113
5.5	Conclusion	114
6	Theoretical aspect of EMHD viscous fluid with corrugated walls in curved channel	116
6.1	Mathematical Formulation	116
6.2	Solution of Problem	119
6.2.1	Zeroth Order System	119
6.2.2	First Order System	119
6.2.3	Second Order System	120
6.2.4	Solution of zeroth order	120
6.2.5	Solution of first order	120
6.2.6	Solution of second order	121
6.3	Graphical consequence	122
6.4	Tables Description	131
6.5	Conclusion	131
7	Flow of EMHD nanofluid in curved channel through corrugated walls	132
7.1	Mathematical model	132
7.2	Solution of Problem:	135
7.2.1	Zeroth Order System	135
7.2.2	First Order System	136

7.2.3	Second Order System	136
7.3	Heat transfer rate	140
7.4	Thermophysical properties	141
7.5	Graphical consequence	141
7.6	Tables Description	152
7.7	Conclusion	153
8	Analysis of EMHD Casson Fluid in curved channel with corrugated walls under metallic nanoparticles	154
8.1	Formulation of problem	154
8.2	Solution of Problem:	158
8.2.1	Zeroth order classification	158
8.2.2	First order classification	158
8.2.3	Second order classification	159
8.3	Heat transfer rate	164
8.4	Thermophysical properties	164
8.5	Graphical consequence	164
8.5.1	Effect of wall roughness on 3D velocity and contour distributions	165
8.5.2	Effect of wall roughness on velocity	169
8.5.3	Effect of wall roughness on temperature	174
8.5.4	Tables Description	176
8.6	Deduction	177
	References	178

Nomenclature

English words	
H	distance between corrugated walls
L	length of channel
p	pressure
Re	Reynolds number
Ha	Hartmann number
Pr	Prandtl number
Gr	Grashof number
Da	Darcy number
R	Radiation parameter
w	velocity component
B	magnetic field
E	electric field
J	current density
x, y, z	x-axis, y-axis and z-axis directions
r, x	radial and axial directions
T	Temperature
k''	thermal conductivity
Q_0	heat generation/absorption
k^*	coefficient of mean absorption
S	constant fluid parameter
q^*	radiative heat flux
k_1	permeability of the medium
R	radius
Nu	Nusselt number
Kn	Knudsen number
B_i	Biot number
k	Curvature parameter
C	Couple stress fluid parameter

Greek words	
ε	amplitude parameter
β_1	velocity slip
γ_1	temperature slip
β	strength of electric field
γ^*	casson parameter
β^*	phase difference
μ	viscosity
ρ	density
σ	electrical conductivity
π	deformation rate component
π_c	critical value
ρC_p	heat coefficient
σ^*	Stefan Boltzmann
η	couple stress viscosity coefficient
μ_β	plastic dynamics viscosity
ζ	thermal expansion coefficient
φ	mean velocity
ϕ	heat absorption coefficient
ω	angular frequency
λ^*	wave number
Φ	nanoparticle volume fraction
θ	dimensionless temperature
τ	shear stress

Subscripts	
nf	nanofluid
hnf	hybrid nanofluid
f	base fluid
l	left
r	right
u''	upper
l''	lower

Chapter 1

Introduction

EMHD micropumps have different points of interest, to be particular essential manufacture process, steady flow force and bidirectional pumping capacity. The principle of EMHD micropump is Lorentz force, which is relating an electric current to the conductive liquid over the channel in the presence of an opposite attractive field. EMHD micropumps have different points of interest, to be particular essential manufacture process, steady flow force and bidirectional pumping capacity. EMHD can be utilized to propel liquids as well as for creating secondary complex flow. The possibility of EMHD micropumps has been exhibited by utilizing both direct flow and rotating flow electric and attractive fields. The EMHD micropumps established by both of direct and alternating current electric and magnetic fields. Roughnesses on surfaces always occurred during the fabrication process. At the microscale level, it is tough to get a totally smooth wall surface. In any case, in practice, roughness dependably exists on the surface of channel walls that happened during the manufacture procedure or because of the adsorption of different species, for example, macromolecules. Surface roughness can be outlined misleadingly to advance axial rotation or blending. Numerous scientists have considered flow and heat transfer of a liquid through corrugated channel. One basic subject among these investigations is geometrical impacts because of wall corrugations on the flow opposition or pressure drop in the channel. The surface roughness is also mimics by wavy boundary, where roughness impacts are magnified by small scale of channel.

The EMHD micropump is one of fundamental nonmechanical micropumps and has diverse applications, for example, liquid pumping, control flow in microfluidic frameworks, and liquid

mixing and blending [1]. Investigation of EMHD micropumps take prodigious consideration due to outstanding submissions in fluid propelling, stirring, fluid chromatography and microcoolers [2, 3]. Reddy et al. [4] explored the EMHD flow variabilities in two-phase. The EMHD significance on fluid flow is investigated by Chakraborty and Paul [5]. Jhorar et al. [6] investigated the electroosmosis modulated biomechanical transport through asymmetric microfluidics channel. Sundaravadivelu and Tso [7] explored the electromagnetic fields impact on the surface tension driven flow in microchannel. Rivero [8] explored the consequences of considering fluid/wall slippage in micropumps under electromagnetic fields by analytical and numerical calculations.

On microscale level, to obtain an absolutely smooth wall surface is incredible. For repetition, roughness on surfaces continuously happened in manufacture procedure and the adsorption of macromolecules. In 1970s researchers presented different number of investigation and mathematical procedures to inspect the influence of wall irregularity. Chu [9] discovered the effect of corrugation on movement inside a microtube. The importance of heat transfer features on MHD flow is deliberated by Tashtoush et al. [10]. Ligrani et al. [11] examined surface roughness on pressure rise and flow rate near wall slip operating with Newtonian water. On Darcy–Brinkman flow the impacts of transverse and longitudinal wall corrugations examined by Ng and Wang [12]. Bergles [12] examined the heat transfer perspectives. Szumbariski et al. [14] studied temporary disturbance development in a wavy channel. Luo et al. [15] inspected two-layer flow in ridged channel. Si and Jian [16] researched EMHD flow of the Jeffrey fluids with longitudinal corrugated walls in microchannels. Nadeem et al. [17] discussed corrugation effects in microchannels through permeable medium. Elshafei et al. [18] discussed the impacts of temperature transmission and pressure drop happening in wavy walls. Nadeem et al. [19] inspected flow in a rectangular duct having Jeffrey fluid. Akbarzadeh et al. [20] discussed the convection of heat in two-phase model by corrugated absorber plates. Phan-Thien [21] examined the Stokes’ flow between two corrugated plates. Flow depends on orientation of the corrugations and phase difference of the corrugation. Bujurke and Kudenatti [22] examined the squeeze film behavior of magnetohydrodynamic (MHD) between irregular rectangular plates. Buren et al. [23] deliberated the wall roughness consequences for EMHD flow corresponding to the corrugations of wall in micro parallel channel. Kwang [24] analyzed the effect of Small–Knudsen-Number flow with slip flow in an annulus with corrugated walls.

Microfluidic systems usually applied in reduced systems for organic, therapeutic which are used by genetic researches and syntheses. One of the important research areas in microfluidics is microelectro mechanical system because of its potential applications as an instrument for concentrate crucial physical and biochemical procedures. Microfluidic greatly influenced in numerous areas for example heat exchange, firewood, detection and corporal element separation. Microfluidics field gradually more considered in both scholarly world and industry due to plausibility and productivity for controlling flows in microscale devices. Microfluidic transport have attractive advantage of passive machineries, especially surface tension. Microfluidic systems are highly desirable due to active pump and a self-contained. Dispensing therapeutic agents is a goal of micropump inventors into the body. Microfluidic can be appeared as micropumps impelled by pressure, magnetohydrodynamic (MHDs), electromagnetohydrodynamic pumps (EMHD), electroosmosis siphons, etc., when driving force is divided. Most microfluidic framework require an independent dynamic pump of a size practically identical with the volume of liquid to be pumped. The key contemplations for them incorporate their reliability, control utilization, activation voltage, cost of fabrication and a dosing exactness similar with fuel pump. First micropump was established by Jan Smits in 1980 to controlled insulin delivery systems for preserving diabetics' blood sugar stage without recurrent needle injections [25].

Darcy's law is very much essential in order to study the fluid flow problems in porous medium. Currently, investigation of fluid flows and heat transfer over porous medium has engrossed much attention. It is a fact that porous medium has many real-world applications. Instances of common porous media phenomena are sea shore sand, sandstone, bile duct, limestone and wood. Another illustration in outflow under a dam which is very imperative [26]. Alamri et al. [27] deliberated the convective radiative nanofluid flow along porous medium. Akbar et al. [28] explored the nanofluid diffusive process in a permeable channel. In an annulus the peristaltic flow through permeable medium is inspected by Mekheimer et al. [29]. Ellahi et al. [30] discussed the impacts of porous medium on two phase flow. Rapits et al. [31] have tackled issues of the progression of a viscous fluid by a permeable medium confined by a vertical surface. Mekheimer and Al-Arabi [32] analyzed peristaltic nonlinear transport in a porous medium for MHD flow. Sayed [33] examined the electrohydrodynamic instability of two superposed viscous and streaming fluids through permeable medium. Varshney [34] examined

the fluctuating progression of a viscous liquid through a permeable medium.

The nanofluids have extraordinary consideration in research because of adequate applications. Nanofluid is basically novel class of fluids which comprises nano-sized elements. Nanofluids have gigantic effect in many submissions for example pharmacological procedures, cross-mechanical appliances, petroleum cells, housing cooler, nuclear device and space invention and several circumstances. Thermal performance of fluids improves by means of nanoscience knowledge. The nanotechnology was first presented by Choi et al. [35]. Later on, Akbar et al. [36] explore the effect of metallic nanoparticles on viscous fluid in an asymmetric channel. Buongiorno [37] suggested that the thermophoresis and Brownian movement assume a key role in the elements of nanofluids. Inside a pipe flow of a nanofluid was studied by Xuan et al. [38] applying a dispersal model. Pramuanjaroenkij et al. [39] deliberated heat transfer ability employing nanofluids. In a permeable network MHD flow of nanofluid considered by Sheikholeslami et al. [40]. The slip effect in a rotating disk is illustrated by Hayat et al. [41]. Darcy flow effect on nanofluids is evaluated by Shehzad [42]. Khanafer et al. [43] presented a model for nanofluids heat transfer in a two-dimensional channel. Sheikholeslami et al. [44] inspected nanofluid involuntary convection in semi annulus. Nasrin et al. [45] defined free convection heat transmission on nanofluid in a cavity. Andreozzi et al. [46] inspected the impacts of nanofluid and spines in channel. Nadeem et al. [47] examined the heat degeneracy impacts on Jeffery nanofluid by using biological analysis.

In vertical channels, the mixed convection has gained extensive significance to upgrade the systems of cooling in engineering. This incorporates present day heat exchangers, atomic reactors, sun based cells and numerous other electronic gadgets. Buoyancy forces are responsible for such type of flows. Heat transfer analysis in the existence of mixed convection is the extensive significance because of its applications in self-cooled or independently cooled fluid metal covers, cooling frameworks for electronic gadgets, sun based vitality accumulation and synthetic procedures. Utilization of nanoparticles as intends to upgrade the flow of heat in low thermal conductivity liquids has turned out to be a novel procedure. The art of nanofluids mechanics has increased significant consideration of propelled analysis from everywhere throughout the world. Iqbal et al. [48] researched the unsteady transport of MHD mixed convection inspired by thermal radiation and partial slip performance. The exact solutions are computed for the

reduced systems of equations. Nanoparticles due to distinct properties have countless deliberation for investigators and the motivation of nanotechnology in numerous submissions are accessible in the literature such as [49-51].

The fundamental fluid's property (viscosity) differ with temperature. It plays a dynamic part in nanofluids. In industrial application the conventional fluids like oil, water and ethylene glycol have been extensively used in fluids heat transfer. Different types of nano fluids are defined as pharmaceutical nanofluids, medicinal nanofluids, environmental nanofluids etc. Currently frequent experiments have been performed with "Hybrid Nanofluid", the cutting edge nanofluid. Another class of fluid is recognized as hybrid nanofluid for noteworthy conductivity and stability. A significant number of heat transfer enhancement studies using different nanofluids type, for example, Al_2O_3 , CNT, Fe_2O_3 , Cu, CuO, Ag, TiO_2 , ZnO, SiO and SiC through a cylinder have been done [52-54]. The Hybrid nanofluid can be accumulated by merging two unalike solid nanoparticles in the base fluids. Picking up the proper mixture of nanoparticles is the principle favoured perspective of exploiting hybrid nanofluid. Encouraging structures can be amended and by the reason of synergistic effect troublesomeness can be enclosed. Recently, hybrid nanofluids have been extensively used in many areas such as micro fluidics, transportation, medical, naval structures and acoustics etc. Mainly, nanofluids flow are eminent for high heat transfer as related to normal fluid. In addition to improve it even further, the hybrid nanofluid is initiated. Suresh et al. [55] deliberated the hybrid nanofluid flow features include with the heat transfer phenomena. Momin [56] did a trial investigation of mixed convection with ($\text{Al}_2\text{O}_3\text{-Cu}/\text{H}_2\text{O}$) hybrid nanofluid for laminar flow in a inclined tube. From that point forward different endeavors subject to Hybrid nanofluid are accounted for see Refs. [57-59].

Presently, it is imperative to note that numerous fluids of industrial significance are non-Newtonian. In real mechanical non-Newtonian fluids are more suitable than Newtonian fluids, because to their applications in oil penetrating, polymer designing, certain partition forms, manufacturing of substances and paper and some other modern procedures [60]. The non-linearity can show itself in an assortment of ways in numerous fields, for example, food, penetrating operations and bio- designing. The Navier–Stokes theory is insufficient for such fluids, and no single constitutive condition is accessible in the literature which displays the properties of all fluids. Subsequently, few non-Newtonian fluid models [61-62] have been proposed relying upon

different physical characters. So as to acquire an exhaustive perception of non-Newtonian fluids and their numerous applications, it is essential to study their flow actions. Because of their application in industry and machinery, couple of issues in fluid mechanics have delighted in the consideration that concurred to flow which includes non-Newtonian fluids.

In classification of the non-Newtonian liquids, Casson model has distinguishing characteristic. This model was displayed by the Casson [63] for progression of viscoelastic fluid in 1959. This model is developed for determining giant shear-rate viscosities when the information of transitional shear-rate are accessible. In the literature, the Casson fluid is in some cases expressed to fit rheological information superior to general viscoelastic models for some materials. Precisely, the Casson fluid depicts the flow qualities of blood exactly at low shear rates and when it moves through little veins. Casson fluids are observed to be material in creating models for blood oxygenator and haemodialysers. The non-linear Casson's constitutive equation has been found to depict precisely the flow curves of suspensions of colors in lithographic varnishes utilized for research of printing inks and silicon suspensions [64]. Eldabe et al. [65] evaluated the heat transfer of MHD Casson fluid flow between two pivoting chambers. Fredrickson [66] inspected the unfaltering progression of a Casson fluid in a tube. Dash et al. [67] explored Casson flow in tube filled through homogeneous permeable medium. Examination of the Casson non-Newtonian blood models in stable and oscillatory flow. Nadeem et al. [68] investigated MHD Casson flow in two horizontal directions past a permeable straight stretching sheet.

The most commonly used Non-Newtonian fluids is Couple Stress fluid, which is actually the generalized form of Newtonian fluid. Ramesh [69] examined peristaltic flow in inclined channel through porous medium. Khan et al. [70] presented definite solution of MHD heat transfer couple stress fluid for peristaltic transport. Kaladhar [71] have investigated the consequence of Joule heating and Hall current on free convection flow of couple stress fluid. Sankad and Nagathan [72] examined peristaltic transport in uniform channel of couple stress fluid. Dhit and Roy [73] explored the impact of channel inclination on couple stress fluid. The stability of buoyancy driven parallel shear flow confined between vertical plates on couple stress fluid is investigated by Shankar et al. [74]. Devakar et al. [75] worked on analytical solutions of couple stress fluid.

All mentioned available studies have been focused to the flows in planar channels or tubes.

In real world issues curved channel are essential significance. In simple channel most of the practical application do not encounter, curved channel increase significantly more important in veins, intestines and arteries. Sato et al. [76] firstly analyzed the flow in a rectangular curved channel for a viscous fluid. Vriend [77] examined the curved microchannel array plates. In curved channel unsteady transport inspected by Ramanamurthy et al. [78]. Hina et al. [79] discussed the impact of nanofluid on curved channel on cilia motion. Eskinazi [80] investigation about fully developed turbulent flows in curved channel. The mathematical examination of hyperbolic tangent fluid in curved tube examined by Nadeem et al. [81]. In the curved channel flow of the pseudoplastic fluid using wall properties and slip conditions were explored by Hina et al. [82]. Fluid motion in a curved channel has been discussed by Dean et al. [83].

Inspired Motivated from the above studies, the them of the current thesis is to digout the effects of corrugation and EMHD for various non-Newtonian fluids. This thesis consist of eight chapters in which first chapter is introductory chapter which other chapters are described as follow.

Chapter two objectives to assess the EMHD flow in microchannel through permeable medium under corrugation effects. The walls corrugations are described by period sine waves with small amplitude. The significant formulation is discussed in the presence of Lorenz force. The corresponding solutions are calculated by using perturbation technique. 3D contours are developed for the small amplitude parameters. This chapter contents are submitted in Physica A: Statistical Mechanics and its Applications.

The aims of chapter three is to investigate the influences of surface wavy roughness on the viscous fluid flow inside microchannel through corrugated walls. The theme to this chapter has the following interesting features. Firstly, to inspect the influence of Lorenz on electromagneto-hydrodynamic flow. Secondly to address the effect of convective conditions. Thirdly the effect of EMHD on nanofluid through the corrugated walls are discussed. Fourth, the Navier-Stokes equations are simplified by utilizing perturbation technique. Fifth the influence of related parameters graphically interpreted. This chapter contents are published in Physica A: Statistical Mechanics and its Applications, Volume 551, 1 August 2020, 124089.

In Chapter four we explored the effect of Couple stress fluid on electromagneto-hydrodynamic flow in a microchannel. The flow is deliberated in the presence of convective conditions. By

employing mathematical computation, we evaluated the wavy effects on velocity for the EMHD flow. The impact of all parameters on velocity and the mean velocity profiles can be analyzed by graphs. This chapter contents are submitted in *Advances in Mechanical Engineering*.

The determination of Chapter five is to examine the consequences of heat generation and heat flow on hybrid nanofluid in microchannel. The heat transfer enhancement by using hybrid nanofluid. We take two-dimensional flow of a Hybrid nanofluid Cu-Al₂O₃/water and nanofluid Cu/water along with Casson fluid. This model is employed to inspect the consequence of thermal radiation, heat generation and porous effect in microchannel with corrugated walls. This chapter contents are submitted in *Journal of Thermal Analysis and Calorimetry*.

Chapter six models the electromagnetohydrodynamic flow in a curved channel of viscous fluid. Amplitude of corrugations of the wavy walls are either in phase or out of phase. The solution of velocity is achieved by employing the perturbation technique. By means of mathematical calculations we investigated the corrugation effects on the EMHD velocity flow. The influence of emerging parameters from obtained solutions are inspected by graphs. This chapter contents are submitted in *Physica A: Statistical Mechanics and its Applications*.

Chapter seven investigates the corrugated effect on nanofluids in curved channel under the influence of electromagnetohydrodynamic flow. Firstly, performed the mathematical modelling and then employing the method of perturbation, we have estimated the analytical solutions. The main observations are summarized in the conclusions. The physical effects of flow variables are graphically discussed. Consequences of Curvature parameter on stresses and Nusselt number are analyzed through tables. The important conclusion is that reducing the unobvious wave effect on the velocity by taking amplitude ratio parameter small. This chapter contents are accepted in *Applied Mathematics-A Journal of Chinese Universities*.

The aims of chapter eight is described the steady EMHD non-Newtonian incompressible and electrical conducting Casson fluid between corrugated walls in the presence of Lorenz force. The Casson fluid model is utilized to characterize the non-Newtonian fluid behavior. The equations are transformed by utilizing the perturbation method. Analytical solution corresponding to momentum and temperature equations are acquired. The heat transfer features are analyzed in detail. This chapter contents are submitted in *Applied Mathematics-A Journal of Chinese Universities*.

Chapter 2

Electromagnetohydrodynamic flow in microchannel by velocity slip and temperature jump through a porous medium under corrugated wall

In this chapter, we have discussed the electromagnetohydrodynamic (EMHD) flow in microchannels by perturbation technique through the porous medium under slightly corrugated walls effects. In microparallel plates we consider incompressible and electrically conducting viscous fluid. With small amplitudes the wall corrugations are described by periodic sine waves. The flow is discussed in the presence of Lorenz force. We discussed the effects of darcy condition on velocity. Impacts of velocity slip and in addition thermal slip have been appropriately dealt with in the present examination. The energy equation is defined by including a heat source factor which simulates either absorption or generation. Systematic solutions assessed for velocity and temperature. By utilizing numerical computations, we investigated the corrugation consequences on EMHD flow. We explicitly clarified the profiles of velocity and temperature and their dependencies on the parameters.

2.1 Mathematical development

We consider EMHD flow of viscous, incompressible and electrically conducting Newtonian fluids between two vertical corrugated walls separated by $2H$ distance. We assumed that the length L of channel in z^* -direction and in x^* -direction width W and the flow is taken due to Lorenz force. The flow is taken opposite to corrugations of the walls. The wavy walls are described by

$$y_l^* = H + \varepsilon H \sin(\lambda^* x^*) \quad \text{and} \quad y_r^* = -H - \varepsilon H \sin(\lambda^* x^*). \quad (2.1)$$

We can applied electric field \mathbf{E}^* and magnetic field \mathbf{B}^* in x^* and y^* direction respectively. Here $\mathbf{J} \times \mathbf{B}^*$ is the Lorenz force taken along the z^* direction and created by electric and magnetic field interaction, where current density is symbolize by \mathbf{J} .

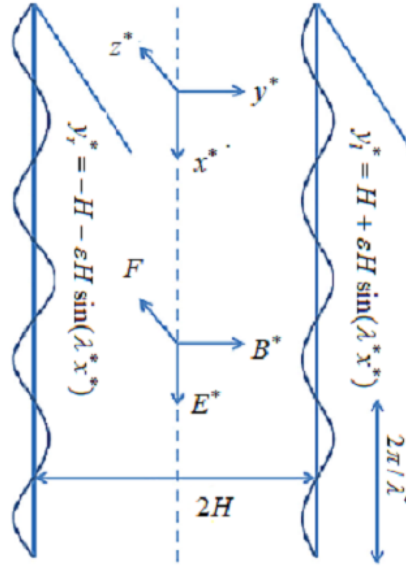


Fig. (2.1): Geometrical sketch of EMHD flow in microchannel.

The basic equations for mass, momentum and temperature are expressed as [84],

$$\nabla^* \mathbf{u}^* = 0. \quad (2.2)$$

$$\rho \frac{\partial \mathbf{u}^*}{\partial t^*} + \rho (\mathbf{u}^* \cdot \nabla^*) \mathbf{u}^* = -\nabla^* p + \mu \nabla^{*2} \mathbf{u}^* + \mathbf{J} \times \mathbf{B}^* + g(\rho \zeta)(T^* - T_r^*) - \frac{\mu}{k_1} \mathbf{u}^*, \quad (2.3)$$

$$(\rho C_p) \frac{DT^*}{Dt^*} = \nabla^* \cdot k'' \nabla^* T^* + Q_0(T^* - T_r^*). \quad (2.4)$$

We choose the velocity in that form

$$\mathbf{u}^* = (0, 0, w^*(x^*, y^*)).$$

Assume that velocity will be maintained by z^* component. The equations are simplified as

$$\rho \frac{\partial w^*}{\partial t^*} = -\frac{\partial p}{\partial z^*} + \mu \left(\frac{\partial^2 w^*}{\partial x^{*2}} + \frac{\partial^2 w^*}{\partial y^{*2}} \right) + \sigma B^* (E^* - B^* w^*) + g(\rho \zeta)(T^* - T_r^*) - \frac{\mu}{k_1} w^*, \quad (2.5)$$

$$(\rho C_p) \left(\frac{\partial T^*}{\partial t^*} \right) = k'' \left(\frac{\partial^2 T^*}{\partial x^{*2}} + \frac{\partial^2 T^*}{\partial y^{*2}} \right) + Q_0(T^* - T_r^*). \quad (2.6)$$

We consider incompressible fluid between microparallel plates and along z^* direction. Adopting channel is open in z^* direction so neglected pressure gradient [85] and the velocity satisfies

$$\rho \frac{\partial w^*}{\partial t^*} = \mu \left(\frac{\partial^2 w^*}{\partial x^{*2}} + \frac{\partial^2 w^*}{\partial y^{*2}} \right) + \sigma B^* (E^* - B^* w^*) + g(\rho \zeta)(T^* - T_r^*) - \frac{\mu}{k_1} w^*. \quad (2.7)$$

Velocity, electric field and temperature in periodical forms are expressed as

$$w^* = R\{\tilde{w}(x^*, y^*)e^{i\omega t^*}\}, \quad E^* = R\{E_0 e^{i\omega t^*}\}, \quad T^* = R\{T(x^*, y^*)e^{i\omega t^*}\}, \quad (2.8)$$

where $R\{ \}$, \tilde{w} , ω , E_0 , i and T denotes real part, amplitude of velocity, angular frequency, electric field, imaginary unit and temperature. Utilizing Eq. (2.8) into Eq. (2.6) and Eq. (2.7), we get

$$i\rho\omega\tilde{w} = \mu \left(\frac{\partial^2\tilde{w}}{\partial x^{*2}} + \frac{\partial^2\tilde{w}}{\partial y^{*2}} \right) + \sigma B^* E_0 - \sigma B^{*2}\tilde{w} - g(\rho\zeta)(T - T_r) - \frac{\mu}{k_1}\tilde{w}. \quad (2.9)$$

$$T\omega i = \alpha \left(\frac{\partial^2 T}{\partial x^{*2}} + \frac{\partial^2 T}{\partial y^{*2}} \right) + \frac{Q_0}{(\rho C_p)}(T - T_r). \quad (2.10)$$

Nondimensional variables are

$$(x, y) = \frac{(x^*, y^*)}{H}, w = \frac{\tilde{w}}{H\omega}, \lambda = \lambda^* H. \quad (2.11)$$

Using Eq. (2.11) into Eqs. (2.9) and (2.10), we get

$$\left(\frac{\partial^2 w}{\partial x^2} + \frac{\partial^2 w}{\partial y^2} \right) - \left(Ha^2 + Re i + \frac{1}{Da} \right) w + Gr\theta + Ha\beta = 0, \quad (2.12)$$

$$\frac{1}{Pr} \left(\frac{\partial^2 \theta}{\partial x^2} + \frac{\partial^2 \theta}{\partial y^2} \right) + \theta(\phi - i) - Si = 0, \quad (2.13)$$

Now non-dimensional quantities are

$$\begin{aligned} Re &= \frac{\rho\omega H^2}{\mu}, \quad Ha = B^* H \left(\frac{\sigma}{\mu} \right)^{\frac{1}{2}}, \quad \beta = E_0 \left(\frac{\sigma}{\mu} \right)^{\frac{1}{2}} / \omega, \quad Da = \frac{k_1}{H^2}, \\ Gr &= \frac{g(\rho\zeta)H(T_l - T_r)}{\mu\omega}, \quad \theta = \frac{T - T_r}{T_l - T_r}, \quad S = \frac{T_r}{(T_l - T_r)}, \quad Pr = \frac{\omega H^2}{\alpha_f}, \quad \phi = \frac{Q_0 H^2}{k''}. \end{aligned} \quad (2.14)$$

The corresponding dimensionless slip conditions are

$$w - \beta_1 \frac{\partial w}{\partial y} = 0 \text{ and } \theta - \gamma_1 \frac{\partial \theta}{\partial y} = 1 \text{ at } y = y_l, \quad (2.15)$$

$$w + \beta_1 \frac{\partial w}{\partial y} = 0 \text{ and } \theta + \gamma_1 \frac{\partial \theta}{\partial y} = 0 \text{ at } y = y_r. \quad (2.16)$$

2.2 Perturbation analysis

In order to solve Eqs. (2.12) and (2.13) using boundary conditions (2.15) and (2.16), we consider the perturbation expansion by writing

$$w(x, y) = w_0(y) + \varepsilon w_1(x, y) + \varepsilon^2 w_2(x, y) + \dots \quad (2.17)$$

$$\theta(x, y) = \theta_0(y) + \varepsilon \theta_1(x, y) + \varepsilon^2 \theta_2(x, y) + \dots \quad (2.18)$$

Now using Eqs.(2.17) and (2.18) into Eqs. (2.12) and (2.13) and the boundary conditions (2.15) and (2.16) are expanded by Taylor series on wavy wall at $y = 1$ and $y = -1$ and collecting like power of ε , one gets the zeroth-order equations as

$$\frac{d^2 w_0}{dy^2} - \left(Ha^2 + Re\,i + \frac{1}{Da} \right) w_0 + Gr\theta_0 + Ha\beta = 0, \quad (2.19)$$

$$\frac{1}{Pr} \frac{d^2 \theta_0}{dy^2} + \theta_0(\phi - i) - Si = 0. \quad (2.20)$$

Corresponding boundary conditions are

$$w_0 - \beta_1 \frac{dw_0}{dy} = 0 \text{ and } \theta_0 - \gamma_1 \frac{d\theta_0}{dy} = 1 \text{ at } y = 1 \text{ and} \quad (2.21)$$

$$w_0 + \beta_1 \frac{dw_0}{dy} = 0 \text{ and } \theta_0 + \gamma_1 \frac{d\theta_0}{dy} = 0 \text{ at } y = -1. \quad (2.22)$$

The first-order perturbation equation is found in the form

$$\left(\frac{\partial^2 w_1}{\partial x^2} + \frac{\partial^2 w_1}{\partial y^2} \right) - \left(Ha^2 + Re\,i + \frac{1}{Da} \right) w_1 + Gr\theta_1 = 0, \quad (2.23)$$

$$\frac{1}{Pr} \left(\frac{\partial^2 \theta_1}{\partial x^2} + \frac{\partial^2 \theta_1}{\partial y^2} \right) + (\phi - i)\theta_1 = 0. \quad (2.24)$$

The corresponding boundary conditions are

$$w_1 + \sin(\lambda x) \frac{dw_0}{dy} - \beta_1 \left(\frac{\partial w_1}{\partial y} + \sin(\lambda x) \frac{d^2 w_0}{dx^2} \right) = 0 \text{ and} \quad (2.25)$$

$$\theta_1 + \sin(\lambda x) \frac{d\theta_0}{dy} - \gamma_1 \left(\frac{\partial \theta_1}{\partial y} + \sin(\lambda x) \frac{d^2 \theta_0}{dx^2} \right) = 0 \text{ at } y = 1.$$

and

$$\begin{aligned} w_1 - \sin(\lambda x) \frac{dw_0}{dy} + \beta_1 \left(\frac{\partial w_1}{\partial y} - \sin(\lambda x) \frac{d^2 w_0}{dx^2} \right) &= 0 \text{ and} \\ \theta_1 - \sin(\lambda x) \frac{d\theta_0}{dy} + \gamma_1 \left(\frac{\partial \theta_1}{\partial y} - \sin(\lambda x) \frac{d^2 \theta_0}{dx^2} \right) &= 0 \text{ at } y = -1. \end{aligned} \quad (2.26)$$

The second-order perturbation equation is found in the form

$$\frac{\partial^2 w_2}{\partial x^2} + \frac{\partial^2 w_2}{\partial y^2} - \left(Ha^2 + Re i + \frac{1}{Da} \right) w_2 + Gr\theta_2 = 0, \quad (2.27)$$

$$\frac{1}{Pr} \left(\frac{\partial^2 \theta_2}{\partial x^2} + \frac{\partial^2 \theta_2}{\partial y^2} \right) + (\phi - i)\theta_2 = 0. \quad (2.28)$$

The corresponding boundary conditions are

$$\begin{aligned} w_2 + \sin(\lambda x) \frac{\partial w_1}{\partial y} + \frac{1}{2} \sin^2(\lambda x) \frac{d^2 w_0}{dy^2} - \beta_1 \left(\frac{\partial w_2}{\partial y} + \sin(\lambda x) \frac{\partial^2 w_1}{\partial y^2} + \frac{1}{2} \sin^2(\lambda x) \frac{d^3 w_0}{dy^3} \right) &= 0, \\ \theta_2 + \sin(\lambda x) \frac{\partial \theta_1}{\partial y} + \frac{1}{2} \sin^2(\lambda x) \frac{d^2 \theta_0}{dy^2} - \gamma_1 \left(\frac{\partial \theta_2}{\partial y} + \sin(\lambda x) \frac{\partial^2 \theta_1}{\partial y^2} + \frac{1}{2} \sin^2(\lambda x) \frac{d^3 \theta_0}{dy^3} \right) &= 0 \text{ at } y = 1, \end{aligned} \quad (2.29)$$

and

$$\begin{aligned} w_2 - \sin(\lambda x) \frac{\partial w_1}{\partial y} + \frac{1}{2} \sin^2(\lambda x) \frac{d^2 w_0}{dy^2} + \beta_1 \left(\frac{\partial w_2}{\partial y} - \sin(\lambda x) \frac{\partial^2 w_1}{\partial y^2} + \frac{1}{2} \sin^2(\lambda x) \frac{d^3 w_0}{dy^3} \right) &= 0, \\ \theta_2 - \sin(\lambda x) \frac{\partial \theta_1}{\partial y} + \frac{1}{2} \sin^2(\lambda x) \frac{d^2 \theta_0}{dy^2} + \gamma_1 \left(\frac{\partial \theta_2}{\partial y} - \sin(\lambda x) \frac{\partial^2 \theta_1}{\partial y^2} + \frac{1}{2} \sin^2(\lambda x) \frac{d^3 \theta_0}{dy^3} \right) &= 0 \text{ at } y = -1. \end{aligned} \quad (2.30)$$

2.3 Solution of the problem

The solution of zero order system (2.19) and (2.20) by utilizing boundary conditions (2.21) and (2.22) we obtained

$$\theta_0(y) = -\frac{Pr Si}{a^2} + e^{ay} A_1 + e^{-ay} A_2, \quad (2.31)$$

$$\begin{aligned}
w_0(y) = & (e^{-y(a+b)}(Dae^{y(a+b)}Gr \Pr \text{Si}(1 + Da(Ha^2 + \text{Re } i)) + a^2(-Da^2e^{y(a+b)}Gr \Pr \text{Si} - A_2Dae^{yb} \\
& Gr(1 + Da(Ha^2 + \text{Re } i)) - A_1Dae^{2y(a+b)}Gr(1 + Da(Ha^2 + \text{Re } i)) - Dae^{y(a+b)}Ha\beta - Da^2 \\
& e^{y(a+b)}Ha^3\beta - Da^2e^{y(a+b)}Ha \text{Re } i\beta - e^{y(a+2b)}(1 + Da(Ha^2 + \text{Re } i))^2B_1 - B_2e^{ya} - 2Dae^{ya} \\
& Ha^2B_2 - Da^2e^{ya}Ha^4B_2 - 2Dae^{ya} \text{Re } iB_2 - 2Da^2e^{ya}Ha^2 \text{Re } iB_2 - Da^2e^{ya} \text{Re } i^2B_2) + a^4 \\
& Dae^{ya}(Dae^{yb}Ha\beta + e^{2yb}(1 + Da(Ha^2 + \text{Re } i))B_1 + B_2 + Da(Ha^2 + \text{Re } i)B_2)))/(a^2(-1 + \\
& a^2Da - Da(Ha^2 + \text{Re } i))(1 + Da(Ha^2 + \text{Re } i))).
\end{aligned} \tag{2.32}$$

with

$$\begin{aligned}
a &= \sqrt{i \Pr - \Pr \phi}, \\
b &= \frac{\sqrt{1 + Da(Ha^2 + \text{Re } i)}}{\sqrt{Da}}.
\end{aligned} \tag{2.33}$$

On the base of conditions (2.25) and (2.26), the first order system solution is

$$\theta_1(x, y) = \sin(\lambda x) f(y), \tag{2.34}$$

$$w_1(x, y) = \sin(\lambda x) g(y), \tag{2.35}$$

here $f(y)$ and $g(y)$ are function of y .

Using Eq. (2.34) into Eqs. (2.35), (2.23) and (2.24), we get

$$\frac{1}{\Pr} \left(\frac{d^2 f(y)}{dy^2} - \lambda^2 \right) f(y) + (\phi - i) f(y) = 0, \tag{2.36}$$

$$\frac{d^2 g(y)}{dy^2} - (\lambda^2 + Ha^2 + \text{Re } i + \frac{1}{Da}) g(y) + Gr f(y) = 0. \tag{2.37}$$

The boundary conditions are transformed in the following form

$$\begin{aligned}
f(y) + \frac{d\theta_0}{dy} - \gamma_1 \left(\frac{df(y)}{dy} + \frac{d^2\theta_0}{dy^2} \right) &= 0 \text{ and} \\
g(y) + \frac{dw_0}{dy} - \beta_1 \left(\frac{dg(y)}{dy} + \frac{d^2w_0}{dy^2} \right) &= 0 \text{ at } y = 1,
\end{aligned} \tag{2.38}$$

and

$$\begin{aligned}
f(y) - \frac{d\theta_0}{dy} + \gamma_1 \left(\frac{df(y)}{dy} - \frac{d^2\theta_0}{dy^2} \right) &= 0 \text{ and} \\
g(y) - \frac{dw_0}{dy} + \beta_1 \left(\frac{dg(y)}{dy} - \frac{d^2w_0}{dy^2} \right) &= 0 \text{ at } y = -1.
\end{aligned} \tag{2.39}$$

Based upon boundary conditions, the solutions of Eqs. (2.36) and (2.37) takes the form

$$f(y) = e^{cy}C_1 + e^{-cy}C_2, \quad (2.40)$$

$$g(y) = -(Da e^{-dy}(C_2 + C_1 e^{2dy})Gr / (-1 + c^2 Da - Da(Ha^2 + \text{Re } i + \lambda^2))) + e^{dy}D_1 + e^{-dy}D_2, \quad (2.41)$$

with

$$\begin{aligned} c &= \sqrt{i \text{Pr} + \lambda^2 - \text{Pr} \phi}, \\ d &= \frac{\sqrt{1 + Da(Ha^2 + \text{Re } i + \lambda^2)}}{\sqrt{Da}}. \end{aligned} \quad (2.42)$$

First order problem solution can be expressed as

$$\theta_1(x, y) = \sin(\lambda x) (e^{cy}C_1 + e^{-cy}C_2) \quad (2.43)$$

$$w_1(x, y) = \sin(\lambda x) \left[-(Da e^{-dy}(C_2 + C_1 e^{2dy})Gr / (-1 + c^2 Da - Da(Ha^2 + \text{Re } i + \lambda^2))) + e^{dy}D_1 + e^{-dy}D_2 \right]. \quad (2.44)$$

The boundary conditions (2.29) and (2.30) of the second order can be simplified by the solutions of (2.31), (2.32), (2.43) and (2.44). Base on boundary conditions, the second order system solutions can be computed as

$$\theta_2(x, y) = h(y) + \cos(2\lambda x) k(y), \quad (2.45)$$

$$w_2(x, y) = m(y) + \cos(2\lambda x) n(y). \quad (2.46)$$

By utilizing Eqs. (2.45) and (2.46) into Eqs. (2.27) and (2.28), we get the following forms

$$\frac{1}{\text{Pr}} \frac{d^2 h(y)}{dy^2} + (\phi - i)h(y) = 0, \quad (2.47)$$

$$\frac{d^2 m(y)}{dy^2} - (Ha^2 + \text{Re } i + \frac{1}{Da})m(y) + Grh(y) = 0. \quad (2.48)$$

The boundary conditions are transformed as

$$\begin{aligned} h(y) + \frac{1}{2}\left(\frac{df(y)}{dy} + \frac{1}{2}\frac{d^2\theta_0}{dy^2}\right) - \gamma_1\left(\frac{dh(y)}{dy} + \frac{1}{2}\left(\frac{d^2f(y)}{dy^2} + \frac{1}{2}\frac{d^3\theta_0}{dy^3}\right)\right) &= 0 \text{ and} \\ m(y) + \frac{1}{2}\left(\frac{dg(y)}{dy} + \frac{1}{2}\frac{d^2w_0}{dy^2}\right) - \beta_1\left(\frac{dm(y)}{dy} + \frac{1}{2}\left(\frac{d^2g(y)}{dy^2} + \frac{1}{2}\frac{d^3w_0}{dy^3}\right)\right) &= 0 \text{ at } y = 1, \end{aligned} \quad (2.49)$$

and

$$\begin{aligned} h(y) - \frac{1}{2}\left(\frac{df(y)}{dy} - \frac{1}{2}\frac{d^2\theta_0}{dy^2}\right) + \gamma_1\left(\frac{dh(y)}{dy} - \frac{1}{2}\left(\frac{d^2f(y)}{dy^2} - \frac{1}{2}\frac{d^3\theta_0}{dy^3}\right)\right) &= 0 \text{ and} \\ m(y) - \frac{1}{2}\left(\frac{dg(y)}{dy} - \frac{1}{2}\frac{d^2w_0}{dy^2}\right) + \beta_1\left(\frac{dm(y)}{dy} - \frac{1}{2}\left(\frac{d^2g(y)}{dy^2} - \frac{1}{2}\frac{d^3w_0}{dy^3}\right)\right) &= 0 \text{ at } y = -1, \end{aligned} \quad (2.50)$$

$$\frac{1}{Pr}\left(\frac{d^2k(y)}{dy^2} - 4\lambda^2\right)k(y) + (\phi - i)k(y) = 0, \quad (2.51)$$

$$\frac{d^2n(y)}{dy^2} - (4\lambda^2 + Ha^2 + Re i + \frac{1}{Da})n(y) + Grk(y) = 0. \quad (2.52)$$

The boundary conditions are transformed in the following form

$$\begin{aligned} k(y) - \frac{1}{2}\left(\frac{df(y)}{dy} + \frac{1}{2}\frac{d^2\theta_0}{dy^2}\right) - \gamma_1\left(\frac{dk(y)}{dy} - \frac{1}{2}\left(\frac{d^2f(y)}{dy^2} + \frac{1}{2}\frac{d^3\theta_0}{dy^3}\right)\right) &= 0 \text{ and} \\ n(y) - \frac{1}{2}\left(\frac{dg(y)}{dy} + \frac{1}{2}\frac{d^2w_0}{dy^2}\right) - \beta_1\left(\frac{dn(y)}{dy} - \frac{1}{2}\left(\frac{d^2g(y)}{dy^2} + \frac{1}{2}\frac{d^3w_0}{dy^3}\right)\right) &= 0 \text{ at } y = 1, \end{aligned} \quad (2.53)$$

and

$$\begin{aligned} k(y) + \frac{1}{2}\left(\frac{df(y)}{dy} - \frac{1}{2}\frac{d^2\theta_0}{dy^2}\right) + \gamma_1\left(\frac{dk(y)}{dy} + \frac{1}{2}\left(\frac{d^2f(y)}{dy^2} - \frac{1}{2}\frac{d^3\theta_0}{dy^3}\right)\right) &= 0 \text{ and} \\ n(y) + \frac{1}{2}\left(\frac{dg(y)}{dy} - \frac{1}{2}\frac{d^2w_0}{dy^2}\right) + \beta_1\left(\frac{dn(y)}{dy} + \frac{1}{2}\left(\frac{d^2g(y)}{dy^2} - \frac{1}{2}\frac{d^3w_0}{dy^3}\right)\right) &= 0 \text{ at } y = -1. \end{aligned} \quad (2.54)$$

By utilizing the above boundary conditions (2.49), (2.50), (2.53) and (2.54) the solutions are expressed as

$$h(y) = e^{ay}E_1 + e^{-ay}E_2, \quad (2.55)$$

$$m(y) = (Dae^{-ay}(E_2 + E_1e^{2ay})Gr)/(1 + Da(-a^2 + Ha^2 + Re i)) + e^{by}F_1 + e^{-by}F_2, \quad (2.56)$$

$$k(y) = e^{ey}G_1 + e^{-ey}G_2, \quad (2.57)$$

$$n(y) = (Dae^{-ey}(G_2 + G_1e^{2ey})Gr/(1 + Da(-e^2 + Ha^2 + Re i + 4\lambda^2))) + e^{fy}H_1 + e^{-fy}H_2, \quad (2.58)$$

with

$$\begin{aligned} e &= \sqrt{iPr + 4\lambda^2 - Pr}\phi, \\ f &= \frac{\sqrt{1 + Da(Ha^2 + Re i + 4\lambda^2)}}{\sqrt{Da}}. \end{aligned} \quad (2.59)$$

Thus the second order solutions finally take the form

$$\theta_2 = e^{ay}E_1 + e^{-ay}E_2 + \cos(2\lambda x)(e^{ey}G_1 + e^{-ey}G_2), \quad (2.60)$$

$$\begin{aligned} w_2 = & (Dae^{-ay}(E_2 + E_1e^{2ay})Gr/(1 + Da(-a^2 + Ha^2 + Re i))) + e^{by}F_1 + e^{-by}F_2 + \cos(2\lambda x) \\ & ((Dae^{-ey}(G_2 + G_1e^{2ey})Gr/(1 + Da(-e^2 + Ha^2 + Re i + 4\lambda^2))) + e^{fy}H_1 + e^{-fy}H_2). \end{aligned} \quad (2.61)$$

Collecting (2.31), (2.43) and (2.60), the approximate temperature solution can be obtained as

$$\theta(x, y) = \theta_0(y) + \varepsilon\theta_1(x, y) + \varepsilon^2\theta_2(x, y) + \dots \quad (2.62)$$

$$\begin{aligned} \theta(x, y) = & -\frac{Pr Si}{a^2} + e^{ay}A_1 + e^{-ay}A_2 + \varepsilon \sin(\lambda x)(e^{cy}C_1 + e^{-cy}C_2) \\ & + \varepsilon^2(e^{ay}E_1 + e^{-ay}E_2 + \cos(2\lambda x)(e^{ey}G_1 + e^{-ey}G_2)). \end{aligned} \quad (2.63)$$

Collecting (2.32), (2.44) and (2.61), the estimated velocity solution can be written as

$$w(x, y) = w_0(y) + \varepsilon w_1(x, y) + \varepsilon^2 w_2(x, y) + \dots \quad (2.64)$$

$$\begin{aligned}
& (e^{-y(a+b)}(Dae^{y(a+b)}Gr \text{ Pr Si}(1 + Da(Ha^2 + \text{Re } i)) + a^2(-Da^2e^{y(a+b)}Gr \text{ Pr Si} - A_2Dae^{yb} \\
& Gr(1 + Da(Ha^2 + \text{Re } i)) - A_1Dae^{2y(a+b)}Gr(1 + Da(Ha^2 + \text{Re } i)) - Dae^{y(a+b)}Ha\beta - Da^2 \\
& e^{y(a+b)}Ha^3\beta - Da^2e^{y(a+b)}Ha \text{ Re } i\beta - e^{y(a+2b)}(1 + Da(Ha^2 + \text{Re } i))^2B_1 - B_2e^{ya} - 2Dae^{ya} \\
& Ha^2B_2 - Da^2e^{ya}Ha^4B_2 - 2Dae^{ya} \text{ Re } iB_2 - 2Da^2e^{ya}Ha^2 \text{ Re } iB_2 - Da^2e^{ya} \text{ Re } i^2B_2) + a^4 \\
w(x, y) = & Dae^{ya}(Dae^{yb}Ha\beta + e^{2yb}(1 + Da(Ha^2 + \text{Re } i))B_1 + B_2 + Da(Ha^2 + \text{Re } i)B_2))/ (a^2(-1 + \\
& a^2Da - Da(Ha^2 + \text{Re } i))(1 + Da(Ha^2 + \text{Re } i))) + \varepsilon \sin(\lambda x) (-Dae^{-dy}(C_2 + C_1e^{2dy})Gr / \\
& (-1 + c^2Da - Da(Ha^2 + \text{Re } i + \lambda^2))) + e^{dy}D_1 + e^{-dy}D_2) + \varepsilon^2((Dae^{-ay}(E_2 + E_1e^{2ay})Gr / \\
& (1 + Da(-a^2 + Ha^2 + \text{Re } i))) + e^{by}F_1 + e^{-by}F_2 + \cos(2\lambda x) ((Dae^{-ey}(G_2 + G_1e^{2ey})Gr / (1 \\
& + Da(-e^2 + Ha^2 + \text{Re } i + 4\lambda^2))) + e^{fy}H_1 + e^{-fy}H_2).
\end{aligned} \tag{2.65}$$

2.4 Volume flow rate

We can define the volume flow rate per unit width of channel as

$$q(x) = \int_{-1-\varepsilon \sin(\lambda x)}^{1+\varepsilon \sin(\lambda x)} w(x, y) dy. \tag{2.66}$$

Substituting (2.57) into (2.58) and expanded the integrals results and disregarding third order term , finally expressed as

$$\begin{aligned}
q(x) = & \int_{-1}^1 w_0(y) dy + \varepsilon \int_{-1}^1 w_1(x, y) dy + \varepsilon^2 (\int_{-1}^1 w_2(x, y) dy + \sin(\lambda x) [w_1(x, y) |_{y=1} \\
& + w_1(x, y) |_{y=-1}] + \frac{1}{2} \sin^2(\lambda x) (\frac{dw_0(y)}{dy} |_{y=1} - \frac{dw_0(y)}{dy} |_{y=-1})) .
\end{aligned} \tag{2.67}$$

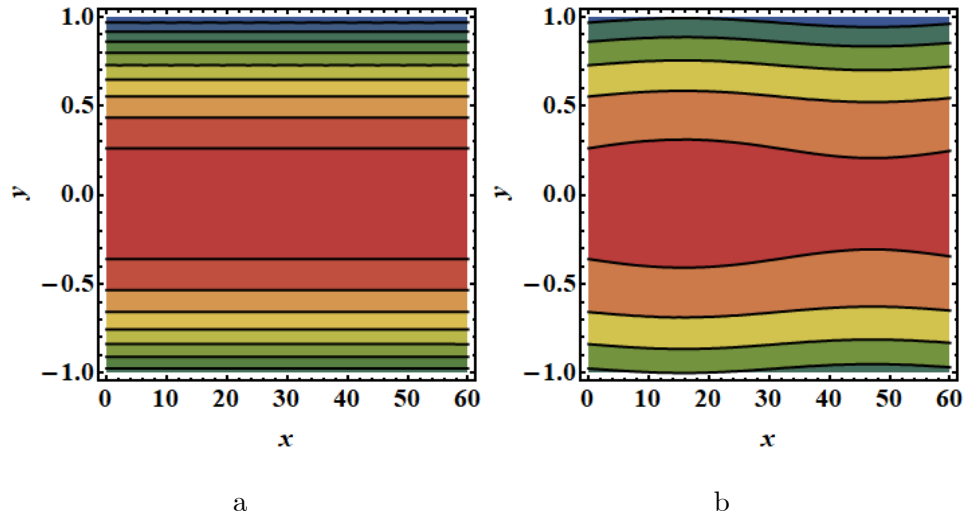
2.5 Graphical consequence

We obtained solutions by using perturbation method for velocity, temperature and volume flow rate of EMHD viscous fluids bounded by microparallel plates with corrugated walls. For general microfluidic analysis, consider $H \sim 100\mu m$ is half height of channel, the conditions of domain on density of water set with physical properties is $\rho \sim 10^3 kgm^{-3}$, the electrical conductivity $\sigma \sim 2.2 \times 10^{-4} - 10^6 Sm^{-1}$ and the viscosity $\mu \sim 10^{-3} kgm^{-1}s^{-1}$. If range of magnetic field is the $O(B^*) \sim 0.018 - 0.44T$, the Hartmann number order $O(Ha)$ using $Ha = B^*H(\sigma/\mu)^{1/2}$ is

taken from 0.0001 to 3. The electric field frequency $O(\omega)$ is changes from the 50 to $500s^{-1}$ and range of the frequency is $0 - 1 \times 10^4 s^{-1}$. The order of Reynolds number $O(Re)$ change between the 0.5 to 5 and the dimensionless parameter is fixed value i.e. $\beta = 5$.

2.5.1 Effect of wall roughness on contour distributions of velocity and temperature

The contour of the non-dimensional velocity and temperature distributions with x and y coordinates for various ε are shown in the Figs. 2.2 – 2.3. Figs. 2.2(a) and 2.3(a) display the influence of velocity and temperature distributions through smooth channels when $\varepsilon = 0$. It is defines from Figs. 2.2 – 2.3 that the wavy phenomenon noticeable with the expansion of the corrugation. We found that the velocity distribution depends on the shape of channel. The asymmetric boundaries of the channels lead to asymmetric velocity. The three-dimensional velocity and contour distributions for various value of variable viscosity are shown in Figs. 2.2 – 2.3. In microchannel, the wall roughness can cause changes in the velocity distribution.



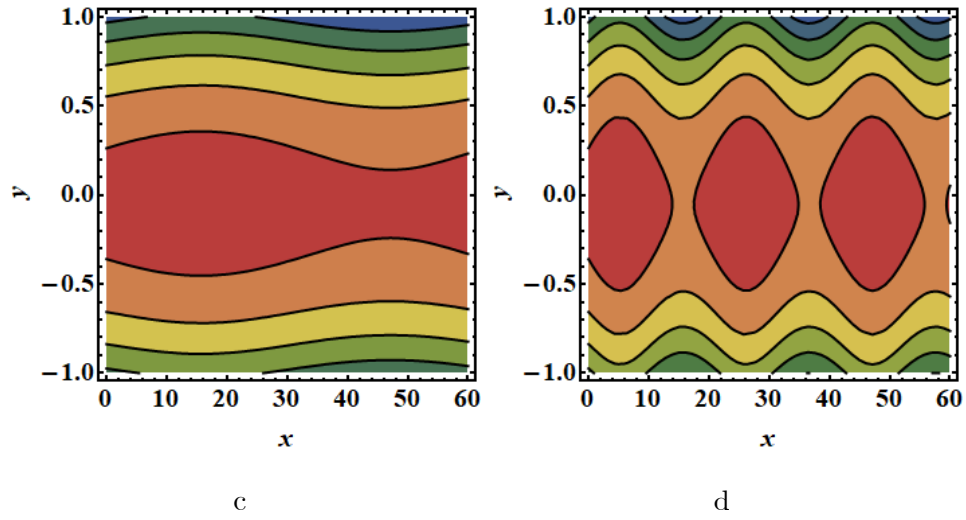
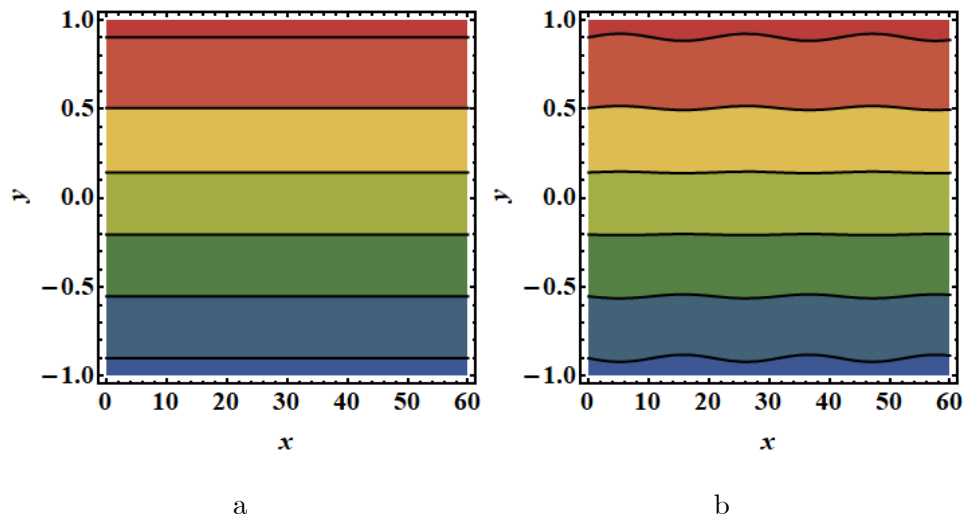


Fig. (2.2): Velocity contours (a, b, c, d) for $\varepsilon = 0, 0.02, 0.05, 0.1$ respectively.



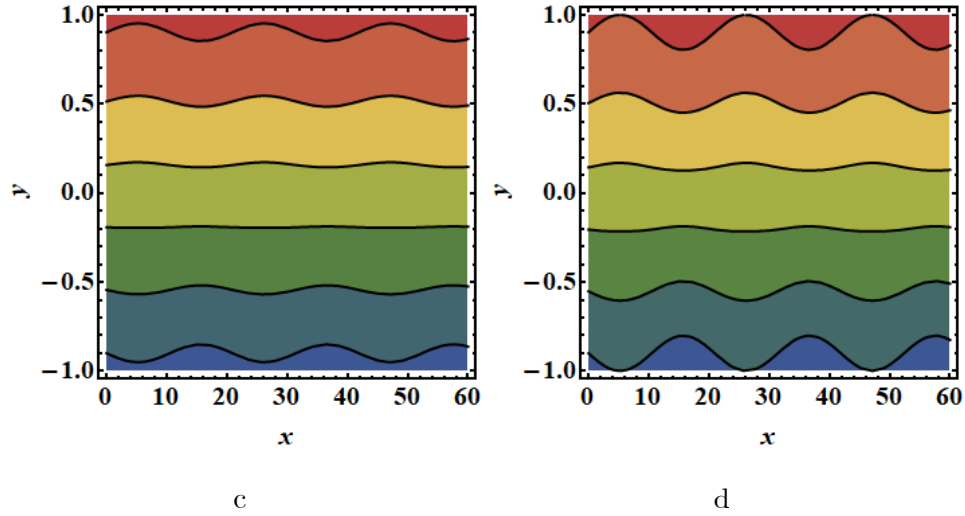


Fig. (2.3): Temperature contours (a, b, c, b) for $\varepsilon = 0, 0.02, 0.05, 0.1$ respectively.

2.5.2 Effect of wall roughness on velocity

The 2D variations of the EMHD velocity w for various values of Reynolds number, Grashof number, velocity-slip parameter furthermore, Darcy number are shown in the Figs. (2.4) to (2.7). Figs. 2.4 – 2.7 focus around the EMHD velocity of different parameter at point $x = 0.5$ and $y = 0$ when we take $\varepsilon = 0.1$ and $\beta = 5$. From these figures, the velocities first grow and then reduce by expanding the y . Fig. (2.4) illustrates that the disparity of the velocity for various estimations of Reynolds number, with increasing Re the velocity w increases. Fig. (2.5) displays that the velocity w declines for distinct values of Gr . Fig. (2.6) illustrates that the velocity w declines due to velocity slip parameter β_1 . Fig. (2.7) displays the impact of Darcy number Da on velocity w . It is inspected that the velocity increases with the increasing Darcy number Da .

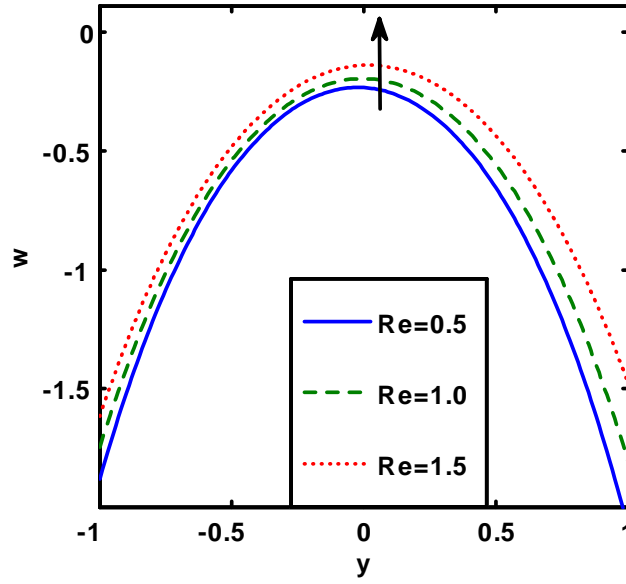


Fig. (2.4): 2D Variation of velocity for Reynolds number Re .

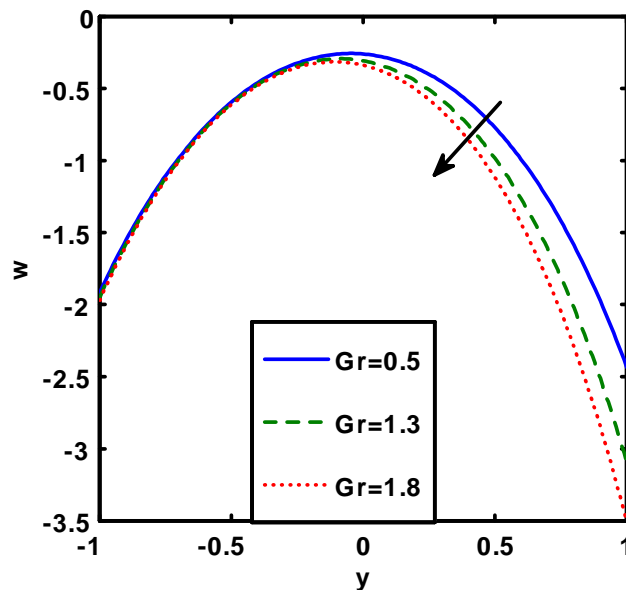


Fig. (2.5): 2D Variation of velocity for Grashof number Gr .

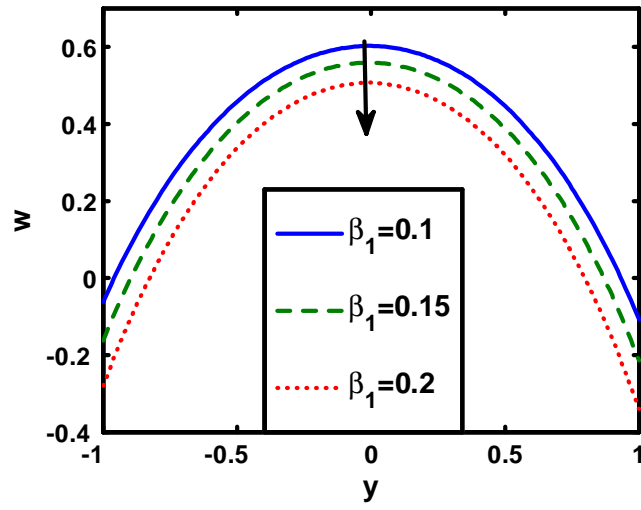


Fig. (2.6): 2D Variation of velocity for velocity slip parameter β_1 .

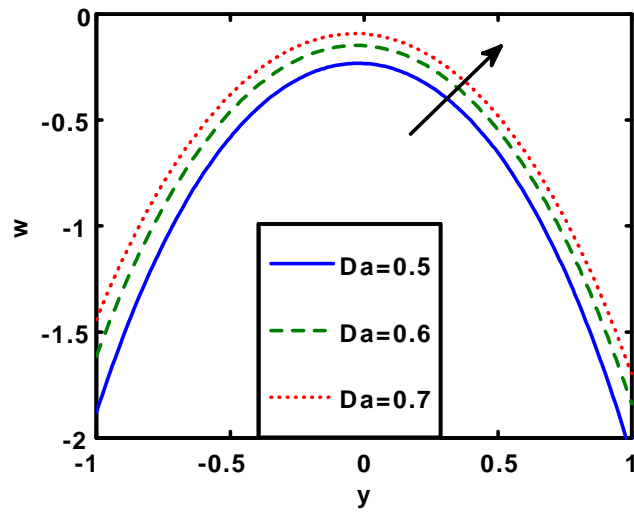


Fig. (2.7): 2D Variation of velocity for Darcy number Da .

2.5.3 Effect of wall roughness on temperature

Figs. 2.8 – 2.11 give some trademark profiles of temperature for distinct values of thermal slip/ temperature jump factor, heat absorption coefficient, Prandtl number and dimensionless parameter respectively. The 2D variation of different parameters γ_1 , ϕ , Pr and S are taken at $x = 0.5$ and $y = 0$. Fig. (2.8) represents the change of θ versus y for numerous values of γ_1 . Temperature plot first declines with the expanding of γ_1 and afterward enlarge with expanding value of γ_1 . Fig. (2.9) emphasizes that as heat generates during flow in channel. Therefore the temperature of the wall enhanced when the heat absorption coefficient ϕ increases. Fig. (2.10) shows that profile of temperature decreases when the Prandtl number Pr increases. Fig. (2.11) shows that profile of temperature decreases when non-dimensional parameter S increases.

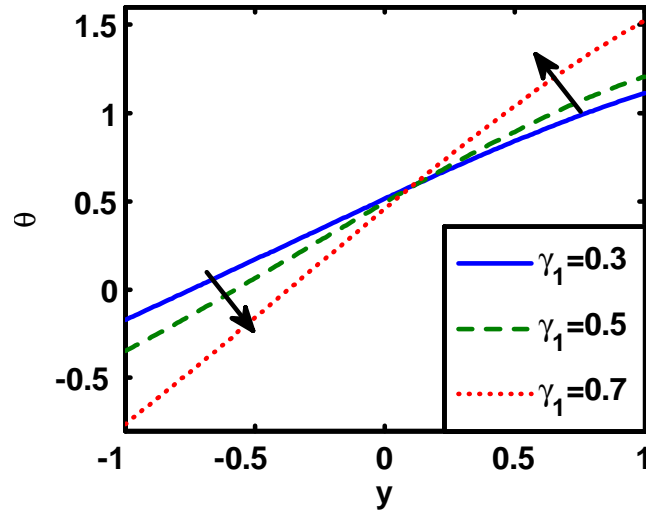


Fig. (2.8): 2D Temperature variation for thermal slip parameter γ_1 .

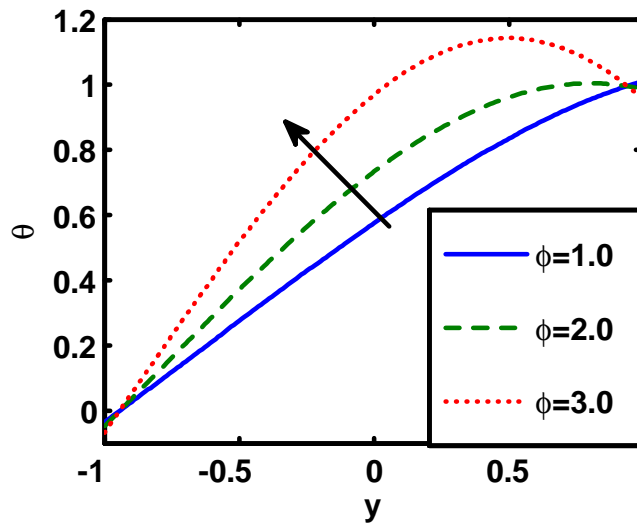


Fig. (2.9): Temperature variation for heat absorption coefficient ϕ .

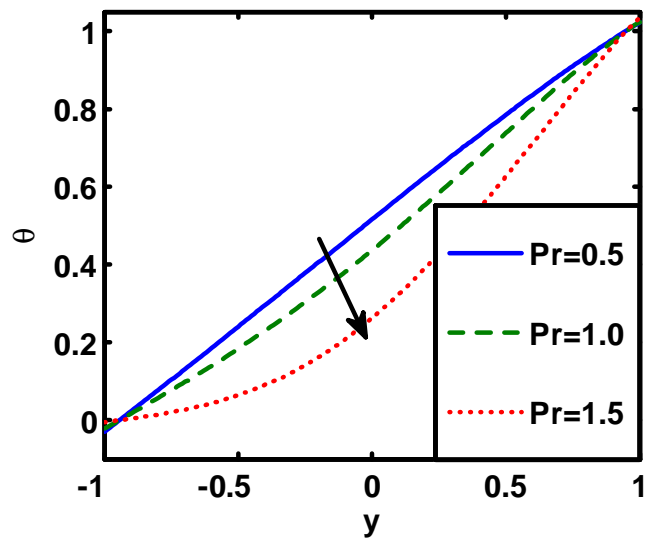


Fig. (2.10): Temperature variation for Prandtl number Pr .

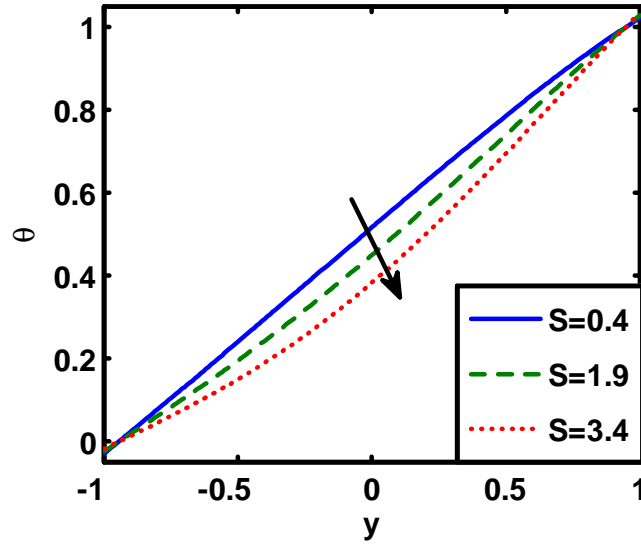


Fig. (2.11): 2Temperature variation for Non-dimensional parameter S .

2.6 Conclusions

The technique of perturbation is utilized to assess EMHD flow behavior through microchannel in the presence of corrugated walls depicted by the sin wave with small amplitude for viscous fluid. The primary outcomes are quickly clarified as

- The unobvious influences of wave can be reduced by small value of ε parameter.
- When amplitude ε approach to 0, the profile of velocity and temperature distributions of flow through the corrugated walls approach to the velocity and temperature distributions of the flow through a smooth channel.
- The velocity and temperature depend on the shape of a channel.
- Velocity grows with expanding assay of Reynolds number, Grashof number and Darcy number.
- Velocity declines for various estimations of slip parameter β_1 .

- Wave phenomenon of velocity becomes obvious with enlargement of corrugation.
- Velocity is more prominent middle of the channel and lesser sides of walls in all cases.
- The profile of temperature at first decreases then increases with effect of jump temperature coefficient γ_1 .
- The profile of temperature increases with ϕ .
- The profile of temperature declines with non-dimensional parameter S and Prandtl number Pr .

Chapter 3

Significance of knudsen number and corrugation on EMHD flow under metallic nanoparticles impact

In this chapter, the impacts of surface wavy roughness on the viscous fluid flow inside microchannel through corrugated walls is examined. The Navier–Stokes equations are simplified by utilizing perturbation technique with incorporated microscopic slip conditions at the wavy wall. The present investigation depends on the assumptions that the corrugations are periodic sinusoidal waves of small amplitude. The considered examination involves the consequence of electromagnetohydrodynamic on the features of the nanofluid through the corrugated walls under the impact of nanoparticle by considering an appropriate mathematical model. The equations are understood through the strategy of perturbation. Examination is introduced by taking water and copper in the presence of convective conditions. Influence of related parameters are interpreted graphically.

3.1 Mathematical model

We inspected the EMHD flow with nanoparticle between two vertical corrugated walls of height $2H$. The microchannel height is taken $100\mu m$ and $0.1H$ is taken amplitude of corrugated wall. The wall surfaces are describe by

$$y_l^* = H + \varepsilon H \sin(\lambda^* x^*) \quad \text{and} \quad y_r^* = -H - \varepsilon H \sin(\lambda^* x^* + \beta^*), \quad (3.1)$$

where λ^* represents the wave length and ε is small amplitude. We can applied electric field \mathbf{E}^* and magnetic field \mathbf{B}^* in x^* and y^* direction respectively, $\mathbf{J} \times \mathbf{B}^*$ is Lorenz force which taken along the z^* direction and created by electric and magnetic field interaction, where current density is symbolize by \mathbf{J} .

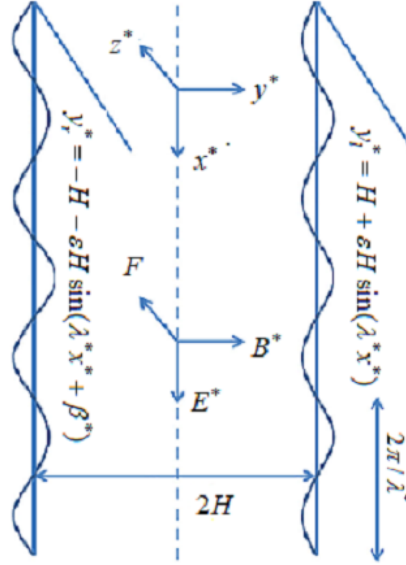


Fig. (3.1): Geometrical sketch of EMHD flow in microchannel.

The formulated problem composed as

$$\nabla^* \mathbf{u}^* = 0, \quad (3.2)$$

$$\rho_{nf} \frac{\partial \mathbf{u}^*}{\partial t^*} + \rho_{nf} (\mathbf{u}^* \cdot \nabla^*) \mathbf{u}^* = -\nabla^* p + \nabla^* \boldsymbol{\tau}^* + \mathbf{J} \times \mathbf{B}^* + g(\rho\zeta)_{nf} (T^* - T_r^*), \quad (3.3)$$

$$(\rho C_p)_{nf} \frac{DT^*}{Dt^*} = \nabla^* k''_{nf} \nabla^* T^* + Q_0(T^* - T_r^*), \quad (3.4)$$

where T^* shows the temperature, Q_0 is heat absorption constant, μ_{nf} , k''_{nf} , ρ_{nf} , ζ_{nf} , $(\rho C_p)_{nf}$ are defined the nanofluid viscosity, thermal conductivity, density, expansion coefficient and heat capacitance.

$$\begin{aligned} \mu_{nf} &= \frac{\mu_f}{(1-\Phi)^{2.5}}, \quad \alpha_{nf} = \frac{k''_{nf}}{(\rho C_p)_{nf}}, \quad \rho_{nf} = (1-\Phi)\rho_f + \Phi\rho_s, \\ (\rho\zeta)_{nf} &= (1-\Phi)(\rho\zeta)_f + \Phi(\rho\zeta)_s, \quad (\rho C_p)_{nf} = (1-\Phi)(\rho C_p)_f + \Phi(\rho C_p)_s, \\ \frac{k''_{nf}}{k''_f} &= \frac{(k''_s + 2k''_f) - 2\Phi(k''_f - k''_s)}{(k''_s + 2k''_f) + \Phi(k''_f - k''_s)}, \quad \frac{\sigma_{nf}}{\sigma_f} = 1 + \frac{(\frac{\sigma_s}{\sigma_f} - 1)\Phi}{(\frac{\sigma_s}{\sigma_f} + 1) - \Phi(\frac{\sigma_s}{\sigma_f} - 1)} \end{aligned} \quad (3.5)$$

Under the considered assumptions only the z^* factor of velocity will be retained. The equations are rearranged as

$$\rho_{nf} \frac{\partial w^*}{\partial t^*} = -\frac{\partial p}{\partial z^*} + \frac{\partial}{\partial x^*} \tau_{x^* z^*}^* + \frac{\partial}{\partial x^*} \tau_{y^* z^*}^* + \frac{\partial}{\partial z^*} \tau_{z^* z^*}^* + \sigma_{nf} B^* (E^* - B^* w^*) + g(\rho\zeta)_{nf} (T^* - T_r^*), \quad (3.6)$$

$$(\rho C_p)_{nf} \left(\frac{\partial T^*}{\partial t^*} \right) = k''_{nf} \left(\frac{\partial^2 T^*}{\partial x^{*2}} + \frac{\partial^2 T^*}{\partial y^{*2}} \right) + Q_0(T^* - T_r^*). \quad (3.7)$$

The simplification and incorporating the values of stresses in Eq. (3.6) yield

$$\rho_{nf} \frac{\partial w^*}{\partial t^*} = -\frac{\partial p}{\partial z^*} + \mu_{nf} \left(\frac{\partial^2 w^*}{\partial x^{*2}} + \frac{\partial^2 w^*}{\partial y^{*2}} \right) + \sigma_{nf} B^* (E^* - B^* w^*) + g(\rho\zeta)_{nf} (T^* - T_r^*). \quad (3.8)$$

The boundary conditions are written as:

$$\begin{aligned} w^*(x^*, y_l^*) &= K_n \frac{dw^*}{dn} \text{ at } y_l^* = H + \varepsilon H \sin(\lambda^* x^*) \\ w^*(x^*, y_r^*) &= K_n \frac{dw^*}{dn} \text{ at } y_r^* = -H - \varepsilon H \sin(\lambda^* x^* + \beta^*) \\ T^*(x^*, y_l^*) &= T_l^*(x^*, y^*) \text{ at } y_l^* = H + \varepsilon H \sin(\lambda^* x^*) \\ k''_{nf} \frac{\partial T^*}{\partial y^*} &= -B(T^* - T_r^*) \text{ at } y_r^* = -H - \varepsilon H \sin(\lambda^* x^* + \beta^*) \end{aligned} \quad (3.9)$$

We assumed that fluid is incompressible and only taken in z^* direction. In z^* direction we

assume that channel is open so pressure gradient is ignored [85] and the velocity satisfies

$$\rho_{nf} \frac{\partial w^*}{\partial t^*} = \mu_{nf} \left(\frac{\partial^2 w^*}{\partial x^{*2}} + \frac{\partial^2 w^*}{\partial y^{*2}} \right) + \sigma_{nf} B^* (E^* - B^* w^*) + g(\rho\zeta)_{nf} (T^* - T_r^*). \quad (3.10)$$

Velocity, electric field and temperature in EMHD flow are express in periodical forms as

$$w^* = R\{\tilde{w}(x^*, y^*)e^{i\omega t^*}\}, \quad E^* = R\{E_0 e^{i\omega t^*}\}, \quad T^* = R\{T(x^*, y^*)e^{i\omega t^*}\}. \quad (3.11)$$

Utilizing Eq. (3.11) into Eqs. (3.7) and (3.10), we get

$$i\rho_{nf}\omega\tilde{w} = \mu_{nf} \left(\frac{\partial^2 \tilde{w}}{\partial x^{*2}} + \frac{\partial^2 \tilde{w}}{\partial y^{*2}} \right) + \sigma_{nf} B^* E_0 - \sigma_{nf} B^{*2} \tilde{w} + g(\rho\zeta)_{nf} (T - T_r), \quad (3.12)$$

$$T\omega i = \alpha_{nf} \left(\frac{\partial^2 T}{\partial x^{*2}} + \frac{\partial^2 T}{\partial y^{*2}} \right) + \frac{Q_0}{(\rho C_p)_{nf}} (T - T_r). \quad (3.13)$$

The dimensionless form of momentum and temperature equations are

$$\frac{\partial^2 w}{\partial x^2} + \frac{\partial^2 w}{\partial y^2} - \frac{\mu_f}{\mu_{nf}} \left(\frac{\sigma_{nf}}{\sigma_f} Ha^2 + \frac{\rho_{nf}}{\rho_f} \text{Re } i \right) w + \frac{\mu_f}{\mu_{nf}} \frac{\sigma_{nf}}{\sigma_f} Ha\beta + \frac{\mu_f}{\mu_{nf}} \frac{(\rho\zeta)_{nf}}{(\rho\zeta)_f} Gr\theta = 0, \quad (3.14)$$

$$\frac{\partial^2 \theta}{\partial x^2} + \frac{\partial^2 \theta}{\partial y^2} + \frac{k''_f}{k''_{nf}} \phi\theta - \text{Pr } i \frac{\alpha_f}{\alpha_{nf}} (S + \theta) = 0. \quad (3.15)$$

The non-dimensional quantities are expressed as

$$\begin{aligned} (x, y) &= \left(\frac{x^*, y^*}{H} \right), \quad \lambda = \lambda^* H, \quad w = \frac{\tilde{w}}{H\omega}, \quad Ha = B^* H \left(\frac{\sigma_f}{\mu_f} \right)^{\frac{1}{2}}, \\ \text{Re} &= \frac{\rho_f \omega H^2}{\mu_f}, \quad \beta = E_0 \left(\frac{\sigma_f}{\mu_f} \right)^{\frac{1}{2}} / \omega, \quad \text{Pr} = \frac{\omega H^2}{\alpha_f}, \quad Bi = \frac{BH}{k''_f}, \\ Gr &= \frac{g(\rho\zeta)_f H(T_l - T_r)}{\mu_f \omega}, \quad \theta = \frac{T - T_r}{T_l - T_r}, \quad S = \frac{T_r}{T_l - T_r}, \quad \phi = \frac{Q_0 H^2}{k''_f}. \end{aligned} \quad (3.16)$$

On the boundary, we expand $w(x, y)$ in the following form as suggested by [10]

$$w(x, y) = w(x, y) + \varepsilon dy w_y(x, y) + \varepsilon^2 \left(\frac{dy^2}{2} w_{yy}(x, y) \right) \dots = K_n \frac{dw}{dn}. \quad (3.17)$$

Thus, on the upper wall and lower walls $\frac{dw}{dn}$ is defined as

$$\frac{dw}{dn} = \nabla w \frac{\nabla(y_l - 1 - \varepsilon \sin(\lambda x))}{|\nabla(y_l - 1 - \varepsilon \sin(\lambda x))|} \quad (3.18)$$

$$= (1 + \varepsilon^2 \lambda^2 \cos^2(\lambda x))^{-\frac{1}{2}} (w_y - \varepsilon \lambda \cos(\lambda x) w_x) \quad (3.19)$$

at $y_l = 1 + \varepsilon \sin(\lambda x)$,

$$\frac{dw}{dn} = \nabla w \frac{\nabla(y_r + 1 + \varepsilon \sin(\lambda x + \beta^*))}{|\nabla(y_r + 1 + \varepsilon \sin(\lambda x + \beta^*))|} \quad (3.20)$$

$$= (1 + \varepsilon^2 \lambda^2 \cos^2(\lambda x + \beta^*))^{-\frac{1}{2}} (w_y - \varepsilon \lambda \cos(\lambda x + \beta^*) w_x) \quad (3.21)$$

at $y_r = -1 - \varepsilon \sin(\lambda x + \beta^*)$,

and boundary conditions on temperature are

$$\theta = 1 \text{ at } y_l = 1 + \varepsilon \sin(\lambda x), \quad (3.22)$$

$$\frac{\partial \theta}{\partial y} + \frac{B_i}{\left(\frac{k''_{nf}}{k''_f}\right)} \theta = 0 \text{ at } y_r = -1 - \varepsilon \sin(\lambda x + \beta^*). \quad (3.23)$$

3.2 Solution of technique

Utilizing regular perturbation technique in above equations, we may define

$$w(x, y) = w_0(y) + \varepsilon w_1(x, y) + \varepsilon^2 w_2(x, y) + \dots \quad (3.24)$$

$$\theta(x, y) = \theta_0(y) + \varepsilon \theta_1(x, y) + \varepsilon^2 \theta_2(x, y) + \dots \quad (3.25)$$

Incorporating Eqs. (3.24) and (3.25) into equations (3.14), (3.15) and boundary condition (3.17), collecting the same powers of ε , we reach at

3.2.1 Zeroth order classification

$$\frac{d^2 \theta_0}{dy^2} + \frac{k''_f}{k''_{nf}} \phi \theta_0 - \text{Pr} i \frac{\alpha_f}{\alpha_{nf}} (S + \theta_0) = 0, \quad (3.26)$$

$$\frac{d^2 w_0}{dy^2} - \frac{\mu_f}{\mu_{nf}} \left(\frac{\sigma_{nf}}{\sigma_f} Ha^2 + \frac{\rho_{nf}}{\rho_f} \text{Re } i \right) w_0 + \frac{\mu_f}{\mu_{nf}} \frac{\sigma_{nf}}{\sigma_f} Ha\beta + \frac{\mu_f}{\mu_{nf}} \frac{(\rho\zeta)_{nf}}{(\rho\zeta)_f} Gr\theta_0 = 0, \quad (3.27)$$

$$\theta_0 = 1 \text{ at } y = 1, \quad \frac{d\theta_0}{dy} + \frac{B_i}{\left(\frac{k''_{nf}}{k''_f}\right)} \theta_0 = 0 \text{ at } y = -1, \quad (3.28)$$

$$w_0 - K_n \frac{dw_0}{dy} = 0 \text{ at } y = 1, \quad w_0 - K_n \frac{dw_0}{dy} = 0 \text{ at } y = -1. \quad (3.29)$$

3.2.2 First order classification

$$\frac{\partial^2 \theta_1}{\partial x^2} + \frac{\partial^2 \theta_1}{\partial y^2} + \frac{k''_f}{k''_{nf}} \phi \theta_1 - \text{Pr } i \frac{\alpha_f}{\alpha_{nf}} \theta_1 = 0, \quad (3.30)$$

$$\frac{\partial^2 w_1}{\partial x^2} + \frac{\partial^2 w_1}{\partial y^2} - \frac{\mu_f}{\mu_{nf}} \left(\frac{\sigma_{nf}}{\sigma_f} Ha^2 + \frac{\rho_{nf}}{\rho_f} \text{Re } i \right) w_1 + \frac{\mu_f}{\mu_{nf}} \frac{\sigma_{nf}}{\sigma_f} Ha\beta + \frac{\mu_f}{\mu_{nf}} \frac{(\rho\zeta)_{nf}}{(\rho\zeta)_f} Gr\theta_1 = 0, \quad (3.31)$$

$$\begin{aligned} \theta_1 + \sin(\lambda x) \left(\frac{d\theta_0}{dy} \right) &= 0 \text{ at } y = 1 \\ \frac{\partial \theta_1}{\partial y} + \sin(\lambda x + \beta^*) \frac{d^2 \theta_0}{dy^2} + \frac{B_i}{\left(\frac{k''_{nf}}{k''_f}\right)} (\theta_1 + \sin(\lambda x + \beta^*) \theta_0) &= 0 \text{ at } y = -1, \end{aligned} \quad (3.32)$$

$$\begin{aligned} w_1 + 2 \sin(\lambda x) \frac{dw_0}{dy} - K_n (2 \sin(\lambda x) \frac{d^2 w_0}{dy^2} + \frac{\partial w_1}{\partial y} - \lambda \cos(\lambda x) \frac{dw_{0x}}{dy}) &= 0 \text{ at } y = 1 \\ w_1 + 2 \sin(\lambda x + \beta^*) \frac{dw_0}{dy} - K_n (2 \sin(\lambda x + \beta^*) \frac{d^2 w_0}{dy^2} + \frac{\partial w_1}{\partial y} - \lambda \cos(\lambda x + \beta^*) \frac{dw_{0x}}{dy}) &= 0 \text{ at } y = -1. \end{aligned} \quad (3.33)$$

3.2.3 Second order classification

$$\frac{\partial^2 \theta_2}{\partial x^2} + \frac{\partial^2 \theta_2}{\partial y^2} + \frac{k''_f}{k''_{nf}} \phi \theta_2 - \text{Pr } i \frac{\alpha_f}{\alpha_{nf}} \theta_2 = 0, \quad (3.34)$$

$$\frac{\partial^2 w_2}{\partial x^2} + \frac{\partial^2 w_2}{\partial y^2} - \frac{\mu_f}{\mu_{nf}} \left(\frac{\sigma_{nf}}{\sigma_f} Ha^2 + \frac{\rho_{nf}}{\rho_f} \text{Re } i \right) w_2 + \frac{\mu_f}{\mu_{nf}} Gr \frac{(\rho\zeta)_{nf}}{(\rho\zeta)_f} \theta_2 = 0, \quad (3.35)$$

$$\begin{aligned}
& \theta_2 + \sin(\lambda x) \frac{\partial \theta_1}{\partial y} + \frac{1}{4}(1 - \cos(2\lambda x)) \frac{d^2 \theta_0}{dy^2} = 0 \text{ at } y = 1 \\
& \frac{\partial^2 \theta_2}{\partial y^2} + \sin(\lambda x + \beta^*) \frac{\partial^2 \theta_1}{\partial y^2} + \frac{1}{4}(1 - \cos(2\lambda x + 2\beta^*)) \frac{d^3 \theta_0}{dy^3} + \frac{B_i}{(k''_{nf})} \\
& (\theta_2 + \sin(\lambda x + \beta^*) \theta_1 + \frac{1}{4}(1 - \cos(2\lambda x + 2\beta^*)) \theta_0) = 0 \text{ at } y = -1,
\end{aligned} \tag{3.36}$$

$$\begin{aligned}
& w_2 + 2 \sin(\lambda x) \frac{\partial w_1}{\partial y} + (1 - \cos(2\lambda x)) \frac{d^2 w_0}{dy^2} - K_n \left(\frac{\partial w_2}{\partial y} + 2 \sin(\lambda x) \frac{\partial^2 w_1}{\partial y^2} + (1 - \cos(2\lambda x)) \frac{d^3 w_0}{dy^3} - \right. \\
& \left. 2\lambda \cos(\lambda x) \sin(\lambda x) \frac{\partial^2 w_0}{\partial x \partial y} - \lambda \cos(\lambda x) \frac{\partial w_1}{\partial x} - \frac{1}{4} \lambda^2 (1 + \cos(2\lambda x)) \frac{dw_0}{dy} \right) = 0 \text{ at } y = 1 \\
& w_2 + 2 \sin(\lambda x + \beta^*) \frac{\partial w_1}{\partial y} + (1 - \cos(2\lambda x + 2\beta^*)) \frac{d^2 w_0}{dy^2} - K_n \left(\frac{\partial w_2}{\partial y} + 2 \sin(\lambda x + \beta^*) \frac{\partial^2 w_1}{\partial y^2} + \right. \\
& \left. (1 - \cos(2\lambda x + 2\beta^*)) \frac{d^3 w_0}{dy^3} - 2\lambda \cos(\lambda x + \beta^*) \sin(\lambda x + \beta^*) \frac{\partial^2 w_0}{\partial x \partial y} - \lambda \cos(\lambda x + \beta^*) \frac{\partial w_1}{\partial x} - \right. \\
& \left. \frac{1}{4} \lambda^2 (1 + \cos(2\lambda x + 2\beta^*)) \frac{dw_0}{dy} \right) = 0 \text{ at } y = 1.
\end{aligned} \tag{3.37}$$

The solution of first order system can be computed by using the following expressions

$$\theta_1(x, y) = \sin(\lambda x) f(y) + \cos(\lambda x) g(y), \tag{3.38}$$

$$w_1(x, y) = \sin(\lambda x) h(y) + \cos(\lambda x) k(y). \tag{3.39}$$

Using Eqs. (3.38) and (3.39) into Eqs. (3.30) and (3.31) and boundary conditions Eqs. (3.32) and (3.33), we get

$$\frac{d^2 f(y)}{dy^2} - \left[\lambda^2 - \frac{k''_{nf}}{k''_{nf}} \phi + \text{Pr} i \frac{\alpha_f}{\alpha_{nf}} \right] f(y), \tag{3.40}$$

$$\frac{d^2 g(y)}{dy^2} - \left[\lambda^2 - \frac{k''_{nf}}{k''_{nf}} \phi + \text{Pr} i \frac{\alpha_f}{\alpha_{nf}} \right] g(y), \tag{3.41}$$

$$\left(\frac{d^2 h(y)}{dy^2} - \lambda^2 h(y) \right) - \frac{\mu_f}{\mu_{nf}} \left(\left(\frac{\sigma_{nf}}{\sigma_f} Ha^2 + \frac{\rho_{nf}}{\rho_f} \text{Re} i \right) h(y) - Gr \frac{(\rho \zeta)_{nf}}{(\rho \zeta)_f} f(y) \right) = 0, \tag{3.42}$$

$$\left(\frac{d^2 k(y)}{dy^2} - \lambda^2 k(y) \right) - \frac{\mu_f}{\mu_{nf}} \left(\left(\frac{\sigma_{nf}}{\sigma_f} Ha^2 + \frac{\rho_{nf}}{\rho_f} \text{Re} i \right) k(y) - Gr \frac{(\rho \zeta)_{nf}}{(\rho \zeta)_f} g(y) \right) = 0, \tag{3.43}$$

$$f(y) + \frac{d\theta_0}{dy} = 0 \text{ at } y = 1, \frac{df}{dy} + \cos \beta^* \frac{d^2 \theta_0}{dy^2} + \frac{B_i}{(k''_{nf})} (f(y) + \theta_0 \cos \beta^*) \text{ at } y = -1, \tag{3.44}$$

$$g(y) = 0 \text{ at } y = 1, \quad \frac{dg}{dy} + \sin \beta^* \frac{d^2 \theta_0}{dy^2} + \frac{B_i}{\left(\frac{k''_{nf}}{k''_f}\right)} (g(y) + \theta_0 \sin \beta^*) \text{ at } y = -1. \quad (3.45)$$

The solution of second order scheme can be evaluated by means of expressions of the form

$$\theta_2(x, y) = l(y) + \sin(2\lambda x)m(y) + \cos(2\lambda x)n(y), \quad (3.46)$$

$$w_2(x, y) = p(y) + \sin(2\lambda x)q(y) + \cos(2\lambda x)r(y). \quad (3.47)$$

Invoking Eqs. (3.46) and (3.47) into Eqs. (3.34) and (3.35) and boundary conditions Eqs. (3.36) and (3.37), we get the resulting differential equations are

$$\frac{d^2 l(y)}{dy^2} + \left(\frac{k''_f}{k''_{nf}} \phi - \frac{\alpha_f}{\alpha_{nf}} \text{Pr } i \right) l(y) = 0, \quad (3.48)$$

$$\frac{d^2 m(y)}{dy^2} - \left(4\lambda^2 - \frac{k''_f}{k''_{nf}} \phi + \frac{\alpha_f}{\alpha_{nf}} \text{Pr } i \right) m(y) = 0, \quad (3.49)$$

$$\frac{d^2 n(y)}{dy^2} - \left(4\lambda^2 - \frac{k''_f}{k''_{nf}} \phi + \frac{\alpha_f}{\alpha_{nf}} \text{Pr } i \right) n(y) = 0, \quad (3.50)$$

$$\frac{d^2 p(y)}{dy^2} - \frac{\mu_f}{\mu_{nf}} \left(\left(\frac{\sigma_{nf}}{\sigma_f} Ha^2 + \frac{\rho_{nf}}{\rho_f} \text{Re } i \right) p(y) - Gr \frac{(\rho\zeta)_{nf}}{(\rho\zeta)_f} l(y) \right) = 0, \quad (3.51)$$

$$\left(\frac{d^2 q(y)}{dy^2} - 4\lambda^2 q(y) \right) - \frac{\mu_f}{\mu_{nf}} \left(\left(\frac{\sigma_{nf}}{\sigma_f} Ha^2 + \frac{\rho_{nf}}{\rho_f} \text{Re } i \right) q(y) - Gr \frac{(\rho\zeta)_{nf}}{(\rho\zeta)_f} m(y) \right) = 0, \quad (3.52)$$

$$\left(\frac{d^2 r(y)}{dy^2} - 4\lambda^2 r(y) \right) - \frac{\mu_f}{\mu_{nf}} \left(\left(\frac{\sigma_{nf}}{\sigma_f} Ha^2 + \frac{\rho_{nf}}{\rho_f} \text{Re } i \right) r(y) - Gr \frac{(\rho\zeta)_{nf}}{(\rho\zeta)_f} n(y) \right) = 0, \quad (3.53)$$

$$l(y) + \frac{1}{2} \left(\frac{df}{dy} + \frac{1}{2} \frac{d^2 \theta_0}{dy^2} \right) = 0 \text{ at } y = 1,$$

$$\begin{aligned} & \frac{d^2 l}{dy^2} + \frac{\cos \beta^*}{2} \frac{d^2 f}{dy^2} + \frac{\sin \beta^*}{2} \frac{d^2 g}{dy^2} + \frac{1}{4} \frac{d^3 \theta_0}{dy^3} + \frac{B_i}{\left(\frac{k''_{nf}}{k''_f}\right)} (l(y) \\ & + \frac{\cos \beta^*}{2} f(y) + \frac{\sin \beta^*}{2} g(y) + \frac{1}{4} \theta_0) \text{ at } y = -1, \end{aligned} \quad (3.54)$$

$$\begin{aligned}
m(y) + \frac{1}{2} \frac{dg}{dy} &= 0 \text{ at } y = 1, \\
\frac{d^2m}{dy^2} + \frac{\cos \beta^*}{2} \frac{d^2g}{dy^2} + \frac{\sin \beta^*}{2} \frac{d^2f}{dy^2} + \frac{\sin 2\beta^*}{4} \frac{d^3\theta_0}{dy^3} + \frac{B_i}{\left(\frac{k^n}{k^n f}\right)} (m(y) \\
&+ \frac{\cos \beta^*}{2} g(y) + \frac{\sin \beta^*}{2} f(y) + \frac{\sin 2\beta^*}{4} \theta_0) \text{ at } y = -1,
\end{aligned} \tag{3.55}$$

$$\begin{aligned}
n(y) - \frac{1}{2} \left(\frac{df}{dy} + \frac{1}{2} \frac{d^2\theta_0}{dy^2} \right) &= 0 \text{ at } y = 1, \\
\frac{d^2n}{dy^2} - \frac{\cos \beta^*}{2} \frac{d^2f}{dy^2} + \frac{\sin \beta^*}{2} \frac{d^2g}{dy^2} - \frac{\cos 2\beta^*}{4} \frac{d^3\theta_0}{dy^3} + \frac{B_i}{\left(\frac{k^n}{k^n f}\right)} (n(y) \\
&- \frac{\cos \beta^*}{2} f(y) + \frac{\sin \beta^*}{2} g(y) - \frac{\cos 2\beta^*}{4} \theta_0) \text{ at } y = -1,
\end{aligned} \tag{3.56}$$

$$\begin{aligned}
p(y) + \frac{d^2w_0}{dy^2} - \frac{dh}{dy} - K_n \left(\frac{d^3w_0}{dy^3} - \frac{d^2h}{dy^2} + \frac{dp}{dy} - \frac{\lambda^2}{2} (h(y) + \frac{1}{2} \frac{dw_0}{dy}) \right) &= 0 \text{ at } y = 1, \\
p(y) + \frac{d^2w_0}{dy^2} + \cos \beta^* \frac{dh}{dy} + \sin \beta^* \frac{dk}{dy} - K_n \left(\frac{d^3w_0}{dy^3} + \cos \beta^* \frac{d^2h}{dy^2} + \sin \beta^* \frac{d^2k}{dy^2} + \frac{dp}{dy} \right. \\
&\left. - \frac{\lambda^2}{2} \left(\frac{dw_0}{dy} + \cos \beta^* h(y) + \sin \beta^* k(y) \right) \right) = 0 \text{ at } y = -1,
\end{aligned} \tag{3.57}$$

$$\begin{aligned}
q(y) + \frac{dk}{dy} - K_n \left(\frac{d^2k}{dy^2} + \frac{dq}{dy} + \frac{\lambda^2}{2} k(y) \right) &= 0 \text{ at } y = 1, \\
q(y) + \sin 2\beta^* \frac{d^2w_0}{dy^2} + \cos \beta^* \frac{dk}{dy} + \sin \beta^* \frac{dh}{dy} - K_n \left(\sin 2\beta^* \frac{d^3w_0}{dy^3} + \cos \beta^* \frac{d^2k}{dy^2} \right. \\
&\left. + \sin \beta^* \frac{d^2h}{dy^2} + \frac{dq}{dy} + \frac{\lambda^2}{2} \left(\sin 2\beta^* \frac{dw_0}{dy} + \cos \beta^* k(y) + \sin \beta^* h(y) \right) \right) = 0 \text{ at } y = -1,
\end{aligned} \tag{3.58}$$

$$\begin{aligned}
r(y) - \frac{d^2 w_0}{dy^2} - \frac{dh}{dy} - K_n \left(-\frac{d^3 w_0}{dy^3} - \frac{d^2 h}{dy^2} + \frac{dr}{dy} - \frac{\lambda^2}{2} \left(h(y) + \frac{1}{2} \frac{dw_0}{dy} \right) \right) &= 0 \text{ at } y = 1, \\
r(y) - \cos 2\beta^* \frac{d^2 w_0}{dy^2} - \cos \beta^* \frac{dh}{dy} + \sin \beta^* \frac{dk}{dy} - K_n \left(-\cos 2\beta^* \frac{d^3 w_0}{dy^3} - \cos \beta^* \frac{d^2 h}{dy^2} \right. \\
\left. + \sin \beta^* \frac{d^2 k}{dy^2} + \frac{dr}{dy} - \frac{\lambda^2}{2} \left(\cos 2\beta^* \frac{dw_0}{dy} + \cos \beta^* h(y) - \sin \beta^* k(y) \right) \right) &= 0 \text{ at } y = -1. \quad (3.59)
\end{aligned}$$

The approximate temperature solution can be obtained as

$$\theta(x, y) = \theta_0(y) + \varepsilon \theta_1(x, y) + \varepsilon^2 \theta_2(x, y) + \dots \quad (3.60)$$

The approximate velocity solution can be demonstrated as

$$w(x, y) = w_0(y) + \varepsilon w_1(x, y) + \varepsilon^2 w_2(x, y) + \dots \quad (3.61)$$

3.3 Heat transfer rate

The Nusselt number determines the convective heat exchange strength, and is defined as follows [86]

$$Nu = \frac{H q_w}{k''_f (T_l^* - T_r^*)}, \quad (3.62)$$

On left and right walls we defined

$$q_w = -k''_{nf} \frac{\partial T^*}{\partial y^*} \Big|_{y^*=y_l^*}, \quad q_w = -k''_{nf} \frac{\partial T^*}{\partial y^*} \Big|_{y^*=y_r^*}, \quad (3.63)$$

From Eqs. (3.62) and (3.63), the Nusselt number can be expressed as

$$Nu = -\frac{k''_{nf}}{k''_f} \frac{\partial \theta}{\partial y} \Big|_{y=y_l}, \quad Nu = -\frac{k''_{nf}}{k''_f} \frac{\partial \theta}{\partial y} \Big|_{y=y_r}. \quad (3.64)$$

3.4 Volume Flow rate

We can define volume flow rate as

$$q(x) = \int_{-1-\varepsilon \sin(\lambda x)}^{1+\varepsilon \sin(\lambda x)} w(x, y) dy. \quad (3.65)$$

Substituting (3.61) into (3.65) and expanded by using the Taylor series the integrals results in x and neglecting third order term, finally volume flow rate written as:

$$q(x) = \int_{-1}^1 w_0(y) dy + \varepsilon \int_{-1}^1 w_1(x, y) dy + \varepsilon^2 \left(\int_{-1}^1 w_2(x, y) dy + \sin(\lambda x) [w_1(x, y) |_{y=1} + w_1(x, y) |_{y=-1}] + \frac{1}{2} \sin^2(\lambda x) \left(\frac{dw_0(y)}{dy} \Big|_{y=1} - \frac{dw_0(y)}{dy} \Big|_{y=-1} \right) \right). \quad (3.66)$$

3.4.1 Mean velocity

On average over the one wavelength $(0, 2\pi/\lambda)$ of the corrugations, thus we defined mean velocity as:

$$w_m = \frac{\lambda}{4\pi} \int_{-1-\varepsilon \sin(\lambda x)}^{1+\varepsilon \sin(\lambda x)} \int_0^{\frac{2\pi}{\lambda}} w(x, y) dx dy. \quad (3.67)$$

Inserting (3.65) into (3.67) and using (3.66), the mean velocity is:

$$w_m = \frac{\lambda}{4\pi} \int_0^{\frac{2\pi}{\lambda}} q(x) dx = w_{0m} [1 + \varepsilon^2 \varphi + O(\varepsilon^4)], \quad (3.68)$$

where

$$\begin{aligned} \varphi = & \frac{1}{8} (3b_1(B_1 - B_2) \cosh(b_1) + 4(D_1 + D_2) \cosh(b_2) + (5b_1(B_1 + B_2) + 8_1(F_1 \\ & + F_2) \sinh(b_1)) / b_1 + (((4(C_1 + C_2) \cosh(a_2) s_2 \mu_f \rho_f) + ((3a_1(A_1 - A_2) \cosh(a_1) \\ & \mu_f (a_2^2 - \lambda^2) s_4 - s_1 \mu_f \rho_f) + (1/a_1) ((5a_1^2(A_1 + A_2) + 8(E_1 + E_2)) \sinh(a_1) 2\mu_f \\ & (a_2^2 - \lambda^2) s_4 - s_1 \mu_f \rho_f)) / (a_1^2 s_4 - \mu_f s_1)) / (((-a_2^2 - \lambda^2) s_4 + s_1 \mu_f \rho_f) (\rho \zeta)_f) \end{aligned} \quad (3.69)$$

The w_{0m} represents the mean velocity for perfectly smooth walls and φ denotes the leading-order perturbations to the mean velocity due to the corrugations.

3.5 Thermophysical properties

The thermophysical properties are

Physical Properties	Water	Copper
C_p (J/kgK)	4179	385
ρ (kg/m ³)	997.1	89333
k "(W/mK)	0.613	400
$\zeta \times 10^5$ (1/K)	21.0	1.67
σ (S/m)	5.0×10^{-2}	$5,96 \times 10^7$
μ (kg/m.sec)	8.90×10^{-4}	-

Table (3.1): Thermo physical effects.

3.6 Graphical consequence

In the previous portion, velocity, temperature and Nusselt number have been determined and results are demonstrated graphically to explore the flow parallel to the wall corrugations. To analyze the impacts of corrugations on the electromagnetically driven flow, the accompanying typical parametric values are utilized. For microfluidic examination, half height of channel is $H_1 \sim 100\mu m$, the conditions of domain set with physical properties of the water density $\rho \sim 10^3 kgm^{-3}$, the electrical conductivity $\sigma \sim 2.2 \times 10^{-4} - 10^6 Sm^{-1}$ and the viscosity $\mu \sim 10^{-3} kgm^{-1}s^{-1}$. If range of magnetic field is the $O(B^*) \sim 0.018 - 0.44$, the valued of order of Hartmann number $O(Ha)$ using $Ha = B^*H(\sigma/\mu)^{1/2}$ is from 0.0001 to 3. The frequency of electric field $O(\omega)$ changes from the 50 to $500s^{-1}$ and range of the frequency is $0 - 1 \times 10^4 s^{-1}$. The Reynolds number order $O(Re)$ changes from the 0.5 to 5 and the dimensionless parameter is fixed value i.e. $\beta = 5$.

3.6.1 Effect of wall roughness on 3D velocity and contour distributions

The three-dimensional velocity and contour distributions for various K_n and B_i when $\beta^* = 0$, $\beta^* = \frac{\pi}{2}$ and $\beta^* = \pi$ are shown in figures 3.2 – 3.7. In microchannel, the wall roughness can cause changes in the velocity distribution. In Figs. (3.2) and (3.5), the phase difference between

two walls is 0° . In Figs. (3.3) and (3.6), the phase difference is 90° and in Figs. (3.4) and (3.7), the phase difference between two walls is 180° . We find that the velocity distribution depends on the shape of channel from Figs. (3.2) to (3.7).

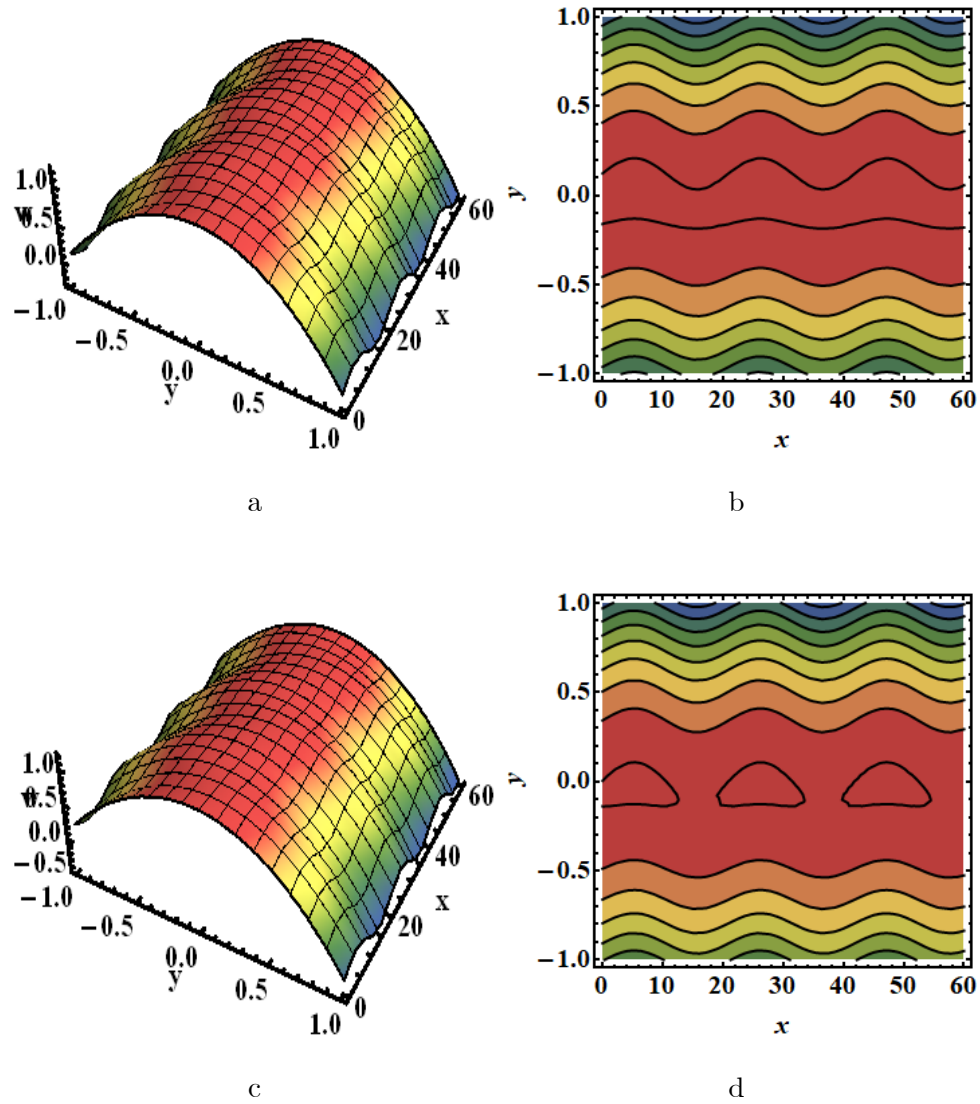


Fig. (3.2): 3D Velocity distribution and contour (a, b, c, d) when $K_n = 0.05$ and $K_n = 0.1$ in phase (i.e. $\beta^* = 0$).

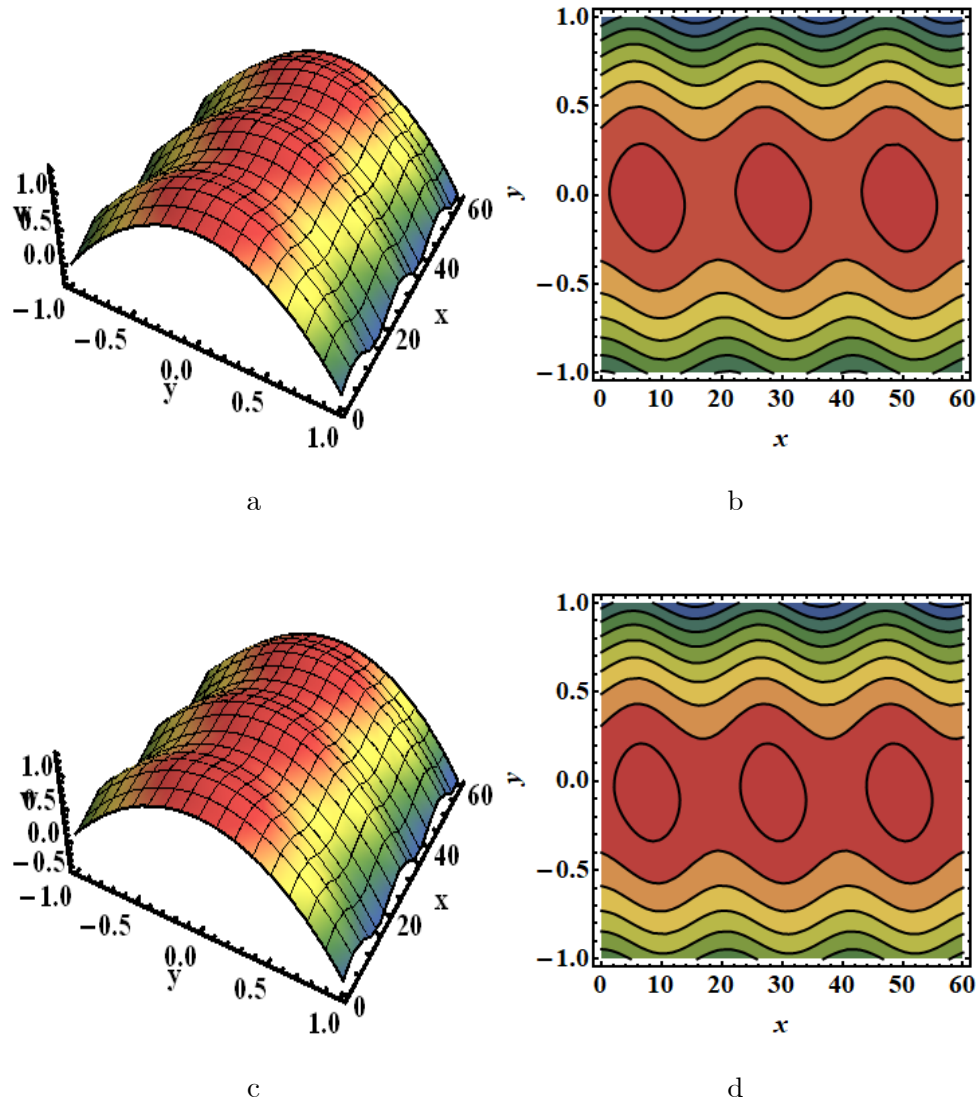


Fig. (3.3): 3D Velocity distribution and contour (a, b, c, d) when $K_n = 0.05$ and $K_n = 0.1$ when $\beta^* = \frac{\pi}{2}$.

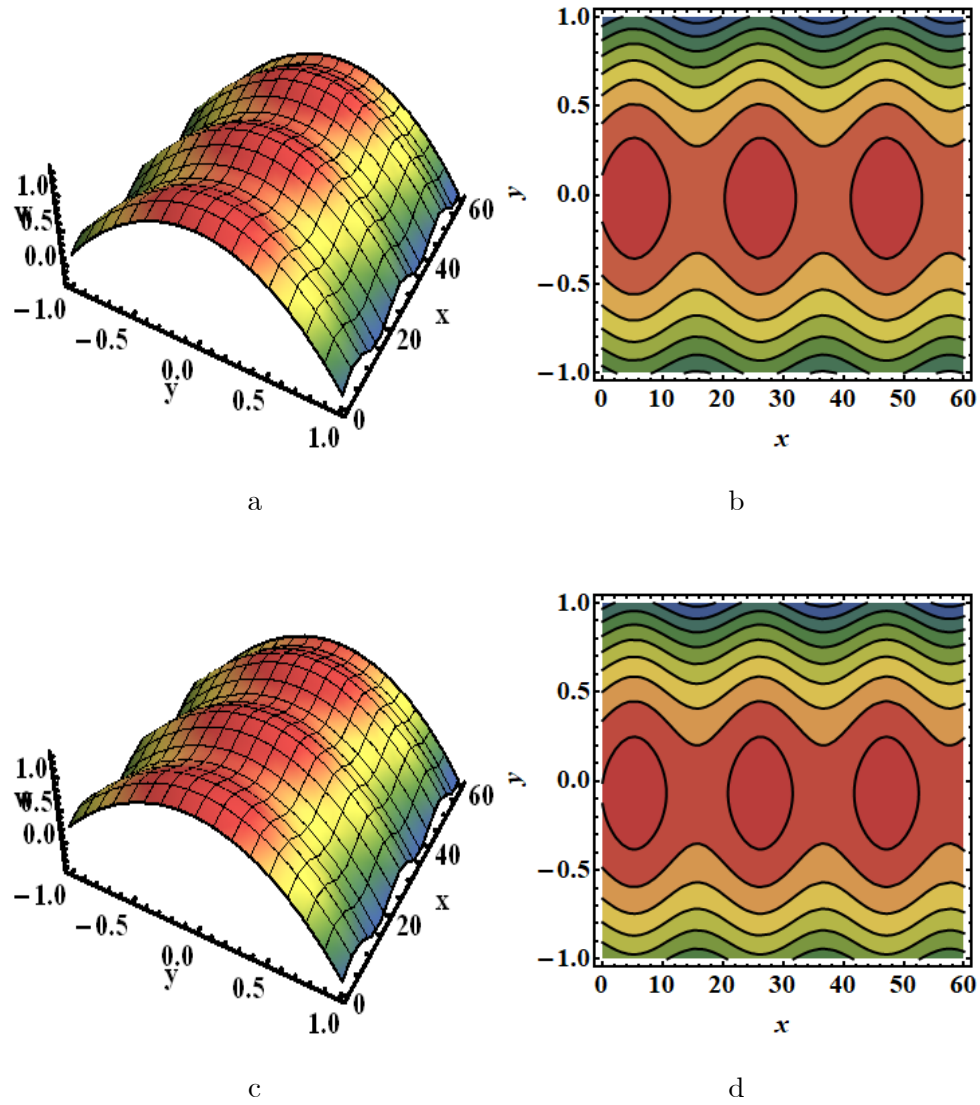


Fig. (3.4): 3D Velocity distribution and contour (a, b, c, d) when $K_n = 0.05$ and $K_n = 0.1$ out of phase (i.e. $\beta^* = \pi$).

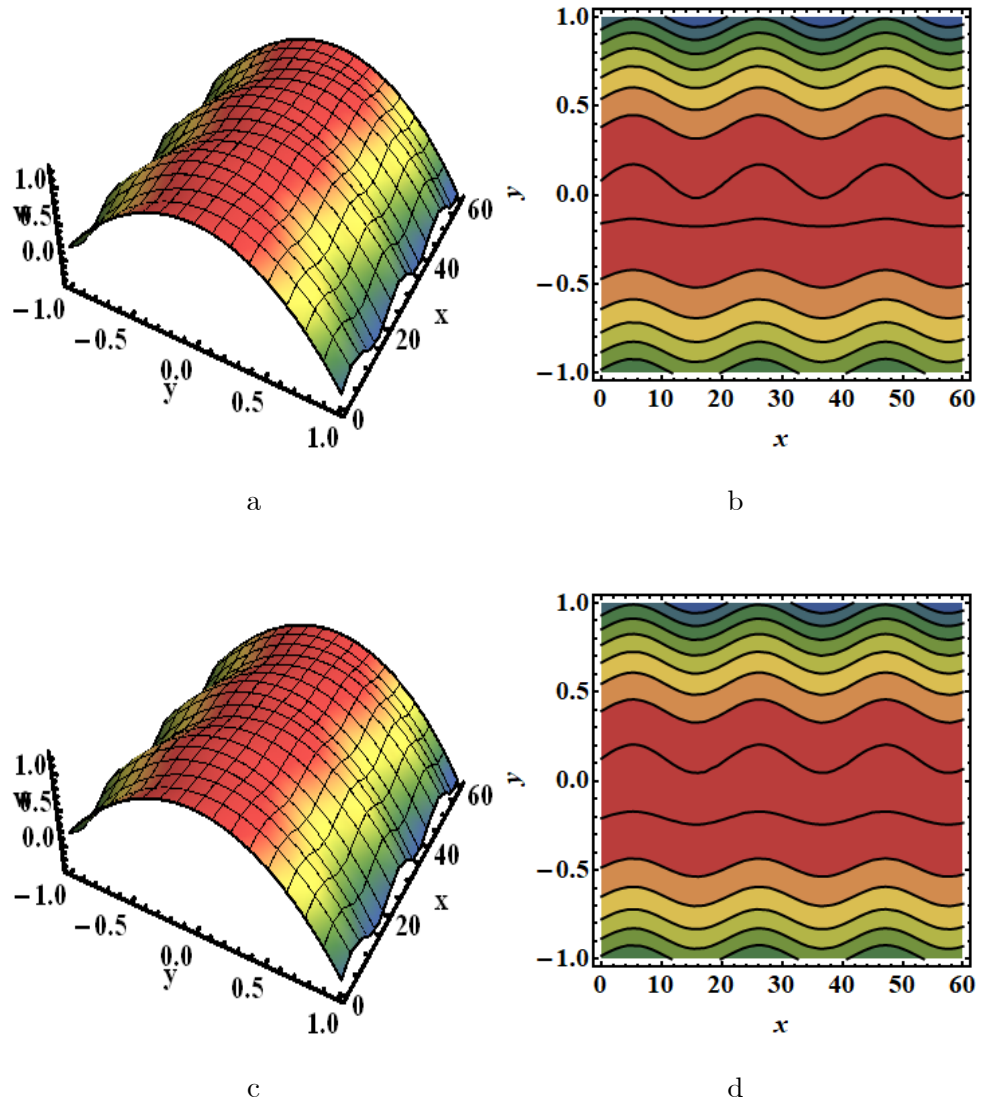


Fig. (3.5): 3D Velocity distribution and contour (a, b, c, d) when $B_i = 4.0$ and $B_i = 8.0$ in phase (i.e. $\beta^* = 0$).

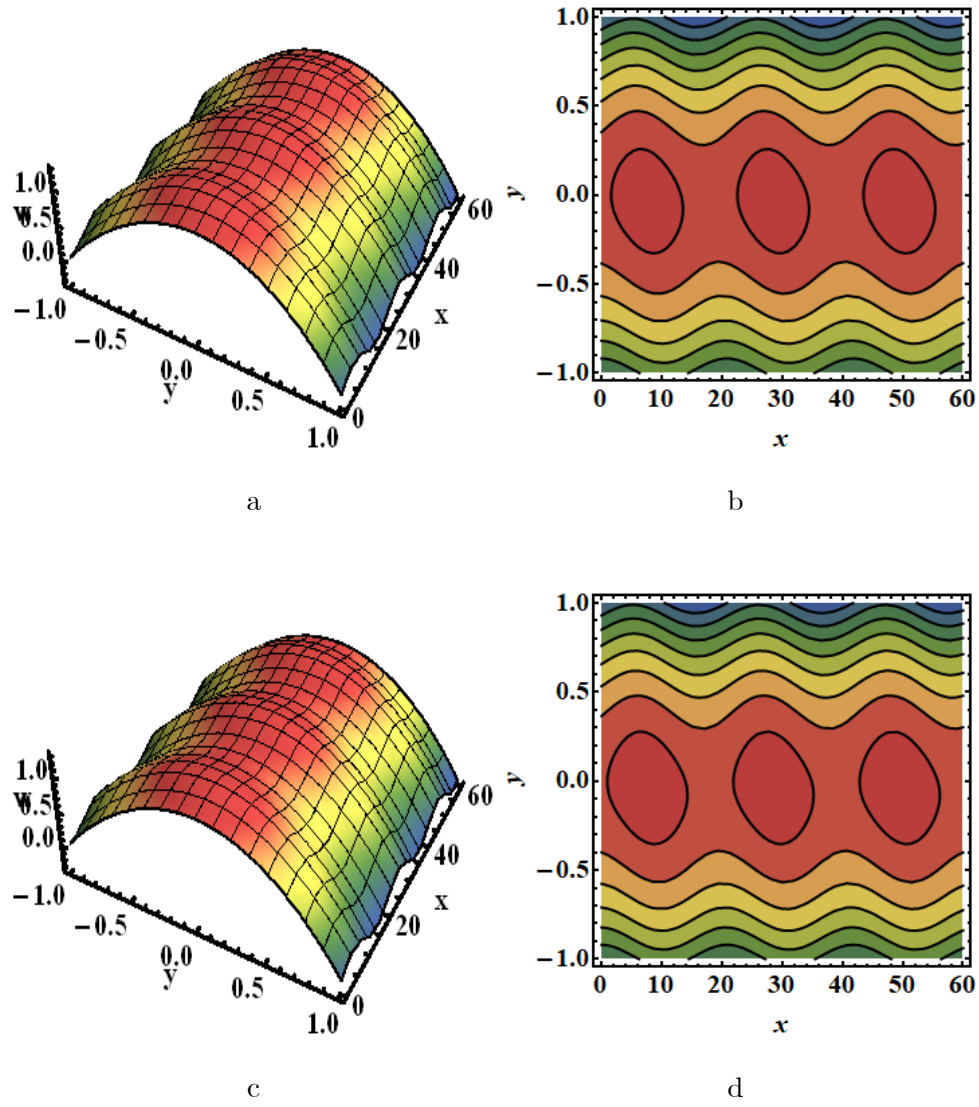


Fig. (3.6): 3D Velocity distribution and contour (a, b, c, d) when $B_i = 4.0$ and $B_i = 8.0$ when $\beta^* = \frac{\pi}{2}$.

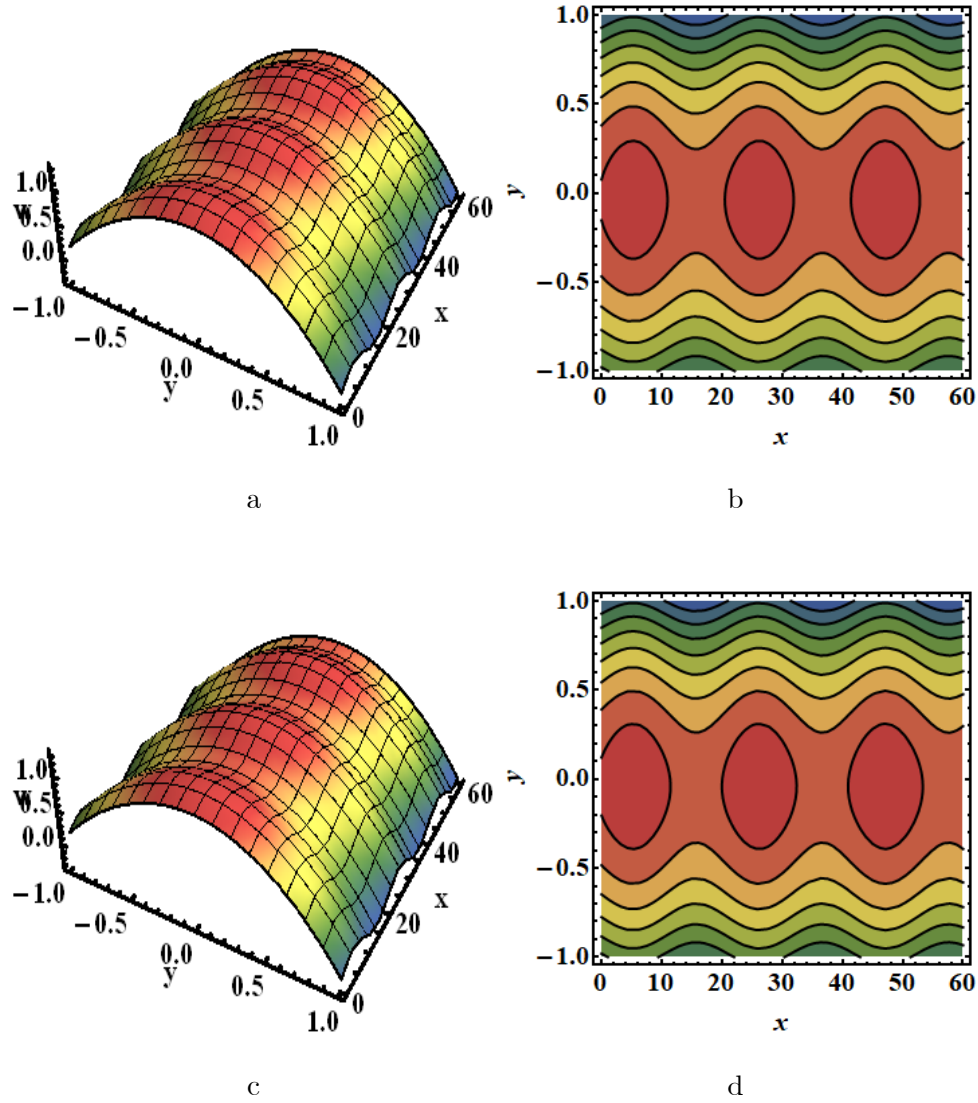


Fig. (3.7): 3D Velocity distribution and contour (a, b, c, d) when $B_i = 4.0$ and $B_i = 8.0$ out of phase (i.e. $\beta^* = \pi$).

3.6.2 Effect of wall roughness on velocity

The 2D variations of the EMHD velocity w for various Gr , Φ , K_n , Pr , B_i , ϕ , Re and Ha are displayed in the Figs. (3.8) to (3.15) when we take $\varepsilon = 0.1$ and $\beta = 5$. Fig. (3.8) demonstrates

that the w increases for various estimate of Grashof number due to effect of declining in viscosity with growing Gr . Fig. (3.9) illustrates the small impact of Φ on the EMHD velocity. Fig. (3.10) shows that the velocity w increases in the portion $[-1, 0]$ and decreases in the portion $[0, 1]$ with increasing value of K_n . Fig. (3.11) shows that the velocity increases for B_i . Fig. (3.12) displays that the velocity w decreases for various estimations of Pr . Fig. (3.13) shows that the velocity w decreases for heat absorption coefficient ϕ . Fig. (3.14) shows that velocity w for Re , with increasing Reynolds number velocity w decreases. The reason is that the rapid oscillation of velocity with small amplitudes for the larger Re . Fig. (3.15) illustrates that velocity w increases for various values of Ha .

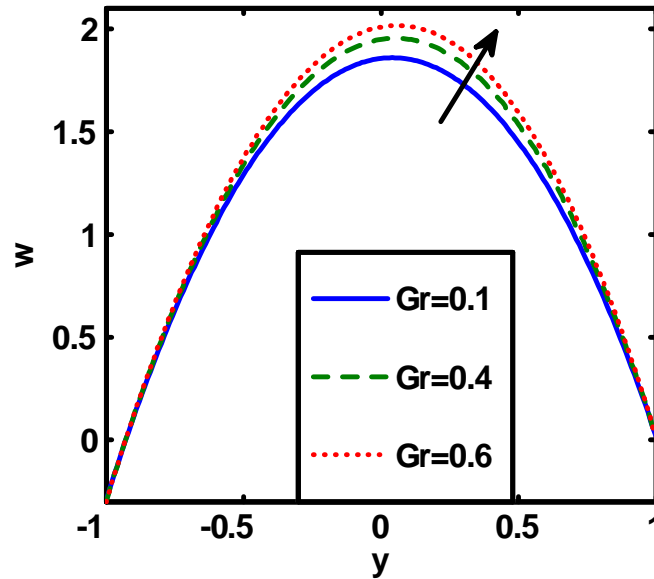


Fig. (3.8): 2D Variation of velocity for Grashof number Gr .

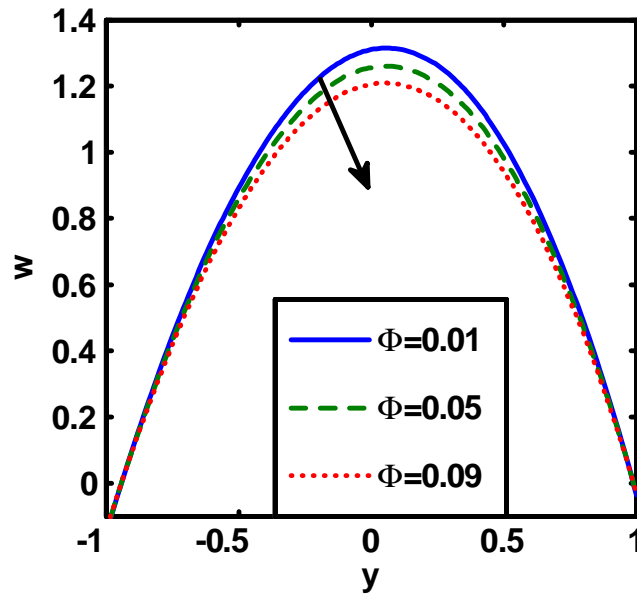


Fig. (3.9): 2D Variation of velocity for nanoparticle volume fraction Φ .

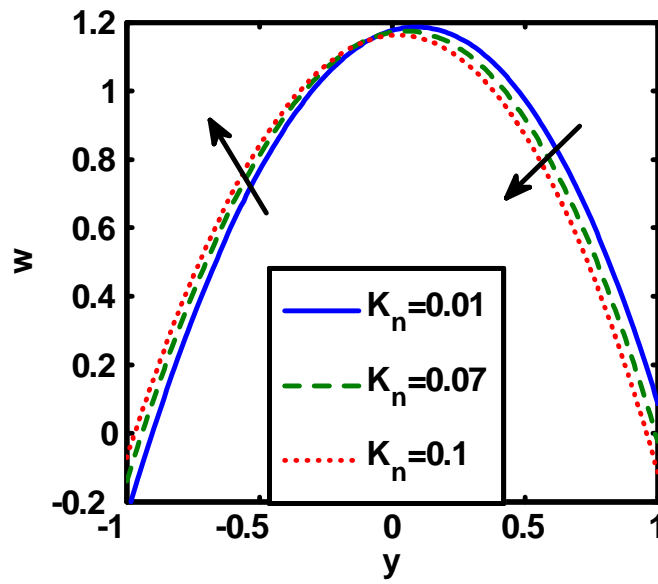


Fig. (3.10): 2D Variation of velocity for knudsen number K_n .

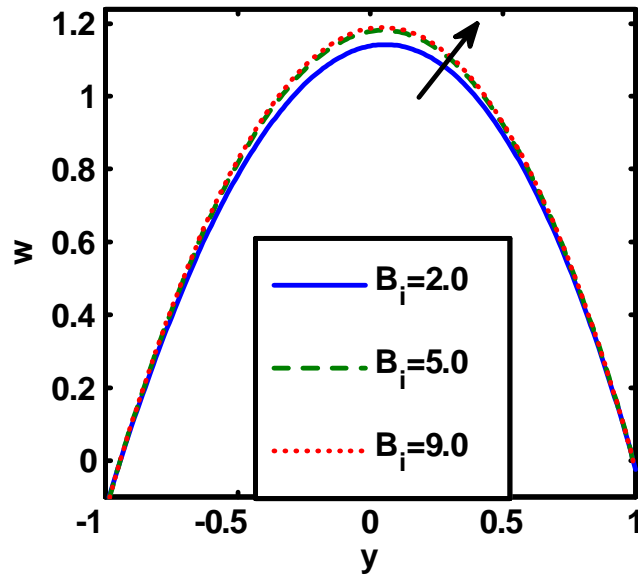


Fig. (3.11): 2D Variation of velocity for biot number B_i .

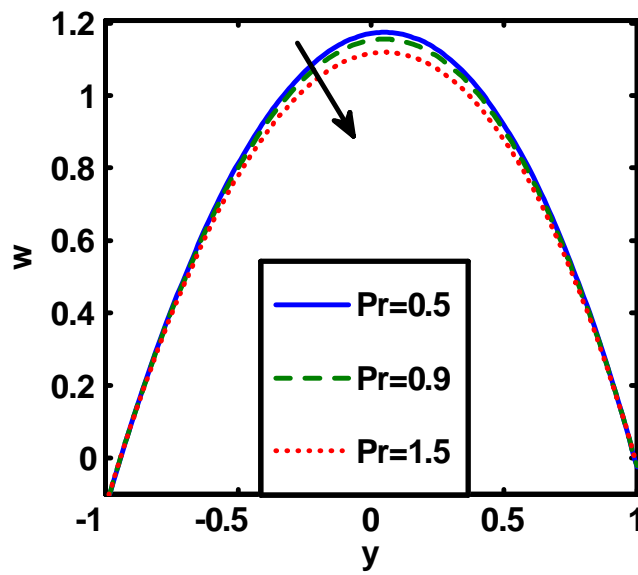


Fig. (3.12): 2D Variation of velocity for Prandtl number Pr .

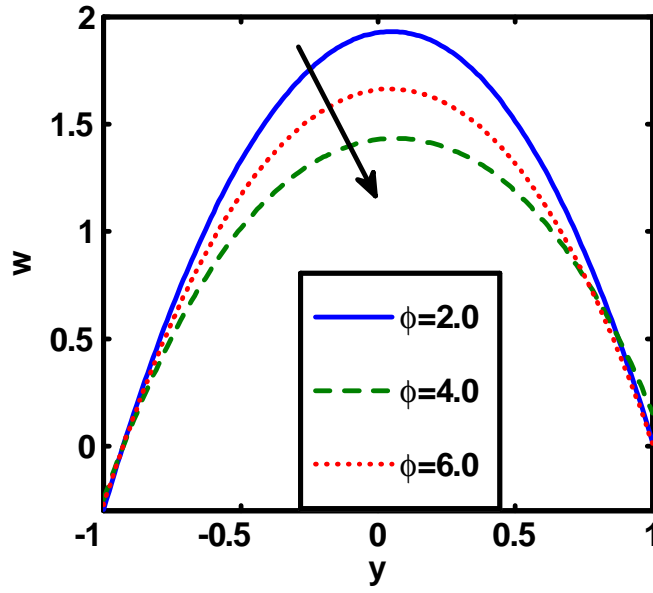


Fig. (3.13): 2D Variation of velocity for heat absorption coefficient ϕ .

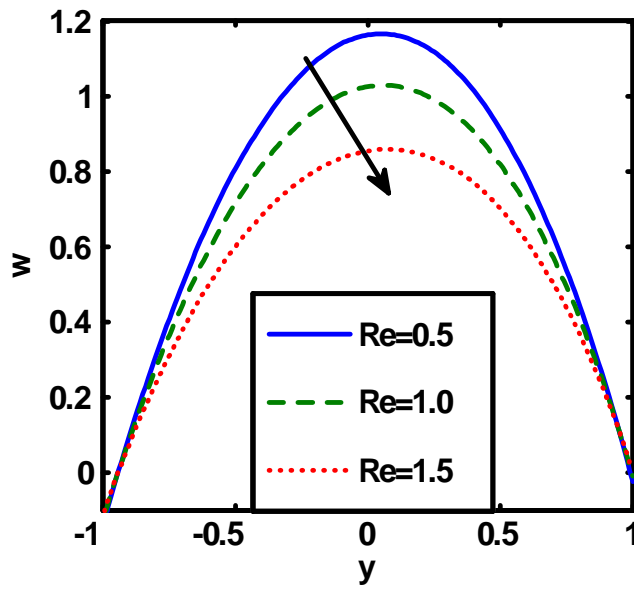


Fig. (3.14): 2D Variation of velocity for Reynolds number Re .

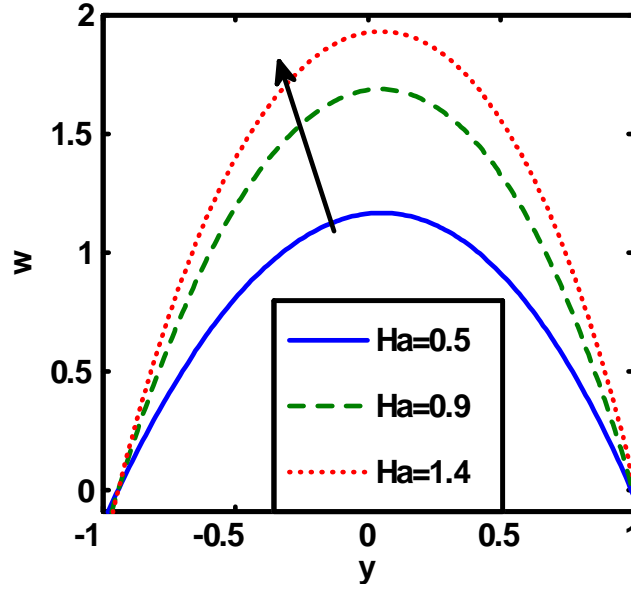


Fig. (3.15): 2D Variation of velocity for hartmann number Ha .

3.6.3 Effect of wall roughness on temperature

The 2D variations of the EMHD temperature θ for various ϕ , Pr , Φ , and B_i are represented in the Figs. (3.16) to (3.19) when we take $\varepsilon = 0.1$ and $\beta = 5$. Fig. (3.16) depicts that profile of temperature increases when the heat absorption coefficient ϕ increases. Fig. (3.17) shows that profile of temperature decreases when the Prandtl number Pr increase. Fig. (3.18) illustrates the result of volume fraction Φ on temperature plot. By enlarges the Φ temperature shows declining effect. Fig. (3.19) shows that profile of temperature increases when the B_i increases.

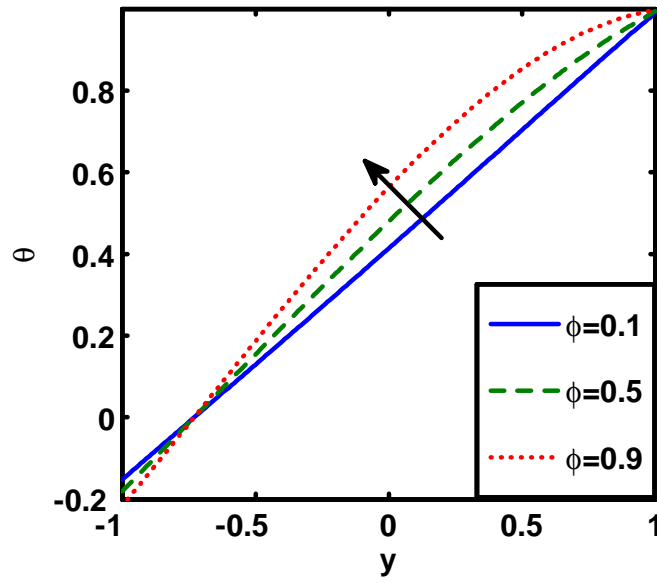


Fig. (3.16): 2D Temperature variation for heat absorption coefficient ϕ .

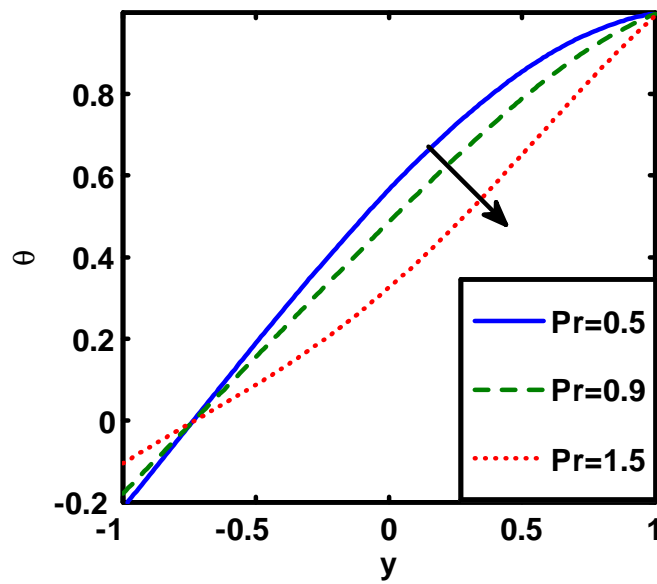


Fig. (3.17): 2D Temperature variation for Prandtl number Pr .

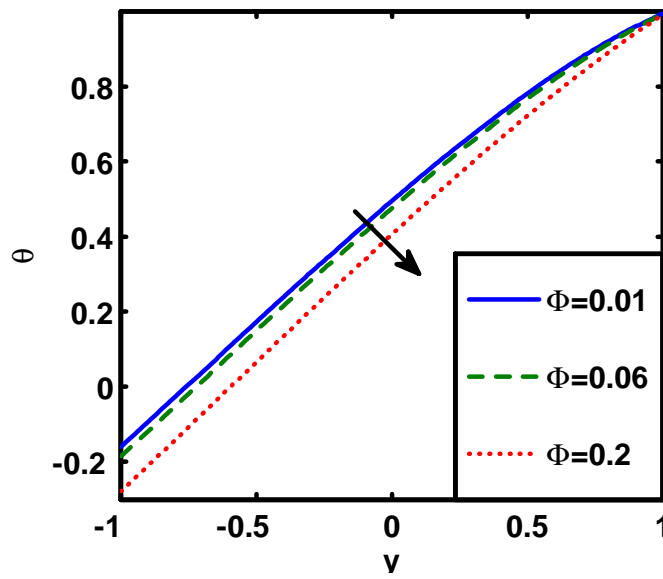


Fig. (3.18): 2D Temperature variation for nanoparticle volume fraction Φ .

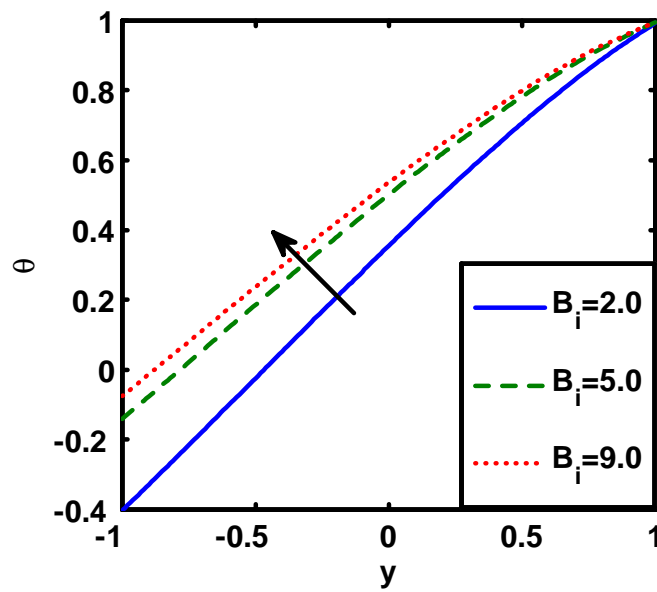


Fig. (3.19): 2D Temperature variation for biot number B_i .

3.7 Tables Description

In this section, the impact of Nusselt number $Nu = -\frac{k_{nf}^*}{k_f^*} \theta'(y_u)$ and $Nu = -\frac{k_{nf}^*}{k_f^*} \theta'(y_l)$ on EMHD flow fluid discussed in microchannel through corrugated walls. Table 3.2 demonstrates that the Nusselt number Nu increases with the increasing value of x at upper wall and lower walls respectively while Nusselt number Nu increases by the rises of Biot number B_i on both walls. Table 3.3 shows that the Nu grows on both walls with the increasing of x and also decreases by the increment in Prandtl number Pr . In this section, the impact of mean velocity φ on Grashof number Gr , Knudsen number K_n , nanoparticle volume fraction Φ explain through the table in microchannel through corrugated walls with variation of hartmann number Ha . Table 3.4 demonstrates that by the increasing value of Ha , Grashof number Gr and Knudsen number K_n the mean velocity φ increases but decreases with the increasing value of nanoparticle volume fraction Φ .

Nu	At left wall			At right wall		
x	$B_i = 5$	$B_i = 7$	$B_i = 9$	$B_i = 5$	$B_i = 7$	$B_i = 9$
0	-0.562202	-0.386915	-0.345996	-0.889901	-0.781847	-0.749193
0.1	-0.559438	-0.385261	-0.344604	-0.887708	-0.780493	-0.748051
0.2	-0.556704	-0.38362	-0.343221	-0.885537	-0.779148	-0.746914
0.3	0.554003	-0.381993	-0.341849	-0.883388	-0.777815	-0.745784
0.4	-0.551337	-0.380383	-0.340489	-0.881265	-0.776493	-0.744662
0.5	-0.548708	-0.378791	-0.339141	-0.879168	-0.775183	-0.743548
0.6	-0.546117	-0.377217	-0.337808	-0.877099	-0.773888	-0.742444
0.7	-0.543567	-0.375663	-0.33649	-0.875061	-0.772608	-0.74135
0.8	-0.541059	-0.374131	0.335188	-0.873053	-0.771343	-0.740267
0.9	-0.538596	-0.37262	-0.333904	-0.871079	-0.770096	-0.739197
1	-0.536178	-0.371134	-0.332638	-0.869138	-0.768867	-0.738141

Table (3.2): Effect of Biot number B_i on Nusselt number Nu .

Nu	At left wall			At right wall		
x	Pr = 0.7	Pr = 1.4	Pr = 2.0	Pr = 0.7	Pr = 1.4	Pr = 2.0
0	-0.202748	-0.583935	-0.967906	-0.789329	-0.559082	-0.319657
0.1	-0.200841	-0.584461	-0.969994	-0.787639	-0.556282	-0.31611
0.2	-0.198953	-0.585007	-0.972089	-0.785964	-0.55352	-0.312636
0.3	-0.197088	-0.585571	-0.974186	-0.784303	-0.550799	-0.309237
0.4	-0.195245	-0.586153	-0.976284	-0.782659	-0.54812	-0.305917
0.5	-0.193427	-0.586752	-0.978381	-0.781032	-0.545486	-0.302677
0.6	-0.191636	-0.587366	-0.980473	-0.779426	-0.5429	-0.29952
0.7	-0.189871	-0.587994	-0.98256	-0.77784	-0.540363	-0.296448
0.8	-0.188134	-0.588636	-0.984638	-0.776276	-0.537878	-0.293463
0.9	-0.186428	-0.589289	-0.986706	-0.774735	-0.535446	-0.290567
1	-0.184752	-0.589952	-0.988759	-0.773219	-0.533069	-0.287761

Table (3.3): Effect of Prandtl number Pr on Nusselt number Nu .

Ha	$Gr = 0.1$	$Gr = 0.6$	$K_n = 0.07$	$K_n = 0.1$	$\Phi = 0.01$	$\Phi = 0.09$
0	0.0728856	0.437313	0.437313	0.459048	0.473643	0.383185
0.1	0.414823	0.77926	0.77926	0.850018	0.797492	0.708564
0.2	0.753043	1.11751	1.11751	1.23761	1.11768	1.0302
0.3	1.08406	1.44858	1.44858	1.61855	1.43059	1.34466,
0.4	1.40484	1.76943	1.76943	1.98997	1.73305	1.6489
0.5	1.71294	2.07758	2.07758	2.34952	2.02252	1.94047
0.6	2.00659	2.37123	2.37123	2.69554	2.29712	2.21756
0.7	2.28475	2.64926	2.64926	3.02696	2.55571	2.47901
0.8	2.54703	2.91121	2.91121	3.3434	2.79784	2.72433
0.9	2.79364	3.15719	3.15719	3.64499	3.02363	2.9536
1	3.02524	3.38781	3.38781	3.93237	3.23372	3.16739

Table (3.4): Effect of Grashof number Gr , Knudsen number K_n , Nanoparticle volume fraction Φ on mean velocity φ .

3.8 Conclusions

The impact of copper nanoparticles on EMHD flow through corrugated walls in microchannel is discussed. The main observations from this theoretical analysis is concise as follows,

- The shape of channel depends on velocity and temperature.
- Velocity increases with Gr , B_i and Ha .
- The velocity declines with rising value of K_n in inner half of channel and rises in outer half of channel.
- With expanding Reynolds number, heat absorption coefficient, nanoparticles and Prandtl number, velocity field decreases.
- Temperature declines with volumetric concentration of nanoparticle Φ and Prandtl number Pr .
- Temperature increases with the heat absorption coefficient ϕ and Biot number B_i .
- Nusselt number expands with Biot number B_i declines with Prandtl number Pr .
- Mean velocity φ increases by the increasing value of Ha , Grashof number Gr and Knudsen number K_n while decreases with the increasing value of nanoparticle volume fraction Φ .

Chapter 4

EMHD flow of Couple stress nanofluid inside a vertical corrugated wavy walls

In this chapter, we have presented the analytical solutions for a flow of the velocity, volume flow rate and mean velocity by using the method of perturbation inside a corrugated surface. For corrugated walls we considered the electromagnetohydrodynamic flow of fluid between the microparallel plates. By employing mathematical computation, we evaluated the wavy effects on velocity for the EMHD flow. The impact of all parameters on velocity and the mean velocity profiles can be analyzed through graphs. With the help of graphs we explain the effect of the Hartmann number, Wave number, Reynolds number and fluid parameter on velocity.

4.1 Mathematical model

Considered the EMHD flow of electrically conducting and an incompressible couple stress fluid between two vertical corrugated walls with $2H$ height. The microchannel height is $100\mu m$ and corrugated wall amplitude is set to be $0.1 H$. Here we have adopted at the middle of the microchannel, the Cartesian coordinate system with a fixed origin. The length L of the channel along z^* direction while width of the channel is assumed to be W along x^* direction are much larger than the layer thickness i.e. $L, W \gg 2H$.

The geometry of flow is shown in Figure 4.1

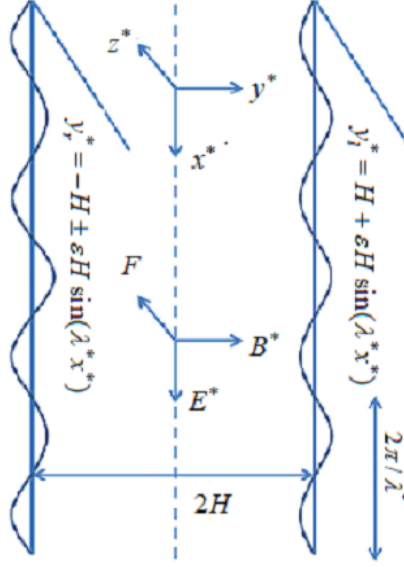


Fig. (4.1): Geometrical sketch of EMHD flow in microchannel.

The equations of lower and upper walls are

$$y_l^* = H + \varepsilon H \sin(\lambda^* x^*) \text{ and } y_r^* = -H \pm \varepsilon H \sin(\lambda^* x^*), \quad (4.1)$$

where ε is small amplitude and λ^* is wave number. We take magnetic field \mathbf{B}^* along y^* direction while along the x^* direction electric field \mathbf{E}^* is applied. Along the z^* direction, we take the Lorentz force which is produced by the contact among the magnetic field \mathbf{B}^* and the electric field \mathbf{E}^* . In the presence of body force the equation of continuity, momentum equation and energy equation of an incompressible couple stress fluid are written as

$$\nabla^* \mathbf{u}^* = 0. \quad (4.2)$$

$$\rho_{nf}(\mathbf{u}^* \cdot \nabla^*) \mathbf{u}^* = -\nabla^* p + \nabla^* \boldsymbol{\tau}^* - \eta \nabla^{*4} \mathbf{u}^* + \mathbf{J} \times \mathbf{B}^* + g(\rho \zeta)_{nf}(T^* - T_r^*). \quad (4.3)$$

$$(\rho C_p)_{nf}(\mathbf{u}^* \cdot \nabla^*) T^* = \nabla^* \cdot k''_{nf} \nabla^* T^* + Q_0. \quad (4.4)$$

where

$$\boldsymbol{\tau}^* = \mu_{nf} \mathbf{A}_1^*, \quad (4.5)$$

$$\mathbf{A}_1^* = \nabla^* \mathbf{u}^* + (\nabla^* \mathbf{u}^*)^t. \quad (4.6)$$

The therrmo physical characteristics of nanofluid are specified as

$$\begin{aligned} \mu_{nf} &= \frac{\mu_f}{(1-\Phi)^{2.5}}, \quad \alpha_{nf} = \frac{k''_{nf}}{(\rho C_p)_{nf}}, \quad \rho_{nf} = (1-\Phi)\rho_f + \Phi\rho_s, \\ (\rho \zeta)_{nf} &= (1-\Phi)(\rho \zeta)_f + \Phi(\rho \zeta)_s, \quad (\rho C_p)_{nf} = (1-\Phi)(\rho C_p)_f + \Phi(\rho C_p)_s, \quad . \\ \frac{k''_{nf}}{k''_f} &= \frac{(k''_s + 2k''_f) - 2\Phi(k''_f - k''_s)}{(k''_s + 2k''_f) + \Phi(k''_f - k''_s)}, \quad \frac{\sigma_{nf}}{\sigma_f} = 1 + \frac{(\frac{\sigma_s}{\sigma_f} - 1)\Phi}{(\frac{\sigma_s}{\sigma_f} + 1) - \Phi(\frac{\sigma_s}{\sigma_f} - 1)} \end{aligned} \quad (4.7)$$

Here ρ_f , ρ_s , ζ_f , ζ_s , k''_f , k''_s , $(\rho C_p)_f$, $(\rho C_p)_s$, σ_f and σ_s represent the densities, thermal expansion, thermal conductivities, heat capacitance and electrical conductivities respectively.

The numerical values of these parameters are given in Table 4.1.

We consider the velocity profile of the following form

$$\mathbf{u}^* = [0, 0, w^*(x^*, y^*)]. \quad (4.8)$$

In the microchannel, we assumed an incompressible fluid to be along the z^* axis direction only. Thus Eqs. (4.3) and (4.4) take the following form

$$-\frac{\partial p}{\partial z^*} + \mu_{nf} \left(\frac{\partial^2 w^*}{\partial x^{*2}} + \frac{\partial^2 w^*}{\partial y^{*2}} \right) - \eta \left(\frac{\partial^4 w^*}{\partial x^{*4}} + \frac{\partial^4 w^*}{\partial y^{*4}} + 2 \frac{\partial^4 w^*}{\partial x^{*2} \partial y^{*2}} \right) + \sigma_{nf} B^* (E^* - B^* w^*) + g(\rho \zeta)_{nf}(T^* - T_r^*) = 0, \quad (4.9)$$

$$\left(\frac{\partial^2 T^*}{\partial x^{*2}} + \frac{\partial^2 T^*}{\partial y^{*2}} \right) + \frac{Q_0}{(\rho C_p)_{nf}} = 0. \quad (4.10)$$

The correspondingly conditions are

$$w^* = 0, T^* = T_l^* \text{ at } y_l^* = H + \varepsilon H \sin(\lambda^* x^*), \quad (4.11)$$

$$w^* = 0, k_{nf} \frac{\partial T^*}{\partial r^*} = -B(T^* - T_r^*) \text{ at } y_r^* = -H \pm \varepsilon H \sin(\lambda^* x^*), \quad (4.12)$$

Suppose along the z^* direction channel is open, so we can ignore the pressure gradient $\partial p / \partial z^*$ along the microchannel [85] and the velocity $w^*(x^*, y^*)$ satisfies

$$\mu_{nf} \left(\frac{\partial^2 w^*}{\partial x^{*2}} + \frac{\partial^2 w^*}{\partial y^{*2}} \right) - \eta \left(\frac{\partial^4 w^*}{\partial x^{*4}} + \frac{\partial^4 w^*}{\partial y^{*4}} + 2 \frac{\partial^4 w^*}{\partial x^{*2} \partial y^{*2}} \right) + \sigma_{nf} B^* (E^* - B^* w^*) + g(\rho\zeta)_{nf} (T^* - T_r^*) = 0. \quad (4.13)$$

Dimensionless quantities that are used in the above equations are

$$(x, y) = \frac{(x^*, y^*)}{H}, \lambda = \lambda^* H, w = \frac{w^*}{U}, Ha = B^* H \left(\frac{\sigma_f}{\mu_f} \right)^{\frac{1}{2}}, \beta = E_0 \left(\frac{\sigma_f}{\mu_f} \right)^{\frac{1}{2}} / U. \quad (4.14)$$

$$C^2 = \frac{\eta}{H^2 \mu_f}, \theta = \frac{T - T_r}{T_l - T_r}, Gr = \frac{g(\rho\zeta)_f H(T_l - T_r)}{\mu_f U}, \phi = \frac{Q_0 H^2}{k_f (T_l - T_r)}, Bi = \frac{BH}{k_f}$$

In the above expression $Gr, \theta, \lambda, Ha, \phi, C^2, Bi, \beta$ represent the Grashof number, dimensionless temperature, wave number, Hartmann number, dimensionless heat source parameter, couple stress parameter, Biot number and non-dimensional parameter respectively. After using the lubrication approach, the continuity equation is exactly satisfied and Eqs. (4.9) and (4.12) are converted into

$$\left(\frac{\partial^2 w}{\partial x^2} + \frac{\partial^2 w}{\partial y^2} \right) - \frac{\mu_f}{\mu_{nf}} \left[C^2 \left(\frac{\partial^4 w}{\partial x^4} + \frac{\partial^4 w}{\partial y^4} + 2 \frac{\partial^4 w}{\partial x^2 \partial y^2} \right) - \frac{\sigma_{nf}}{\sigma_f} (Ha^2 w + \frac{\sigma_{nf}}{\sigma_f} Ha \beta) - g \frac{(\rho\zeta)_{nf}}{(\rho\zeta)_f} Gr \theta \right] = 0, \quad (4.15)$$

$$\left(\frac{\partial^2 \theta}{\partial x^2} + \frac{\partial^2 \theta}{\partial y^2} \right) + \frac{k''_f}{k''_{nf}} \phi = 0. \quad (4.16)$$

The corresponding non-dimensional boundary conditions are

$$\theta = 1 \text{ at } y_l = 1 + \varepsilon \sin(\lambda x), \quad (4.17)$$

$$\frac{\partial \theta}{\partial y} + \frac{Bi}{\left(\frac{k_{nf}}{k_f} \right)} \theta = 0 \text{ at } y_r = -1 - \varepsilon \sin(\lambda x + \beta^*). \quad (4.18)$$

$$\begin{aligned}
w &= 0 \text{ at } y_l = 1 + \varepsilon \sin(\lambda x) \text{ and } y_r = -1 \pm \varepsilon \sin(\lambda x), \\
w_{yy} &= 0 \text{ at } y_l = 1 + \varepsilon \sin(\lambda x) \text{ and } y_r = -1 \pm \varepsilon \sin(\lambda x), \\
w_{yy} &= 0 \text{ at } y_l = 1 + \varepsilon \sin(\lambda x) \text{ and } y_r = -1 \pm \varepsilon \sin(\lambda x), \\
\theta &= 1 \text{ at } y_l = 1 + \varepsilon \sin(\lambda x), \\
\frac{\partial \theta}{\partial y} + \frac{B_i}{\left(\frac{k''_{nf}}{k''_f}\right)} \theta &= 0 \text{ at } y_r = -1 \pm \varepsilon \sin(\lambda x).
\end{aligned} \tag{4.19}$$

In above Eq. (4.17), $y_l = y_l^* / H$, $y_r = y_r^* / H$, the ‘-’symbol means the half period out of phase and ‘+’sign means wavy walls corrugation in phase.

4.2 Solution by Perturbation method

By applying Taylor series, we can expand the boundary conditions in Eq. (4.17). If there is no roughness then the velocity is function of y only while in the presence of surface roughness the x direction variation is also considered. With the consideration of small amplitude $\varepsilon \ll 1$, we can apply the perturbation technique to solve Eqs. (4.15) and (4.16). Then velocity and temperature function written as

$$\begin{aligned}
w(x, y) &= w_0(y) + \varepsilon w_1(x, y) + \varepsilon^2 w_2(x, y) + \dots \\
\theta(x, y) &= \theta_0(y) + \varepsilon \theta_1(x, y) + \varepsilon^2 \theta_2(x, y) + \dots
\end{aligned} \tag{4.20}$$

By utilizing Eq. (4.18) into Eqs. (4.15) and (4.16) and boundary conditions (4.17), comparing the similar powers of the ε , we obtain the following systems.

4.2.1 Zero Order classification

$$\frac{d^2 \theta_0}{dy^2} + \frac{k''_f}{k''_{nf}} \phi = 0, \tag{4.21}$$

$$\frac{d^2 w_0}{dy^2} - \frac{\mu_f}{\mu_{nf}} \left[C^2 \frac{d^4 w_0}{dy^4} - \frac{\sigma_{nf}}{\sigma_f} (H a^2 w_0 + \frac{\sigma_{nf}}{\sigma_f} H a \beta) - g \frac{(\rho \zeta)_{nf}}{(\rho \zeta)_f} Gr \theta_0 \right] = 0 \tag{4.22}$$

The required boundary conditions are

$$\theta_0|_{y=1} = 1, \quad \frac{d\theta_0}{dy}|_{y=-1} = -\frac{B_i}{\left(\frac{k^n}{k^n_f}\right)}\theta_0|_{y=-1} = 0 \quad (4.23)$$

$$\begin{aligned} w_0|_{y=1} &= 0, \quad w_0|_{y=-1} = 0 \\ w_{0yy}|_{y=1} &= 0, \quad w_{0yy}|_{y=-1} = 0 \end{aligned} \quad (4.24)$$

4.2.2 First Order classification

$$\left(\frac{\partial^2\theta_1}{\partial x^2} + \frac{\partial^2\theta_1}{\partial y^2}\right) = 0, \quad (4.25)$$

$$\left(\frac{\partial^2 w_1}{\partial x^2} + \frac{\partial^2 w_1}{\partial y^2}\right) - \frac{\mu_f}{\mu_{nf}} \left[C^2 \left(\frac{\partial^4 w_1}{\partial x^4} + \frac{\partial^4 w_1}{\partial y^4} + 2 \frac{\partial^4 w_1}{\partial x^2 \partial y^2} \right) - \frac{\sigma_{nf}}{\sigma_f} (Ha^2 w_1 + \frac{\sigma_{nf}}{\sigma_f} Ha\beta) - g \frac{(\rho\zeta)_{nf}}{(\rho\zeta)_f} Gr\theta_1 \right] = 0. \quad (4.26)$$

The boundary conditions are

$$\begin{aligned} \theta_1|_{y=1} &= -\sin(\lambda x) \left(\frac{d\theta_0}{dy} \right)_{y=1} \\ \frac{\partial\theta_1}{\partial y}|_{y=-1} &= \left(\mp \sin(\lambda x) \frac{d^2\theta_0}{dy^2} \Big|_{y=-1} - \frac{B_i}{\left(\frac{k^n}{k^n_f}\right)} (\theta_1 \mp \sin(\lambda x)\theta_0) \right)_{y=-1}, \end{aligned} \quad (4.27)$$

$$\begin{aligned} w_1|_{y=1} &= -\sin(\lambda x) \left(\frac{dw_0}{dy} \right)_{y=1}, \quad w_1^\pm|_{y=-1} = \mp \sin(\lambda x) \left(\frac{dw_0}{dy} \right)_{y=-1}, \\ w_{1yy}|_{y=1} &= -\sin(\lambda x) \left(\frac{d^3 w_0}{dy^3} \right)_{y=1}, \quad w_{1yy}^\pm|_{y=-1} = \mp \sin(\lambda x) \left(\frac{d^3 w_0}{dy^3} \right)_{y=-1}. \end{aligned} \quad (4.28)$$

4.2.3 Second Order classification

$$\left(\frac{\partial^2\theta_2}{\partial x^2} + \frac{\partial^2\theta_2}{\partial y^2}\right) = 0, \quad (4.29)$$

$$\left(\frac{\partial^2 w_2}{\partial x^2} + \frac{\partial^2 w_2}{\partial y^2}\right) - \frac{\mu_f}{\mu_{nf}} \left[C^2 \left(\frac{\partial^4 w_2}{\partial x^4} + \frac{\partial^4 w_2}{\partial y^4} + 2 \frac{\partial^4 w_2}{\partial x^2 \partial y^2} \right) - \frac{\sigma_{nf}}{\sigma_f} (Ha^2 w_2 + \frac{\sigma_{nf}}{\sigma_f} Ha\beta) - g \frac{(\rho\zeta)_{nf}}{(\rho\zeta)_f} Gr\theta_2 \right] = 0. \quad (4.30)$$

The boundary conditions are

$$\theta_2 \big|_{y=1} = \left(-\sin(\lambda x) \frac{\partial \theta_1}{\partial r} + \frac{\sin^2(\lambda x)}{2} \frac{d^2 \theta_0}{dy^2} \right)_{y=1},$$

$$\frac{\partial^2 \theta_2}{\partial y^2} \big|_{y=1} = \left(\mp \sin(\lambda x) \frac{\partial^2 \theta_1}{\partial y^2} - \frac{\sin^2(\lambda x)}{2} \frac{d^3 \theta_0}{dy^3} - \frac{B_i}{\left(\frac{k''}{k''} n_f\right)} (\theta_2 \mp \sin(\lambda x) \theta_1 - \frac{\sin^2(\lambda x)}{2} \theta_0) \right)_{y=-1}. \quad (4.31)$$

$$w_2 \big|_{y=1} = -\sin(\lambda x) \left(\frac{\partial w_1}{\partial y} \right)_{y=1} - \frac{1}{2} \sin^2(\lambda x) \left(\frac{d^2 w_0}{dy^2} \right)_{y=1},$$

$$w_2^\pm \big|_{y=-1} = \mp \sin(\lambda x) \left(\frac{\partial w_1}{\partial y} \right)_{y=-1} - \frac{1}{2} \sin^2(\lambda x) \left(\frac{d^2 w_0}{dy^2} \right)_{y=-1} \quad (4.32)$$

$$w_{2yy} \big|_{y=1} = -\sin(\lambda x) \left(\frac{\partial^3 w_1}{\partial y^3} \right)_{y=1} - \frac{1}{2} \sin^2(\lambda x) \left(\frac{d^4 w_0}{dy^4} \right)_{y=1},$$

$$w_{2yy}^\pm \big|_{y=-1} = \mp \sin(\lambda x) \left(\frac{\partial^3 w_1}{\partial y^3} \right)_{y=-1} - \frac{1}{2} \sin^2(\lambda x) \left(\frac{d^4 w_0}{dy^4} \right)_{y=-1}$$

Solution of zero order classification

By utilizing boundary conditions we obtained the zero order solution as

$$\theta_0(y) = A_{11} + A_{12}y - \frac{y^2 \phi k''_f}{2k''_{nf}} \quad (4.33)$$

$$w_0(y) = e^{-yb_1} B_{11} + e^{yb_1} B_{12} + e^{-yb_2} B_{13} + e^{yb_2} B_{14} - \frac{\beta}{Ha} + (Gr(\rho\zeta)_{nf} \sigma_f (-2\phi k''_f \mu_{nf} \sigma_f + Ha^2 (y^2 \phi k''_f - 2(A_{11} + A_{12}y)k''_{nf}) \mu_f \sigma_{nf}) / 2Ha^4 k''_{nf} \mu_f (\rho\zeta)_f \sigma_{nf}^2), \quad (4.34)$$

where

$$b_1 = \sqrt{\frac{\mu_{nf}}{2C^2 \mu_f} - \frac{\sqrt{\mu_{nf}^2 \sigma_f + 4C^2 Ha^2 \mu_f^2 \sigma_{nf}}}{2C^2 \mu_f \sqrt{\sigma_f}}}, \quad (4.35)$$

$$b_2 = \sqrt{\frac{\mu_{nf}}{2C^2 \mu_f} + \frac{\sqrt{\mu_{nf}^2 \sigma_f + 4C^2 Ha^2 \mu_f^2 \sigma_{nf}}}{2C^2 \mu_f \sqrt{\sigma_f}}},$$

where A_{11} , A_{12} , B_{11} , B_{12} , B_{13} and B_{14} are constants.

Solution of first order classification

By utilizing the solutions (4.31) and (4.32) into Eqs. (4.25) and (4.26), we can adopt solution of the first order classification as

$$\theta_1(x, y) = \sin(\lambda x) f(y),$$

$$w_1(x, y) = \sin(\lambda x) g(y), \quad (4.36)$$

where $f(y)$ and $g(y)$ is function of the y .

Employing Eq. (4.34) in Eqs. (4.23) and (4.24), we get the following form of first order system

$$\frac{d^2 f(y)}{dy^2} - \lambda^2 f(y) = 0, \quad (4.37)$$

$$\left(\frac{d^2 g(y)}{dy^2} - \lambda^2 g(y) \right) - \frac{\mu_f}{\mu_{nf}} \left[C^2 \left(\frac{d^4 g(y)}{dy^4} - 2\lambda^2 \frac{d^2 g(y)}{dy^2} + \lambda^4 g(y) \right) - \frac{\sigma_{nf}}{\sigma_f} H a^2 g(y) - \frac{(\rho\zeta)_{nf}}{(\rho\zeta)_f} G r f(y) \right] = 0. \quad (4.38)$$

The boundary conditions yield the form

$$f|_{y=1} = -\frac{d\theta_0}{dy}|_{y=1}, \quad \frac{df^\pm(y)}{dy}|_{y=-1} = \mp \left(\frac{d^2\theta_0}{dy^2} - \frac{B_i}{\left(\frac{k''_{nf}}{k''_f}\right)} (f^\pm(y) \mp \theta_{0y=-1}) \right), \quad (4.39)$$

$$\begin{aligned} g|_{y=1} &= -\frac{dw_0}{dy}|_{y=1}, \quad g^\pm|_{y=-1} = \mp \frac{dw_0}{dy}|_{y=-1}, \\ g_{yy}|_{y=-1} &= -\frac{d^3 w_0}{dy^3}|_{y=1}, \quad g_{yy}^\pm|_{y=-1} = \mp \frac{d^3 w_0}{dy^3}|_{y=-1}. \end{aligned} \quad (4.40)$$

Under the above boundary conditions (4.37) and (4.38), the solution of the Eqs. (4.35) and (4.36) are directly written as

$$f^\pm(y) = \begin{aligned} &e^{y\lambda} A_{21} + e^{-y\lambda} A_{22}, \\ &e^{y\lambda} A_{31} + e^{-y\lambda} A_{32}, \end{aligned} \quad (4.41)$$

$$\begin{aligned} g^\pm(y) &= \begin{aligned} &e^{-yb_3} B_{21} + e^{yb_3} B_{22} + e^{-yb_4} B_{23} + e^{yb_4} B_{24} - (Gr e^{-y\lambda} (e^{2y\lambda} A_{21} + A_{22}) (\rho\zeta)_{nf} \sigma_f / H a^2 (\rho\zeta)_f \sigma_{nf}), \\ &e^{-yb_3} B_{31} + e^{yb_3} B_{32} + e^{-yb_4} B_{33} + e^{yb_4} B_{34} - (Gr e^{-y\lambda} (e^{2y\lambda} A_{31} + A_{32}) (\rho\zeta)_{nf} \sigma_f / H a^2 (\rho\zeta)_f \sigma_{nf}), \end{aligned} \\ &\quad (4.42) \end{aligned}$$

where A_{21} , A_{22} , A_{31} , A_{32} , B_{21} , B_{22} , B_{23} , B_{24} , B_{31} , B_{32} , B_{33} and B_{34} are constants.

Using (4.39) and (4.40) into equation (4.34), the solution of first order system take the form

$$\theta_1^\pm(x, y) = \begin{aligned} &\sin(\lambda x) (e^{y\lambda} A_{21} + e^{-y\lambda} A_{22}), \\ &\sin(\lambda x) (e^{y\lambda} A_{31} + e^{-y\lambda} A_{32}), \end{aligned} \quad (4.43)$$

$$\begin{aligned}
w_1^\pm(x, y) = & \sin(\lambda x) (e^{-yb_3} B_{21} + e^{yb_3} B_{22} + e^{-yb_4} B_{23} + e^{yb_4} B_{24} - (Gre^{-y\lambda} \\
& (e^{2y\lambda} A_{21} + A_{22})(\rho\zeta)_{nf}\sigma_f/Ha^2(\rho\zeta)_f\sigma_{nf})), \\
& \sin(\lambda x) (e^{-yb_3} B_{31} + e^{yb_3} B_{32} + e^{-yb_4} B_{33} + e^{yb_4} B_{34} - (Gre^{-y\lambda} \\
& (e^{2y\lambda} A_{31} + A_{32})(\rho\zeta)_{nf}\sigma_f/Ha^2(\rho\zeta)_f\sigma_{nf})),
\end{aligned} \tag{4.44}$$

where

$$\begin{aligned}
b_3 &= \sqrt{\frac{4\lambda^2 C^2 \mu_f + 2\mu_{nf}}{C^2 \mu_f} - \frac{2\sqrt{\mu_{nf}^2 \sigma_f + 4C^2 Ha^2 \mu_f^2 \sigma_{nf}}}{C^2 \mu_f \sqrt{\sigma_f}}}, \\
b_4 &= \sqrt{\frac{4C^2 \lambda^2 \mu_f + 2\mu_{nf}}{C^2 \mu_f} + \frac{2\sqrt{\mu_{nf}^2 \sigma_f + 4C^2 Ha^2 \mu_f^2 \sigma_{nf}}}{C^2 \mu_f \sqrt{\sigma_f}}}.
\end{aligned} \tag{4.45}$$

4.2.4 Solution of second order classification

The boundary conditions (4.29) and (4.30) of second order classification can be simplified by utilizing the solutions of (4.31), (4.32), (4.41) and (4.42). Under the boundary conditions (4.29) and (4.30), we can adopt solution of the second order classification as

$$\begin{aligned}
\theta_2^\pm(x, y) &= h^\pm(y) + \cos(2\lambda x) k^\pm(y), \\
w_2^\pm(x, y) &= m^\pm(y) + \cos(2\lambda x) n^\pm(y).
\end{aligned} \tag{4.46}$$

By applying Eq. (4.44) into Eqs.(4.27) and (4.28), we get the following forms

$$\frac{d^2 h^\pm(y)}{dy^2} = 0, \tag{4.47}$$

$$\frac{d^2 k^\pm(y)}{dy^2} - 4\lambda^2 k^\pm(y) = 0, \tag{4.48}$$

$$\frac{d^2 m^\pm(y)}{dy^2} - \frac{\mu_f}{\mu_{nf}} \left[C^2 \frac{d^4 m^\pm(y)}{dy^4} - \frac{\sigma_{nf}}{\sigma_f} Ha^2 m^\pm(y) - \frac{(\rho\zeta)_{nf}}{\rho\zeta}_f Gr h^\pm(y) \right] = 0, \tag{4.49}$$

$$\begin{aligned}
& \left(\frac{d^2 n^\pm(y)}{dy^2} - 4\lambda^2 n^\pm(y) \right) - \frac{\mu_f}{\mu_{nf}} \left[C^2 \left(\frac{d^4 n^\pm(y)}{dy^4} - 8\lambda^2 \frac{d^2 n^\pm(y)}{dy^2} \right) \right. \\
& \left. + 16\lambda^4 n^\pm(y) - \frac{\sigma_{nf}}{\sigma_f} Ha^2 n^\pm(y) - \frac{(\rho\zeta)_{nf}}{\rho\zeta}_f Gr k^\pm(y) \right] = 0.
\end{aligned} \tag{4.50}$$

The boundary conditions of two functions are

$$\begin{aligned}
h^\pm(y) \Big|_{y=1} &= -\frac{1}{2} \left(\frac{df^\pm(y)}{dr} + \frac{1}{2} \frac{d^2\theta_0}{dr^2} \right)_{y=1}, \\
\frac{dh^\pm(y)}{dy} \Big|_{y=-1} &= - \left(\frac{1}{2} \left(\frac{d^2f^\pm(y)}{dy^2} + \frac{1}{2} \frac{d^3\theta_0}{dy^3} \right) + \frac{B_i}{\left(\frac{k^n}{k^n f}\right)} \left(h^\pm(y) + \frac{1}{2} (f^\pm(y) + \frac{1}{2}\theta_0(y)) \right) \right)_{y=-1},
\end{aligned} \tag{4.51}$$

$$\begin{aligned}
m^\pm(y) \Big|_{y=1} &= -\frac{1}{2} \left(\frac{dg^\pm(y)}{dy} + \frac{1}{2} \frac{d^2w_0}{dy^2} \right)_{y=1}, \\
m^\pm(y) \Big|_{y=-1} &= -\frac{1}{2} \left(\mp \frac{dg^\pm(y)}{dy} - \frac{1}{2} \frac{d^2w_0}{dy^2} \right)_{y=-1}, \\
\frac{d^2m^\pm(y)}{dy^2} \Big|_{y=1} &= -\frac{1}{2} \left(\frac{d^3g^\pm(y)}{dy^3} + \frac{1}{2} \frac{d^4w_0}{dy^4} \right)_{y=1}, \\
\frac{d^2m^\pm(y)}{dy^2} \Big|_{y=-1} &= -\frac{1}{2} \left(\pm \frac{d^3g^\pm(y)}{dy^3} + \frac{1}{2} \frac{d^4w_0}{dy^4} \right)_{y=-1},
\end{aligned} \tag{4.52}$$

$$\begin{aligned}
n^\pm(y) \Big|_{y=1} &= \frac{1}{2} \left(\frac{dg^\pm(y)}{dy} + \frac{1}{2} \frac{d^2w_0}{dy^2} \right)_{y=1}, \\
n^\pm(y) \Big|_{y=-1} &= -\frac{1}{2} \left(\pm \frac{dg^\pm(y)}{dy} - \frac{1}{2} \frac{d^2w_0}{dy^2} \right)_{y=-1}, \\
\frac{d^2n^\pm(y)}{dy^2} \Big|_{y=1} &= \frac{1}{2} \left(\frac{d^3g^\pm(y)}{dy^3} + \frac{1}{2} \frac{d^4w_0}{dy^4} \right)_{y=1}, \\
\frac{d^2n^\pm(y)}{dy^2} \Big|_{y=-1} &= -\frac{1}{2} \left(\mp \frac{d^3g^\pm(y)}{dy^3} - \frac{1}{2} \frac{d^4w_0}{dy^4} \right)_{y=-1}.
\end{aligned} \tag{4.53}$$

By utilizing the above boundary conditions (4.49) to (4.51), the exact solutions can be obtained as

$$h^\pm(y) = \begin{aligned} &A_{41} + A_{42}y, \\ &A_{61} + A_{62}y, \end{aligned} \tag{4.54}$$

$$\begin{aligned}
m^\pm(y) &= \begin{aligned} &e^{-yb_1} B_{41} + e^{yb_1} B_{42} + e^{-yb_2} B_{43} + e^{yb_2} B_{44} - (Gr(A_{41} + A_{42}y)(\rho\zeta)_{nf}\sigma_f/Ha^2(\rho\zeta)_f\sigma_{nf}), \\ &e^{-yb_1} B_{61} + e^{yb_1} B_{62} + e^{-yb_2} B_{63} + e^{yb_2} B_{64} - (Gr(A_{61} + A_{62}y)(\rho\zeta)_{nf}\sigma_f/Ha^2(\rho\zeta)_f\sigma_{nf}), \end{aligned} \\ &\tag{4.55}
\end{aligned}$$

$$k^\pm(y) = \begin{aligned} &e^{2y\lambda} A_{51} + e^{-2y\lambda} A_{52}, \\ &e^{2y\lambda} A_{71} + e^{-2y\lambda} A_{72}, \end{aligned} \tag{4.56}$$

$$\begin{aligned}
n^\pm(y) &= \begin{aligned} &e^{-yb_5} B_{51} + e^{yb_5} B_{52} + e^{-yb_6} B_{53} + e^{yb_6} B_{54} - (Gr e^{-2y\lambda} (e^{4y\lambda} A_{51} + A_{52})(\rho\zeta)_{nf}\sigma_f/Ha^2(\rho\zeta)_f\sigma_{nf}), \\ &e^{-yb_5} B_{71} + e^{yb_5} B_{72} + e^{-yb_6} B_{73} + e^{yb_6} B_{74} - (Gr e^{-2y\lambda} (e^{4y\lambda} A_{71} + A_{72})(\rho\zeta)_{nf}\sigma_f/Ha^2(\rho\zeta)_f\sigma_{nf}), \end{aligned} \\ &\tag{4.57}
\end{aligned}$$

where

$$\begin{aligned}
b_5 &= \sqrt{\frac{16C^2\lambda^2\mu_f+2\mu_{nf}}{C^2\mu_f} - \frac{2\sqrt{\mu_{nf}^2\sigma_f+4C^2Ha^2\mu_f^2\sigma_{nf}}}{C^2\mu_f\sqrt{\sigma_f}}}, \\
b_6 &= \sqrt{\frac{16C^2\lambda^2\mu_f+2\mu_{nf}}{C^2\mu_f} + \frac{2\sqrt{\mu_{nf}^2\sigma_f+4C^2Ha^2\mu_f^2\sigma_{nf}}}{C^2\mu_f\sqrt{\sigma_f}}},
\end{aligned} \tag{4.58}$$

where $A_{41}, A_{42}, A_{51}, A_{52}, A_{61}, A_{62}, A_{71}, A_{72}, B_{41}, B_{42}, B_{43}, B_{44}, B_{51}, B_{52}, B_{53}, B_{54}, B_{61}, B_{62}, B_{63}, B_{64}, B_{71}, B_{72}, B_{73}$ and B_{74} are constants.

The solution of second order classification can be written as

$$\begin{aligned}
\theta_2^\pm(x, y) &= A_{41} + A_{42}y + \cos(2\lambda x)(e^{2y\lambda}A_{51} + e^{-2y\lambda}A_{52}), \\
&A_{61} + A_{62}y + \cos(2\lambda x)(e^{2y\lambda}A_{71} + e^{-2y\lambda}A_{72}),
\end{aligned} \tag{4.59}$$

$$\begin{aligned}
&e^{-yb_1}B_{41} + e^{yb_1}B_{42} + e^{-yb_2}B_{43} + e^{yb_2}B_{44} - (Gr(A_{41} + A_{42}y)(\rho\zeta)_{nf}\sigma_f/Ha^2(\rho\zeta)_f\sigma_{nf}) \\
&+ \cos(2\lambda x)(e^{-yb_5}B_{51} + e^{yb_5}B_{52} + e^{-yb_6}B_{53} + e^{yb_6}B_{54} - (Gre^{-2y\lambda}(e^{4y\lambda}A_{51} + A_{52})\sigma_f \\
&(\rho\zeta)_{nf}/Ha^2(\rho\zeta)_f\sigma_{nf})), \\
w_2^\pm(x, y) &= e^{-yb_1}B_{61} + e^{yb_1}B_{62} + e^{-yb_2}B_{63} + e^{yb_2}B_{64} - (Gr(A_{61} + A_{62}y)(\rho\zeta)_{nf}\sigma_f/Ha^2(\rho\zeta)_f\sigma_{nf}) \\
&+ \cos(2\lambda x)e^{-yb_5}B_{71} + e^{yb_5}B_{72} + e^{-yb_6}B_{73} + e^{yb_6}B_{74} - (Gre^{-2y\lambda}(e^{4y\lambda}A_{71} + A_{72})\sigma_f \\
&(\rho\zeta)_{nf}/Ha^2(\rho\zeta)_f\sigma_{nf}).
\end{aligned} \tag{4.60}$$

Collecting the solutions of zero, first and second order systems, the approximate solutions can be denoted as

$$\theta(x, y) = \theta_0(y) + \varepsilon\theta_1^\pm(x, y) + \varepsilon^2\theta_2^\pm(x, y) + \dots \tag{4.61}$$

$$w(x, y) = w_0(y) + \varepsilon w_1^\pm(x, y) + \varepsilon^2 w_2^\pm(x, y) + \dots \tag{4.62}$$

4.2.5 Volume flow rate

We can define the volume flow rate as

$$q(x) = \int_{-1-\varepsilon\sin(\lambda x)}^{1+\varepsilon\sin(\lambda x)} w(x, y)dy, \tag{4.63}$$

$$q(x) = \int_{-1}^1 w_0(y)dy + \varepsilon \int_{-1}^1 w_1(x, y)dy + \varepsilon^2 (\int_{-1}^1 w_2(x, y)dy + \sin(\lambda x)[w_1(x, y)|_{y=1} + w_1(x, y)|_{y=-1}] + \frac{1}{2} \sin^2(\lambda x) (\frac{dw_0(y)}{dy}|_{y=1} - \frac{dw_0(y)}{dy}|_{y=-1})) \quad (4.64)$$

4.2.6 Mean velocity

The mean velocity on average over one wavelength $(0, 2\pi/\lambda)$ of the corrugations as

$$w_m^\pm = \frac{\lambda}{4\pi} \int_{-1 \pm \varepsilon \sin(\lambda x)}^{1 + \varepsilon \sin(\lambda x)} \int_0^{\frac{2\pi}{\lambda}} w^\pm(x, y) dx dy. \quad (4.65)$$

Inserting (4.61) into (4.63) and using (4.62), the mean velocity takes the form

$$w_m^\pm = \frac{\lambda}{4\pi} \int_0^{\frac{2\pi}{\lambda}} q^\pm(x) dx = w_{0m} [1 + \varepsilon^2 \varphi^\pm + O(\varepsilon^4)], \quad (4.66)$$

where w_{0m} indicates the mean velocity for the perfectly smooth walls and φ^\pm indicates the leading order perturbations to a mean velocity due to the corrugations. When φ^\pm is positive then mean velocity increases, while when φ^\pm is negative then mean velocity decreases.

4.3 Thermophysical properties of water and silver

The thermophysical properties are

Physical Properties	Water	Silver
$C_p(J/kgK)$	4179	235
$\rho(kg/m^3)$	997.1	10,500
$k''(W/mK)$	0.613	429
$\zeta \times 10^5 (1/K)$	21.0	1.89
$\sigma(S/m)$	5.0×10^{-2}	6.3×10^7
$\mu(kg/m.sec)$	8.90×10^{-4}	-

Table (4.1): Thermo physical effects.

4.4 Graphical consequence

In this portion, the graphical behavior of couple stress fluid discussed between the corrugated walls. For microfluidic investigation the height of channel is $H \sim 100\mu m$, electric field frequency changes from 50 to $500s^{-1}$, the Hartmann number between 0.0001 to 3. The Reynolds number changes from 0.5 to 5, $\beta = 5$ is the fixed dimensionless parameter. In order to decrease the unclear influence of the wave, we established the small parameter ε as 0.1.

For three dimensional disparities, the electromagnetohydrodynamic (EMHD) velocity distributions and contour of the couple stress parameter C are shown in Figs. (4.2) and (4.3). In 3D Figs. (4.2), 0° is the phase difference between the walls. During the 3D plots of Figs. (4.3) the phase difference is equal to the 180° between two walls. We observe that, in the 3D Figs. (4.2) and (4.3) the velocity distribution depends upon the shape of the channel. Figs. (4.2) and (4.3) illustrates the velocity distribution for distinct values of C and wavy phenomenon becomes obvious on velocity with the increase of the corrugation and the phase difference is 180° between the walls.

The electromagnetohydrodynamic velocity w^\pm distribution for different parameters Ha , Gr , Φ , C , ϕ and B_i are shown in the Figs. (4.4) to (4.9) when we take $\varepsilon = 0.1$ and $\beta = 5$. From these figures, the velocities increase and then decline with the y . Fig. (4.4) shows that the velocity w^\pm increases with increasing Hartmann number Ha . Fig. (4.5) shows that small effect on velocity w^\pm for distinct values values of Gr . Fig. (4.6) displays that w^\pm declines for various values of Φ as a effect of decreasing in heat transfer rate. Fig. (4.7) shows that velocity w^\pm decreases with couple stress parameter C . Fig. (4.8) displays that w^\pm increases for heat absorption coefficient ϕ . Fig. (4.9) illustrates that the velocity w^\pm increases for values of biot number B_i . We found out, the EMHD velocities in phase are weaker than out of phase.

The 2D variation of the EMHD temperature θ^\pm distribution in phase and out phase for parameters ϕ and B_i are exposed in Figs. (4.10) and (4.11). Fig. (4.10) shows that profile of temperature increases when the heat absorption coefficient ϕ are increase. Fig. (4.11) describes the outcome of B_i on temperature. By enlarges value of biot number B_i temperature shows increasing effect.

The impact of mean velocity φ^\pm on EMHD flow of Couple stress fluid discussed in the microchannel through corrugated walls. Table 4.2 and Table 4.3 expressed the behavior of

couple stress parameter and Grashof number on the mean velocity φ^\pm . Table 4.2 demonstrates that mean velocity rises by increasing value of x for couple stress parameter C and Grashof number Gr and the mean velocity φ^+ decreases with the couple stress parameter C and Grashof number Gr . Table 4.3 displays mean velocity φ^- enlarges by increasing value of x for couple stress parameter C and Grashof number Gr and the mean velocity φ^+ increases with the couple stress parameter C and Grashof number Gr .

4.5 Graphs

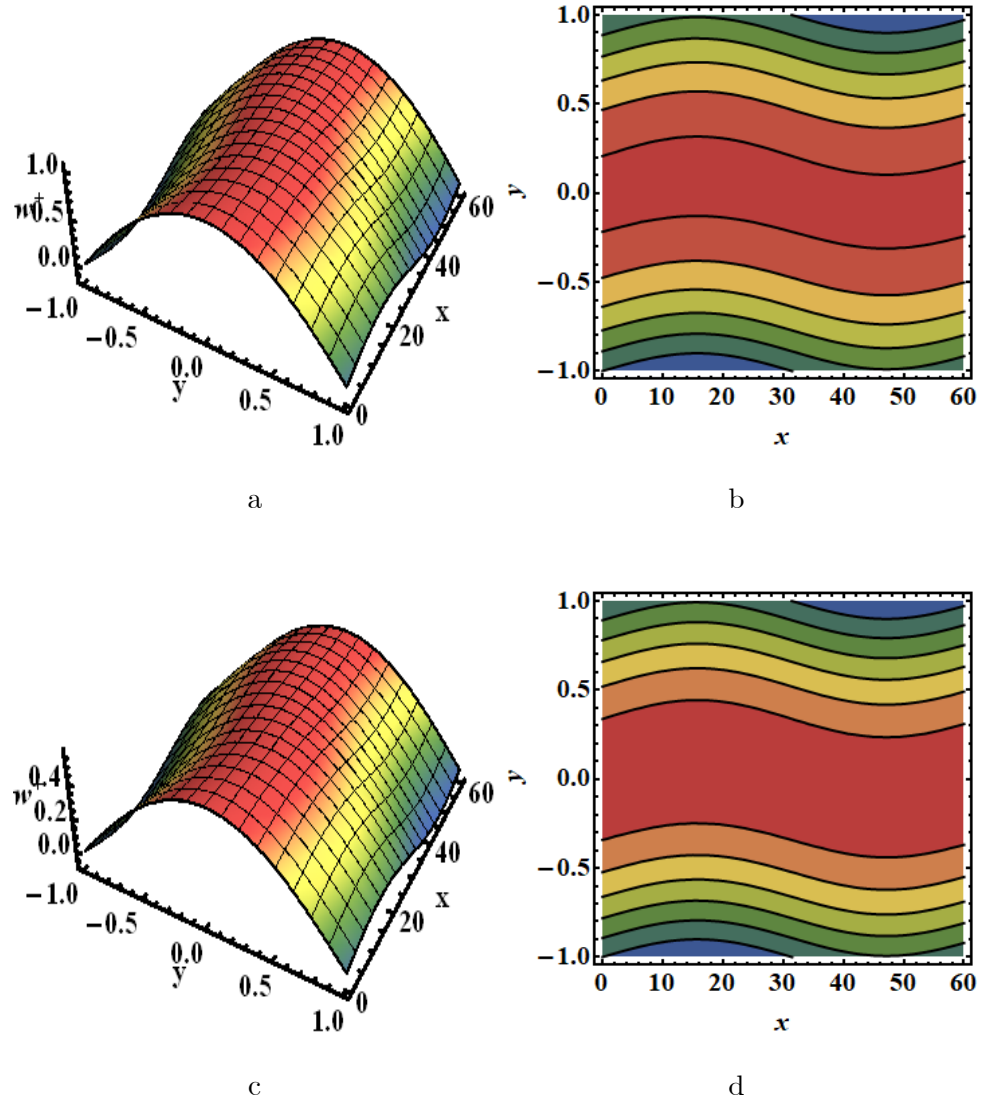


Fig. (4.2): 3D Velocity distribution and contour (a, b, c, d) when fluid parameter $C = 0.5$ and $C = 1.5$ in phase.

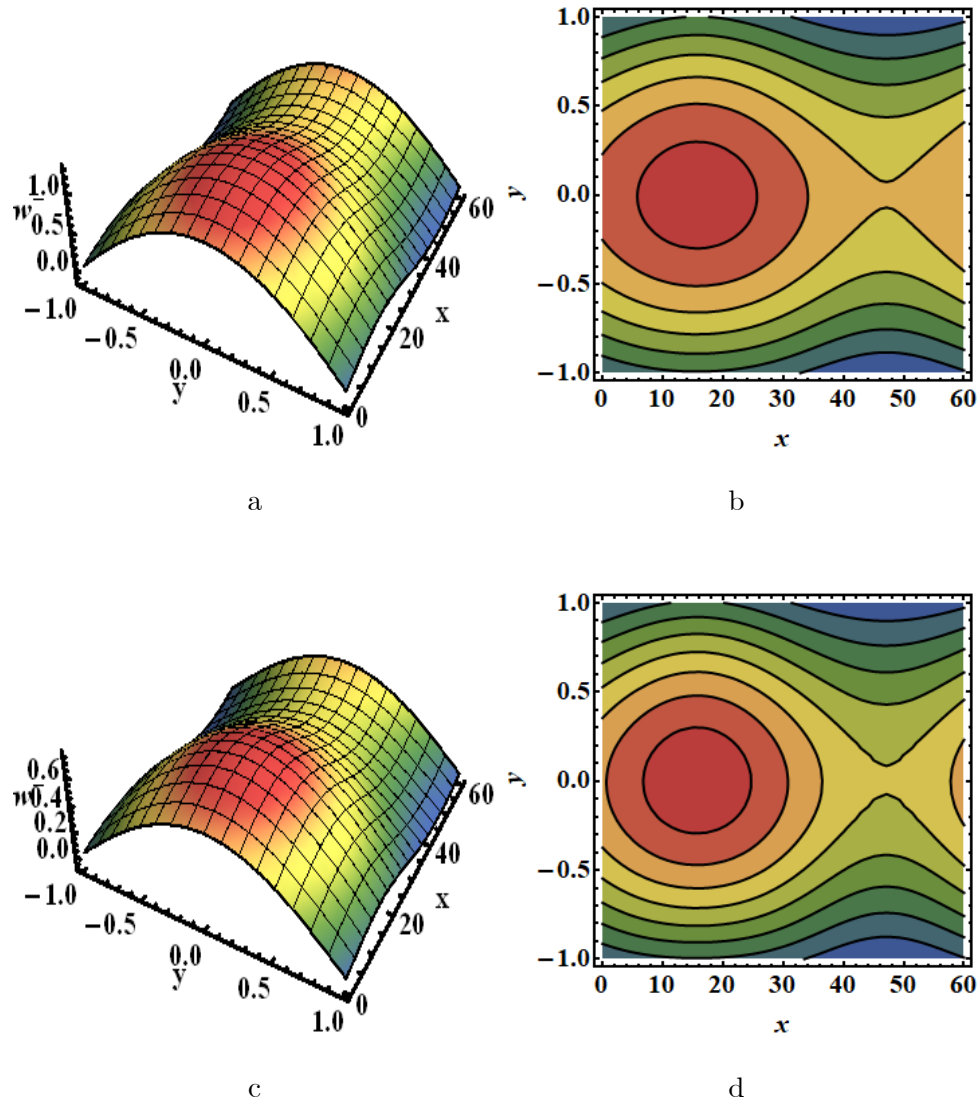


Fig. (4.3): 3D Velocity distribution and contour (a, b, c, d) when fluid parameter $C = 0.5$ and $C = 1.5$ out of phase.

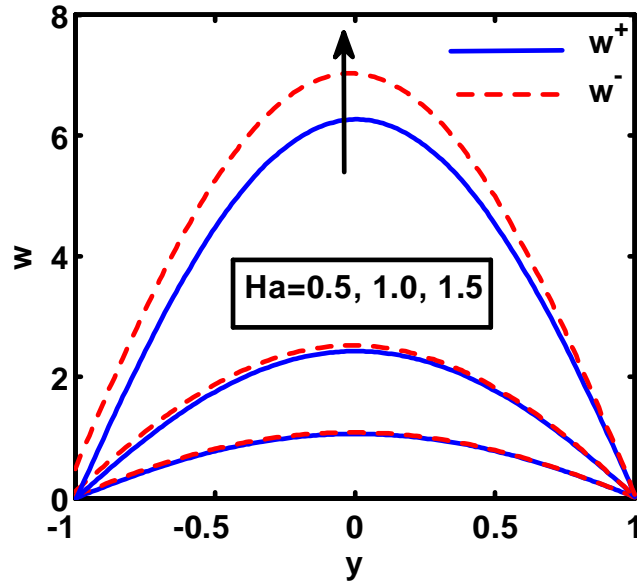


Fig. (4.4): 2D Variation of velocity for hartmann number Ha .

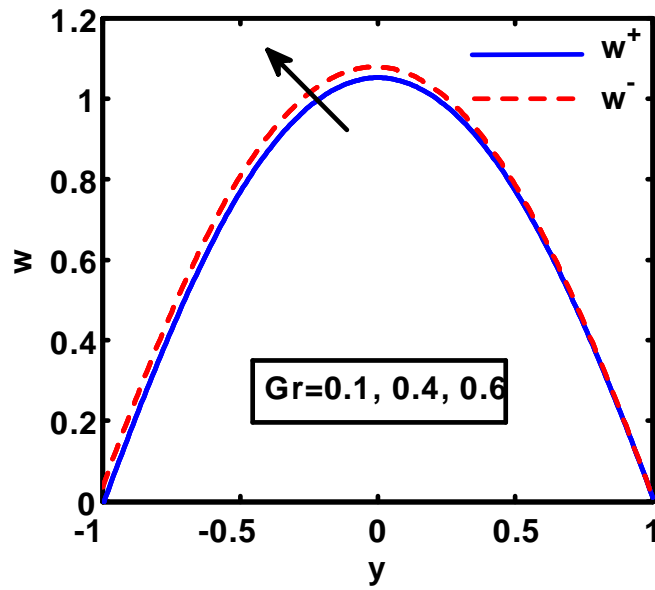


Fig. (4.5): 2D Variation of velocity for Grashof number Gr .

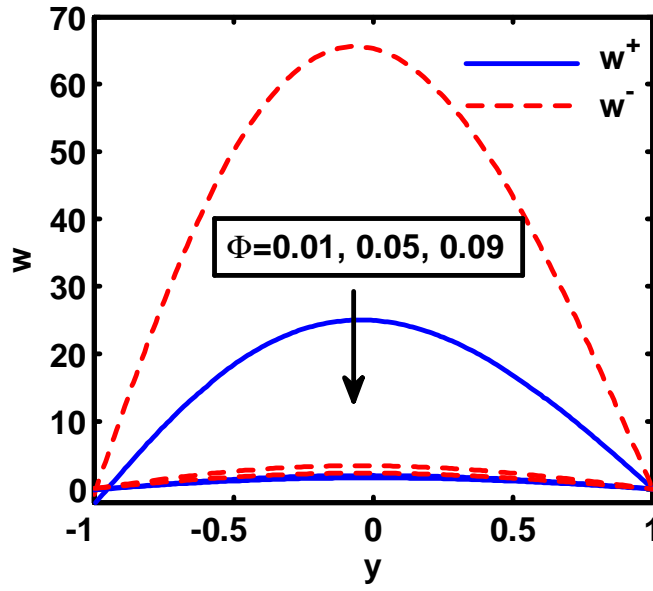


Fig. (4.6): 2D Variation of velocity for nanoparticle volume fraction Φ .

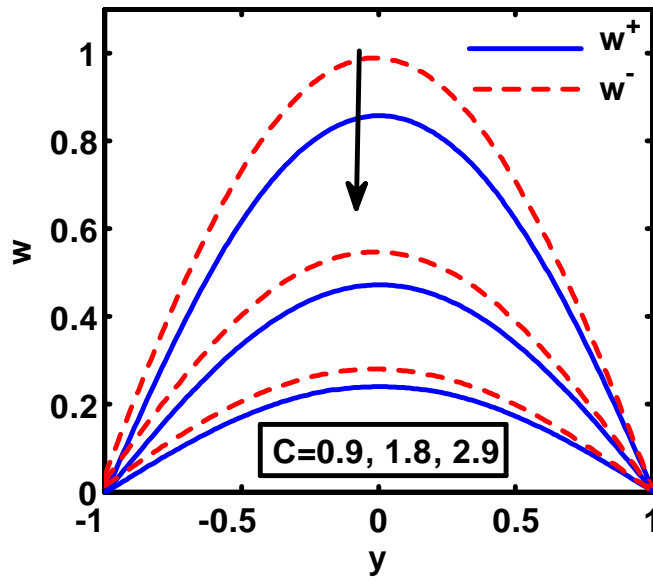


Fig. (4.7): 2D Variation of velocity for couple stress parameter C .

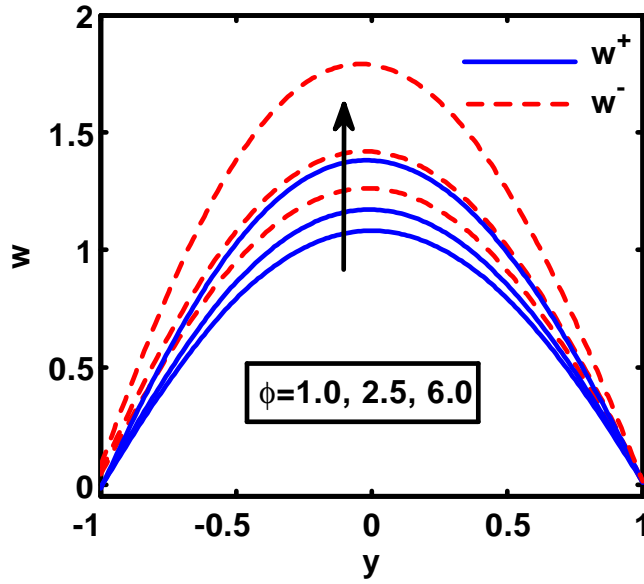


Fig. (4.8): 2D Variation of velocity for heat source coefficient ϕ .

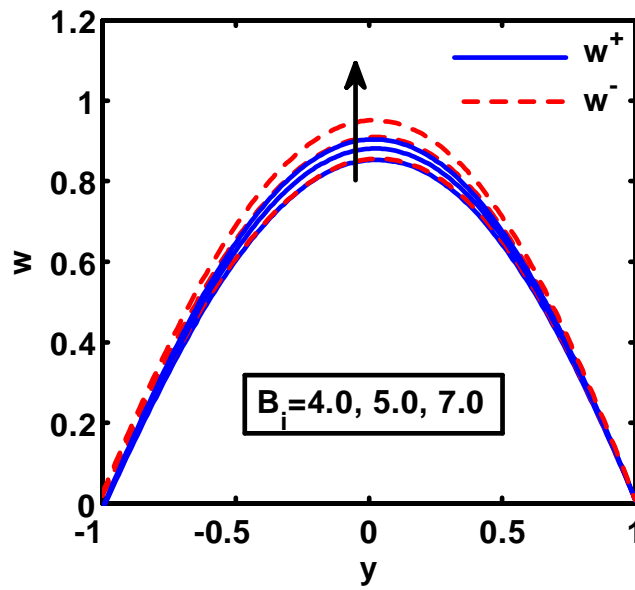


Fig. (4.9): 2D Variation of velocity for biot number B_i .

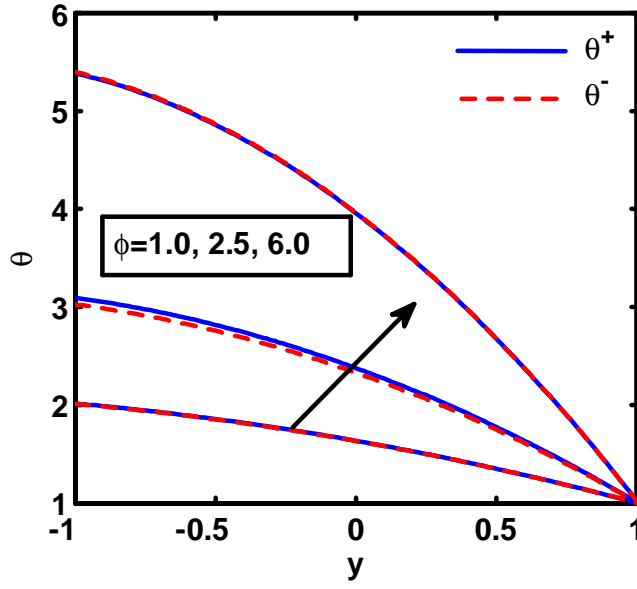


Fig. (4.10): 2D Variation of temperature for heat source coefficient ϕ .

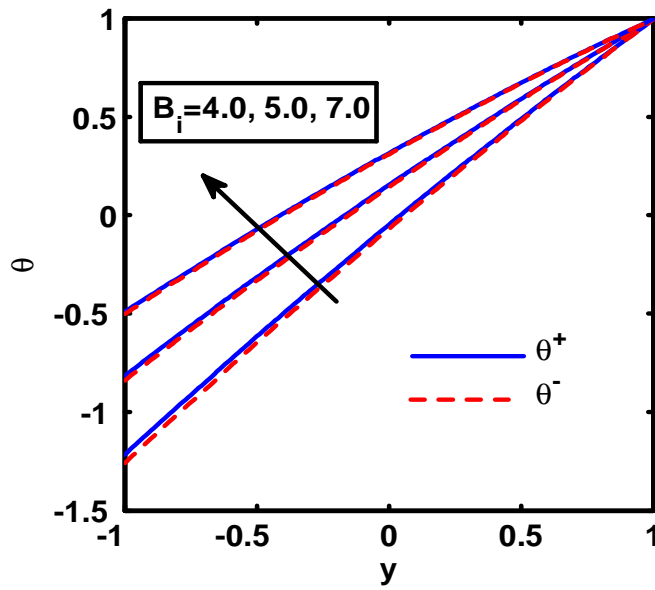


Fig. (4.11): 2D Variation of temperature for biot number B_i .

For Mean velocity φ^+						
x	$C = 0.5$	$C = 1.5$	$C = 2.0$	$Gr = 0.1$	$Gr = 0.4$	$Gr = 0.6$
0	-0.499662	-0.256531	-0.182453	-0.395093	-0.551947	-0.656516
0.1	-0.415546	-0.212912	-0.151429	-0.320551	-0.463044	-0.55804
0.2	-0.333973	-0.170617	-0.121347	-0.248347	-0.376787	-0.462413
0.3	-0.254987	-0.129667	-0.0922233	-0.178519	-0.293221	-0.369688
0.4	-0.178627	-0.0900846	-0.0640716	-0.111105	-0.212388	-0.27991
0.5	-0.104929	-0.0518868	-0.0369053	-0.0461341	-0.134326	-0.19312
0.6	-0.033932	-0.0150902	-0.010736	0.016365	-0.0590674	-0.109356
0.7	0.0343625	0.0202915	0.0144265	0.0763693	0.0133591	-0.0286477
0.8	0.099906	0.0542466	0.0385739	0.133859	0.0829295	0.0489766
0.9	0.162689	0.0867657	0.0616996	0.188819	0.149625	0.123495
1	0.222698	0.117842	0.0837984	0.241236	0.213429	0.194891

Table. (4.2): Effect of fluid parameter C and Grashof number Gr on mean velocity φ^+ .

For Mean velocity φ^-						
x	$C = 0.5$	$C = 1.5$	$C = 2.0$	$Gr = 0.1$	$Gr = 0.4$	$Gr = 0.6$
0	2.77896	2.09495	1.64963	2.35469	2.99109	3.41535
0.1	2.79108	2.09997	1.65245	2.36572	3.00376	3.42913
0.2	2.80039	2.10385	1.65463	2.37426	3.01345	3.43958
0.3	2.80687	2.10658	1.65616	2.38032	3.02015	3.4467
0.4	2.81051	2.10815	1.65703	2.38387	3.02383	3.45047
0.5	2.8113	2.10856	1.65726	2.38491	3.0245	3.45089
0.6	2.80925	2.10781	1.65683	2.38345	3.02215	3.44795
0.7	2.80434	2.10591	1.65574	2.37948	3.01678	3.44165
0.8	2.7966	2.10284	1.65401	2.373	3.0084	3.43201
0.9	2.78603	2.09862	1.65162	2.36403	2.99703	3.41903
1	2.77265	2.09326	1.64859	2.35259	2.98268	3.40274

Table. (4.3): Effect of fluid parameter C and Grashof number Gr on mean velocity φ^- .

4.6 Conclusions

- The main results are briefly explained as
- The shape of channel depends on velocity distribution.
- The velocities profiles in phase and out of phase are asymmetric and symmetric, respectively.
- The unobvious wave effects on the velocity reducing by small value of ε parameter.
- With the increases in Hartmann number velocity field increases.
- Velocity have small impact for various values of Gr .
- EMHD velocity decreases with the increasing nanoparticle volume fraction and couple stress parameter .
- The EMHD velocity increases with the increasing heat absorption coefficient and volume fraction .
- The temperature fields increases for value of heat absorption coefficient and biot number.
- The mean velocity parameter φ^+ decreases with couple stress parameter C and Grashof number Gr .
- The mean velocity parameter φ^- increases with couple stress parameter C and Grashof number Gr .

Chapter 5

Impacts of heat generation and heat flow on $\text{Al}_2\text{O}_3\text{-Cu}$ /water hybrid nanofluid in microchannel under corrugated walls through porous medium

The heat transfer enhancement by using hybrid nanofluid is another class of study to enhance the heat transfer rate is discussed in this chapter. The major purpose of present examination is to observe behaviour of Hybrid nanofluid in microchannel through permeable medium with corrugated walls. Here, we take two dimensional flow of a Hybrid nanofluid $\text{Cu} - \text{Al}_2\text{O}_3/\text{water}$ and nanofluid Cu/water along with casson fluid. This model is employed to inspect the consequence of thermal radiation, heat generation and porous effect in microchannel with corrugated walls. Results for temperature and velocity are calculated. Final section of this paper is devoted for the graphical discussion of velocity, temperature and stream functions.

5.1 Problem formulation

Let us considered electrically conducting and incompressible Casson fluid with electrical conductivity and density for an EMHD flow between corrugated walls of height $2H$. The amplitude of corrugated wall is $0.1H$ and the height of microchannel is supposed to $100\mu m$. With the fixed origin at the center of the microchannel, we choose the Cartesian coordinate system. We take the length L along z^* direction and the width of the channel W along x^* direction, the width and the length much greater than thickness of the layer i.e. $W, L \gg 2H$.

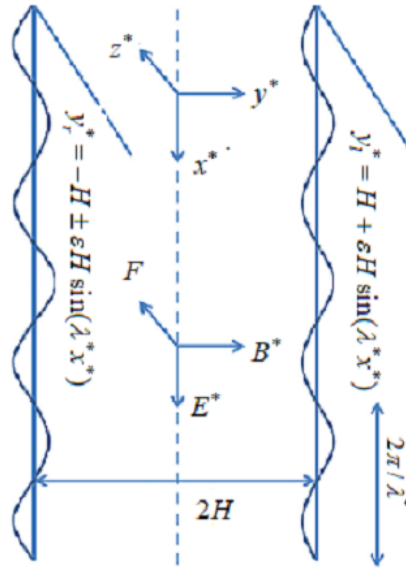


Fig. (5.1): Geometrical sketch of EMHD flow in microchannel.

Along the x^* direction the electric field \mathbf{E}^* is applied while magnetic field \mathbf{B}^* is taken along y^* direction. Lorentz force $\mathbf{J} \times \mathbf{B}^*$ is generated by the magnetic \mathbf{B}^* and electric field \mathbf{E}^* interaction is taken along the z^* direction, where current density is represented by $\mathbf{J} = \sigma(\mathbf{E}^* + \mathbf{u}^* \times \mathbf{B}^*)$.

The rheological equation of Casson fluid is [66]

$$\tau_{ij} = \begin{cases} 2(\mu_\beta + p_y/\sqrt{2\pi})e_{ij}, \pi \succ \pi_c \\ 2(\mu_\beta + p_y/\sqrt{2\pi})e_{ij}, \pi \prec \pi_c \end{cases}, \quad (5.1)$$

where τ_{ij} is the stress tensor component, π is the component of deformation, π_c is critical value, μ_β is the plastic dynamics viscosity and p_y yield stress. Location of right and left wavy walls are

$$y_r^* = -H \pm \varepsilon H \sin(\lambda^* x^*) \quad \text{and} \quad y_l^* = H + \varepsilon H \sin(\lambda^* x^*), \quad (5.2)$$

where ε is small amplitude and λ^* is the wave number.

Velocity field for the fluid is given by

$$\mathbf{u}^* = [0, 0, w^*(x^*, y^*)]. \quad (5.3)$$

The formulated problem for Casson hybrid nanofluid as,

$$\frac{\partial w^*}{\partial z^*} = 0, \quad (5.4)$$

$$-\frac{\partial p}{\partial z^*} + \frac{\partial}{\partial x^*} \tau_{x^* z^*}^* + \frac{\partial}{\partial x^*} \tau_{y^* z^*}^* + \frac{\partial}{\partial x^*} \tau_{z^* z^*}^* + \sigma B^* (E^* - B^* w^*) - \frac{\mu_{hnf}}{k_1} w^* + g(\rho\zeta)_{hnf} (T^* - T_r^*) = 0, \quad (5.5)$$

$$k''_{hnf} \left(\frac{\partial^2 T^*}{\partial x^{*2}} + \frac{\partial^2 T^*}{\partial y^{*2}} \right) + Q_0 (T^* - T_r^*) - \frac{\partial q^*}{\partial y^*}, \quad (5.6)$$

where ρ_{hnf} , ζ_{hnf} and k''_{hnf} are density, thermal expansion and thermal conductivity of hybrid nanofluid respectively. The dimensional coefficient of heat generation/ absorption is represented by Q_0 , q^* is radiative heat flux defined by [87]

$$q^* = \frac{4\sigma^*}{3k^*} \frac{\partial T^{*4}}{\partial y^*}, \quad (5.7)$$

where σ^* , k^* denoted Stefan-Boltzmann value and coefficient of mean absorption. It is supposed that the variations of temperature is small, therefore the term T^{*4} might be written as

$$T^{*4} = 4T^*T_r^{*3} - 3T_r^{*4}. \quad (5.8)$$

The nondimensional parameters utilized in the problem are characterized as pursues:

$$(x, y) = \left(\frac{x^*, y^*}{H}\right), \lambda = \lambda^* H, w = \frac{w^*}{U}, \beta = E_0 \left(\frac{\sigma}{\mu_f}\right)^{\frac{1}{2}} / U, \phi = \frac{Q_0 H^2}{k''_f}, Da = \frac{k_1}{H^2}, \quad (5.9)$$

$$T = T^*, Ha = B^* H \left(\frac{\sigma}{\mu_f}\right)^{\frac{1}{2}}, \theta = \frac{T - T_r}{T_l - T_r}, Gr = \frac{g(\rho\zeta)_f H(T_l - T_r)}{\mu_f U}, R = \frac{4\sigma^* T_r^3}{3k^* k''_f}$$

Dimensionless form of momentum and temperature equations are, we get

$$\left(1 + \frac{1}{\gamma^*}\right) \left(\frac{\partial^2 w}{\partial x^2} + \frac{\partial^2 w}{\partial y^2}\right) - \frac{1}{Da} w + \frac{\mu_f}{\mu_{hnf}} (Ha\beta + Ha^2 w) + \frac{(\rho\zeta)_{hnf}}{(\rho\zeta)_f} Gr\theta = 0, \quad (5.10)$$

$$\frac{k''_{hnf}}{k''_f} \frac{\partial^2 \theta}{\partial x^2} + \left(\frac{k''_{hnf}}{k''_f} + R\right) \frac{\partial^2 \theta}{\partial y^2} + \phi\theta = 0. \quad (5.11)$$

The corresponding non-dimensional boundary conditions are

$$w = 0 \text{ at } y_l = 1 + \varepsilon \sin(\lambda x) \text{ and } y_r = -1 \pm \varepsilon \sin(\lambda x), \quad (5.12)$$

$$\theta = 1 \text{ at } y_l = 1 + \varepsilon \sin(\lambda x), \theta = 0 \text{ at } y_r = -1 \pm \varepsilon \sin(\lambda x). \quad (5.13)$$

In Eqs. (5.12) and (5.13), $y_l = y_l^*/H$, $y_r = y_r^*/H$.

5.2 Solution of Problem

The velocity w and temperature θ are functions of y only when there is no roughness and the existence of surface roughness the x direction variation can also be considered. By assuming small amplitude $\varepsilon \ll 1$, we solve Eqs. (5.10) and (5.11) with the help of perturbation technique by taking small parameter . Then by expanding velocity and temperature function as

$$w(x, y) = w_0(y) + \varepsilon w_1(x, y) + \varepsilon^2 w_2(x, y) + \dots \quad (5.14)$$

$$\theta(x, y) = \theta_0(y) + \varepsilon \theta_1(x, y) + \varepsilon^2 \theta_2(x, y) + \dots \quad (5.15)$$

By utilizing Eqs. (5.14) and (5.15) into Eqs. (5.10) and (5.11), we get

$$\begin{aligned} & \left(\left(1 + \frac{1}{\gamma^*}\right) \left(\frac{\partial^2}{\partial x^2} + \frac{\partial^2}{\partial y^2} \right) - \frac{1}{Da} + \frac{\mu_f}{\mu_{hnf}} Ha^2 \right) (w_0(y) + \varepsilon w_1(x, y) + \varepsilon^2 w_2(x, y) + \dots) \\ & + \frac{\mu_f}{\mu_{hnf}} (Ha\beta) + \frac{(\rho\zeta)_{hnf}}{(\rho\zeta)_f} Gr (\theta_0(y) + \varepsilon \theta_1(x, y) + \varepsilon^2 \theta_2(x, y) + \dots) = 0, \end{aligned} \quad (5.16)$$

$$\left(\frac{k''_{hnf}}{k''_f} \frac{\partial^2}{\partial x^2} + \left(\frac{k''_{hnf}}{k''_f} + R \right) \frac{\partial^2}{\partial y^2} + \phi \right) (\theta_0(y) + \varepsilon \theta_1(x, y) + \varepsilon^2 \theta_2(x, y) + \dots) = 0. \quad (5.17)$$

By using Taylor series, we can expand the boundary conditions (5.12) and (5.13) at $y = 1$ and $y = -1$, respectively

$$\begin{aligned} 0 = w \Big|_{y=1+\varepsilon \sin(\lambda x)} &= (w_0 + \varepsilon w_1 + \varepsilon^2 w_2)_{y=1} + \varepsilon \sin(\lambda x) \\ & \left(\frac{dw_0}{dy} + \varepsilon \frac{\partial w_1}{\partial y} \right)_{y=1} + \frac{\varepsilon^2 \sin^2(\lambda x)}{2} \left(\frac{d^2 w_0}{dy^2} \right)_{y=1} + O(\varepsilon^3), \end{aligned} \quad (5.18)$$

$$\begin{aligned} 0 = w^\pm \Big|_{y=-1 \pm \varepsilon \sin(\lambda x)} &= (w_0 + \varepsilon w_1^\pm + \varepsilon^2 w_2^\pm)_{y=-1} \pm \varepsilon \sin(\lambda x) \\ & \left(\frac{dw_0}{dy} + \varepsilon \frac{\partial w_1}{\partial y} \right)_{y=-1} + \frac{\varepsilon^2 \sin^2(\lambda x)}{2} \left(\frac{d^2 w_0}{dy^2} \right)_{y=-1} + O(\varepsilon^3), \end{aligned} \quad (5.19)$$

$$\begin{aligned} 1 = \theta \Big|_{y=1+\varepsilon \sin(\lambda x)} &= (\theta_0 + \varepsilon \theta_1 + \varepsilon^2 \theta_2)_{y=1} + \varepsilon \sin(\lambda x) \\ & \left(\frac{d\theta_0}{dy} + \varepsilon \frac{\partial \theta_1}{\partial y} \right)_{y=1} + \frac{\varepsilon^2 \sin^2(\lambda x)}{2} \left(\frac{d^2 \theta_0}{dy^2} \right)_{y=1} + O(\varepsilon^3), \end{aligned} \quad (5.20)$$

$$\begin{aligned} 0 = \theta^\pm \Big|_{y=-1 \pm \varepsilon \sin(\lambda x)} &= (\theta_0 + \varepsilon \theta_1^\pm + \varepsilon^2 \theta_2)_{y=-1} \pm \varepsilon \sin(\lambda x) \\ & \left(\frac{d\theta_0}{dy} + \varepsilon \frac{\partial \theta_1}{\partial y} \right)_{y=-1} + \frac{\varepsilon^2 \sin^2(\lambda x)}{2} \left(\frac{d^2 \theta_0}{dy^2} \right)_{y=-1} + O(\varepsilon^3), \end{aligned} \quad (5.21)$$

where the ‘-’ sign in above equation represented half period out of phase and ‘+’ sign is the case for corrugation in phase and by equating the like powers of ε from Eqs. (5.16) to (5.21), the following systems are acquire.

5.2.1 Zero Order classification

The zero order classification given as,

$$\left(\frac{k''_{hnf}}{k''_f} + R\right) \frac{d^2\theta_0}{dy^2} + \phi\theta_0 = 0, \quad (5.22)$$

$$\left(1 + \frac{1}{\gamma^*}\right) \frac{d^2w_0}{dy^2} - \frac{1}{Da}w_0 + \frac{\mu_f}{\mu_{hnf}}(Ha\beta + Ha^2w_0 + \frac{(\rho\zeta)_{hnf}}{(\rho\zeta)_f}Gr\theta_0) = 0, \quad (5.23)$$

with the following boundary conditions

$$\theta_0|_{y=1} = 1, \quad \theta_0|_{y=-1} = 0, \quad (5.24)$$

$$w_0|_{y=1} = 0, \quad w_0|_{y=-1} = 0. \quad (5.25)$$

5.2.2 First Order classification

The first order classification can be expressed as,

$$\frac{k''_{hnf}}{k''_f} \frac{\partial^2\theta_1}{\partial x^2} + \left(\frac{k''_{hnf}}{k''_f} + R\right) \frac{\partial^2\theta_1}{\partial y^2} + \phi\theta_1 = 0, \quad (5.26)$$

$$\left(1 + \frac{1}{\gamma^*}\right) \left(\frac{\partial^2w_1}{\partial x^2} + \frac{\partial^2w_1}{\partial y^2}\right) - \frac{1}{Da}w_1 + \frac{\mu_f}{\mu_{hnf}}(Ha\beta + Ha^2w_1 + \frac{(\rho\zeta)_{hnf}}{(\rho\zeta)_f}Gr\theta_1) = 0, \quad (5.27)$$

with the following boundary conditions

$$\theta_1|_{y=1} = -\sin(\lambda x) \left(\frac{d\theta_0}{dy}\right)_{y=1}, \quad \theta_1^\pm|_{y=-1} = \mp \sin(\lambda x) \left(\frac{d\theta_0}{dy}\right)_{y=-1}, \quad (5.28)$$

$$w_1|_{y=1} = -\sin(\lambda x) \left(\frac{dw_0}{dy}\right)_{y=1}, \quad w_1^\pm|_{y=-1} = \mp \sin(\lambda x) \left(\frac{dw_0}{dy}\right)_{y=-1}. \quad (5.29)$$

5.2.3 Second Order classification

The second order classification can be expressed as

$$\frac{k''_{hnf}}{k''_f} \frac{\partial^2 \theta_2}{\partial x^2} + \left(\frac{k''_{hnf}}{k''_f} + R \right) \frac{\partial^2 \theta_2}{\partial y^2} + \phi \theta_2 = 0, \quad (5.30)$$

$$\left(1 + \frac{1}{\gamma^*}\right) \left(\frac{\partial^2 w_2}{\partial x^2} + \frac{\partial^2 w_2}{\partial y^2} \right) - \frac{1}{Da} w_2 + \frac{\mu_f}{\mu_{hnf}} (Ha\beta + Ha^2 w_2 + \frac{(\rho\zeta)_{hnf}}{(\rho\zeta)_f} Gr \theta_2) = 0, \quad (5.31)$$

with the following boundary conditions

$$\theta_2 \Big|_{y=1} = -\sin(\lambda x) \left(\frac{\partial \theta_1}{\partial y} \right)_{y=1} - \frac{1}{2} \sin^2(\lambda x) \left(\frac{d^2 \theta_0}{dy^2} \right)_{y=1}, \quad (5.32)$$

$$\theta_2^\pm \Big|_{y=-1} = \mp \sin(\lambda x) \left(\frac{\partial \theta_1}{\partial y} \right)_{y=-1} - \frac{1}{2} \sin^2(\lambda x) \left(\frac{d^2 \theta_0}{dy^2} \right)_{y=-1}, \quad (5.33)$$

$$w_2 \Big|_{y=1} = -\sin(\lambda x) \left(\frac{\partial w_1}{\partial y} \right)_{y=1} - \frac{1}{2} \sin^2(\lambda x) \left(\frac{d^2 w_0}{dy^2} \right)_{y=1}, \quad (5.34)$$

$$w_2^\pm \Big|_{y=-1} = \mp \sin(\lambda x) \left(\frac{\partial w_1}{\partial y} \right)_{y=-1} - \frac{1}{2} \sin^2(\lambda x) \left(\frac{d^2 w_0}{dy^2} \right)_{y=-1}. \quad (5.35)$$

Solution of zeroth order

By solving zero order classification with the corresponding boundary conditions from Eqs. (5.22) to (5.25), we obtained

$$\theta_0(y) = e^{-ya_1} A_1 + e^{ya_2} A_2, \quad (5.36)$$

$$w_0(y) = \frac{e^{-yb_1} B_1 + e^{yb_2} B_2 + Da\mu_f(Ha\beta / (-DaHa^2\mu_f + \mu_{hnf}) - e^{-ya_1}(A_1 + A_2 e^{2ya_2})Gr(\rho\zeta)_{hnf} / ((DaHa^2\mu_f + (-1 + Da(1 + \frac{1}{\gamma^*})a_1^2)\mu_{hnf})(\rho\zeta)_f))}{e^{2ya_2})Gr(\rho\zeta)_{hnf} / ((DaHa^2\mu_f + (-1 + Da(1 + \frac{1}{\gamma^*})a_1^2)\mu_{hnf})(\rho\zeta)_f)}, \quad (5.37)$$

with

$$a_1 = \sqrt{\frac{\phi k''_f}{-Rk''_f - k''_{hnf}}}, \quad (5.38)$$

$$b_1 = \sqrt{\frac{DaHa^2\mu_f + \mu_{hnf}}{Da(1 + \frac{1}{\gamma^*})\mu_{hnf}}}.$$

5.2.4 Solution of first order

Within the boundary conditions (5.28) and (5.29), we can assume the solution to the first order classification can be denoted as

$$\theta_1(x, y) = \sin(\lambda x) f(y), \quad (5.39)$$

$$w_1(x, y) = \sin(\lambda x) g(y), \quad (5.40)$$

where $f(y)$ and $g(y)$ are the functions of y .

By employing Eqs. (5.39) and (5.40) into (5.26) to (5.29), we get

$$\left(\frac{k''_{hnf}}{k''_f} + R\right) \frac{d^2 f(y)}{dy^2} - \lambda^2 \frac{k''_{hnf}}{k''_f} f(y) + \phi f(y) = 0, \quad (5.41)$$

$$\left(1 + \frac{1}{\gamma^*}\right) \left(\frac{d^2 g(y)}{dy^2} - \lambda^2 g(y)\right) - \frac{1}{Da} g(y) + \frac{\mu_f}{\mu_{hnf}} (Ha^2 g(y) + \frac{(\rho\zeta)_{hnf}}{(\rho\zeta)_f} Gr f(y)) = 0, \quad (5.42)$$

while boundary conditions yield the following form

$$f_{y=1} = -\frac{d\theta_0}{dy}, \quad f_{y=-1}^{\pm} = \mp \frac{d\theta_0}{dy}, \quad (5.43)$$

$$g_{y=1} = -\frac{dw_0}{dy}, \quad g_{y=-1}^{\pm} = \mp \frac{dw_0}{dy}. \quad (5.44)$$

By using the boundary conditions (5.43) and (5.44), the solution of (5.41) and (5.42) is directly obtained as

$$f^{\pm}(y) = \begin{aligned} & e^{-a_2 y} C_1 + e^{a_2 y} C_2, \\ & e^{-a_2 y} C'_1 + e^{a_2 y} C'_2, \end{aligned} \quad (5.45)$$

$$g_y^{\pm} = \begin{aligned} & e^{-b_2 y} D_1 + e^{b_2 y} D_2 - (Dae^{-ya_2}(C_1 + C_2 e^{2a_2 y}) Gr \mu_f (\rho\zeta)_{hnf} / \\ & ((DaHa^2 \mu_f + (-1 - Da(1 + \frac{1}{\gamma^*})(\lambda^2 - a_2^2)) \mu_{hnf})(\rho\zeta)_f)), \\ & e^{-b_2 y} D'_1 + e^{b_2 y} D'_2 - (Dae^{-ya_2}(C'_1 + C'_2 e^{2a_2 y}) Gr \mu_f (\rho\zeta)_{hnf} / \\ & ((DaHa^2 \mu_f + (-1 - Da(1 + \frac{1}{\gamma^*})(\lambda^2 - a_2^2)) \mu_{hnf})(\rho\zeta)_f)) \end{aligned} \quad (5.46)$$

where

$$\begin{aligned} a_2 &= \sqrt{\frac{-\phi k''_f + \lambda^2 k''_{hnf}}{R k''_f + k''_{hnf}}} \\ b_2 &= \sqrt{\frac{-DaHa^2\mu_f + \mu_{hnf} + Da(1 + \frac{1}{\gamma^*})\lambda^2\mu_{hnf}}{Da(1 + \frac{1}{\gamma^*})\mu_{hnf}}} \end{aligned} \quad (5.47)$$

The first order solutions finally take the form

$$\theta_1^\pm(x, y) = \begin{cases} \sin(\lambda x) (e^{-a_2 y} C_1 + e^{a_2 y} C_2), \\ \sin(\lambda x) (e^{-a_2 y} C'_1 + e^{a_2 y} C'_2), \end{cases} \quad (5.48)$$

$$w_1^\pm(x, y) = \begin{cases} \sin(\lambda x) (e^{-b_2 y} D_1 + e^{b_2 y} D_2 - (Da e^{-y a_2} (C_1 + C_2 e^{2a_2 y}) \setminus \mu_f(\rho\zeta)_{hnf} \\ Gr / ((DaHa^2\mu_f + (-1 - Da(1 + \frac{1}{\gamma^*})(\lambda^2 - a_2^2))\mu_{hnf})(\rho\zeta)_f))), \\ \sin(\lambda x) (e^{-b_2 y} D'_1 + e^{b_2 y} D'_2 - (Da e^{-y a_2} (C'_1 + C'_2 e^{2a_2 y}) \mu_f(\rho\zeta)_{hnf} \\ Gr / ((DaHa^2\mu_f + (-1 - Da(1 + \frac{1}{\gamma^*})(\lambda^2 - a_2^2))\mu_{hnf})(\rho\zeta)_f))). \end{cases} \quad (5.49)$$

5.2.5 Solution of second order

On the base of zeroth order solutions (5.36) and (5.37) and first order solutions (5.48) and (5.49), we can assume second order solutions as

$$\theta_2^\pm(x, y) = h^\pm(y) + \cos(2\lambda x) k^\pm(y), \quad (5.50)$$

$$w_2^\pm(x, y) = m^\pm(y) + \cos(2\lambda x) n^\pm(y). \quad (5.51)$$

By putting Eqs. (5.50) and (5.51) into (5.30) to (5.35), we obtained

$$\left(\frac{k''_{hnf}}{k''_f} + R\right) \frac{d^2 h^\pm(y)}{dy^2} + \phi h^\pm(y) = 0, \quad (5.52)$$

$$\left(\frac{k''_{hnf}}{k''_f} + R\right) \frac{d^2 k^\pm(y)}{dy^2} - 4\lambda^2 \frac{k''_{hnf}}{k''_f} k^\pm(y) + \phi k^\pm(y) = 0, \quad (5.53)$$

$$\left(1 + \frac{1}{\gamma^*}\right) \frac{d^2 m^\pm(y)}{dy^2} - \frac{1}{Da} m^\pm(y) + \frac{\mu_f}{\mu_{hnf}} (Ha^2 m^\pm(y) + \frac{(\rho\zeta)_{hnf}}{(\rho\zeta)_f} Gr h^\pm(y)) = 0. \quad (5.54)$$

$$(1 + \frac{1}{\gamma^*}) (\frac{d^2 n^\pm(y)}{dy^2} - 4\lambda^2 n^\pm(y)) - \frac{1}{Da} n^\pm(y) + \frac{\mu_f}{\mu_{hnf}} (Ha^2 n^\pm(y) + \frac{(\rho\zeta)_{hnf}}{(\rho\zeta)_f} Gr k^\pm(y)) = 0. \quad (5.55)$$

The relevant boundary conditions are

$$h^\pm = -\frac{1}{2} (\frac{df}{dy} + \frac{1}{2} \frac{d^2\theta_0}{dy^2}) \text{ at } y = 1, -\frac{1}{2} (\pm \frac{df}{dy} - \frac{1}{2} \frac{d^2\theta_0}{dy^2}) \text{ at } y = -1, \quad (5.56)$$

$$k^\pm = \frac{1}{2} (\frac{df}{dy} + \frac{1}{2} \frac{d^2\theta_0}{dy^2}) \text{ at } y = 1, -\frac{1}{2} (\pm \frac{df}{dy} - \frac{1}{2} \frac{d^2\theta_0}{dy^2}) \text{ at } y = -1, \quad (5.57)$$

$$m^\pm = -\frac{1}{2} (\frac{dg}{dy} + \frac{1}{2} \frac{d^2w_0}{dy^2}) \text{ at } y = 1, -\frac{1}{2} (\pm \frac{dg}{dy} - \frac{1}{2} \frac{d^2w_0}{dy^2}) \text{ at } y = -1, \quad (5.58)$$

$$n^\pm = \frac{1}{2} (\frac{dg}{dy} + \frac{1}{2} \frac{d^2w_0}{dy^2}) \text{ at } y = 1, -\frac{1}{2} (\pm \frac{dg}{dy} - \frac{1}{2} \frac{d^2w_0}{dy^2}) \text{ at } y = -1. \quad (5.59)$$

By utilizing the boundary conditions (5.56) to (5.59) and (5.52) to (5.55), the solutions are

$$h^\pm(y) = \begin{aligned} & e^{-a_1 y} E_1 + e^{a_1 y} E_2, \\ & e^{-a_1 y} E'_1 + e^{a_1 y} E'_2, \end{aligned} \quad (5.60)$$

$$k^\pm(y) = \begin{aligned} & \sin(a_3 y) G_1 + \cos(a_3 y) G_2, \\ & \sin(a_3 y) G'_1 + \cos(a_3 y) G'_2, \end{aligned} \quad (5.61)$$

$$m^\pm(y) = \begin{aligned} & e^{-b_1 y} F_1 + e^{b_1 y} F_2 - (Dae^{-y a_1} (E_1 + E_2 e^{2a_1 y}) Gr(\rho\zeta)_{hnf} \\ & \mu_f / ((DaHa^2 \mu_f + (-1 + Da(1 + \frac{1}{\gamma^*}) a_1^2 \mu_{hnf})(\rho\zeta)_f)), \\ & e^{-b_1 y} F'_1 + e^{b_1 y} F'_2 - (Dae^{-y a_1} (E'_1 + E'_2 e^{2a_1 y}) Gr(\rho\zeta)_{hnf} \\ & \mu_f / ((DaHa^2 \mu_f + (-1 + Da(1 + \frac{1}{\gamma^*}) a_1^2 \mu_{hnf})(\rho\zeta)_f)). \end{aligned} \quad (5.62)$$

$$n^\pm(y) = \begin{aligned} & e^{-b_3 y} H_1 + e^{b_3 y} H_2 - (Dae^{-y a_1} (\sin(a_3 y) G_1 + \cos(a_3 y) G_2) (\rho\zeta)_{hnf} \\ & \mu_f / ((DaHa^2 \mu_f - (1 + Da(1 + \frac{1}{\gamma^*}) (4\lambda^2 + a_3^2) \mu_{hnf})(\rho\zeta)_f)), \\ & e^{-b_3 y} H'_1 + e^{b_3 y} H'_2 - (Dae^{-y a_1} (\sin(a_3 y) G'_1 + \cos(a_3 y) G'_2) (\rho\zeta)_{hnf} \\ & \mu_f / ((DaHa^2 \mu_f - (1 + Da(1 + \frac{1}{\gamma^*}) (4\lambda^2 + a_3^2) \mu_{hnf})(\rho\zeta)_f)), \end{aligned} \quad (5.63)$$

with

$$\begin{aligned} a_3 &= \sqrt{\frac{\phi k_f'' - 4\lambda^2 k_{hnf}''}{Rk_f'' + k_{hnf}''}}, \\ b_3 &= \sqrt{\frac{-DaHa^2\mu_f + \mu_{hnf} + 4Da(1 + \frac{1}{\gamma^*})\lambda^2\mu_{hnf}}{Da(1 + \frac{1}{\gamma^*})\mu_{hnf}}}. \end{aligned} \quad (5.64)$$

The second order solutions finally take the form

$$\begin{aligned} \theta_2^\pm &= e^{-a_1 y} E_1 + e^{a_1 y} E_2 + \cos(2\lambda x) (\sin(a_3 y) G_1 + \cos(a_3 y) G_2), \\ &e^{-a_1 y} E'_1 + e^{a_1 y} E'_2 + \cos(2\lambda x) (\sin(a_3 y) G'_1 + \cos(a_3 y) G'_2), \end{aligned} \quad (5.65)$$

$$\begin{aligned} w_2^\pm &= e^{-b_1 y} F_1 + e^{b_1 y} F_2 - (Dae^{-ya_1} (E_1 + E_2 e^{2a_1 y}) Gr(\rho\zeta)_{hnf} \mu_f / ((DaHa^2\mu_f + (-1 + Da \\ &(1 + \frac{1}{\gamma^*})a_1^2\mu_{hnf})(\rho\zeta)_f)) + \cos(2\lambda x) e^{-b_3 y} H_1 + e^{b_3 y} H_2 - (Dae^{-ya_1} (\sin(a_3 y) G_1 + \\ &\cos(a_3 y) G_2)(\rho\zeta)_{hnf} \mu_f / ((DaHa^2\mu_f - (1 + Da(1 + \frac{1}{\gamma^*}))(4\lambda^2 + a_3^2)\mu_{hnf})(\rho\zeta)_f)), \\ &e^{-b_1 y} F'_1 + e^{b_1 y} F'_2 - (Dae^{-ya_1} (E'_1 + E'_2 e^{2a_1 y}) Gr(\rho\zeta)_{hnf} \mu_f / ((DaHa^2\mu_f + (-1 + Da \\ &(1 + \frac{1}{\gamma^*})a_1^2)\mu_{hnf})(\rho\zeta)_f)) + \cos(2\lambda x) e^{-b_3 y} H'_1 + e^{b_3 y} H'_2 - (Dae^{-ya_1} (\sin(a_3 y) G'_1 + \\ &\cos(a_3 y) G'_2)(\rho\zeta)_{hnf} \mu_f / ((DaHa^2\mu_f - (1 + Da(1 + \frac{1}{\gamma^*}))(4\lambda^2 + a_3^2)\mu_{hnf})(\rho\zeta)_f)). \end{aligned} \quad (5.66)$$

By collection of Eqs. (5.36), (5.37), (5.48), (5.49), (5.65) and (5.66), we obtain the approximate velocity and temperature solution as

$$\theta^\pm(x, y) = \theta_0(y) + \varepsilon\theta_1^\pm(x, y) + \varepsilon^2\theta_2^\pm(x, y) + \dots \quad (5.67)$$

$$w^\pm(x, y) = w_0(y) + \varepsilon w_1^\pm(x, y) + \varepsilon^2 w_2^\pm(x, y) + \dots \quad (5.68)$$

5.2.6 Volume flow rate

We can define volume flow rate as

$$q^\pm(x) = \int_{-1 \pm \varepsilon \sin(\lambda x)}^{1 + \varepsilon \sin(\lambda x)} w^\pm(x, y) dy. \quad (5.69)$$

Utilizing Eq.(5.68) into (5.69) and by using Taylor series we can expand the integral results in x and third order term neglecting, we finally obtained the expression of volume flow as

$$q^\pm(x) = \int_{-1}^1 w_0(y)dy + \varepsilon \int_{-1}^1 w_1^\pm(x, y)dy + \varepsilon^2 \left(\int_{-1}^1 w_2^\pm(x, y)dy + \sin(\lambda x) [w_1^\pm(x, y) |_{y=1} \mp w_1^\pm(x, y) |_{y=-1}] + \frac{1}{2} \sin^2(\lambda x) \left(\frac{dw_0(y)}{dy} |_{y=1} - \frac{dw_0(y)}{dy} |_{y=-1} \right) \right). \quad (5.70)$$

5.2.7 Mean velocity

Mean velocity over one wavelength $(0, 2\pi/\lambda)$ on averaging of the corrugations, can be evaluated as

$$w_m^\pm = \frac{\lambda}{4\pi} \int_{-1 \pm \varepsilon \sin(\lambda x)}^{1 + \varepsilon \sin(\lambda x)} \int_0^{\frac{2\pi}{\lambda}} w^\pm(x, y) dx dy. \quad (5.71)$$

By putting Eq. (5.70) into Eq. (5.71), the mean velocity becomes

$$w_m^\pm = \frac{\lambda}{4\pi} \int_0^{\frac{2\pi}{\lambda}} q^\pm(x) dx = w_{0m} [1 + \varepsilon^2 \varphi^\pm + O(\varepsilon^4)], \quad (5.72)$$

where w_{0m} shows the mean velocity for perfectly smooth walls and φ^\pm denotes the leading order perturbations to mean velocity due to the corrugations. When φ^\pm be negative then mean velocity decreased while for positive φ^\pm the mean velocity increases.

5.2.8 Heat transfer rate

Nusselt number determines the convective heat exchange strength, and is expressed as follows [86]

$$Nu^\pm = \frac{Hq_w}{k''_f(T_l^* - T_r^*)}, \quad (5.73)$$

where

$$q_w = -k''_{nf} \frac{\partial T^*}{\partial y^*} |_{y^*=y_l^*}. \quad (5.74)$$

From Eqs. (5.73) and (5.74), we get

$$Nu^\pm = -\frac{k''_{nf}}{k''_f} \frac{\partial \theta}{\partial y} \Big|_{y=y_i} . \quad (5.75)$$

5.3 Thermophysical properties

The thermophysical properties are

Physical Properties	Fluid Phase (water)	Al ₂ O ₃	Copper
$\rho(kg/m^3)$	997.1	3970	8933
$k''(W/mK)$	0.613	40	400
$\zeta \times 10^5 (1/K)$	21.0	5.1	1.67

Table (5.1): Thermo physical properties.

Properties		Nanofluid (Cu-water)
Density (ρ)		$\rho_{nf} = (1 - \Phi_1)\rho_f + \Phi_1\rho_{s1}$
Viscosity (μ)		$\mu_{nf} = \frac{\mu_f}{(1-\Phi_1)^{2.5}}$
Thermal expansion (ζ)		$\zeta_{nf} = (1 - \Phi_1)\zeta_f + \Phi_1\zeta_{s1}$
Thermal conductivity (k'')		$\frac{k''_{nf}}{k''_f} = \frac{k''_{s1} + (n-1)k''_f - (n-1)\Phi_1(k''_f - k''_{s1})}{k''_{s1} + (n-1)k''_f + \Phi_1(k''_f - k''_{s1})}$
Properties		Hybrid Nanofluid (Al ₂ O ₃ –water)
Density (ρ)		$\rho_{hnf} = ((1 - \Phi_2)((1 - \Phi_1)\rho_f + \Phi_1\rho_{s1}) + \Phi_2\rho_{s2})$
Viscosity (μ)		$\mu_{hnf} = \frac{\mu_f}{(1-\Phi_1)^{2.5}(1-\Phi_2)^{2.5}}$
Thermal expansion (ζ)		$\zeta_{hnf} = ((1 - \Phi_2)((1 - \Phi_1)\zeta_f + \Phi_1\zeta_{s1}) + \Phi_2\zeta_{s2})$
Thermal conductivity (k'')		$\frac{k''_{hnf}}{k''_{bf}} = \frac{k''_{s2} + (n-1)k''_{bf} - (n-1)\Phi_2(k''_{bf} - k''_{s2})}{k''_{s2} + (n-1)k''_{bf} + \Phi_2(k''_{bf} - k''_{s2})}$ where $\frac{k''_{bf}}{k''_f} = \frac{k''_{s1} + (n-1)k''_f - (n-1)\Phi_1(k''_f - k''_{s1})}{k''_{s1} + (n-1)k''_f + \Phi_1(k''_f - k''_{s1})}$

Table (5.2): Thermo physical properties.

For the nanoparticles, we take the $n = 3$. The subscripts of the parameters s_1 , s_2 , f , hnf and nf represent the solid nanoparticle of copper, alumina, fluid, hybrid nanofluid and nanofluid respectively. The thermophysical characteristics of fluid at 25°C and particles are given in Table 5.1.

5.4 Graphical consequence

This portion dedicated for investigation of the copper and aluminum oxide nanoparticles for some emerging parameters of flow on corrugated walls under porous effect through the graph of stream line, velocity and temperature profile. half height of channel is $H \sim 100\mu m$, for the general microfluidic analysis. The electrical conductivity $\sigma \sim 2.2 \times 10^{-4} - 10^6 Sm^{-1}$, if the magnetic field range is the $O(B^*) \sim 0.018 - 0.44T$, the order of Hartmann number between 0.0001 to 3. The graphs are drawn by taking the parameters constants, for example, $0.005 \preceq \Phi_2 \preceq 0.09$, $\Phi_1 = 0.1, \beta = 5$.

We describe the graphical effects of velocity and temperature for the distinct values of Grashof number Gr , Casson parameter γ^* , heat generation ϕ , darcy number Da , Φ_2 , radiation parameter R . We set $\varepsilon = 0.1$ as a small parameter because small parameter ε reducing the unobvious effects.

In 3D (three-dimensional) disparity and contour of velocity and temperature for hybrid nanofluid and nanofluid for radiation parameter R are shown in Figs. (5.2) to (5.9), respectively. In 3D Figs. (5.2), (5.4) and (5.6), (5.8), the phase difference between the walls is 0° . In 3D Figs. (5.3), (5.5) and (5.7), (5.9), the phase difference between the walls is 180° . In three dimensional graphs of Figs. (5.2) and (5.6) shown the consequence of radiation parameter R on velocity and temperature for nanofluid and Figs. (5.4) and (5.8) shown the consequence of radiation parameter on w and θ for hybrid nanofluid, the effect of corrugation are more prominent for hybrid nanofluid as compare to nanofluid is in phase. In three dimensional graphs of Figs. (5.3) and (5.7) shown the impact radiation parameter R on velocity and temperature for nanofluid and Figs. (5.5) and (5.9) shown the outcome radiation parameter R on velocity and temperature for hybrid nanofluid, the effect of corrugation are more prominent for nanofluid as compare to hybrid nanofluid is out of phase. The wavy phenomenon of the distribution of velocity and temperature becomes clear in Figs. (5.2) to (5.9) with increase of the corrugation, especially when the phase difference between the two walls is 180° .

The 2D (two-dimensional) variations of the EMHD velocity w^\pm in phase and out phase for Grashof number Gr , Casson parameter γ^* , Heat source parameter ϕ , Darcy number Da , nanoparticle volume fraction Φ_2 , Radiation parameter R are represents in the Figs. (5.10) to (5.15) by taking $\varepsilon = 0.1$ and $\beta = 5$. From these Figs., the velocities at first grow and then reduce.

Particularly, Figs. (5.10) and (5.11) shown the distinction of velocity profiles for the Grashof number Gr and Casson parameter γ^* . Velocity plots grow rapidly for nanofluid (Cu /water) as contrary to hybrid nanofluid ($Cu - Al_2O_3$ /water) by expanding the estimations of Gr and γ^* . Figs. (5.12) and (5.13) demonstrated the velocity plots for ϕ and Da . Velocity plot enlarge quickly for nanofluid (Cu /water) as related to hybrid nanofluid ($Cu - Al_2O_3$ /water) by expanding ϕ and Da . Figs. (5.14) and (5.15) shown the disparity of velocity for the distinct result of nanoparticle volume fraction Φ_2 and Radiation parameter R . It is seen that velocity plots reduced for hybrid nanofluid ($Cu - Al_2O_3$ /water) rapidly as compared to nanofluid (Cu /water) by increasing the values of nanoparticle volume fraction Φ_2 and Radiation parameter R . We can observe that, the EMHD velocities in phase are weaker than out of phase.

The 2D (two-dimensional) disparity of the EMHD temperature for non-dimensional parameters heat source parameter ϕ and radiation parameter R and at the point $x = 0.5$ and $y = 0$ are shown in the Figs. (5.16) and (5.17). For various values of heat source parameter ϕ , Fig. (5.16) describes the variation of the temperature. With increment in heat source parameter ϕ , there is an increase in temperature θ^\pm . Fig. (5.17) shows that for different values radiation parameter R temperature θ^\pm decreases.

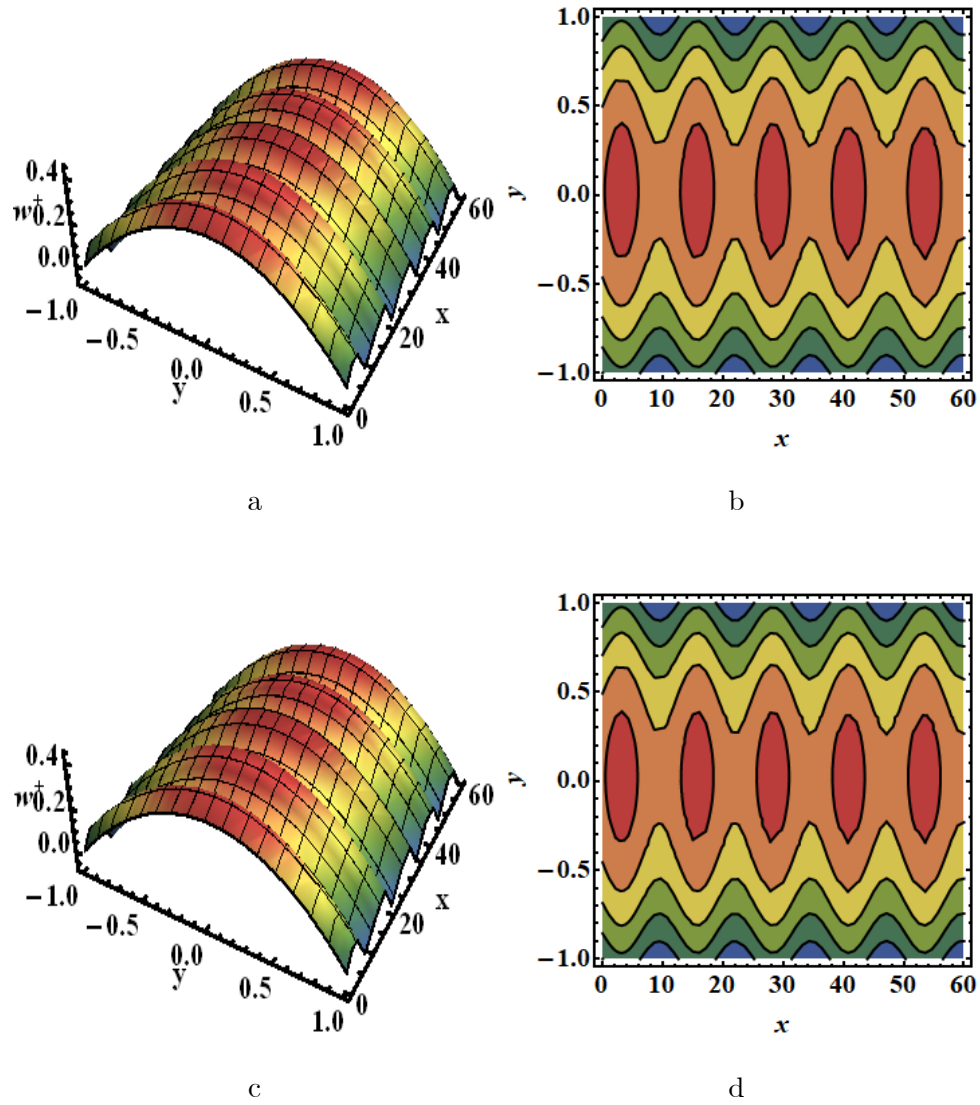


Fig. (5.2): 3D Velocity distribution and contour (a, b, c, d) for $R = 0.5$ and $R = 2$ in phase for nanofluid.

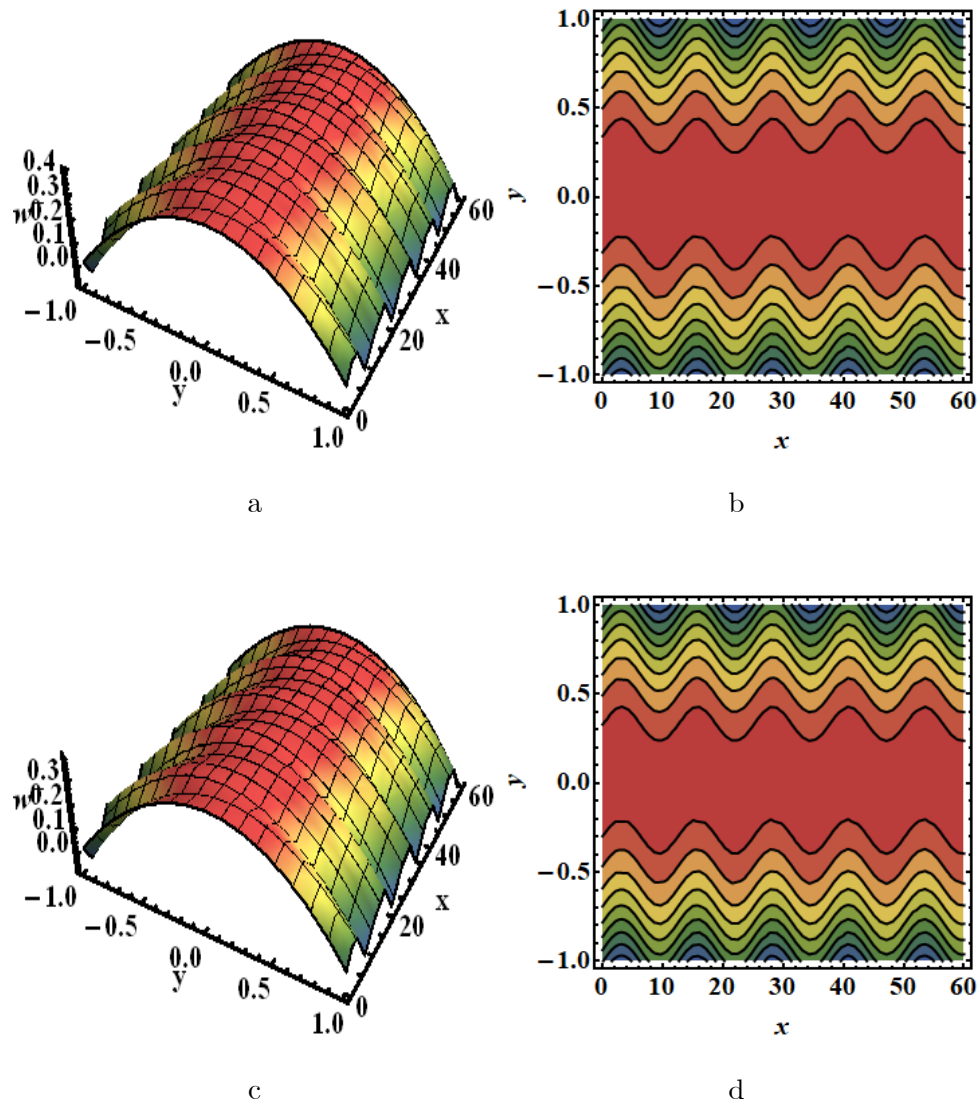


Fig. (5.3): 3D Velocity distribution and contour (a, b, c, d) for $R = 0.5$ and $R = 2$ out of phase for nanofluid.

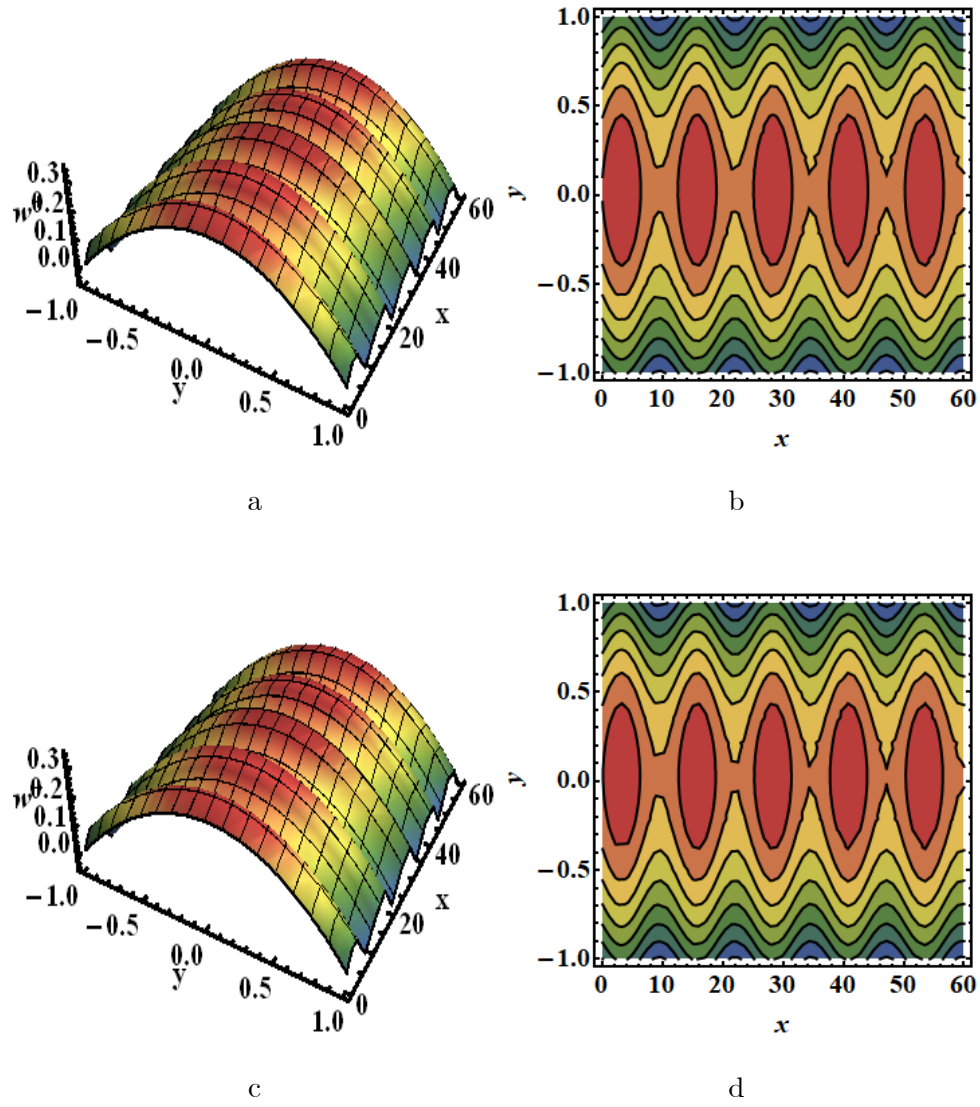


Fig. (5.4): 3D Velocity distribution and contour (a, b, c, d) for $R = 0.5$ and $R = 2$ in phase for hybrid nanofluid.

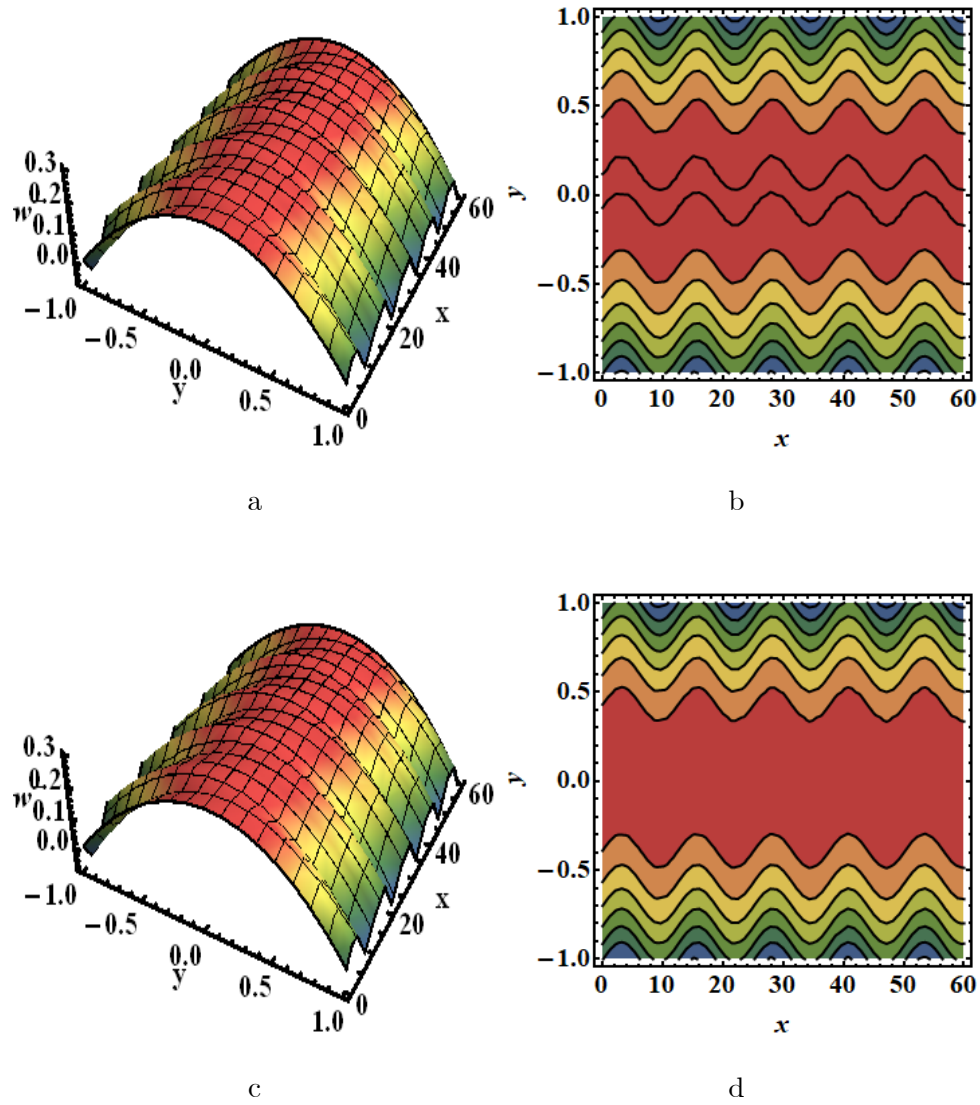


Fig. (5.5): 3D Velocity distribution and contour (a, b, c, d) for $R = 0.5$ and $R = 2$ out of phase for hybrid nanofluid.

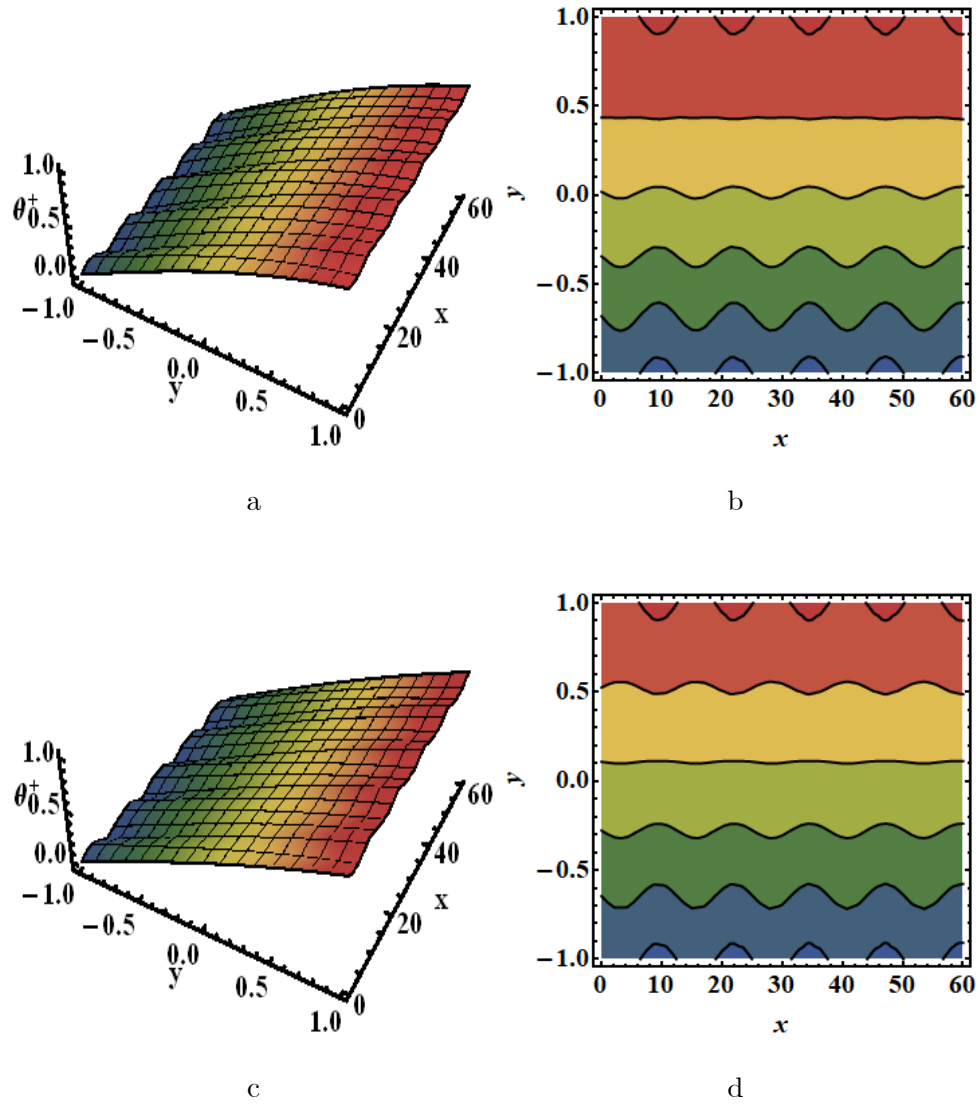


Fig. (5.6): 3D Temperature distribution and contour (a, b, c, d) for $R = 0.5$ and $R = 2$ in phase for nanofluid.

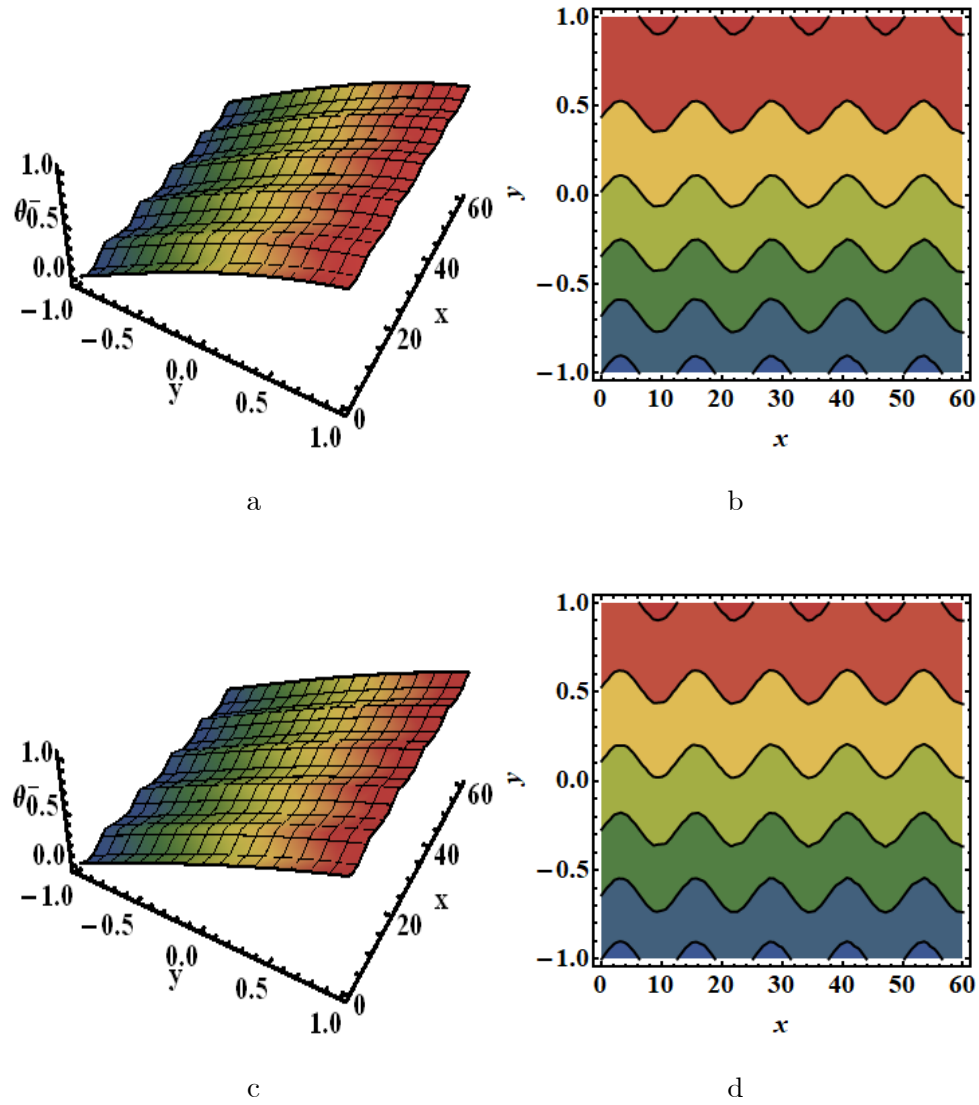


Fig. (5.7): 3D Temperature distribution and contour (a, b, c, d) for $R = 0.5$ and $R = 2$ out of phase for nanofluid.

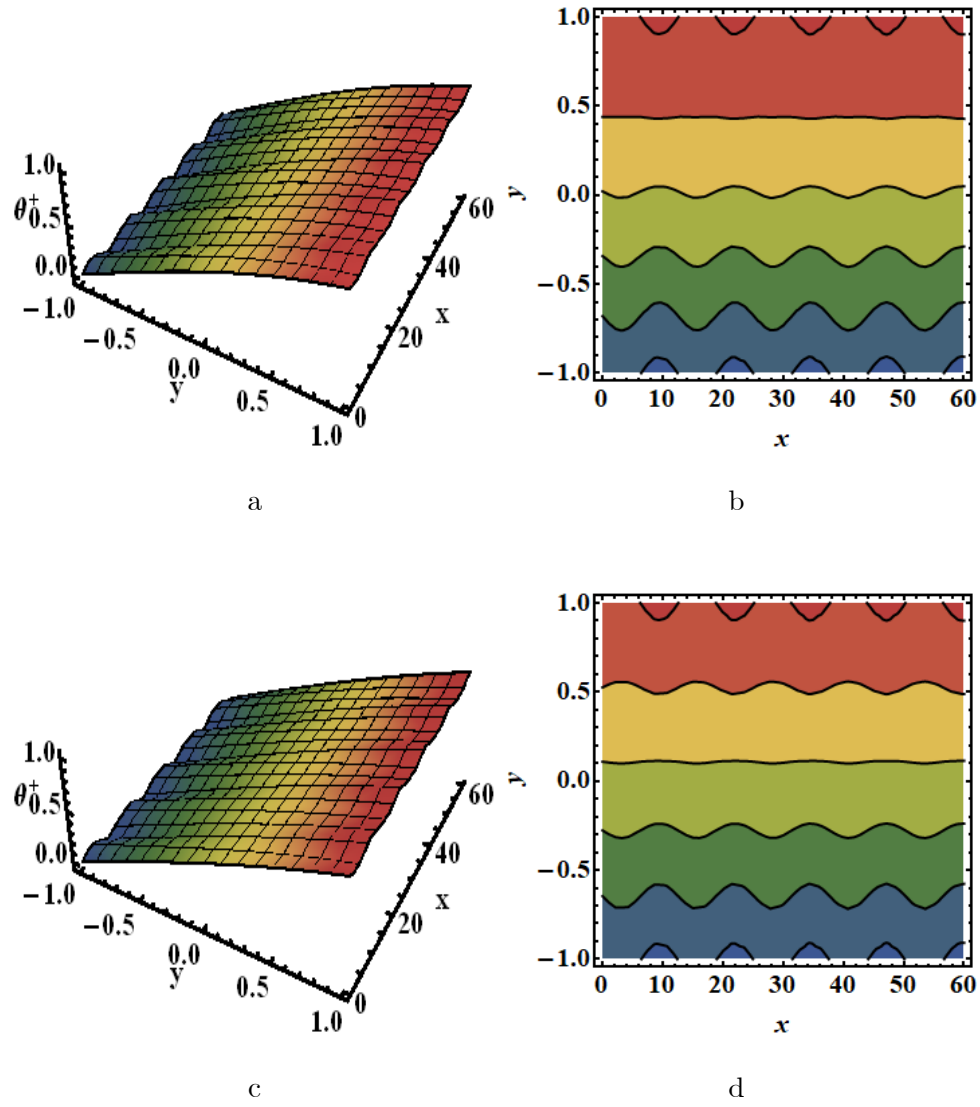


Fig. (5.8): 3D Temperature distribution and contour (a, b, c, d) for $R = 0.5$ and $R = 2$ in phase for hybrid nanofluid.

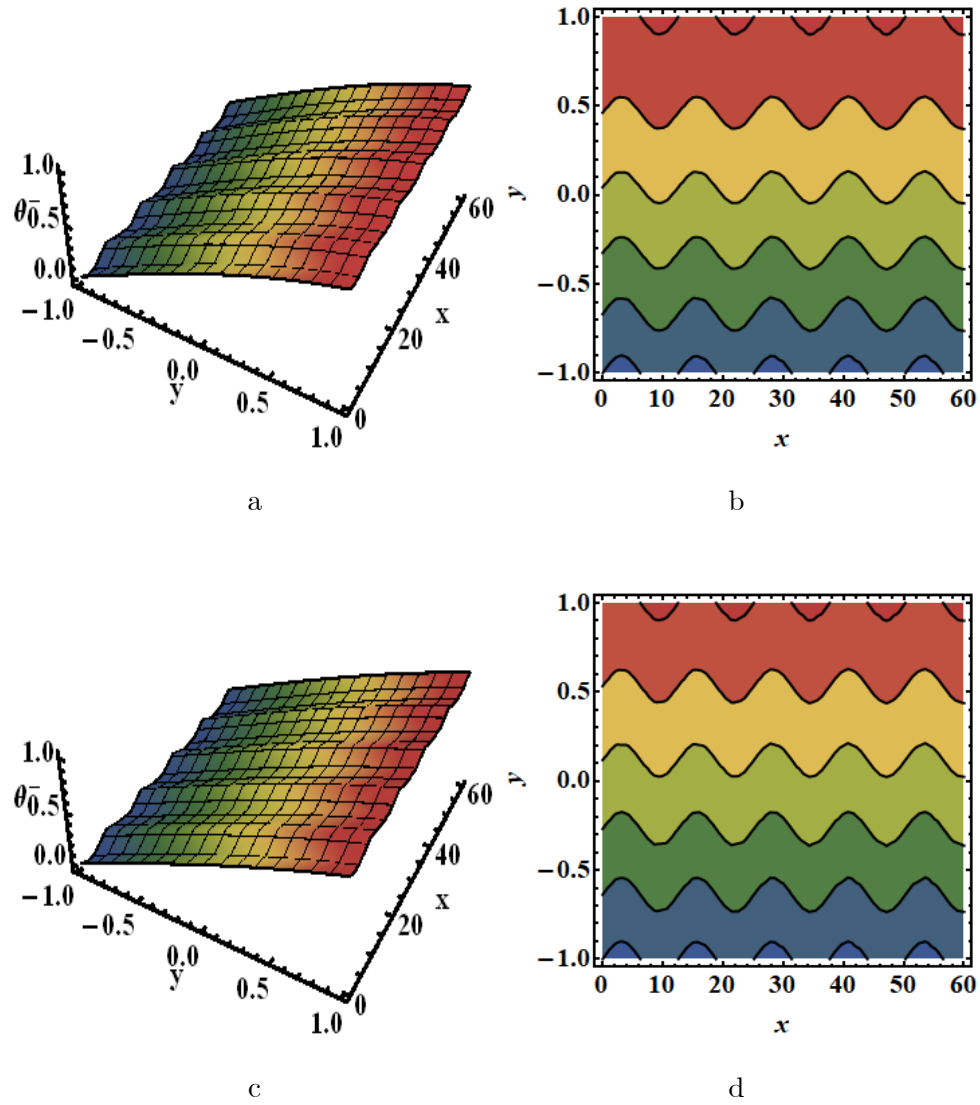


Fig. (5.9): 3D Temperature distribution and contour (a, b, c, d) for $R = 0.5$ and $R = 2$ out of phase for hybrid nanofluid.

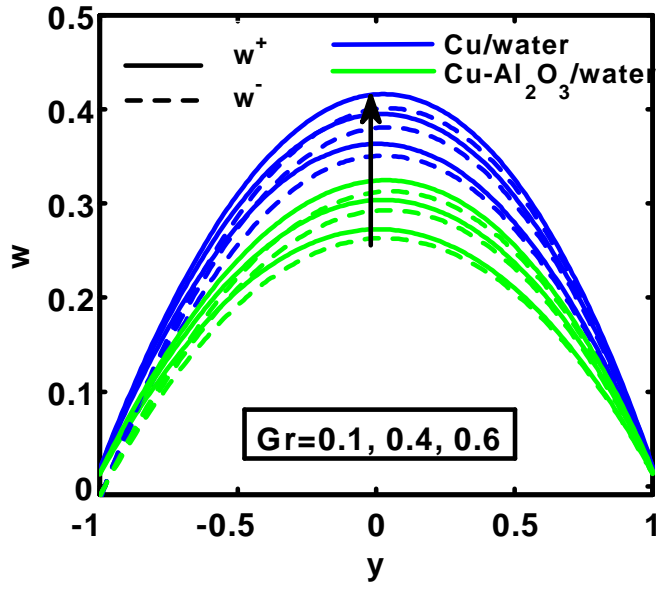


Fig. (5.10): 2D Variation of velocity for Grashof number Gr .

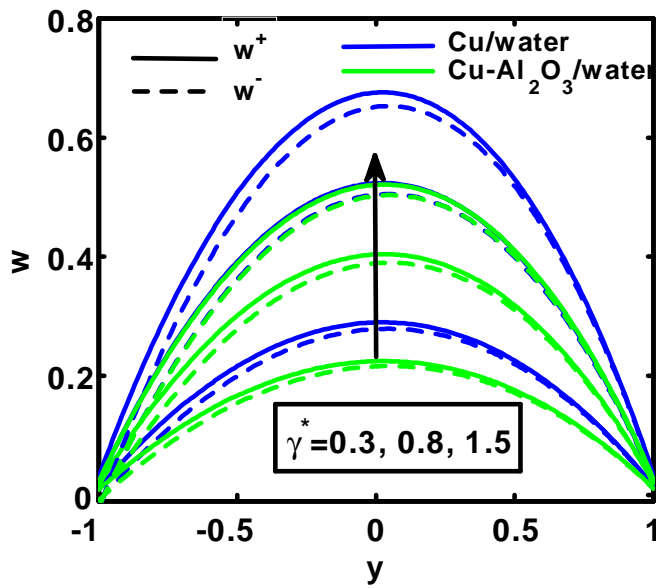


Fig. (5.11): 2D Variation of velocity for Casson parameter γ^* .

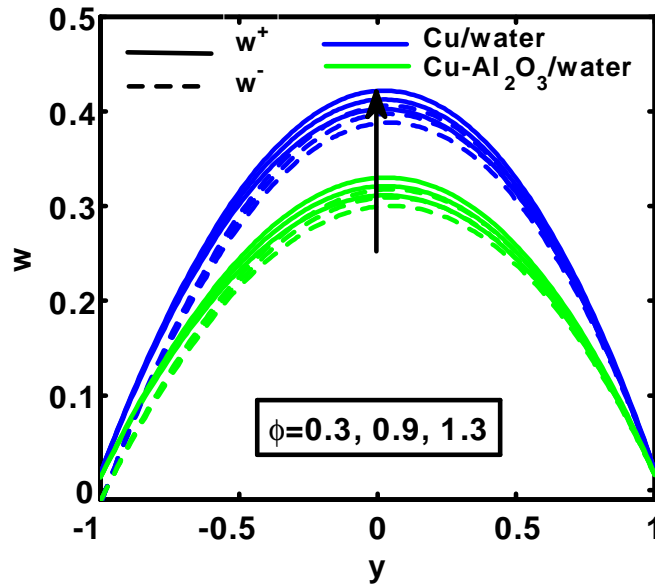


Fig. (5.12): 2D Variation of velocity for heat source parameter ϕ .

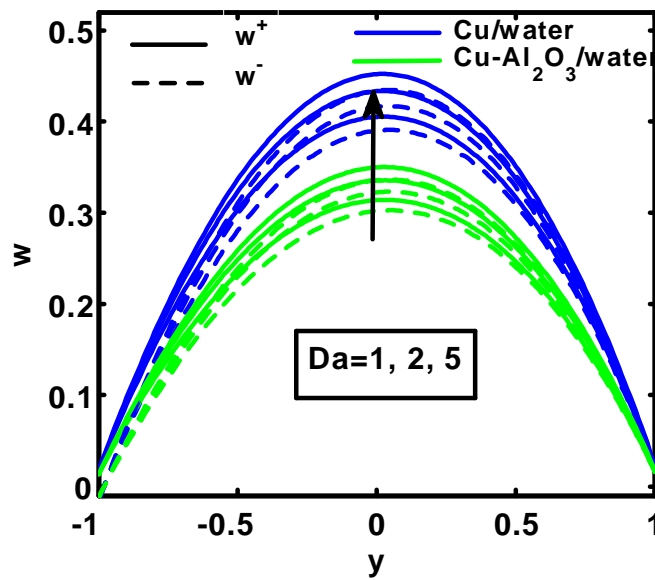


Fig. (5.13): 2D Variation of velocity for Darcy number Da .

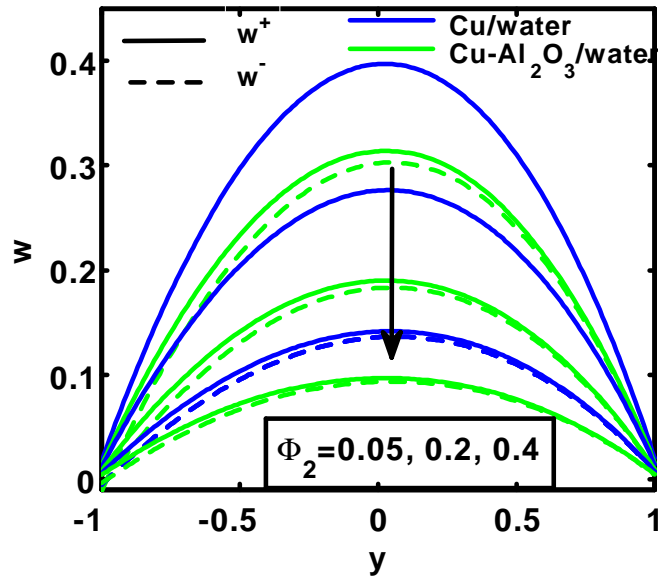


Fig. (5.14): 2D Variation of velocity for Volume fraction Φ_2 .

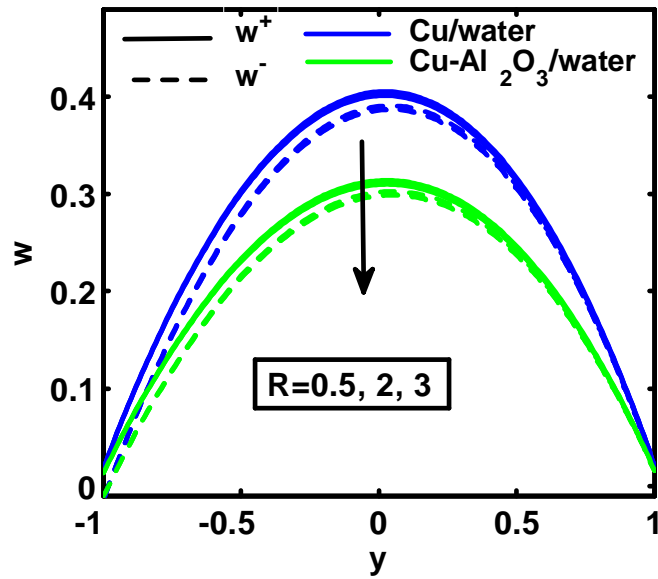


Fig. (5.15): 2D Variation of velocity for Radiation parameter R .

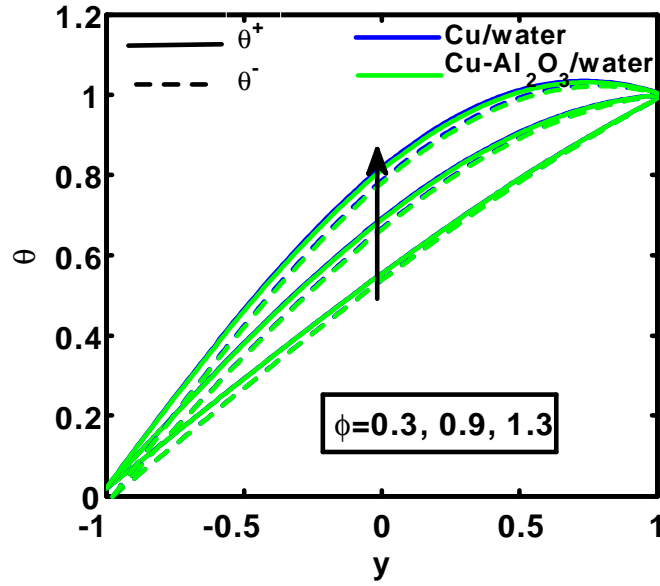


Fig. (5.16): 2D Variation of temperature for heat source parameter ϕ .

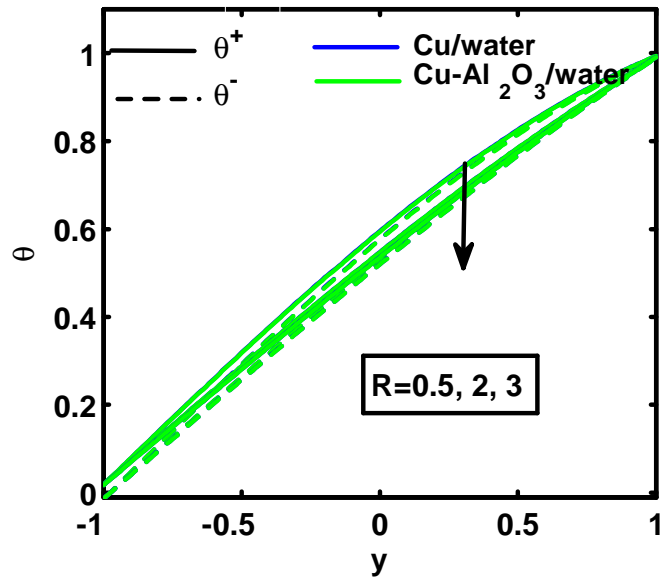


Fig. (5.17): 2D Variation of temperature for Radiation parameter R .

5.4.1 Tables Description

In this section, the impact of Nusselt number $Nu^\pm = -\frac{k''_{nf}\theta'(y_u)}{k''_f}$ on EMHD flow of Casson fluid for nano fluid (Cu/water) and hybrid nanofluid (Cu - Al₂O₃/water) discussed in the microchannel through corrugated walls under porous medium. This section expressed the behavior of Radiation parameter R on the Nusselt number Nu^\pm . Table 5.3 demonstrates that Nu^+ declines with expanding value of x and increases by the rise of the Radiation parameter R for both the nano fluid (Cu/water) and hybrid nanofluid (Cu - Al₂O₃/water). Table 5.4 shows that the Nu^- declines with expanding value of x and increases by the rise of the Radiation parameter R for both the nano fluid (Cu/water) and hybrid nanofluid (Cu - Al₂O₃/water).

For Nusselt number Nu^+						
For nano fluid (Cu/water)				For hybrid nanofluid		
x	$R = 0.5$	$R = 2$	$R = 3$	$R = 0.5$	$R = 2$	$R = 3$
0	0.348705	0.468788	0.498593	0.385843	0.486562	0.51363
0.1	0.34049	0.461955	0.492098	0.377783	0.479654	0.50703
0.2	0.33203	0.454929	0.485422	0.369491	0.472551	0.500248
0.3	0.323422	0.447791	0.478644	0.36106	0.465339	0.493364
0.4	0.314764	0.440623	0.471841	0.352585	0.458097	0.486455
0.5	0.306149	0.433501	0.465086	0.34416	0.450906	0.479597
0.6	0.297668	0.426501	0.458449	0.335872	0.443839	0.47286
0.7	0.289406	0.419691	0.451996	0.327805	0.436967	0.466312
0.8	0.281144	0.413133	0.445787	0.320035	0.430353	0.460013
0.9	0.273841	0.406887	0.439874	0.31263	0.424056	0.454017
1	0.266675	0.401003	0.434308	0.305654	0.418127	0.448374

Table (5.3): Impact of the Radiation parameter R on Nusselt number Nu^+ .

For Nusselt number Nu^-						
For nano fluid (Cu/water)			For hybrid nanofluid			
x	$R = 0.5$	$R = 2$	$R = 3$	$R = 0.5$	$R = 2$	$R = 3$
0	0.313892	0.438894	0.469855	0.324607	0.449201	0.48037
0.1	0.313096	0.438459	0.469522	0.323788	0.448751	0.480024
0.2	0.312261	0.438004	0.469173	0.322931	0.44828	0.479663
0.3	0.311398	0.437534	0.468813	0.322042	0.447793	0.47929
0.4	0.310512	0.437053	0.468445	0.321132	0.447296	0.478908
0.5	0.309613	0.436566	0.468073	0.320209	0.446792	0.478522
0.6	0.30871	0.436078	0.4677	0.319281	0.446287	0.478136
0.7	0.307812	0.435593	0.467329	0.318358	0.445786	0.477752
0.8	0.306927	0.435117	0.466966	0.317449	0.445293	0.477375
0.9	0.306065	0.434654	0.466613	0.316563	0.444815	0.47701
1	0.305234	0.43421	0.466274	0.31571	0.444355	0.476658

Table (5.4): Impact of the Radiation parameter R on Nusselt number Nu^- .

5.5 Conclusion

The outline of present work is ordered as follows

- The unobvious effect reduces by small value of ε on velocity and temperature.
- The shape of channel depends on velocity distribution.
- The velocity for the Grashof number, Casson parameter, Heat source parameter and Darcy number increase with increasing value of parameters.
- The velocity profiles increase rapidly for nanofluid (Cu/water) as compared to hybrid nanofluid (Cu - Al₂O₃/water) for Grashof number, Casson parameter, Heat source parameter and Darcy number.
- The temperature for both nanofluid and hybrid nanofluid is increasing with heat source parameter ϕ .

- The temperature for both nanofluid and hybrid nanofluid is decreasing with the positive values of radiation parameter R parameter.
- The velocities profiles in phase are weaker than out of phase.

Chapter 6

Theoretical aspect of EMHD viscous fluid with corrugated walls in curved channel

In this chapter, we have investigation base on the electromagnetohydrodynamic (EMHD) flow effects on viscous fluid through corrugated walls in the curved channel. Amplitude of corrugations of the wavy walls are either in phase or out of phase. At first performed the mathematical modelling and then the solution of velocity is achieved by employing the perturbation technique. By means of mathematical calculations we investigated the corrugation effects on the EMHD velocity flow. The influence of emerging parameters from obtained solutions are inspected by plotting the graphs. The important conclusion is that reducing the unobvious wave effect on the velocity by taking amplitude ratio parameter small.

6.1 Mathematical Formulation

The EMHD flow viscous and an incompressible fluid between fixed corrugated wall in a curved channel with height $2H$, center at O and radius R' is considered. The flow induced in the channel by sine waves by small amplitude ε along the corrugated walls of the channel. The wavy walls are located at

$$r_u^* = H + \varepsilon H \sin(\lambda^* x^*) \text{ and } r_l^* = -H \pm \varepsilon H \sin(\lambda^* x^*). \quad (6.1)$$

where ε is small amplitude and λ^* is wave number. We take magnetic field \mathbf{B}^* along y^* direction while along the x^* direction electric field \mathbf{E}^* is applied. Along the z^* direction, we take the Lorentz force which is produced by the contact among the magnetic field \mathbf{B}^* and the electric field \mathbf{E}^* .

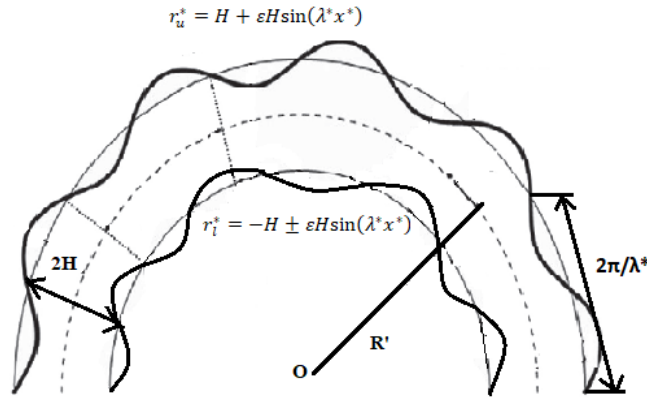


Fig. (6.1): Geometrical sketch of EMHD flow in microchannel.

Defining velocity field as

$$\mathbf{u}^* = (0, 0, w^*(X^*, R^*, t)). \quad (6.2)$$

For present flow the basic equations are

Continuity equation

$$\nabla^* \mathbf{u}^* = 0. \quad (6.3)$$

Momentum equation

$$\rho \frac{\partial \mathbf{u}^*}{\partial t^*} + \rho (\mathbf{u}^* \cdot \nabla^*) \mathbf{u}^* = -\nabla^* p + \nabla^* \boldsymbol{\tau}^* + \mathbf{J} \times \mathbf{B}^*. \quad (6.4)$$

Suppose along the z^* direction channel is open, so we can ignore the pressure gradient $\partial p / \partial z^*$ along the microchannel [85] and the velocity $w^*(x^*, y^*)$ satisfies

$$\rho \frac{\partial w^*}{\partial t^*} = \frac{1}{\dot{R} + R^*} \frac{\partial}{\partial R^*} (R^* + \dot{R}) \bar{\tau}_{Z^* R^*} + \frac{\dot{R}}{\dot{R} + R^*} \bar{\tau}_{Z^* X^*} + \sigma B^* (E^* - (\frac{\dot{R}}{\dot{R} + R^*})^2 B^* w^*), \quad (6.5)$$

where

$$\bar{\tau}_{Z^* R^*} = \mu \frac{\partial w^*}{\partial R^*}, \quad \bar{\tau}_{Z^* X^*} = \mu \frac{\dot{R}}{\dot{R} + R^*} \frac{\partial w^*}{\partial X^*}. \quad (6.6)$$

Corresponding no-slip boundary conditions expressed as

$$w^*(X^*, R_{u^*}^*) = w^*(X^*, R_{p^*}^*) = 0. \quad (6.7)$$

In complex forms the EMHD velocity, electric field and stress components can be written as

$$w^* = R\{\tilde{w}(X^*, R_{u^*}^*) e^{i\omega t^*}\}, \quad E^* = R\{E_0 e^{i\omega t^*}\}, \quad \bar{\tau}_{ij} = R\{\tau_{ij} e^{i\omega t^*}\}, \quad (6.8)$$

where real part of function denotes by $R\{\}$, ω is angular frequency, \tilde{w} , E_0 and τ_{ij} are velocity amplitude, electric field and stress component. Using Eq. (6.8) into Eq. (6.5), we get

$$i\rho\omega\tilde{w} = \frac{1}{\dot{R} + R^*} \frac{\partial}{\partial R^*} (R^* + \dot{R}) \tau_{Z^* R^*} + \frac{\dot{R}}{R^* + \dot{R}} \tau_{Z^* X^*} + \sigma B^* (E^* - (\frac{\dot{R}}{\dot{R} + R^*})^2 B^* \tilde{w}). \quad (6.9)$$

Bring out the non dimensionless parameters as

$$\begin{aligned} (r, x) &= \frac{(R^*, X^*)}{H}, \quad \lambda = \lambda^* H, \quad w = \frac{\tilde{w}}{H\omega}, \quad k = \frac{\dot{R}}{H}, \quad z = Z^*, \\ \text{Re} &= \frac{\rho\omega H^2}{\mu}, \quad Ha = B^* H \left(\frac{\sigma}{\mu}\right)^{\frac{1}{2}}, \quad \beta = E_0 \left(\frac{\sigma}{\mu}\right)^{\frac{1}{2}} / \omega. \end{aligned} \quad (6.10)$$

The dimensionless momentum equation stated in the following form

$$\frac{\partial^2 w}{\partial r^2} + \frac{1}{r+k} \frac{\partial w}{\partial r} + \frac{k}{r+k} \frac{\partial^2 w}{\partial x^2} - \left(\text{Re } i + \left(\frac{k}{r+k} \right)^2 Ha^2 \right) w + Ha\beta = 0. \quad (6.11)$$

The corresponding non-dimensional boundary conditions define as

$$w = 0, \quad r_{w^+} = 1 + \varepsilon \sin(\lambda x), \quad r_{w^-} = -1 \pm \varepsilon \sin(\lambda x). \quad (6.12)$$

In Eq. (6.12), $r_{w^+} = r_{w^+}^*/H$, $r_{w^-} = r_{w^-}^*/H$, the ‘+’ symbol means the corrugation is in phase and for out of phase ‘-’ symbol is used.

6.2 Solution of Problem

By using regular perturbation technique in above equation:

$$w(r, x) = w_0(r) + \varepsilon w_1(r, x) + \varepsilon^2 w_2(r, x) + \dots \quad (6.13)$$

Equating the like power of ε after using the Eq.(6.13) into Eqs. (6.11) and (6.12), we get the systems as

6.2.1 Zeroth Order System

$$\frac{\partial^2 w_0}{\partial r^2} + \frac{1}{r+k} \frac{\partial w_0}{\partial r} - \left(\text{Re } i + \left(\frac{k}{r+k} \right)^2 Ha^2 \right) w_0 + Ha\beta = 0, \quad (6.14)$$

$$w_0|_{r=1} = 0, \quad w_0|_{r=-1} = 0. \quad (6.15)$$

6.2.2 First Order System

$$\frac{\partial^2 w_1}{\partial r^2} + \frac{1}{r+k} \frac{\partial w_1}{\partial r} + \frac{k}{r+k} \frac{\partial^2 w_1}{\partial x^2} - \left(\text{Re } i + \left(\frac{k}{r+k} \right)^2 Ha^2 \right) w_1 = 0, \quad (6.16)$$

$$w_1|_{r=1} = -\sin(\lambda x) \left(\frac{dw_0}{dr} \right)_{r=1}, \quad w_1|_{r=-1} = \mp \sin(\lambda x) \left(\frac{dw_0}{dr} \right)_{r=-1}. \quad (6.17)$$

6.2.3 Second Order System

$$\frac{\partial^2 w_2}{\partial r^2} + \frac{1}{r+k} \frac{\partial w_2}{\partial r} + \frac{k}{r+k} \frac{\partial^2 w_2}{\partial x^2} - (\text{Re } i + (\frac{k}{r+k})^2 H a^2) w_2 = 0, \quad (6.18)$$

$$\begin{aligned} w_2 |_{r=1} &= -\sin(\lambda x) \left(\frac{\partial w_1}{\partial r} \right)_{r=1} - \frac{1}{2} \sin^2(\lambda x) \left(\frac{d^2 w_0}{dr^2} \right)_{r=1}, \\ w_2^\pm |_{r=-1} &\mp \sin(\lambda x) \left(\frac{\partial w_1}{\partial r} \right)_{r=-1} - \frac{1}{2} \sin^2(\lambda x) \left(\frac{d^2 w_0}{dr^2} \right)_{r=-1}. \end{aligned} \quad (6.19)$$

6.2.4 Solution of zeroth order

Under the boundary conditions the zero-order solution can be expressed as:

$$\begin{aligned} w_0(r) = & \text{BesselJ}[kHa, -i(k+r)]A_1 + \text{BesselY}[kHa, -i(k+r)\sqrt{\text{Re } i}]A_2 + \frac{1}{-8k+2k^3Ha^2} \\ & (k+r)^2 \beta ((2+kHa) \text{Hypergeometric0F1}[1+kHa, \frac{1}{4}(k+r)^2 \text{Re } i] \\ & \text{HypergeometricPFQ}[\{1-\frac{kHa}{2}\}, \{1-kHa, 2-\frac{kHa}{2}\}, \frac{1}{4}(k+r)^2 \text{Re } i] \\ & + (-2+kHa) \text{Hypergeometric0F1}[1-kHa, \frac{1}{4}(k+r)^2 \text{Re } i] \\ & \text{HypergeometricPFQ}[\{1+\frac{kHa}{2}\}, \{2+\frac{kHa}{2}, 1+kHa\}, \frac{1}{4}(k+r)^2 \text{Re } i]). \end{aligned} \quad (6.20)$$

6.2.5 Solution of first order

Base on the boundary conditions (6.17), we can assume the solution of first order as

$$w_1(r, x) = \sin(\lambda x) f(r), \quad (6.21)$$

where $f(r)$ is function of r .

Using Eq.(6.21) into Eq.(6.16), we get

$$\frac{d^2 f(r)}{dr^2} + \frac{1}{(k+r)} \frac{df(r)}{dr} - \left[\frac{(\lambda k)^2}{(k+r)^2} + \text{Re } i + H a^2 \frac{k^2}{(k+r)^2} \right] f(r) = 0. \quad (6.22)$$

Correspondingly boundary conditions are transformed as

$$f(r) + \frac{dw_0}{dr} = 0 \text{ at } r = 1, f(r) \pm \frac{dw_0}{dr} = 0 \text{ at } r = -1. \quad (6.23)$$

The solution of first order problem can be expressed as

$$w_1^\pm(r, x) = \sin(\lambda x) \begin{cases} \text{BesselJ}[k\sqrt{Ha^2 + \lambda^2}, -i(k+r)\sqrt{\text{Re } i}]B_1 + \\ \text{BesselY}[k\sqrt{Ha^2 + \lambda^2}, -i(k+r)\sqrt{\text{Re } i}]B_2 \\ \text{BesselJ}[k\sqrt{Ha^2 + \lambda^2}, -i(k+r)\sqrt{\text{Re } i}]B'_1 + \\ \text{BesselY}[k\sqrt{Ha^2 + \lambda^2}, -i(k+r)\sqrt{\text{Re } i}]B'_2 \end{cases}, \quad (6.24)$$

6.2.6 Solution of second order

Base on the boundary conditions (6.19), second order system solution in supposed form is considered as

$$w_2^\pm(r, x) = g^\pm(r) + \cos(2\lambda x) h^\pm(r), \quad (6.25)$$

where $g^\pm(r)$ and $h^\pm(r)$ are function of r only.

By utilizing Eq.(6.25) into Eq. (6.18), we get the following forms

$$\frac{d^2 g^\pm(r)}{dr^2} + \frac{1}{(k+r)} \frac{dg^\pm(r)}{dr} - [\text{Re } i + Ha^2 \frac{k^2}{(k+r)^2}] g^\pm(r) = 0, \quad (6.26)$$

$$\frac{d^2 h^\pm(r)}{dr^2} + \frac{1}{(k+r)} \frac{dh^\pm(r)}{dr} - [\frac{4(\lambda k)^2}{(k+r)^2} + \text{Re } i + Ha^2 \frac{k^2}{(k+r)^2}] h^\pm(r) = 0. \quad (6.27)$$

The boundary conditions of the functions $g^\pm(r)$ and $h^\pm(r)$ are

$$g^\pm(r) + \frac{1}{2} \left(\frac{df(r)}{dr} + \frac{1}{2} \frac{d^2 w_0}{dr^2} \right) \text{ at } r = 1, g^\pm(r) \pm \frac{1}{2} \left(\frac{df(r)}{dr} \mp \frac{1}{2} \frac{d^2 w_0}{dr^2} \right) \text{ at } r = -1, \quad (6.28)$$

$$h^\pm(r) - \frac{1}{2} \left(\frac{df(r)}{dr} + \frac{1}{2} \frac{d^2 w_0}{dr^2} \right) \text{ at } r = 1, h^\pm(r) \pm \frac{1}{2} \left(\frac{df(r)}{dr} \mp \frac{1}{2} \frac{d^2 w_0}{dr^2} \right) \text{ at } r = -1. \quad (6.29)$$

Second order solution can be written as.

$$\begin{aligned}
w_2^\pm = & \text{BesselJ}[kHa, -i(k+r)\sqrt{\text{Re } i}]C_1 + \text{BesselY}[kHa, -i(k+r)\sqrt{\text{Re } i}]C_2 + \cos(2\lambda x) \\
& \text{BesselJ}[k\sqrt{Ha^2 + 4\lambda^2}, -i(k+r)\sqrt{\text{Re } i}]D_1 + \text{BesselY}[k\sqrt{Ha^2 + 4\lambda^2}, -i(k+r)\sqrt{\text{Re } i}]D_2 \\
& \text{BesselJ}[kHa, -i(k+r)\sqrt{\text{Re } i}]C'_1 + \text{BesselY}[kHa, -i(k+r)\sqrt{\text{Re } i}]C'_2 + \cos(2\lambda x) \\
& \text{BesselJ}[k\sqrt{Ha^2 + 4\lambda^2}, -i(k+r)\sqrt{\text{Re } i}]D'_1 + \text{BesselY}[k\sqrt{Ha^2 + 4\lambda^2}, -i(k+r)\sqrt{\text{Re } i}]D'_2
\end{aligned} \tag{6.30}$$

Collecting Eqs.(6.20), (6.24) and (6.30), the approximate velocity solution can be evaluated as

$$w^\pm(r, x) = w_0(r) + \varepsilon w_1^\pm(r, x) + \varepsilon^2 w_2^\pm(r, x) + \dots \tag{6.31}$$

6.3 Graphical consequence

In this portion, the graphical outcomes of the viscous fluid are explored by EMHD flow in a curved channel with corrugated walls. All graphical effects are attained by using the MATLAB software. This portion is expressly arranged to inspect the impact of embedded constraints on flow quantities. Plots for 3D variations and contour of velocity and 2D variations of velocity are shown and dissected through Figs. (6.2) to (6.7) respectively. Specifically, the Reynolds parameters Re and curvature parameter k have been seen.

In Figs.(6.2) and (6.3), the phase difference among the two corrugated walls equals 0° . In Figs. (6.4) to (6.5), the phase difference between walls equals 180° . It is found that trapped bolus are appear for out-of-phase corrugations when ε is small. From the 3D plots of Figs. (6.2) to (6.5), we explored that the velocity distribution depends upon the shape of channel. When the corrugations are in phase, the wave phenomenon in the center of channel becomes obvious, as appeared in Figs. (6.2) to (6.5). As shown in Figs. (6.2) to (6.5), the wave phenomenon of the flow shape becomes obvious with the expansion of the corrugation. The wavy pattern increases by increase the value of parameters.

In Figs. (6.6) and (6.7), the velocities w^\pm are plotted against r for various estimations of parameters the Reynolds parameters Re and curvature parameter k when we take $\varepsilon = 0.1$ and $\beta = 5$. In particular, it can be found in Figs. (6.6) and (6.7), that the velocity amplitude achieves the maximum value at the middle of the channel. Fig. (6.6) demonstrates that the

velocity w^\pm decreases with increasing Reynolds number. The reason is that for the larger the rapid oscillation of velocity with smaller amplitudes. Fig.(6.7) illustrates that the velocity w^\pm decreases for curvature parameter k in the portion $[-1, 0]$ with increases in k , where as velocity it increases in the portion $[0, 1]$. The maximum value of velocity in curved channel shifts from the center towards the lower wall. We can find that, the EMHD velocities in phase are weaker than out of phase.

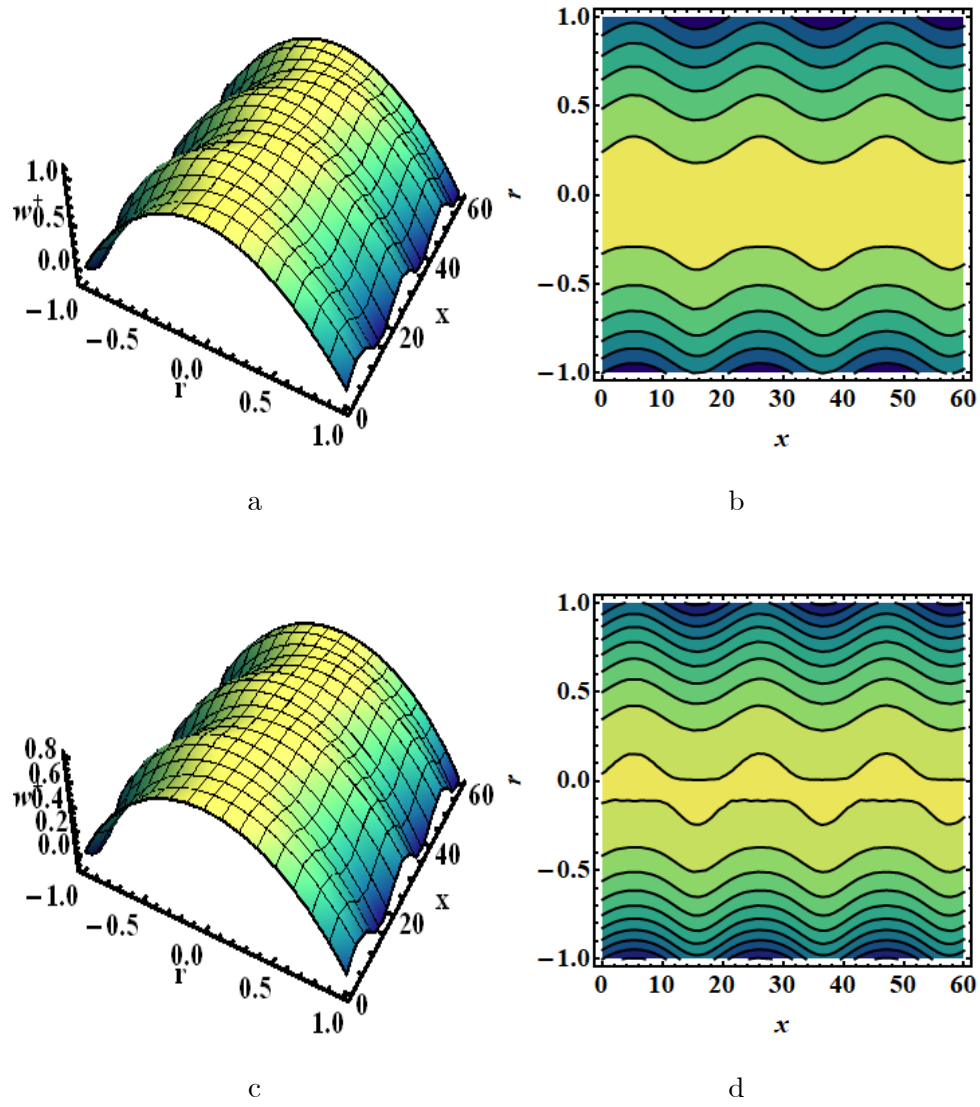


Fig. (6.2): 3D Velocity distribution and contour (a, b, c, d) for $Re = 0.6$ and $Re = 1.7$ in phase.

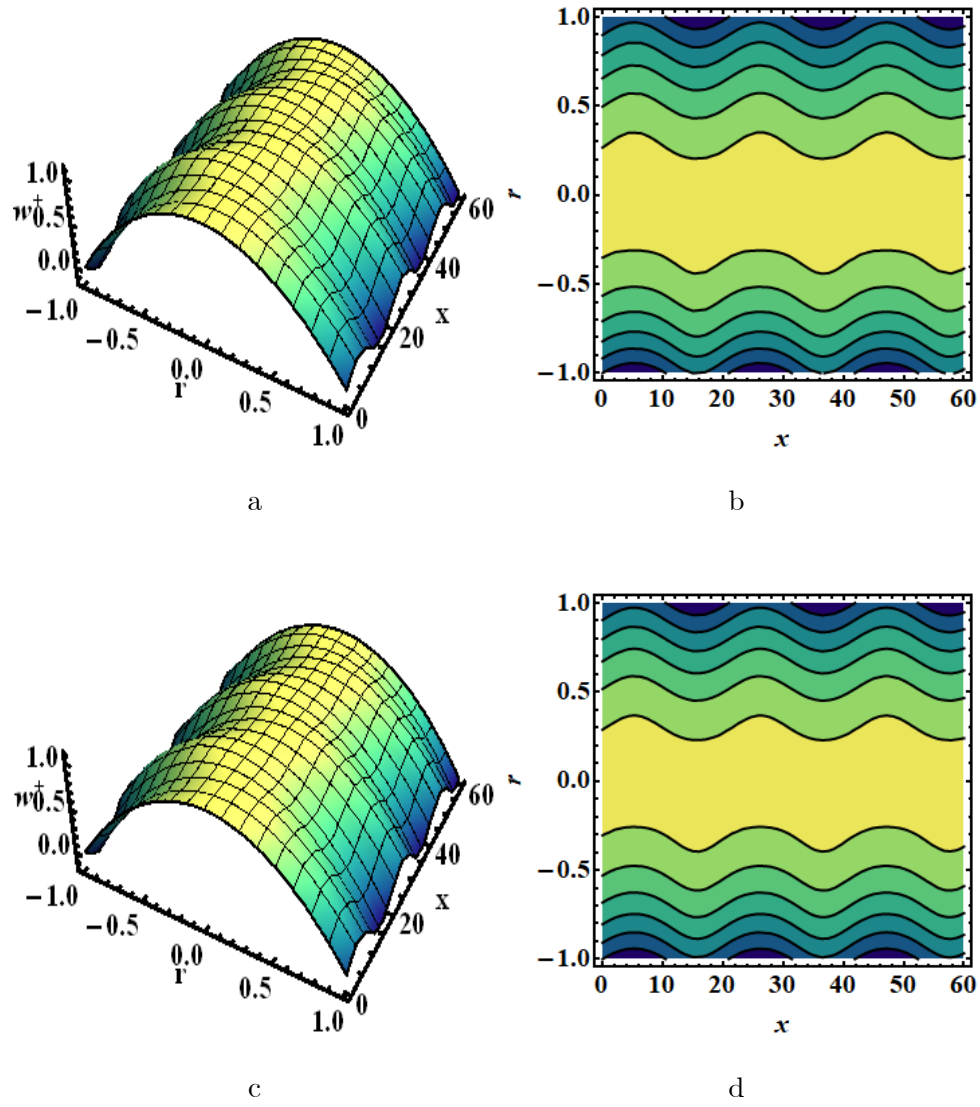


Fig. (6.3): 3D Velocity distribution and contour (a, b, c, d) for $k = 3.0$ and $k = 15$ in phase.

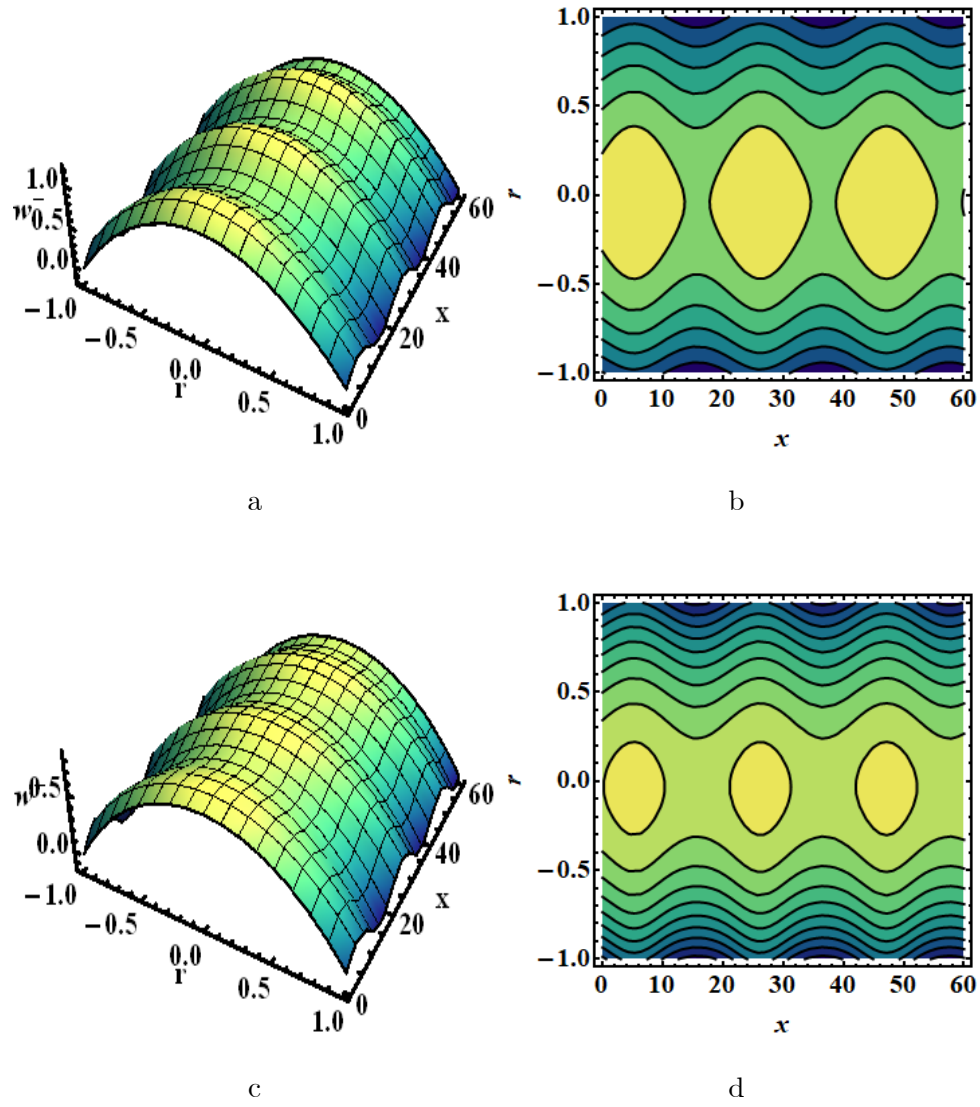


Fig. (6.4): 3D Velocity distribution and contour (a, b, c, d) for $Re = 0.6$ and $Re = 1.7$ out phase.

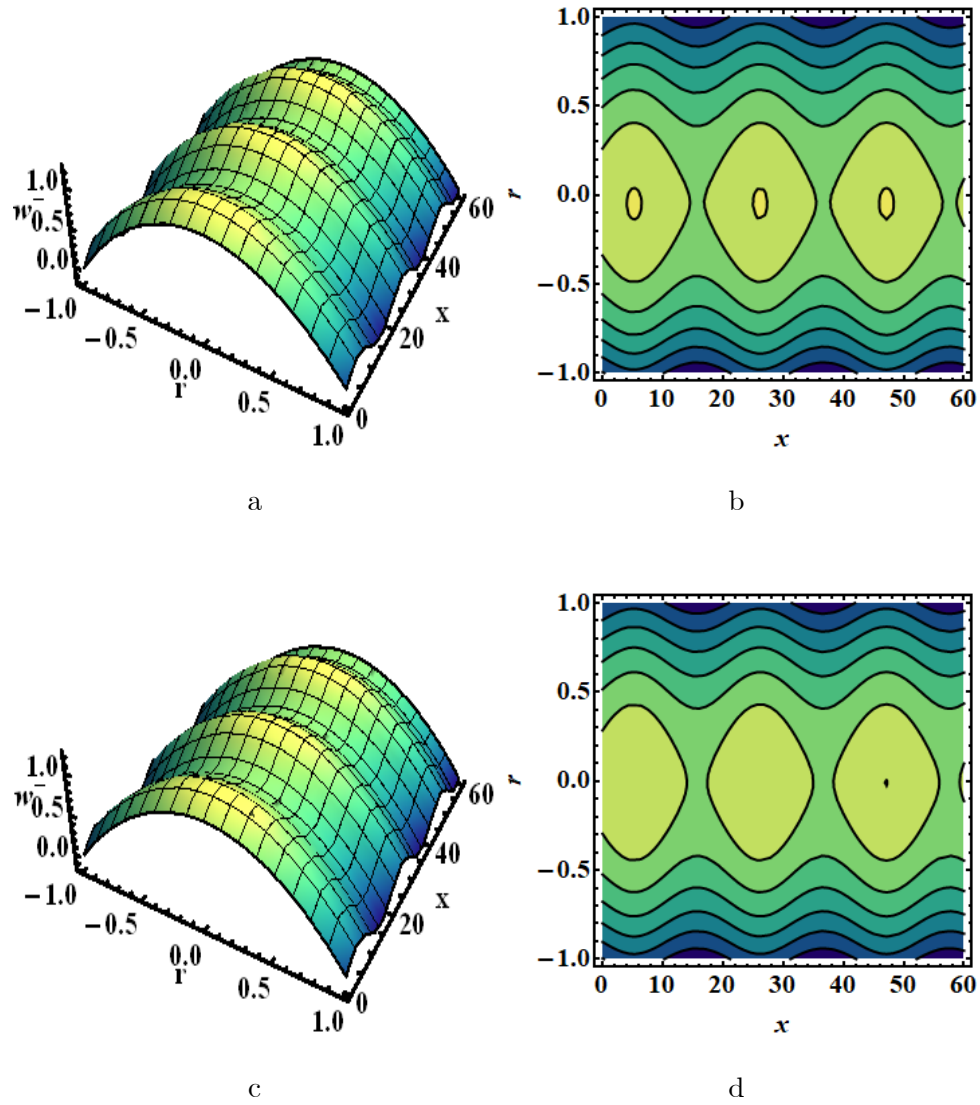


Fig. (6.5): 3D Velocity distribution and contour (a, b, c, d) for $k = 3.0$ and $k = 15$ out phase.

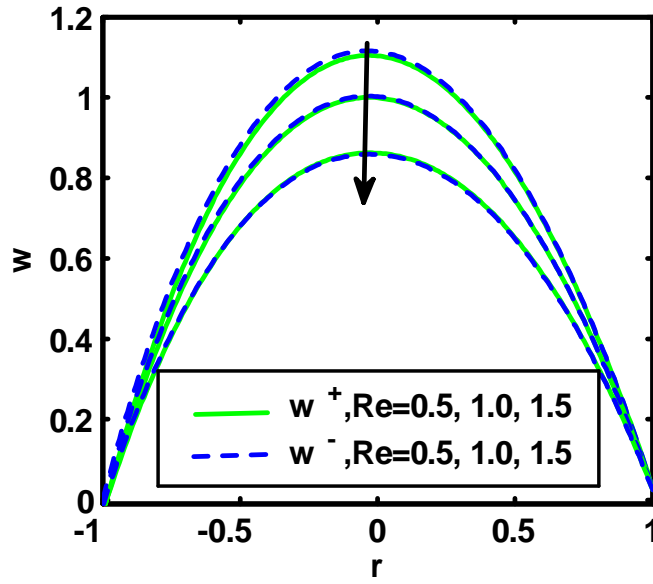


Fig. (6.6): 2D Variation of velocity for Reynolds number Re .

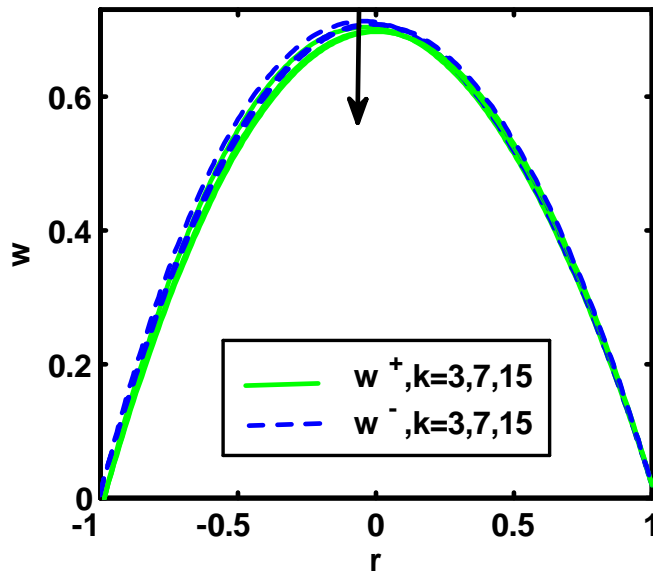


Fig. (6.7): 2D Variation of velocity for Curvature parameter k .

r	$k = 3$	$k = 7$	$k = 12$
-1	2.15359	1.96843	1.92498
-0.8	1.5868	1.51916	1.50131
-0.6	1.10327	1.10303	1.1019
-0.4	0.677796	0.712567	0.721596
-0.2	0.291429	0.34125	0.355449
0	-0.0675845	-0.0166458	-0.00122718
0.2	-0.407992	-0.366113	-0.352811
0.4	-0.736208	-0.711458	-0.703309
0.6	-1.05695	-1.05631	-1.05629
0.8	-1.05695	-1.40361	-1.41481
1	-1.68858	-1.75556	-1.78133

Table (6.1): Effect of curvature parameter k on stress component τ_{zr}^+ .

r	$k = 3$	$k = 7$	$k = 12$
-1	2.11532	1.96843	1.89557
-0.8	1.55722	1.49273	1.47588
-0.6	1.08031	1.08053	1.07987
-0.4	0.65891	0.693301	0.702441
-0.2	0.275897	0.32461	0.338686
0	-0.0806089	-0.0311831	-0.0160419
0.2	-0.419146	-0.379008	-0.36609
0.4	-0.745984	-0.723121	-0.715439
0.6	-1.06575	-1.06711	-1.06764
0.8	-1.38177	-1.41389	-1.42573
1	-1.69634	-1.76565	-1.79215

Table (6.2): Effect of curvature parameter k on stress component τ_{zr}^- .

r	$k = 3$	$k = 7$	$k = 12$
-1	0.018365	0.0194658	0.0198482
-0.8	0.018686	0.0197808	0.0201616
-0.6	0.0189403	0.0200241	0.0204017
-0.4	0.0191269	0.0201949	0.0205677
-0.2	0.019245	0.0202929	0.0206593
0	0.019294	0.0203177	0.0206762
0.2	0.0192735	0.0202693	0.0206188
0.4	0.0191835	0.0201482	0.0204874
0.6	0.0190242	0.0199547	0.0202827
0.8	0.0187959	0.0196899	0.0200056
1	0.0184994	0.0193546	0.0196574

Table (6.3): Effect of curvature parameter k on stress component τ_{zx}^+ .

r	$k = 3$	$k = 7$	$k = 12$
-1	0.0299634	0.0331521	0.0343054
-0.8	0.0305791	0.0338156	0.0349872
-0.6	0.0310898	0.0343622	0.0355477
-0.4	0.0314924	0.0347887	0.035984
-0.2	0.0317843	0.0350926	0.0362932
0	0.0319632	0.0352714	0.036473
0.2	0.032027	0.0353232	0.0365215
0.4	0.0319742	0.0352467	0.0364374
0.6	0.0318038	0.0350408	0.0362197
0.8	0.031515	0.0347052	0.035868
1	0.0311078	0.0342399	0.0353825

Table (6.4): Effect of curvature parameter k on stress component τ_{zx}^- .

6.4 Tables Description

In this section, the impact of stress components on EMHD flow discussed in curved channel through corrugated walls. This section expressed the behavior of curvature parameter k on the stress components τ_{zr}^{\pm} and τ_{zx}^{\pm} . Table 6.1 and Table 6.2 demonstrate that the stress components τ_{zr}^{+} and τ_{zr}^{-} decreased with the increasing value of r and furthermore decrease with the rise of the curvature parameter k . Table 6.3 and table 6.4 show that the stress components τ_{zx}^{+} and τ_{zx}^{-} increased with the increasing value of r and also enlarge with the increment of curvature parameter k .

6.5 Conclusion

The impact of corrugated wall roughness on the viscous EMHD flow in a curved channel is calculated in this paper. Perturbation technique is applied to examine the problem. From the above results, the following deductions are drawn.

- The wavy phenomenon in the center becomes obvious when the amplitude ε is small with in phase and out of phase corrugations.
- The contour plots from the solutions of the velocity, it is found that trapped bolus are appear for out-of-phase corrugations.
- The wavy phenomenon increases by enlarge the parameters values.
- The velocity amplitude achieves maximum value in middle of channel.
- The velocity plot decreases with expanding value of Reynolds number. The reason is that for the larger the rapid oscillation of velocity with smaller amplitudes.
- The velocity profile declines with rising value of k in inner half of channel and rise in outer half of channel.
- The EMHD velocities in phase are weaker than out of phase.
- Stress components τ_{zr}^{\pm} decrease with the rise of the curvature parameter while stress components τ_{zx}^{\pm} increase with the increasing value of the curvature parameter.

Chapter 7

Flow of EMHD nanofluid in curved channel through corrugated walls

The corrugated effect on nanofluids in curved channel under the influence of electromagnetohydrodynamic is discussed in this chapter. Investigation is carried out by water based nanofluids using copper nanoparticle. Firstly performed the mathematical modelling and then employing the method of perturbation, we have estimated the analytical solutions. By mean of mathematical calculations we examined the corrugation effects on EMHD flow. The physical effects of flow variables are graphically discussed. Moreover, consequence of Curvature parameter on stresses and Nusselt number are discussed through tables. The velocity and temperature decline when the curvature parameter increases. The electromagnetohydrodynamic (EMHD) velocity and temperature distributions show that 0° is the phase difference between the two walls for in phase and the phase difference is equal to the 180° between two walls for out of phase. The important conclusion is that reducing the unobvious wave effect on the velocity by taking amplitude ratio parameter small.

7.1 Mathematical model

Consider a EMHD flow of laminar, incompressible and electrically conducting fluid between corrugated wall in the curved channel separated by a distance $2H$, center at O and radius R' is considered. The flow induced in the channel by sine waves with small amplitude ε along the

corrugated walls of the channel. The wavy walls are located a

$$r_w^* = H + \varepsilon H \sin(\lambda^* x^*) \text{ and } r_p^* = -H \pm \varepsilon H \sin(\lambda^* x^*) \quad (7.1)$$

where ε is small amplitude and λ^* is wave number. We take magnetic field \mathbf{B}^* along y^* direction while along the x^* direction electric field \mathbf{E}^* is applied. Along the \mathbf{z}^* direction, we take the Lorentz force which is produced by the contact among the magnetic field \mathbf{B}^* and the electric field \mathbf{E}^* .

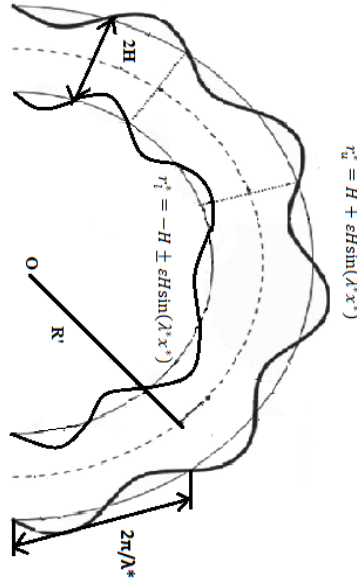


Fig. (7.1): Geometrical sketch of EMHD flow in microchannel.

Defining the velocity field as

$$\mathbf{u}^* = (0, 0, w^*(X^*, R^*)). \quad (7.2)$$

For present flow we considered the following basic equations

Continuity equation

$$\nabla^* \mathbf{u}^* = 0. \quad (7.3)$$

Equation of motion

$$\left(\frac{1}{\dot{R} + R^*} \frac{\partial}{\partial R^*} (R^* + \dot{R}) \bar{\tau}_{Z^* R^*}\right) + \frac{\dot{R}}{\dot{R} + R^*} \bar{\tau}_{Z^* X^*} + \sigma_{nf} B^* \left(E^* - \left(\frac{\dot{R}}{\dot{R} + R^*}\right)^2 B^* w^*\right) + g(\rho\zeta)_{nf} (T^* - T_l^*) = 0. \quad (7.4)$$

Energy equation

$$k''_{nf} \left(\frac{1}{\dot{R} + R^*} \frac{\partial}{\partial R^*} \left((R^* + \dot{R}) \frac{\partial T^*}{\partial R^*} \right) + \left(\frac{\dot{R}}{\dot{R} + R^*} \right)^2 \frac{\partial^2 T^*}{\partial X^{*2}} \right) + Q_0 = 0. \quad (7.5)$$

In addition, assuming that in z^* direction channel is open and pressure gradient can be ignored, the Navier-Stokes Eq. (7.4) along the z^* direction [85] as

$$\left(\frac{1}{\dot{R} + R^*} \frac{\partial}{\partial R^*} (R^* + \dot{R}) \bar{\tau}_{Z^* R^*}\right) + \frac{\dot{R}}{\dot{R} + R^*} \bar{\tau}_{Z^* X^*} + \sigma_{nf} B^* \left(E^* - \left(\frac{\dot{R}}{\dot{R} + R^*}\right)^2 B^* w^*\right) + g(\rho\zeta)_{nf} (T^* - T_l^*) = 0, \quad (7.6)$$

where

$$\bar{\tau}_{Z^* R^*} = \mu_{nf} \frac{\partial w^*}{\partial R^*}, \quad \bar{\tau}_{Z^* X^*} = \mu_{nf} \frac{\dot{R}}{\dot{R} + R^*} \frac{\partial w^*}{\partial X^*}. \quad (7.7)$$

Corresponding no-slip boundary conditions expressed as

$$\begin{aligned} w^*(X^*, R_{u^*}^*) &= 0 \text{ at } R_{u^*}^* = H + \varepsilon H \sin(\lambda^* X^*), \\ w^*(X^*, R_{l^*}^*) &= 0 \text{ at } R_{l^*}^* = -H \pm \varepsilon H \sin(\lambda^* X^*), \\ T^*(X^*, R_{u^*}^*) &= T_{u^*}^*(X^*, R_{u^*}^*) \text{ at } R_{u^*}^* = H + \varepsilon H \sin(\lambda^* X^*), \\ T^*(X^*, R_{l^*}^*) &= T_{l^*}^*(X^*, R_{l^*}^*) \text{ at } R_{l^*}^* = -H \pm \varepsilon H \sin(\lambda^* X^*). \end{aligned} \quad (7.8)$$

Bring out the following dimensionless variables

$$\begin{aligned} (r, x) &= \frac{(R^*, X^*)}{H}, \quad \lambda = \lambda^* H, \quad w = \frac{w^*}{U}, \quad k = \frac{\dot{R}}{H}, \quad Ha = B^* H \left(\frac{\sigma_f}{\mu_f} \right)^{\frac{1}{2}}, \\ \beta &= E_0 \left(\frac{\sigma_f}{\mu_f} \right)^{\frac{1}{2}} / U, \quad \theta = \frac{T - T_{l^*}}{T_{u^*} - T_{l^*}}, \quad Gr = \frac{g(\rho\zeta)_f H (T_{u^*} - T_{l^*})}{\mu_f U}, \quad \phi = \frac{Q_0 H^2}{k''_{nf} (T_{u^*} - T_{l^*})}. \end{aligned} \quad (7.9)$$

Here Ha , Gr , β , θ , ϕ and k represents Hartmann number, Grashof number, non-dimensional parameter, temperature, heat absorption coefficient and curvature parameter. The dimensionless momentum and temperature equation stated in the following form

$$\frac{\mu_{nf}}{\mu_f} \left(\frac{\partial^2 w}{\partial r^2} + \frac{1}{r+k} \frac{\partial w}{\partial r} + \left(\frac{k}{r+k} \right)^2 \frac{\partial^2 w}{\partial x^2} \right) + \frac{\sigma_{nf}}{\sigma_f} \left(Ha\beta + \left(\frac{k}{r+k} \right)^2 Ha^2 w \right) + \frac{(\rho\zeta)_{nf}}{(\rho\zeta)_f} Gr\theta = 0, \quad (7.10)$$

$$\frac{\partial^2 \theta}{\partial r^2} + \frac{1}{r+k} \frac{\partial \theta}{\partial r} + \left(\frac{k}{r+k} \right)^2 \frac{\partial^2 \theta}{\partial x^2} + \phi \frac{k''_f}{k''_{nf}} = 0. \quad (7.11)$$

The corresponding dimensionless boundary conditions yield the form

$$w = 0, \quad r_u'' = 1 + \varepsilon \sin(\lambda x), \quad r_l'' = -1 \pm \varepsilon \sin(\lambda x), \quad (7.12)$$

$$\theta = 1, \quad r_u'' = 1 + \varepsilon \sin(\lambda x), \quad \theta = 0, \quad r_l'' = -1 \pm \varepsilon \sin(\lambda x). \quad (7.13)$$

7.2 Solution of Problem:

By using regular perturbation technique in above equations, we define the following form

$$w(r, x) = w_0(r) + \varepsilon w_1(r, x) + \varepsilon^2 w_2(r, x) + \dots \quad (7.14)$$

$$\theta(r, x) = \theta_0(r) + \varepsilon \theta_1(r, x) + \varepsilon^2 \theta_2(r, x) + \dots \quad (7.15)$$

Substituting above equations into Eqs. (7.10) to (7.13) and computing the like powers of ε yield

7.2.1 Zeroth Order System

$$\frac{\partial^2 \theta_0}{\partial r^2} + \frac{1}{r+k} \frac{\partial \theta_0}{\partial r} + \phi \frac{k''_f}{k''_{nf}} = 0, \quad (7.16)$$

$$\frac{\mu_{nf}}{\mu_f} \left(\frac{\partial^2 w_0}{\partial r^2} + \frac{1}{r+k} \frac{\partial w_0}{\partial r} \right) + \frac{\sigma_{nf}}{\sigma_f} \left(Ha\beta + \left(\frac{k}{r+k} \right)^2 Ha^2 w_0 \right) + \frac{(\rho\zeta)_{nf}}{(\rho\zeta)_f} Gr\theta_0 = 0, \quad (7.17)$$

$$\theta_0 \mid_{r=1} = 1, \quad \theta_0 \mid_{r=-1} = 0, \quad (7.18)$$

$$w_0 \mid_{r=1} = 0, \quad w_0 \mid_{r=-1} = 0. \quad (7.19)$$

7.2.2 First Order System

$$\frac{\partial^2 \theta_1}{\partial r^2} + \frac{1}{r+k} \frac{\partial \theta_1}{\partial r} + \left(\frac{k}{r+k}\right)^2 \frac{\partial^2 \theta_1}{\partial x^2} = 0, \quad (7.20)$$

$$\frac{\mu_{nf}}{\mu_f} \left(\frac{\partial^2 w_1}{\partial r^2} + \frac{1}{r+k} \frac{\partial w_1}{\partial r} + \left(\frac{k}{r+k}\right)^2 \frac{\partial^2 w_1}{\partial x^2} \right) + \frac{\sigma_{nf}}{\sigma_f} \left(\frac{k}{r+k}\right)^2 Ha^2 w_1 + \frac{(\rho\zeta)_{nf}}{(\rho\zeta)_f} Gr \theta_1 = 0, \quad (7.21)$$

$$\theta_1 |_{r=1} = -\sin(\lambda x) \left(\frac{d\theta_0}{dr} \right)_{r=1}, \quad \theta_1^\pm |_{r=-1} = \mp \sin(\lambda x) \left(\frac{d\theta_0}{dr} \right)_{r=-1}, \quad (7.22)$$

$$w_1 |_{r=1} = -\sin(\lambda x) \left(\frac{dw_0}{dr} \right)_{r=1}, \quad w_1^\pm |_{r=-1} = \mp \sin(\lambda x) \left(\frac{dw_0}{dr} \right)_{r=-1}. \quad (7.23)$$

7.2.3 Second Order System

$$\frac{\partial^2 \theta_2}{\partial r^2} + \frac{1}{r+k} \frac{\partial \theta_2}{\partial r} + \left(\frac{k}{r+k}\right)^2 \frac{\partial^2 \theta_2}{\partial x^2} = 0, \quad (7.24)$$

$$\frac{\mu_{nf}}{\mu_f} \left(\frac{\partial^2 w_2}{\partial r^2} + \frac{1}{r+k} \frac{\partial w_2}{\partial r} + \left(\frac{k}{r+k}\right)^2 \frac{\partial^2 w_2}{\partial x^2} \right) + \frac{\sigma_{nf}}{\sigma_f} \left(\frac{k}{r+k}\right)^2 Ha^2 w_2 + \frac{(\rho\zeta)_{nf}}{(\rho\zeta)_f} Gr \theta_2 = 0, \quad (7.25)$$

$$\theta_2 |_{r=1} = -\sin(\lambda x) \left(\frac{\partial \theta_1}{\partial r} \right)_{r=1} - \frac{1}{2} \sin^2(\lambda x) \left(\frac{d^2 \theta_0}{dr^2} \right)_{r=1}, \quad (7.26)$$

$$\theta_2^\pm |_{r=-1} = \mp \sin(\lambda x) \left(\frac{\partial \theta_1}{\partial r} \right)_{r=-1} - \frac{1}{2} \sin^2(\lambda x) \left(\frac{d^2 \theta_0}{dr^2} \right)_{r=-1},$$

$$w_2 |_{r=1} = -\sin(\lambda x) \left(\frac{\partial w_1}{\partial r} \right)_{r=1} - \frac{1}{2} \sin^2(\lambda x) \left(\frac{d^2 w_0}{dr^2} \right)_{r=1}, \quad (7.27)$$

$$w_2^\pm |_{r=-1} = \mp \sin(\lambda x) \left(\frac{\partial w_1}{\partial r} \right)_{r=-1} - \frac{1}{2} \sin^2(\lambda x) \left(\frac{d^2 w_0}{dr^2} \right)_{r=-1}.$$

Solution of zeroth order

Under the boundary conditions the zero-order solution can be expressed as:

$$\theta_0(r) = A_2 + \left(-\frac{1}{2} \phi(r(2k+r) - 2k^2 \ln(k+r))k\right)_f + 2A_1 \ln(k+r)k\right)_{nf} / 2k_{nf}, \quad (7.28)$$

$$w_0(y) = \left\{ \begin{array}{l} (-Gr(k+r)^2 \phi k''_f \mu_f (\rho\zeta)_{nf} \sigma_f (16(-5k^2 - 2kr - r^2 + 8k^2 \ln(k+r)) u_{nf}^2 \sigma_f^2 + k^2 Ha^2 \\ (k^2 - 4kr - 2r^2 + 10k^2 \ln(k+r)) \mu_f \mu_{nf} \sigma_f \sigma_{nf} + k^4 Ha^4 (-r(2k+r) + 2 \ln(k+r)) \\ k^2 u_f^2 \sigma_{nf}^2) + 4k''_{nf} a (B_1 \cos(a_1 \ln(k+r)) b (\rho\zeta)_f + B_2 \sin(a_1 \ln(k+r)) (\rho\zeta)_f b + \mu_f \\ (k+r)^2 (4\mu_{nf} \sigma_f (-Gr(-A_1 + A_2 + A_1 \ln(k+r)) (\rho\zeta)_{nf} \sigma_f - c) - k^2 Ha^2 \mu_f \sigma_{nf} (Gr \\ (A_2 + A_1 \ln(k+r)) (\rho\zeta)_{nf} \sigma_f + a_1)))) / (4(\rho\zeta)_f k_{nf} b a), \end{array} \right. \quad (7.29)$$

with

$$\begin{aligned} a &= 16\mu_{nf} \sigma_f + k^2 Ha^2 \mu_f \sigma_{nf}, \\ b &= (4\mu_{nf} \sigma_f + k^2 Ha^2 \mu_f \sigma_{nf})^2, \\ c &= Ha \beta (\rho\zeta)_f \sigma_{nf}, \\ a_1 &= \frac{k Ha \sqrt{\mu_f \sigma_{nf}}}{\sqrt{\mu_{nf} \sigma_f}}. \end{aligned} \quad (7.30)$$

Solution of first order

Under the boundary conditions (7.22) and (7.23), we can assume the solution of first order system as

$$\begin{aligned} \theta_1(r, x) &= \sin(\lambda x) f(r), \\ w_1(r, x) &= \sin(\lambda x) g(r), \end{aligned} \quad (7.31)$$

where $f(r)$ and $g(r)$ is function of r .

Using Eq. (7.31) into Eqs. (7.20) to (7.23), we get

$$\frac{d^2 f(r)}{dr^2} + \frac{1}{(k+r)} \frac{df(r)}{dr} - \frac{k^2}{(k+r)^2} \lambda^2 f(r) = 0, \quad (7.32)$$

$$\frac{\mu_{nf}}{\mu_f} \left(\frac{d^2 g(r)}{dr^2} + \frac{1}{(k+r)} \frac{dg(r)}{dr} - \lambda^2 \left(\frac{k}{r+k} \right)^2 g(r) \right) + \frac{\sigma_{nf}}{\sigma_f} \left(\frac{k}{r+k} \right)^2 Ha^2 g(r) + \frac{(\rho\zeta)_{nf}}{(\rho\zeta)_f} Gr f(r) = 0. \quad (7.33)$$

with the following boundary conditions

$$f_{r=1} = -\frac{d\theta_0}{dr}, \quad f_{r=-1} = \mp \frac{d\theta_0}{dr}, \quad (7.34)$$

$$g_{r=1} = -\frac{dw_0}{dr}, \quad g_{r=-1} = \mp \frac{dw_0}{dr}. \quad (7.35)$$

The solution of first order problem can be expressed as

$$\theta_1^\pm(r, x) = \sin(\lambda x) \begin{cases} \sin(\lambda x) (C_1 \cosh(k\lambda \ln(k+r)) + iC_2 \sinh(k\lambda \ln(k+r))), \\ \sin(\lambda x) (C'_1 \cosh(k\lambda \ln(k+r)) + iC'_2 \sinh(k\lambda \ln(k+r))). \end{cases} \quad (7.36)$$

$$w_1^\pm(r, x) = \begin{cases} \sin(\lambda x) (D_1 \cosh(a_2 \ln(k+r)) + iD_2 \sinh(a_2 \ln(k+r)) + (Gr(k+r))^2 \sigma_f (\rho\zeta)_{nf} \\ \mu_f (4((C_1 - iC_2 k\lambda) \cosh(k\lambda \ln(k+r)) + i(C_2 + iC_1 k\lambda) \sinh(k\lambda \ln(k+r))) \mu_{nf} \\ \sigma_f \sinh(k\lambda \ln(k+r)) + k^2 Ha^2 C_1 \cosh(k\lambda \ln(k+r)) + \sinh(k\lambda \ln(k+r))) iC_2 \\ \mu_f \sigma_{nf}) / ((\rho\zeta)_f 16(-1 + k^2 \lambda^2) u_{nf}^2 \sigma_f^2 - 8k^2 Ha^2 \mu_f \mu_{nf} \sigma_f \sigma_{nf} - k^4 Ha^4 \mu_f^2 \sigma_{nf}^2)) \\ \sin(\lambda x) (D'_1 \cosh(a_2 \ln(k+r)) + iD'_2 \sinh(a_2 \ln(k+r)) + (Gr(k+r))^2 (\rho\zeta)_{nf} \\ \mu_f \sigma_f (4((C'_1 - iC'_2 k\lambda) \cosh(k\lambda \ln(k+r)) + \sinh(k\lambda \ln(k+r))) i(C'_2 + iC'_1 k\lambda) \\ \mu_{nf} \sigma_f + k^2 Ha^2 C'_1 \cosh(k\lambda \ln(k+r)) + iC'_2 \sinh(k\lambda \ln(k+r))) \mu_f \sigma_{nf}) / \\ ((\rho\zeta)_f 16(-1 + k^2 \lambda^2) u_{nf}^2 \sigma_f^2 - 8k^2 Ha^2 \mu_f \mu_{nf} \sigma_f \sigma_{nf} - k^4 Ha^4 \mu_f^2 \sigma_{nf}^2)) \end{cases}, \quad (7.37)$$

$$a_2 = \frac{k \sqrt{\lambda^2 \mu_{nf} \sigma_f - Ha^2 \mu_f \sigma_{nf}}}{\sqrt{\mu_{nf} \sigma_f}}. \quad (7.38)$$

Solution of second order

The boundary conditions (7.26) and (7.27) can be simplified by applying the solution of zero and first order. Under conditions we can suppose the solution as

$$\theta_2^\pm(r, x) = h^\pm(r) + \cos(2\lambda x) k^\pm(r), \quad (7.39)$$

$$w_2^\pm(r, x) = m^\pm(r) + \cos(2\lambda x) n^\pm(r), \quad (7.40)$$

where $h^\pm(r)$, $k^\pm(r)$, $m^\pm(r)$ and $n^\pm(r)$ are function of r only.

By employing Eq.(7.39) and Eq.(7.40) into Eq. (7.24) and Eq. (7.25), we get the following forms

$$\frac{d^2 h^\pm(r)}{dr^2} + \frac{1}{k+r} \frac{dh^\pm(r)}{dr} = 0, \quad (7.41)$$

$$\frac{d^2 k^\pm(r)}{dr^2} + \frac{1}{(k+r)} \frac{dk^\pm(r)}{dr} - \frac{4\lambda^2 k^2}{(k+r)^2} \lambda^2 k^\pm(r) = 0, \quad (7.42)$$

$$\frac{\mu_{nf}}{\mu_f} \left(\frac{d^2 m^\pm(r)}{dr^2} + \frac{1}{(k+r)} \frac{dm^\pm(r)}{dr} \right) + \frac{\sigma_{nf}}{\sigma_f} \left(\frac{k}{r+k} \right)^2 H a^2 m^\pm(r) + \frac{(\rho\zeta)_{nf}}{(\rho\zeta)_f} Gr h^\pm(r) = 0, \quad (7.43)$$

$$\frac{\mu_{nf}}{\mu_f} \left(\frac{d^2 n^\pm(r)}{dr^2} + \frac{1}{(k+r)} \frac{dn^\pm(r)}{dr} \right) - 4\lambda^2 \left(\frac{k}{r+k} \right)^2 n^\pm(r) + \frac{\sigma_{nf}}{\sigma_f} \left(\frac{k}{r+k} \right)^2 H a^2 n^\pm(r) + \frac{(\rho\zeta)_{nf}}{(\rho\zeta)_f} Gr k^\pm(r) = 0. \quad (7.44)$$

and boundary conditions are

$$h^\pm = \begin{cases} -\frac{1}{2} \left(\frac{df}{dr} + \frac{1}{2} \frac{d^2 \theta_0}{dr^2} \right) & \text{at } r = 1, \\ -\frac{1}{2} \left(\pm \frac{df}{dr} - \frac{1}{2} \frac{d^2 \theta_0}{dr^2} \right) & \text{at } r = 1, \end{cases} \quad (7.45)$$

$$k^\pm = \begin{cases} \frac{1}{2} \left(\frac{df}{dr} + \frac{1}{2} \frac{d^2 \theta_0}{dr^2} \right) & \text{at } r = 1, \\ -\frac{1}{2} \left(\pm \frac{df}{dr} - \frac{1}{2} \frac{d^2 \theta_0}{dr^2} \right) & \text{at } r = 1, \end{cases} \quad (7.46)$$

$$m^\pm = \begin{cases} -\frac{1}{2} \left(\frac{dg}{dr} + \frac{1}{2} \frac{d^2 w_0}{dr^2} \right) & \text{at } r = 1, \\ -\frac{1}{2} \left(\pm \frac{dg}{dr} - \frac{1}{2} \frac{d^2 w_0}{dr^2} \right) & \text{at } r = 1, \end{cases}, \quad (7.47)$$

$$n^\pm = \begin{cases} \frac{1}{2} \left(\frac{dg}{dr} + \frac{1}{2} \frac{d^2 w_0}{dr^2} \right) & \text{at } r = 1, \\ -\frac{1}{2} \left(\pm \frac{dg}{dr} - \frac{1}{2} \frac{d^2 w_0}{dr^2} \right) & \text{at } r = 1. \end{cases} \quad (7.48)$$

Thus the solution of second order system can be obtained as

$$\theta_2^\pm = \begin{cases} E_2 + E_1 \ln(k+r) + \cos(2\lambda x) (G_1 \cosh(2k\lambda \ln(k+r)) + iG_2 \sinh(2k\lambda \ln(k+r))), \\ E'_2 + E'_1 \ln(k+r) + \cos(2\lambda x) (G'_1 \cosh(2k\lambda \ln(k+r)) + iG'_2 \sinh(2k\lambda \ln(k+r))), \end{cases} \quad (7.49)$$

$$w_2^\pm = \left\{ \begin{array}{l} F_1 \cosh(a_1 \ln(k+r)) + F_2 \sinh(a_1 \ln(k+r)) + (Gr(k+r))^2 \mu_f (\rho\zeta)_{nf} \sigma_f (-4((\\ -E_1 + E_2) E_1 \ln(k+r)) \mu_{nf} \sigma_f - k^2 Ha^2 (E_2 + E_1 \ln(k+r)) \mu_f \sigma_{nf}) / ((\rho\zeta)_f b) \\ + \cos(2\lambda x) (H_1 \cosh(a_3 \ln(k+r)) + i H_2 \sinh(a_3 \ln(k+r)) + (Gr(\rho\zeta)_{nf} \mu_f \sigma_f \\ (\cosh(2k\lambda \ln(k+r)) + i \sinh(2k\lambda \ln(k+r))) (4(G_2 + 2iG_1 k\lambda) \mu_{nf} \sigma_f + G_1 k^2 \\ Ha^2 \mu_f \sigma_{nf}))) / ((\rho\zeta)_f 16(-1 + 4k^2 \lambda^2) u_{nf}^2 \sigma_f^2 - 8k^2 Ha^2 \mu_f \mu_{nf} \sigma_f \sigma_{nf} - k^4 Ha^4 \mu_f^2 \sigma_{nf}^2)) \\ F'_1 \cosh(a_1 \ln(k+r)) + F'_2 \sinh(a_1 \ln(k+r)) + (Gr(k+r))^2 \mu_f (\rho\zeta)_{nf} \sigma_f (-4((\\ -E'_1 + E'_2) E'_1 \ln(k+r)) \mu_{nf} \sigma_f - k^2 Ha^2 (E'_2 + E'_1 \ln(k+r)) \mu_f \sigma_{nf}) / ((\rho\zeta)_f b) + \\ \cos(2\lambda x) (H'_1 \cosh(a_3 \ln(k+r)) + i H'_2 \sinh(a_3 \ln(k+r)) + (Gr(k+r))^2 (\rho\zeta)_{nf} \\ \mu_f \sigma_f (\cosh(2k\lambda \ln(k+r)) (4(G'_1 - 2iG'_2 k\lambda) \mu_{nf} \sigma_f + G'_1 k^2 Ha^2 \mu_f \sigma_{nf}) + i \sinh(2k\lambda \\ \ln(k+r)) (4(G'_2 + 2iG'_1 k\lambda) \mu_{nf} \sigma_f + G'_1 k^2 Ha^2 \mu_f \sigma_{nf}))) / ((\rho\zeta)_f 16(-1 + 4k^2 \lambda^2) u_{nf}^2 \\ \sigma_f^2 - 8k^2 Ha^2 \mu_f \mu_{nf} \sigma_f \sigma_{nf} - k^4 Ha^4 \mu_f^2 \sigma_{nf}^2)) \end{array} \right. , \quad (7.50)$$

with

$$a_3 = \frac{k \sqrt{4\lambda^2 \mu_{nf} \sigma_f - Ha^2 \mu_f \sigma_{nf}}}{\sqrt{\mu_{nf} \sigma_f}}. \quad (7.51)$$

Collecting Eqs.(7.28), (7.29), (7.36), (7.37), (7.49) and (7.50), the approximate velocity and temperature solution as

$$\theta^\pm(r, x) = \theta_0(r) + \varepsilon \theta_1^\pm(r, x) + \varepsilon^2 \theta_2^\pm(r, x) + \dots \quad (7.52)$$

$$w^\pm(r, x) = w_0(r) + \varepsilon w_1^\pm(r, x) + \varepsilon^2 w_2^\pm(r, x) + \dots \quad (7.53)$$

Evaluation of constants have been done by using Mathematica 9.

7.3 Heat transfer rate

Nusselt number determines the convective heat exchange strength. Defined as follows [86]

$$Nu = \frac{Hq_w}{k''_f (T_u^* - T_p^*)}, \quad (7.54)$$

On upper and lower walls we defined

$$q_w = -k''_{nf} \frac{\partial T^*}{\partial r^*} \Big|_{r^*=r_u^*} . \quad (7.55)$$

From Eqs. (7.54) and (7.55), the Nusselt number can be expressed as

$$Nu = -\frac{k''_{nf}}{k''_f} \frac{\partial \theta}{\partial r} \Big|_{r=r_u} . \quad (7.56)$$

7.4 Thermophysical properties

The thermophysical properties are

Physical Properties	Water	Copper
$C_p(J/kgK)$	4179	385
$\rho(kg/m^3)$	997.1	8933
$k''(W/mK)$	0.613	400
$\zeta \times 10^5 (1/K)$	21.0	1.67
$\sigma(S/m)$	5.0×10^{-2}	5.96×10^7
$\mu(kg/m.sec)$	8.90×10^{-4}	-

Table (7.1): Thermo physical effects.

7.5 Graphical consequence

In this part, the graphical impacts of viscous fluid are investigated by EMHD flow in a curved channel with corrugated walls. All graphical outcomes are achieved by utilizing the MATLAB programming. This segment is explicitly arranged to investigate the impact of inserted parameters on flow quantities. Plots 3D variations of velocity and contour are appeared dismembered through Figs. (7.2) to (7.5) respectively.

The 3D variations and contour plots are acquired from the solutions of the velocity w^\pm and temperature θ^\pm for curvature parameter k are shown in Figs. (7.2) to (7.5). In Figs. (7.2) and (7.4) the phase difference among the two corrugated walls equals is 0° . Figs. (7.2) and (7.4) shows that bolus increase with expanding value of curvature parameter k . In Figs. (7.3) and (7.5), the phase difference between walls equals to 180° . It is found that trapped bolus

increases with enlarging curvature parameter k out-of-phase corrugations when ε is small. As shows in Figs. (7.2) to (7.5), the wave phenomenon of the flow shape becomes obvious with the expansion of the corrugation. The wavy pattern increases by increase the value of parameters.

In Figs. (7.6) to(7.12), the velocities w^\pm and temperature θ^\pm are plotted against r for various estimations of parameters the Hartmann number Ha , Volumetric concentration Φ , Grashof number Gr , Curvature parameter k and Heat absorption coefficient ϕ when we take $\varepsilon = 0.1$ and $\beta = 5$. Specifically, it can be found in Figs. (7.6) to (7.10), that the velocity amplitude accomplishes the maximum value at the middle of the channel. Fig. (7.6) shows that the velocity w^\pm increases with expanding Hartmann number. Fig. (7.7) demonstrates that the velocity w^\pm declines for various estimations of Volumetric concentration of nanoparticles Φ . Fig. (7.8) shows that the velocity w^\pm increases with Grashof number. Fig. (7.9) demonstrates that the velocity w^\pm decreases for curvature parameter k . Fig. (7.10) admits that EMHD velocity w^\pm increases for various values of heat absorption coefficient ϕ . We can found that, the EMHD velocities in phase are weaker than out of phase. Fig. (7.11) shows that profile of temperature θ^\pm decreases when the curvature parameter k increases. Fig. (7.12) depicts the consequence of Heat absorption coefficient ϕ on temperature plot. Temperature variation grows when the ϕ increases.

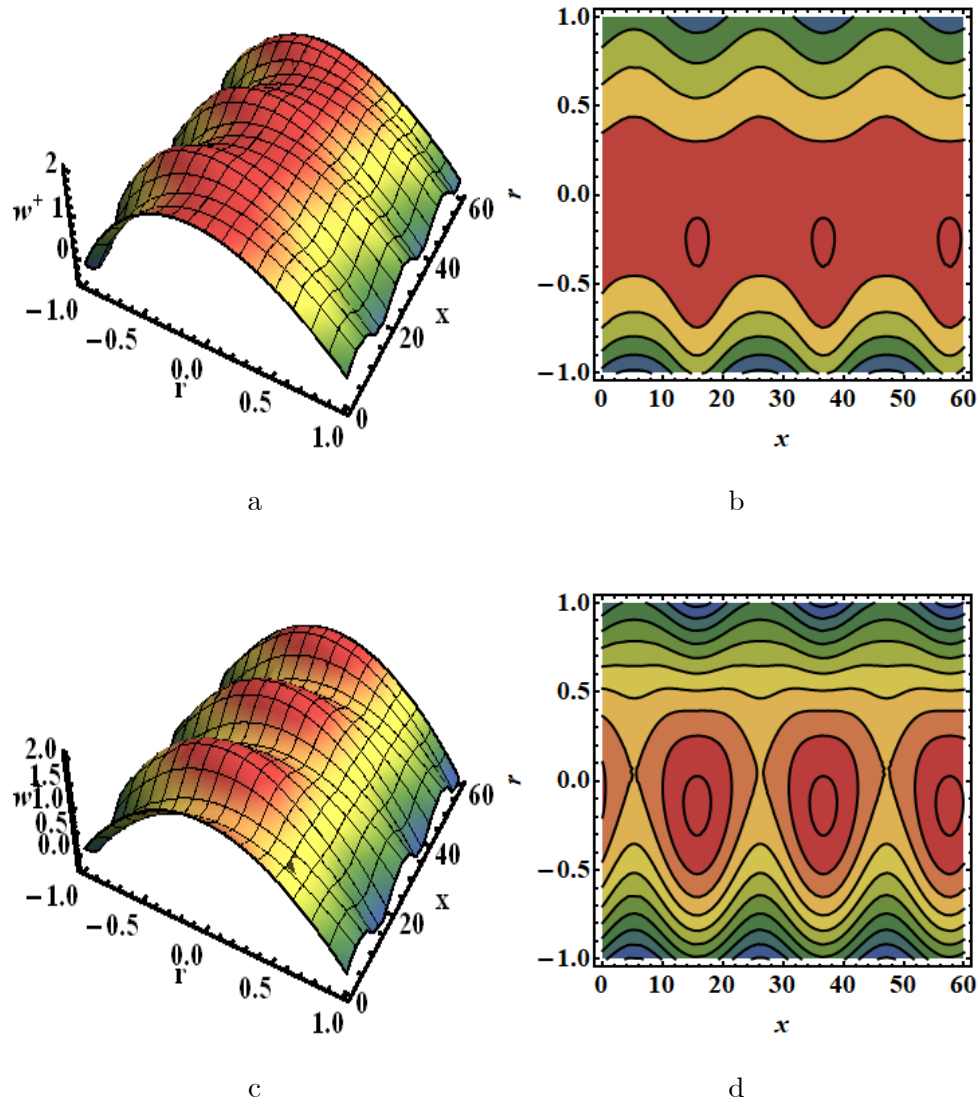


Fig. (7.2): 3D Velocity distribution and contour (a, b, c, d) for $k = 1.5$ and $k = 3.5$ in phase.

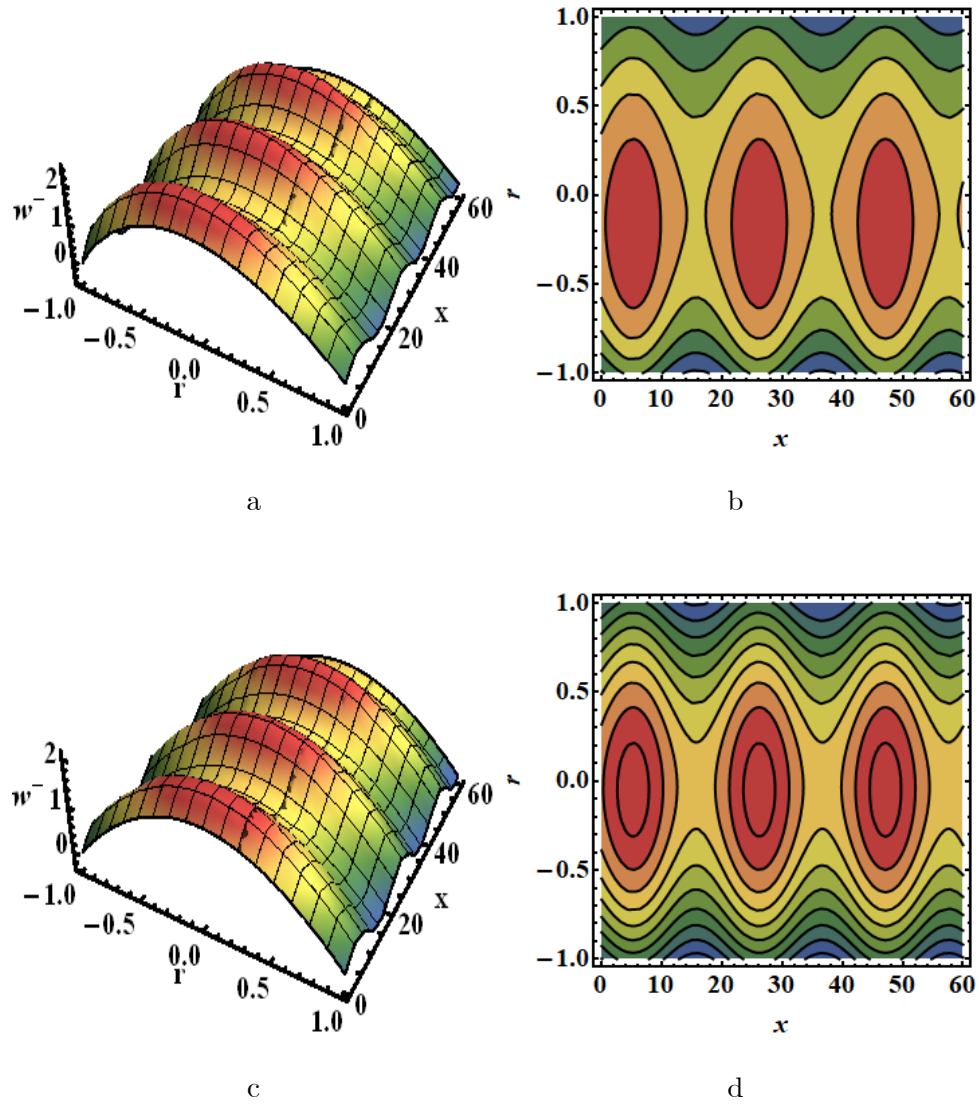


Fig. (7.3): 3D Velocity distribution and contour (a, b, c, d) for $k = 1.5$ and $k = 3.5$ out of phase.

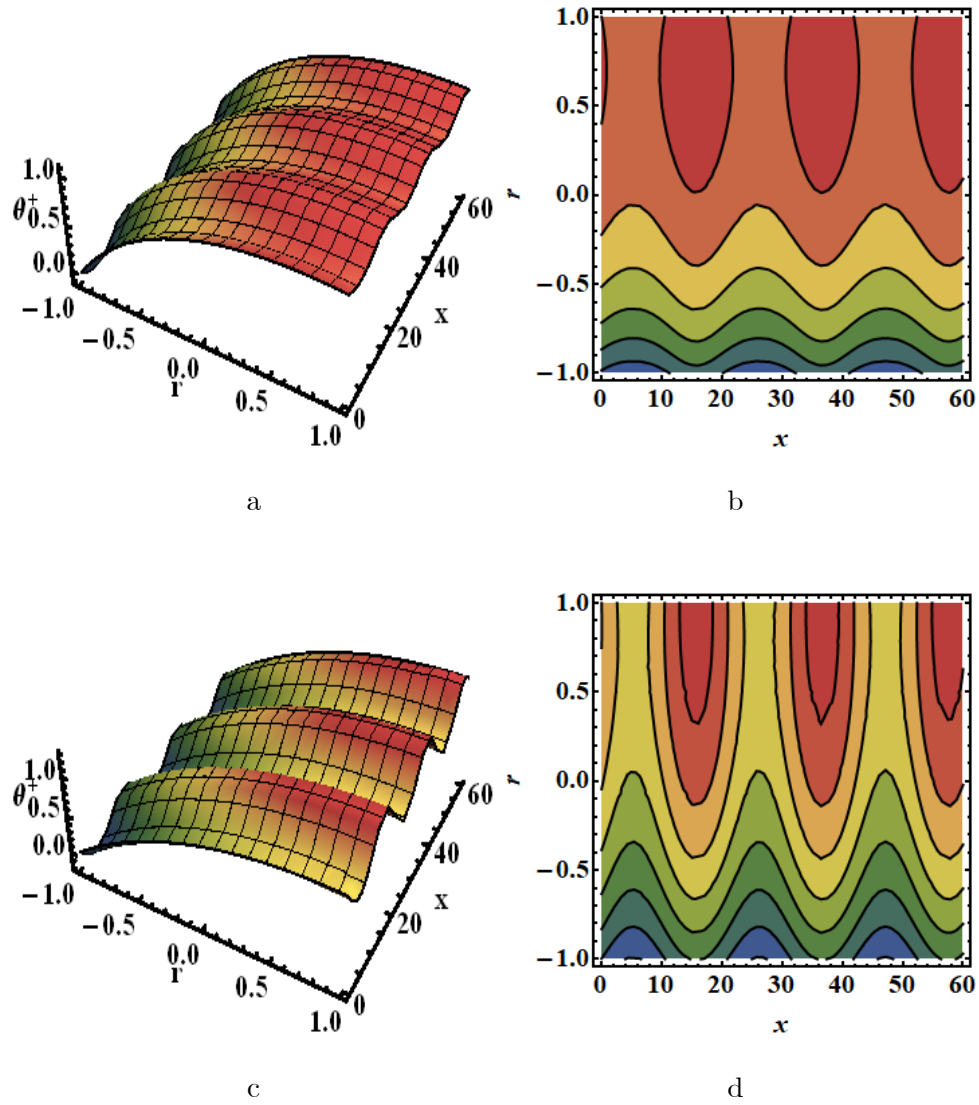
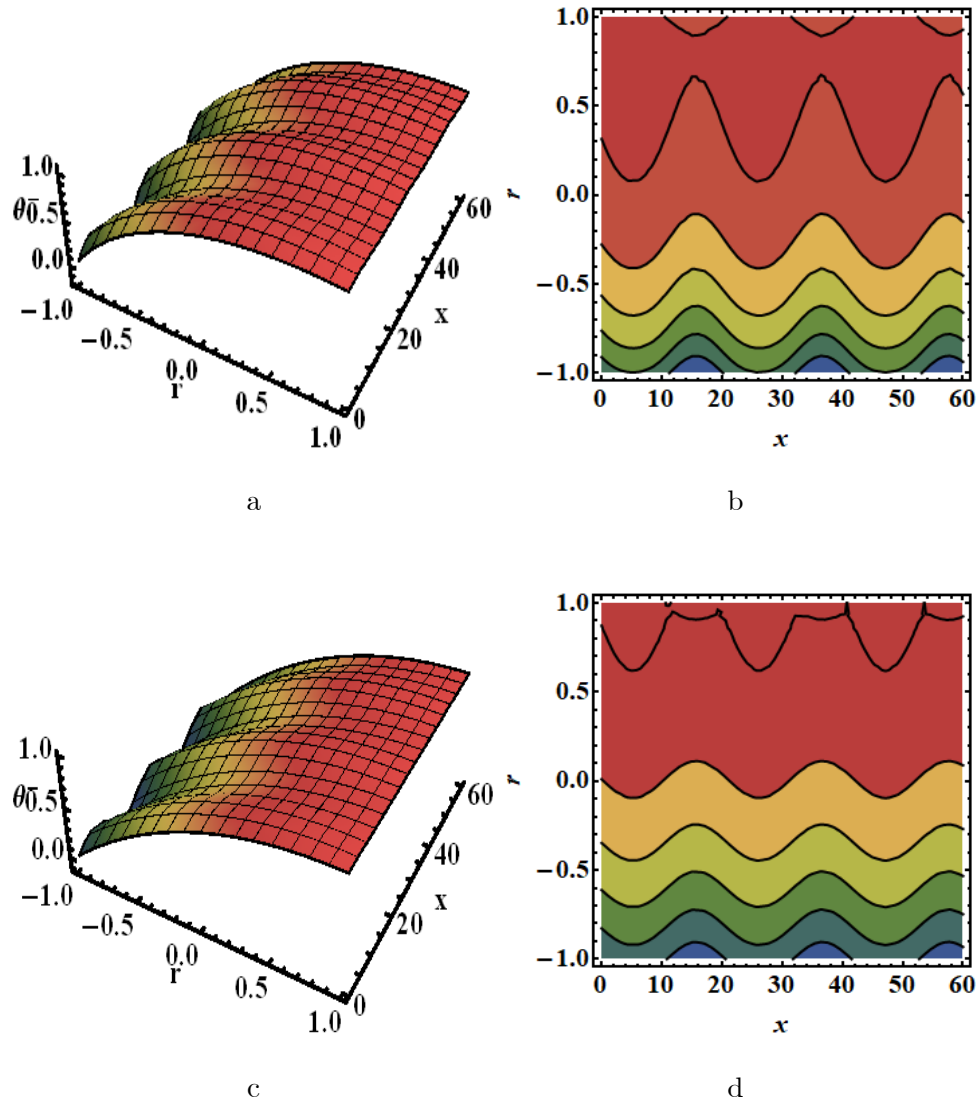


Fig. (7.4): 3D Temperature distribution and contour (a, b, c, d) for $k = 1.5$ and $k = 3.5$ in phase.



Figs. (7.5): 3D Temperature contour for Curvature parameter $k = 1.5$ and $k = 3.5$ out of phase.

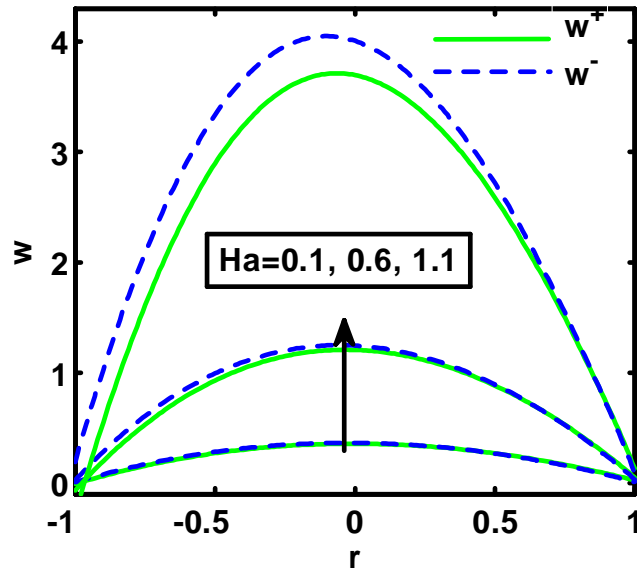


Fig. (7.6): 2D Variation of velocity for Hartmann number Ha .

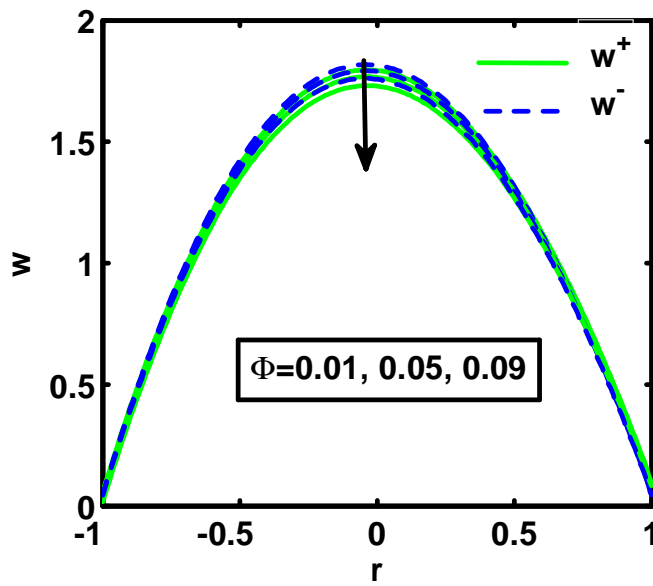


Fig. (7.7): 2D Variation of velocity for Volumetric concentration of nanoparticles Φ .

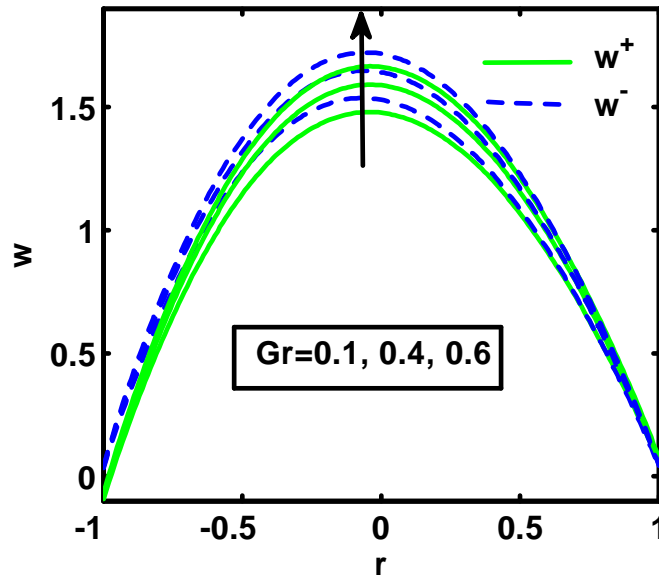


Fig. (7.8): 2D Variation of velocity for Grashof number Gr .

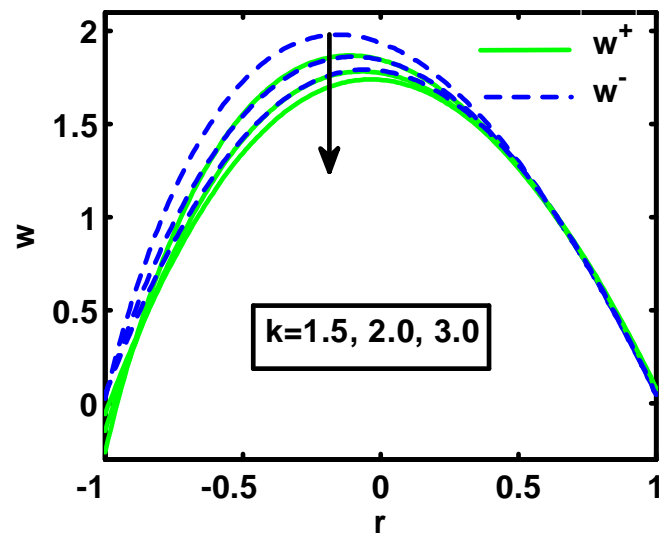


Fig. (7.9): 2D Variation of velocity for Curvature parameter k .

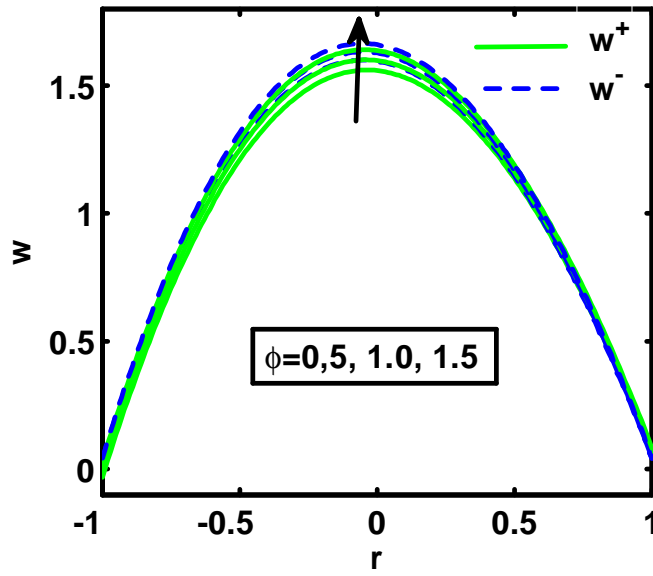


Fig. (7.10): 2D Variation of velocity for Heat absorption coefficient ϕ .

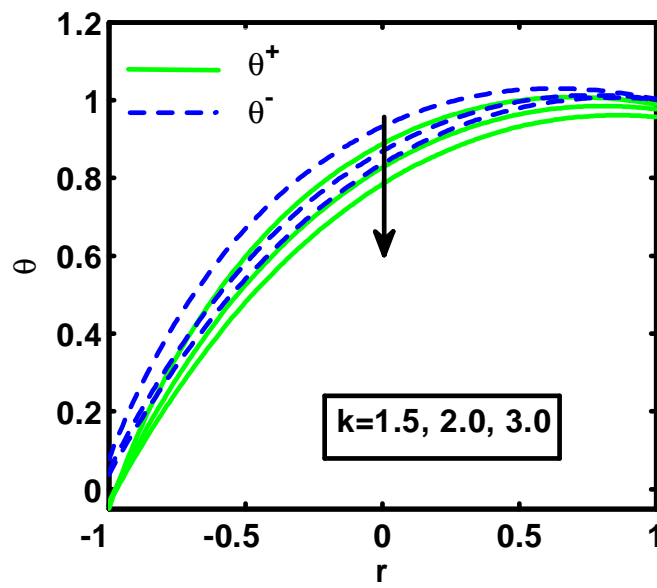


Fig. (7.11): 2D Variation of temperature for Curvature parameter k .

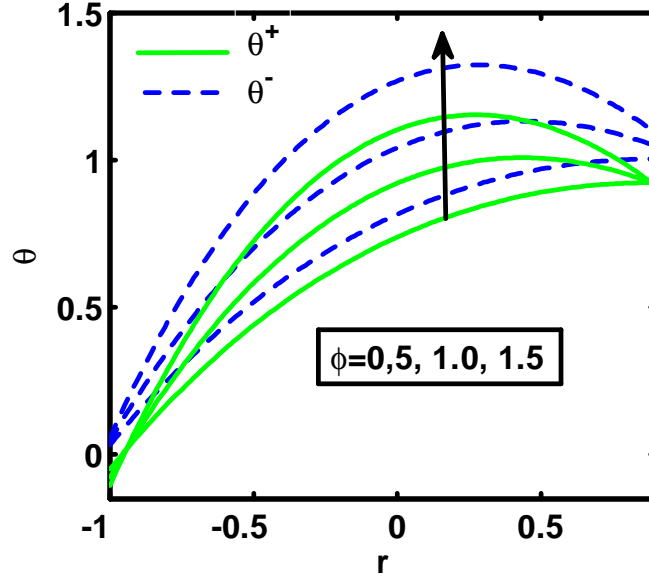


Fig. (7.12): 2D Variation of temperature for Heat absorption coefficient ϕ .

r	τ_{rz}^+ in phase			τ_{rz}^- out of phase		
	$k = 2.5$	$k = 4.0$	$k = 5.0$	$k = 2.5$	$k = 4.0$	$k = 5.0$
-1	5.00097	4.38566	3.28585	4.90409	4.34458	4.20501
-0.8	3.77671	3.52612	2.56966	3.67526	3.4262	3.35829
-0.6	2.64766	2.65359	1.84091	2.54358	2.50167	2.48748
-0.4	1.61499	1.78832	1.11609	1.50944	1.58999	1.61143
-0.2	0.671711	0.943975	0.407727	0.565348	0.703732	0.744382
0	-0.191463	0.129656	-0.274713	-0.298267	-0.148966	-0.102962
0.2	-0.983743	-0.648739	-0.92417	-1.09082	-0.963014	-0.922668
0.4	-1.71342	-1.38752	-1.53542	-1.82074	-1.73542	-1.70892
0.6	-2.3876	-2.08454	-2.10465	-2.49521	-2.46461	-2.45756
0.8	-3.01223	-2.73868	-2.62915	-3.12025	-3.14998	-3.16565
1	-3.59224	-3.34955	-3.10702	-3.7008	-3.79156	-3.83125

Table (7.2): Impact of curvature parameter k on Stress components $\tau_{rz}^{\pm} = \frac{\mu_{nf}}{\mu_f} \frac{\partial w}{\partial r}$

		τ_{rx}^+ in phase			τ_{rx}^- out of phase		
r	$k = 2.5$	$k = 4.0$	$k = 5.0$	$k = 2.5$	$k = 4.0$	$k = 5.0$	
-1	-0.231029	-0.178203	-0.20903	0.244095	0.172208	0.156072	
-0.8	-0.172401	-0.220363	-0.520479	0.222807	0.169103	0.15621	
-0.6	-0.12452	-0.239668	-0.732131	0.201311	0.163309	0.153674	
-0.4	-0.0848175	-0.240199	-0.855576	0.180792	0.15574	0.149153	
-0.2	-0.0513982	-0.225175	-0.900917	0.161743	0.147063	0.143193	
0	-0.0228554	-0.19715	-0.876924	0.144326	0.137764	0.136231	
0.2	0.00186674	-0.158159	-0.791185	0.12854	0.128201	0.128614	
0.4	0.0235702	-0.109826	-0.650256	0.114309	0.118631	0.120617	
0.6	0.0428717	-0.0534562	-0.459789	0.101526	0.109244	0.112459	
0.8	0.0602508	0.0098998	-0.22465	0.0900729	0.100176	0.104314	
1	0.0760844	0.0793949	0.0509706	0.0798331	0.0915214	0.0963176	

Table (7.3): Impact of curvature parameter k on Stress components $\tau_{rx}^{\pm} = \frac{\mu_{nf}}{\mu_f} \frac{k}{r+k} \frac{\partial w}{\partial x}$.

r	$k = 1.5$	$k = 2.5$	$k = 3.5$
-1	-0.133035	-0.0331892	0.0577811
-0.8	-0.134987	-0.0389481	0.0395459
-0.6	-0.137009	-0.0447724	0.0211779
-0.4	-0.139093	-0.0506403	0.00274853
-0.2	-0.141234	-0.0565299	-0.0156717
0	-0.143423	-0.0624198	-0.0340141
0.2	-0.145653	-0.0682885	-0.0522116
0.4	-0.147916	-0.0741149	-0.0701992
0.6	-0.150202	-0.0798783	-0.0879144
0.8	-0.152501	-0.0855585	-0.105297
1	-0.154804	-0.0911357	-0.12229

Table (7.4): Impact of curvature parameter k on Nusselt number Nu^+ .

x	$k = 1.5$	$k = 2.5$	$k = 3.5$
-1	-0.135427	-0.0414312	-0.00237821
-0.8	-0.141131	-0.0471789	-0.00826093
-0.6	-0.146811	-0.0529364	-0.0141611
-0.4	-0.152444	-0.0586804	-0.0200548
-0.2	-0.158007	-0.0643883	-0.0259191
0	-0.163478	-0.0700387	-0.0317317
0.2	-0.168839	-0.075611	-0.0374716
0.4	-0.17407	-0.0810858	-0.0431184
0.6	-0.179156	-0.0864449	-0.0486533
0.8	-0.184083	-0.0916713	-0.0540582
1	-0.188836	-0.0967492	-0.0593164

Table (7.5): Impact of curvature parameter k on Nusselt number Nu^- .

7.6 Tables Description

In this section, we discussed the impact of stress components and Nusselt number on EMHD flow in curved channel through corrugated walls. This section expressed the behavior of curvature parameter k on the stress components τ_{zr}^{\pm} and τ_{zx}^{\pm} and Nusselt number Nu^{\pm} . Table 7.2 demonstrates that the stress components τ_{zr}^+ and τ_{zr}^- decrease with the increasing value of r and furthermore decrease with the rise of the curvature parameter k . Table 7.3 shows that the stress components τ_{zx}^+ and τ_{zx}^- increase with the increasing value of r and also expand with the increment in the value of curvature parameter k . The impact of Nusselt number $Nu = -\frac{k''_{nf}}{k''_f} \theta'(y_u)$ on EMHD flow of nanofluid discussed in microchannel through corrugated walls. Table 7.4 and Table 7.5 demonstrate that the Nusselt number Nu^{\pm} decrease with the increasing value of x and increase with increment in the value of curvature parameter k .

7.7 Conclusion

The consequence of corrugated wall roughness on the viscous EMHD flow in a curved channel is determined in this paper. Perturbation technique is applied to inspect the issue. From the above outcomes, the accompanying reasonings are drawn.

- The wavy phenomenon in the center becomes obvious when the amplitude ε is small with in phase and out of phase corrugations.
- The contour plots from the solutions of the velocity, it is found that trapped bolus are appeared for out-of-phase corrugations.
- The wavy phenomenon increases by increasing in the estimation of parameters.
- The velocity amplitude accomplishes the maximum value on the channel center.
- The velocity enlarges for various values of Ha and Gr .
- The velocity declines for various estimations of Volumetric concentration of nanoparticles Φ and curvature parameter k .
- The EMHD velocity w^\pm increases by increment in heat absorption coefficient ϕ .
- The profile of temperature θ^\pm decreases when the curvature parameter k and increases when the ϕ increases.
- The bolus increase with enlarging the value of curvature parameter k in phase and out of phase corrugations when ε is small.
- The EMHD velocities in phase are weaker than out of phase.
- Stress components τ_{zr}^\pm decrease with the rise of the curvature parameter while stress components τ_{zx}^\pm increase with the increasing value of the curvature parameter.
- The Nusselt number Nu^\pm decrease with the increasing value of x and increase with increment in the value of curvature parameter k .

Chapter 8

Analysis of EMHD Casson Fluid in curved channel with corrugated walls under metallic nanoparticles

The main object of this chapter is to deal the steady EMHD non-Newtonian incompressible and electrical conducting Casson fluid between corrugated walls in the presence of Lorenz force has been examined. The Casson fluid model is utilized to characterize the non-Newtonian fluid behavior. The equations are transformed by utilizing the perturbation method. Analytical solution corresponding to momentum and temperature equations are acquired. The heat transfer features are analyzed and discussed in detail.

8.1 Formulation of problem

Deliberate the steady, incompressible and electrically conducting Casson fluid between corrugated wall in the curved channel separated by a distance $2H$, center at O and radius R' is considered. The flow induced in the channel by sine waves with amplitude ε in the corrugated walls of the a channel. The wavy walls are located at

$$r_{u^*}^* = H + \varepsilon H \sin(\lambda^* x^*) \text{ and } r_{l^*}^* = -H \pm \varepsilon H \sin(\lambda^* x^*). \quad (8.1)$$

where ε is small amplitude and λ^* is wave number. We take magnetic field \mathbf{B}^* along y^* direction while along the x^* direction electric field \mathbf{E}^* is applied. Along the z^* direction, we take the Lorentz force which is produced by the contact among the magnetic field \mathbf{B}^* and the electric field \mathbf{E}^* .

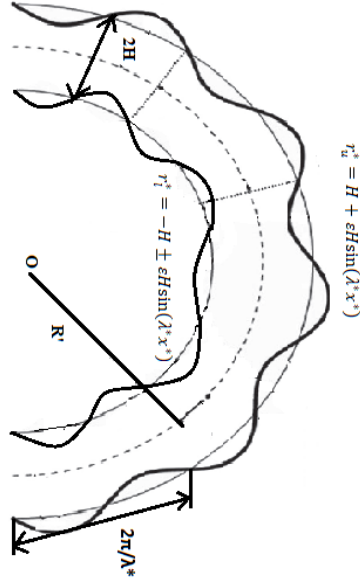


Fig. (8.1): Geometrical sketch of EMHD flow in microchannel.

The rheological equation of Casson fluid is [66]

$$\tau_{ij} = \begin{cases} 2(\mu_\beta + p_y/\sqrt{2\pi})e_{ij}, \pi \succ \pi_c \\ 2(\mu_\beta + p_y/\sqrt{2\pi})e_{ij}, \pi \prec \pi_c \end{cases}, \quad (8.2)$$

where τ_{ij} is the stress tensor component, π is the component of deformation, π_c is critical value, μ_β is the plastic dynamics viscosity and p_y yield stress.

Velocity field expressed as

$$\mathbf{u}^* = (0, 0, w^*(X^*, R^*)). \quad (8.3)$$

For present situation the flow equations are

$$\frac{\partial w^*}{\partial z^*} = 0, \quad (8.4)$$

$$\left(\frac{1}{\dot{R} + R^*} \frac{\partial}{\partial R^*} (R^* + \dot{R}) \bar{\tau}_{Z^*R^*}\right) + \frac{\dot{R}}{\dot{R} + R^*} \bar{\tau}_{Z^*X^*} + \sigma_{nf} B^* (E^* - \left(\frac{\dot{R}}{\dot{R} + R^*}\right)^2 B^* w^*) + g(\rho\zeta)_{nf} (T^* - T_l^*) = 0, \quad (8.5)$$

$$k''_{nf} \left(\frac{1}{\dot{R} + R^*} \frac{\partial}{\partial R^*} ((R^* + \dot{R}) \frac{\partial T^*}{\partial R^*}) + \left(\frac{\dot{R}}{\dot{R} + R^*}\right)^2 \frac{\partial^2 T^*}{\partial X^{*2}} \right) + Q_0 = 0. \quad (8.6)$$

In above equations, T represents the temperature and Q_0 shows heat absorption constant. $(\rho_{nf}, \mu_{nf}, \sigma_{nf}, k''_{nf}, \zeta_{nf}, (\rho C_p)_{nf})$ denotes nanofluid (density, viscosity, electrical conductivity, thermal conductivity, thermal expansion coefficient, heat capacitance). These constants are

$$\begin{aligned} \mu_{nf} &= \frac{\mu_f}{(1 - \Phi)^{2.5}}, \quad \alpha_{nf} = \frac{k''_{nf}}{(\rho C_p)_{nf}}, \quad \rho_{nf} = (1 - \Phi)\rho_f + \Phi\rho_s, \\ (\rho\zeta)_{nf} &= (1 - \Phi)(\rho\zeta)_f + \Phi(\rho\zeta)_s, \quad (\rho C_p)_{nf} = (1 - \Phi)(\rho C_p)_f + \Phi(\rho C_p)_s, \\ \frac{k''_{nf}}{k''_f} &= \frac{(k''_s + 2k''_f) - 2\Phi(k''_f - k''_s)}{(k''_s + 2k''_f) + \Phi(k''_f - k''_s)}, \quad \frac{\sigma_{nf}}{\sigma_f} = 1 + \frac{(\frac{\sigma_s}{\sigma_f} - 1)\Phi}{(\frac{\sigma_s}{\sigma_f} + 1) - \Phi(\frac{\sigma_s}{\sigma_f} - 1)}. \end{aligned} \quad (8.7)$$

Here $\rho_f, \rho_s, \zeta_f, \zeta_s, k''_f, k''_s, (\rho C_p)_f, (\rho C_p)_s, \sigma_f$ and σ_s represents the densities, thermal expansion coefficients, thermal conductivities, heat capacitance and electrical conductivities respectively. Suppose along the z^* direction channel is open, so we can ignore the pressure gradient $\partial p/\partial z^*$ along the microchannel [85] and the velocity $w^*(x^*, y^*)$ satisfies

$$\left(\frac{1}{\dot{R} + R^*} \frac{\partial}{\partial R^*} (R^* + \dot{R}) \bar{\tau}_{Z^*R^*}\right) + \frac{\dot{R}}{\dot{R} + R^*} \bar{\tau}_{Z^*X^*} + \sigma_{nf} B^* (E^* - \left(\frac{\dot{R}}{\dot{R} + R^*}\right)^2 B^* w^*) + g(\rho\zeta)_{nf} (T^* - T_l^*) = 0, \quad (8.8)$$

where

$$\bar{\tau}_{Z^*R^*} = \left(1 + \frac{1}{\gamma^*}\right) \frac{\mu_{nf}}{\mu_f} \frac{\partial w^*}{\partial R^*}, \quad \bar{\tau}_{Z^*X^*} = \left(1 + \frac{1}{\gamma^*}\right) \frac{\mu_{nf}}{\mu_f} \frac{\dot{R}}{\dot{R} + R^*} \frac{\partial w^*}{\partial X^*}, \quad (8.9)$$

where $\gamma^* = \mu_\beta \sqrt{2\pi_c}/p_y$.

The boundary conditions are

$$\begin{aligned} w^*(X^*, R_{u''}^*) &= 0 \text{ at } R_{u''}^* = H + \varepsilon H \sin(\lambda^* X^*), \\ w^*(X^*, R_{l''}^*) &= 0 \text{ at } R_{l''}^* = -H \pm \varepsilon H \sin(\lambda^* X^*), \end{aligned} \quad (8.10)$$

$$\begin{aligned} T^*(X^*, R_{u''}^*) &= T_{u''}^*(X^*, R_{u''}^*) \text{ at } R_{u''}^* = H + \varepsilon H \sin(\lambda^* X^*), \\ k''_{nf} \frac{\partial T^*}{\partial r^*} &= -B(T^* - T_{l''}^*) \text{ at } R_{l''}^* = -H \pm \varepsilon H \sin(\lambda^* X^*). \end{aligned} \quad (8.11)$$

By Introducing dimensionless variables

$$\begin{aligned} (r, x) &= \frac{(R^*, X^*)}{H}, \lambda = \lambda^* H, w = \frac{w^*}{U}, k = \frac{\hat{R}}{H}, Ha = B^* H \left(\frac{\sigma_f}{\mu_f} \right)^{\frac{1}{2}}, \\ \beta &= E_0 \left(\frac{\sigma_f}{\mu_f} \right)^{\frac{1}{2}} / U, \theta = \frac{T - T_{l''}}{T_{u''} - T_{l''}}, Gr = \frac{g(\rho\zeta)_f H(T_{u''} - T_{l''})}{\mu_f U}, \phi = \frac{Q_0 H^2}{k''_f (T_{u''} - T_{l''})}. \end{aligned} \quad (8.12)$$

Dimensionless form of equations are

$$\frac{\mu_{nf}}{\mu_f} \left(1 + \frac{1}{\gamma^*} \right) \left(\frac{\partial^2 w}{\partial r^2} + \frac{1}{r+k} \frac{\partial w}{\partial r} + \left(\frac{k}{r+k} \right)^2 \frac{\partial^2 w}{\partial x^2} \right) + \frac{\sigma_{nf}}{\sigma_f} \left(Ha\beta + \left(\frac{k}{r+k} \right)^2 Ha^2 w \right) + \frac{(\rho\zeta)_{nf}}{(\rho\zeta)_f} Gr\theta = 0, \quad (8.13)$$

$$\frac{\partial^2 \theta}{\partial r^2} + \frac{1}{r+k} \frac{\partial \theta}{\partial r} + \left(\frac{k}{r+k} \right)^2 \frac{\partial^2 \theta}{\partial x^2} + \phi \frac{k''_f}{k''_{nf}} = 0. \quad (8.14)$$

The corresponding non-dimensional conditions are

$$\begin{aligned} w &= 0 \text{ at } r_{u''} = 1 + \varepsilon \sin(\lambda x), \\ w &= 0 \text{ at } r_{l''} = -1 \pm \varepsilon \sin(\lambda x), \\ \theta &= 1 \text{ at } r_{u''} = 1 + \varepsilon \sin(\lambda x), \\ \frac{\partial \theta}{\partial r} + \frac{B_i}{\left(\frac{k''_{nf}}{k''_f} \right)} \theta &= 0 \text{ at } r_{l''} = -1 \pm \varepsilon \sin(\lambda x). \end{aligned} \quad (8.15)$$

8.2 Solution of Problem:

We use the perturbation approximation by taking ε as the small parameter

$$w(r, x) = w_0(r) + \varepsilon w_1(r, x) + \varepsilon^2 w_2(r, x) + \dots \quad (8.16)$$

$$\theta(r, x) = \theta_0(r) + \varepsilon \theta_1(r, x) + \varepsilon^2 \theta_2(r, x) + \dots \quad (8.17)$$

Equating the like power of ε after using the Eq.(8.16), Eq. (8.17) into Eqs. (8.13) to (8.14), we get the following systems as

8.2.1 Zeroth order classification

$$\frac{d^2\theta_0}{dr^2} + \frac{1}{r+k} \frac{d\theta_0}{dr} + \phi \frac{k''_f}{k''_{nf}} = 0, \quad (8.18)$$

$$\frac{\mu_{nf}}{\mu_f} \left(1 + \frac{1}{\gamma^*}\right) \left(\frac{d^2 w_0}{dr^2} + \frac{1}{r+k} \frac{dw_0}{dr}\right) + \frac{\sigma_{nf}}{\sigma_f} \left(Ha\beta + \left(\frac{k}{r+k}\right)^2 Ha^2 w_0\right) + \frac{(\rho\zeta)_{nf}}{(\rho\zeta)_f} Gr\theta_0 = 0, \quad (8.19)$$

$$\theta_0 \quad | \quad r=1 = 1, \quad \frac{d\theta_0}{dr} + \frac{B_i}{\left(\frac{k''_{nf}}{k''_f}\right)} \theta_0 = 0 \quad |_{r=-1} = 0, \quad (8.20)$$

$$w_0 \quad | \quad r=1 = 0, \quad w_0 \quad |_{r=-1} = 0. \quad (8.21)$$

8.2.2 First order classification

$$\frac{\partial^2 \theta_1}{\partial r^2} + \frac{1}{r+k} \frac{\partial \theta_1}{\partial r} + \left(\frac{k}{r+k}\right)^2 \frac{\partial^2 \theta_1}{\partial x^2} = 0, \quad (8.22)$$

$$\frac{\mu_{nf}}{\mu_f} \left(1 + \frac{1}{\gamma^*}\right) \left(\frac{\partial^2 w_1}{\partial r^2} + \frac{1}{r+k} \frac{\partial w_1}{\partial r} + \left(\frac{k}{r+k}\right)^2 \frac{\partial^2 w_1}{\partial x^2}\right) + \frac{\sigma_{nf}}{\sigma_f} \left(\frac{k}{r+k}\right)^2 Ha^2 w_1 + \frac{(\rho\zeta)_{nf}}{(\rho\zeta)_f} Gr\theta_1 = 0, \quad (8.23)$$

$$\theta_1 + \sin(\lambda x) \left(\frac{d\theta_0}{dy}\right) = 0 \quad \text{at } r = 1, \quad (8.24)$$

$$\frac{\partial \theta_1}{\partial r} \pm \sin(\lambda x) \frac{d^2 \theta_0}{dy^2} + \frac{B_i}{\left(\frac{k''_{nf}}{k''_f}\right)} (\theta_1 \pm \sin(\lambda x) \theta_0) = 0 \quad \text{at } r = -1, \quad (8.25)$$

$$w_1 + \sin(\lambda x) \left(\frac{dw_0}{dr} \right) = 0 \text{ at } r = 1, \quad (8.26)$$

$$w_1 \pm \sin(\lambda x) \left(\frac{dw_0}{dr} \right) = 0 \text{ at } r = -1. \quad (8.27)$$

8.2.3 Second order classification

$$\frac{\partial^2 \theta_2}{\partial r^2} + \frac{1}{r+k} \frac{\partial \theta_2}{\partial r} + \left(\frac{k}{r+k} \right)^2 \frac{\partial^2 \theta_2}{\partial x^2} = 0, \quad (8.28)$$

$$\frac{\mu_{nf}}{\mu_f} \left(1 + \frac{1}{\gamma^*} \right) \left(\frac{\partial^2 w_2}{\partial r^2} + \frac{1}{r+k} \frac{\partial w_2}{\partial r} + \left(\frac{k}{r+k} \right)^2 \frac{\partial^2 w_2}{\partial x^2} \right) + \frac{\sigma_{nf}}{\sigma_f} \left(\frac{k}{r+k} \right)^2 H a^2 w_2 + \frac{(\rho\zeta)_{nf}}{(\rho\zeta)_f} G r \theta_2 = 0, \quad (8.29)$$

$$\theta_2 + \sin(\lambda x) \frac{\partial \theta_1}{\partial r} + \frac{\sin^2(\lambda x)}{2} \frac{d^2 \theta_0}{dy^2} = 0 \text{ at } r = 1, \quad (8.30)$$

$$\frac{\partial^2 \theta_2}{\partial r^2} \pm \sin(\lambda x) \frac{\partial^2 \theta_1}{\partial r^2} + \frac{\sin^2(\lambda x)}{2} \frac{d^3 \theta_0}{dy^3} + \frac{B_i}{\left(\frac{k_{nf}}{k_f} \right)} (\theta_2 \pm \sin(\lambda x) \theta_1 + \frac{\sin^2(\lambda x)}{2} \theta_0) = 0 \text{ at } r = -1, \quad (8.31)$$

$$w_2 + \sin(\lambda x) \frac{\partial w_1}{\partial r} + \frac{1}{2} \sin^2(\lambda x) \left(\frac{d^2 w_0}{dr^2} \right) = 0 \text{ at } r = 1, \quad (8.32)$$

$$w_2 \pm \sin(\lambda x) \left(\frac{\partial w_1}{\partial r} \right) + \frac{1}{2} \sin^2(\lambda x) \left(\frac{d^2 w_0}{dr^2} \right) = 0 \text{ at } r = 1. \quad (8.33)$$

Zeroth order solution

Under the boundary conditions the zero-order solution can be expressed as:

$$\theta_0(r) = A_2 + \left(-\frac{1}{2} \phi(r(2k+r) - 2k^2 \text{Log}(k+r)) k''_f + 2A_1 \text{Log}(k+r) \right) k''_{nf} / 2k''_{nf}, \quad (8.34)$$

$$w_0(y) = \left\{ \begin{array}{l} (-Gr(k+r)^2 \phi k''_f \mu_f (\rho\zeta)_{nf} \sigma_f (16r^2(-5k^2 - 2kr - r^2 + 8k^2 \text{Log}(k+r)) u_{nf}^2 \sigma_f^2 + 4Ha^2 \\ k^2(1 + \frac{1}{\gamma^*})(k^2 - 4kr - 2r^2 + 10k^2 \text{Log}(k+r)) \mu_f \mu_{nf} \sigma_f \sigma_{nf} + k^4 Ha^4(-r(2k+r) + 2 \\ k^2 \text{Log}(k+r)) u_f^2 \sigma_{nf}^2) + 4k_{nf}(16(1 + \frac{1}{\gamma^*}) \mu_{nf} \sigma_f + k^2 Ha^2 \mu_f \sigma_{nf})(B_1 \cos(a_1 \text{Log}(k+r)) \\ (\rho\zeta)_f b_1 + B_2 \sin(a_1 \text{Log}(k+r)) (\rho\zeta)_f b_1 + (k+r)^2 \mu_f (4(1 + \frac{1}{\gamma^*}) \mu_{nf} \sigma_f (-Gr(-A_1 + \\ A_2 + A_1 \text{Log}(k+r)) (\rho\zeta)_{nf} \sigma_f - Ha\beta(\rho\zeta)_f \sigma_{nf}) - k^2 Ha^2 \mu_f \sigma_{nf} (Gr(A_2 + A_1 \text{Log}(k+r)) \\ ((\rho\zeta)_{nf} \sigma_f + Ha\beta(\rho\zeta)_f \sigma_{nf})))) / (4(\rho\zeta)_f k''_{nf} b_1 b_2) \end{array} \right. , \quad (8.35)$$

with

$$\begin{aligned} a_1 &= \frac{kHa\sqrt{\mu_f \sigma_{nf}}}{\sqrt{(1 + \frac{1}{\gamma^*}) \mu_{nf} \sigma_f}}, \\ b_1 &= (4(1 + \frac{1}{\gamma^*}) \mu_{nf} \sigma_f + k^2 Ha^2 \mu_f \sigma_{nf})^2, \\ b_2 &= 16(1 + \frac{1}{\gamma^*}) \mu_{nf} \sigma_f + k^2 Ha^2 \mu_f \sigma_{nf}. \end{aligned} \quad (8.36)$$

First order solution

Under the boundary conditions (8.24) to (8.27), we can assume first order solution as

$$\theta_1(r, x) = \sin(\lambda x) f(r), \quad (8.37)$$

$$w_1(r, x) = \sin(\lambda x) g(r), \quad (8.38)$$

where $f(r)$ and $g(r)$ is function of r .

Using Eq.(8.37) and (8.38) into Eq.(8.22) to (8.27), we get

$$\frac{d^2 f(r)}{dr^2} + \frac{1}{(k+r)} \frac{df(r)}{dr} - \frac{k^2}{(k+r)^2} \lambda^2 f(r) = 0, \quad (8.39)$$

$$\frac{\mu_{nf}}{\mu_f} (1 + \frac{1}{\gamma^*}) \left(\frac{d^2 g(r)}{dr^2} + \frac{1}{(k+r)} \frac{dg(r)}{dr} - \lambda^2 \left(\frac{k}{r+k} \right)^2 g(r) \right) + \frac{\sigma_{nf}}{\sigma_f} \left(\frac{k}{r+k} \right)^2 Ha^2 g(r) + \frac{(\rho\zeta)_{nf}}{(\rho\zeta)_f} Gr f(r) = 0. \quad (8.40)$$

Correspondingly boundary conditions are transformed as

$$f(r) + \frac{d\theta_0}{dr} = 0 \text{ at } r = 1, \quad \frac{df^\pm(r)}{dr} \pm \frac{d^2\theta_0}{dr^2} + \frac{Bi}{\left(\frac{k^n}{k^n_f}\right)} (f^\pm(r) \pm \theta_0) \text{ at } r = -1, \quad (8.41)$$

$$g(r) + \frac{dw_0}{dr} = 0 \text{ at } r = 1, \quad g^\pm(r) \pm \frac{dw_0}{dr} = 0 \text{ at } r = -1. \quad (8.42)$$

The solution of first order problem can be expressed as

$$\theta_1^\pm(r, x) = \begin{cases} \sin(\lambda x) (C_1 \cosh(k\lambda \text{Log}(k+r)) + iC_2 \sinh(k\lambda \text{Log}(k+r))) \\ \sin(\lambda x) (C'_1 \cosh(k\lambda \text{Log}(k+r)) + iC'_2 \sinh(k\lambda \text{Log}(k+r))) \end{cases}, \quad (8.43)$$

$$w_1^\pm(r, x) = \begin{cases} \sin(\lambda x) (D_1 \cosh(a_2 \text{Log}(k+r)) + iD_2 \sinh(a_2 \text{Log}(k+r)) + (Gr(k+r)^2 \mu_f (\rho\zeta)_{nf} \sigma_f (4(1 + \frac{1}{\gamma^*}) ((C_1 - iC_2 k\lambda) \cosh(k\lambda \text{Log}(k+r)) + i(C_2 + iC_1 k\lambda) \sinh(k\lambda \text{Log}(k+r))) \\ \mu_{nf} \sigma_f + k^2 Ha^2 (C_1 \cosh(k\lambda \text{Log}(k+r)) + iC_2 \sinh(k\lambda \text{Log}(k+r))) \mu_f \sigma_{nf})) / ((\rho\zeta)_f (16(1 + \frac{1}{\gamma^*})^2 (-1 + k^2 \lambda^2) u_{nf}^2 \sigma_f^2 - 8k^2 Ha^2 (1 + \frac{1}{\gamma^*}) \mu_f \mu_{nf} \sigma_f \sigma_{nf} - k^4 Ha^4 \mu_f^2 \sigma_{nf}^2)) \\ \sin(\lambda x) (D'_1 \cosh(a_2 \text{Log}(k+r)) + iD'_2 \sinh(a_2 \text{Log}(k+r)) + (Gr(k+r)^2 \mu_f (\rho\zeta)_{nf} \sigma_f (k^2 \mu_f Ha^2 \sigma_{nf} (\cosh(k\lambda \text{Log}(k+r)) C'_1 + i \sinh(k\lambda \text{Log}(k+r)) C'_2) + 4(1 + \frac{1}{\gamma^*}) \mu_{nf} \sigma_f (\sinh(k\lambda \text{Log}(k+r)) (-k\lambda C'_1 + iC'_2) + \cosh(k\lambda \text{Log}(k+r)) (C'_1 - iC'_2 k\lambda)))) / ((\rho\zeta)_f (16(1 + \frac{1}{\gamma^*})^2 (-1 + k^2 \lambda^2) u_{nf}^2 \sigma_f^2 - 8k^2 Ha^2 (1 + \frac{1}{\gamma^*}) \mu_f \mu_{nf} \sigma_f \sigma_{nf} - k^4 Ha^4 \mu_f^2 \sigma_{nf}^2)) \end{cases}, \quad (8.44)$$

$$a_2 = \frac{k \sqrt{(1 + \frac{1}{\gamma^*}) \lambda^2 \mu_{nf} \sigma_f - Ha^2 \mu_f \sigma_{nf}}}{\sqrt{(1 + \frac{1}{\gamma^*}) \mu_{nf} \sigma_f}}. \quad (8.45)$$

Second order solution

The boundary conditions (8.30) to (8.33) can be simplified by applying the solution of first and second order system. Base on boundary conditions assume the solution as

$$\theta_2^\pm(r, x) = h^\pm(r) + \cos(2\lambda x) k^\pm(r), \quad (8.46)$$

$$w_2^\pm(r, x) = m^\pm(r) + \cos(2\lambda x) n^\pm(r), \quad (8.47)$$

where $h^\pm(r)$, $k^\pm(r)$, $m^\pm(r)$ and $n^\pm(r)$ are function of r only.

By employing Eq.(8.46) and Eq.(8.47) into Eq. (8.28) and Eq. (8.33), we get the following forms

$$\frac{d^2 h^\pm(r)}{dr^2} + \frac{1}{k+r} \frac{dh^\pm(r)}{dr} = 0, \quad (8.48)$$

$$\frac{d^2 k^\pm(r)}{dr^2} + \frac{1}{(k+r)} \frac{dk^\pm(r)}{dr} - \frac{4\lambda^2 k^2}{(k+r)^2} \lambda^2 k^\pm(r) = 0, \quad (8.49)$$

$$\frac{\mu_{nf}}{\mu_f} \left(1 + \frac{1}{\gamma_*}\right) \left(\frac{d^2 m^\pm(r)}{dr^2} + \frac{1}{(k+r)} \frac{dm^\pm(r)}{dr}\right) + \frac{\sigma_{nf}}{\sigma_f} \left(\frac{k}{r+k}\right)^2 H a^2 m^\pm(r) + \frac{(\rho\zeta)_{nf}}{(\rho\zeta)_f} G r h^\pm(r) = 0, \quad (8.50)$$

$$\frac{\mu_{nf}}{\mu_f} \left(1 + \frac{1}{\gamma_*}\right) \left(\frac{d^2 n^\pm(r)}{dr^2} + \frac{1}{(k+r)} \frac{dn^\pm(r)}{dr}\right) - 4 \left(\frac{\lambda k}{r+k}\right)^2 n^\pm(r) + \frac{\sigma_{nf}}{\sigma_f} \left(\frac{H a k}{r+k}\right)^2 n^\pm(r) + \frac{(\rho\zeta)_{nf}}{(\rho\zeta)_f} G r k^\pm(r) = 0. \quad (8.51)$$

The boundary conditions are

$$h^\pm(r) - \frac{1}{2} \left(\frac{df}{dr} + \frac{1}{2} \frac{d^2 \theta_0}{dr^2}\right) = 0 \text{ at } r = 1, \quad (8.52)$$

$$\frac{dh^\pm}{dr} \pm \frac{1}{2} \left(\frac{d^2 f}{dr^2} + \frac{1}{2} \frac{d^3 \theta_0}{dr^3}\right) + \frac{B_i}{\left(\frac{k_{nf}^*}{k_f^*}\right)} (h(r) \pm \frac{1}{2}(f(r) + \frac{1}{2}\theta_0(r))) \text{ at } r = -1, \quad (8.53)$$

$$m^\pm(r) + \frac{1}{2} \left(\frac{dg}{dr} + \frac{1}{2} \frac{d^2 w_0}{dr^2}\right) = 0 \text{ at } r = 1, \quad (8.54)$$

$$m^\pm(r) + \frac{1}{2} \left(\pm \frac{dg}{dr} - \frac{1}{2} \frac{d^2 w_0}{dr^2}\right) = 0 \text{ at } r = -1, \quad (8.55)$$

$$n^\pm(r) - \frac{1}{2} \left(\frac{dg}{dr} + \frac{1}{2} \frac{d^2 w_0}{dr^2}\right) = 0 \text{ at } r = 1, \quad (8.56)$$

$$n^\pm(r) + \frac{1}{2} \left(\pm \frac{dg}{dr} - \frac{1}{2} \frac{d^2 w_0}{dr^2}\right) = 0 \text{ at } r = -1. \quad (8.57)$$

Second order solution can be evaluated as

$$\theta_2^\pm = \begin{cases} E_2 + E_1 \text{Log}(k+r) + \cos(2\lambda x) (G_1 \cosh(2k\lambda \text{Log}(k+r)) + iG_2 \sinh(2k\lambda \text{Log}(k+r))), \\ E_2' + E_1' \text{Log}(k+r) + \cos(2\lambda x) (G_1' \cosh(2k\lambda \text{Log}(k+r)) + iG_2' \sinh(2k\lambda \text{Log}(k+r))), \end{cases} \quad (8.58)$$

$$w_2^\pm = \begin{cases} F_1 \cosh(a_1 \text{Log}(k+r)) + F_2 \sinh(a_1 \text{Log}(k+r)) + (Gr(k+r)^2 \mu_f (\rho\zeta)_{nf} \sigma_f ((1 + \frac{1}{\gamma^*}) \\ -4(-E_1 + E_2 + E_1 \text{Log}(k+r)) \mu_{nf} \sigma_f - k^2 Ha^2 (E_2 + E_1 \text{Log}(k+r)) \mu_f \sigma_{nf})) / ((\rho\zeta)_f b_1) \\ + \cos(2\lambda x) (H_1 \cosh(a_3 \text{Log}(k+r)) + iH_2 \sinh(a_3 \text{Log}(k+r)) + (Gr(k+r)^2 \mu_f (\rho\zeta)_{nf} \\ \sigma_f (4(1 + \frac{1}{\gamma^*}) ((G_1 - 2iG_2 k\lambda) \cosh(2k\lambda \text{Log}(k+r)) + i(G_2 + 2iG_1 k\lambda) \sinh(2k\lambda \text{Log} \\ (k+r))) \mu_{nf} \sigma_f + k^2 Ha^2 (G_1 \cosh(2k\lambda \text{Log}(k+r)) + iG_2 \sinh(2k\lambda \text{Log}(k+r))) \mu_f \sigma_{nf}) / \\ ((\rho\zeta)_f 16(1 + \frac{1}{\gamma^*})^2 (-1 + 4k^2 \lambda^2) u_{nf}^2 \sigma_f^2 - 8k^2 Ha^2 (1 + \frac{1}{\gamma^*}) \mu_f \mu_{nf} \sigma_f \sigma_{nf} - k^4 Ha^4 \mu_f^2 \sigma_{nf}^2)) \\ F_1' \cosh(a_1 \text{Log}(k+r)) + F_2' \sinh(a_1 \text{Log}(k+r)) - (Gr(k+r)^2 \mu_f (\rho\zeta)_{nf} \sigma_f (4(1 + \frac{1}{\gamma^*}) \\ \mu_{nf} \sigma_f ((-1 + \text{Log}(k+r)) E_1' + E_2') + k^2 Ha^2 \mu_f \sigma_{nf} (E_1' \text{Log}(k+r) + E_2')))) / ((\rho\zeta)_f b_1) + \\ \cos(2\lambda x) (H_1' \cosh(a_3 \text{Log}(k+r)) + iH_2' \sinh(a_3 \text{Log}(k+r)) + (Gr(k+r)^2 (\rho\zeta)_{nf} \mu_f \\ \sigma_f (i \sinh(2k\lambda \text{Log}(k+r)) (k^2 Ha^2 \mu_f \sigma_{nf} G_2' + 4(1 + \frac{1}{\gamma^*}) \mu_{nf} \sigma_f ((2iG_1' k\lambda + G_2')) + \\ \cosh(2k\lambda \text{Log}(k+r)) (k^2 Ha^2 \mu_f \sigma_{nf} G_1' + 4(1 + \frac{1}{\gamma^*}) \mu_{nf} \sigma_f ((G_1' - 2iG_2' k\lambda + G_2'))))) / \\ ((\rho\zeta)_f 16(1 + \frac{1}{\gamma^*})^2 (-1 + 4k^2 \lambda^2) u_{nf}^2 \sigma_f^2 - 8k^2 Ha^2 (1 + \frac{1}{\gamma^*}) \mu_f \mu_{nf} \sigma_f \sigma_{nf} - k^4 Ha^4 \mu_f^2 \sigma_{nf}^2)) \end{cases}, \quad (8.59)$$

with

$$a_3 = \frac{k \sqrt{4(1 + \frac{1}{\gamma^*}) \lambda^2 \mu_{nf} \sigma_f - Ha^2 \mu_f \sigma_{nf}}}{\sqrt{(1 + \frac{1}{\gamma^*}) \mu_{nf} \sigma_f}}. \quad (8.60)$$

Collecting Eqs.(8.34), (8.35) (8.43) (8.44) (8.58) and (8.59), the approximate velocity and temperature solution as

$$\theta^\pm(r, x) = \theta_0(r) + \varepsilon \theta_1^\pm(r, x) + \varepsilon^2 \theta_2^\pm(r, x) + \dots \quad (8.61)$$

$$w^\pm(r, x) = w_0(r) + \varepsilon w_1^\pm(r, x) + \varepsilon^2 w_2^\pm(r, x) + \dots \quad (8.62)$$

Evaluation of constants have been done by using Mathematica 9.

8.3 Heat transfer rate

Nusselt number determines convective heat exchange strength. Expresses as [86]

$$Nu = \frac{Hq_w}{k''_f(T_u^* - T_l^*)} \quad (8.63)$$

On upper wall it is defined as

$$q_w = -k''_{nf} \frac{\partial T^*}{\partial r^*} \Big|_{r^*=r_u^*} \quad (8.64)$$

From Eqs. (8.61) and (8.63), the Nusselt number can be expressed as

$$Nu = -\frac{k''_{nf}}{k''_f} \frac{\partial \theta}{\partial r} \Big|_{r=r_u^*} \quad (8.65)$$

8.4 Thermophysical properties

The thermophysical properties are

Physical Properties	Water	Copper	Silver
$C_p(J/kgK)$	4179	385	235
$\rho(kg/m^3)$	997.1	8933	10,500
$k''(W/mK)$	0.613	400	429
$\zeta \times 10^5 (1/K)$	21.0	1.67	1.89
$\sigma(S/m)$	5.0×10^{-2}	5.96×10^7	6.3×10^7
$\mu(kg/m.sec)$	8.90×10^{-4}	-	-

Table (8.1): Thermo physical effects.

8.5 Graphical consequence

In the previous portion, velocity, temperature and Nusselt number have been determined and results are demonstrated graphically to explore the flow parallel to the wall corrugations. To analyze the impacts of corrugations on the electromagnetically driven flow, the accompanying typical parametric values are utilized. For microfluidic examination, half height

of channel is $H \sim 100 \mu m$, the conditions of domain set with physical properties of the water density $\rho \sim 10^3 kg m^{-3}$, the electrical conductivity $\sigma \sim 2.2 \times 10^{-4} - 10^6 Sm^{-1}$ and the viscosity $\mu \sim 10^{-3} kg m^{-1} s^{-1}$. If range of magnetic field is the $O(B^*) \sim 0.018 - 0.44$, the value of order of Hartmann number $O(Ha)$ using $Ha = B^* H (\sigma/\mu)^{1/2}$ is from 0.0001 to 3. The frequency of electric field $O(\omega)$ changes from the 50 to $500 s^{-1}$ and range of the frequency is $0 - 1 \times 10^4 s^{-1}$. The Reynolds number order $O(Re)$ changes from the 0.5 to 5 and the dimensionless parameter is fixed value i.e. $\beta = 5$.

8.5.1 Effect of wall roughness on 3D velocity and contour distributions

The three-dimensional velocity and contour distributions for Casson parameter γ^* , when $\gamma^* = 0.7$, and $\gamma^* = 1.8$ for copper and silver nanoparticles are shown in Figs. 8.2 – 8.5. The wall roughness can cause changes in the velocity distribution. In Figs. (8.2) and (8.4), the phase difference between the walls is 0° . In Figs. (8.3) and (8.5), the phase difference between the walls is 180° . From the Figs. (8.2) to (8.5), we find that the velocity distribution depends on the shape of channel. Corrugation effect is more prominent for silver nanoparticle as compared to copper nanoparticle.

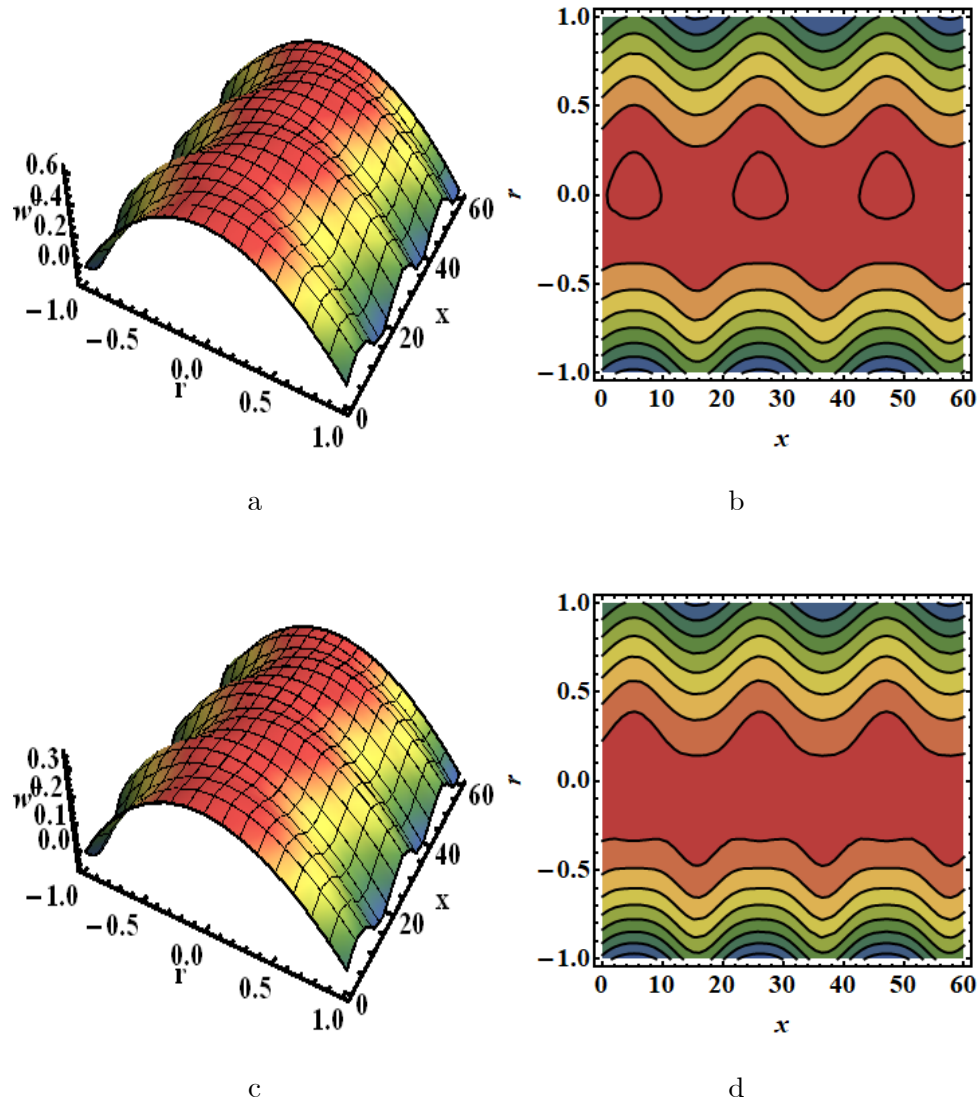


Fig. (8.2): 3D Velocity distribution and contour for $\gamma^* = 0.7$ in phase for copper (*a, b*) and silver (*c, d*).

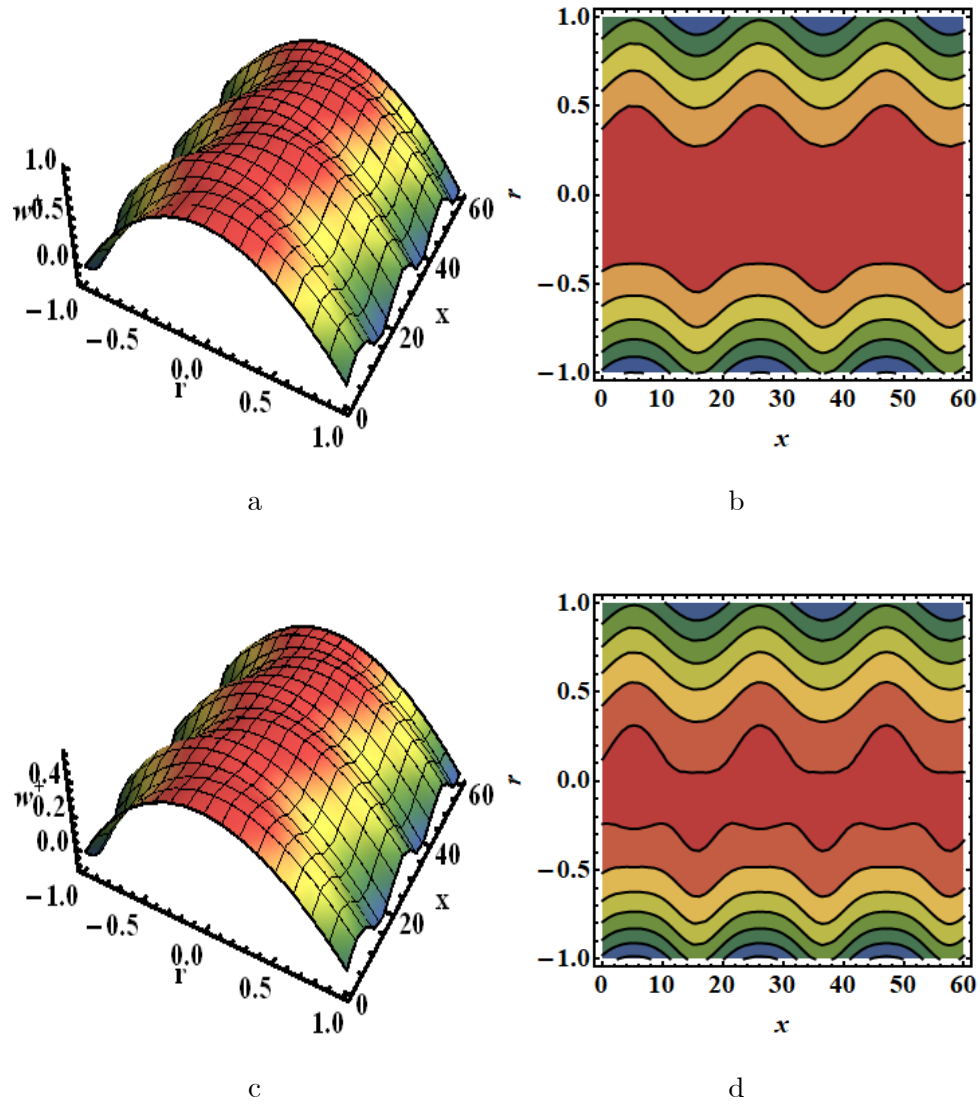


Fig. (8.3): 3D Velocity distribution and contour for $\gamma^* = 1.8$ in phase for copper (*a, b*) and silver (*c, d*).

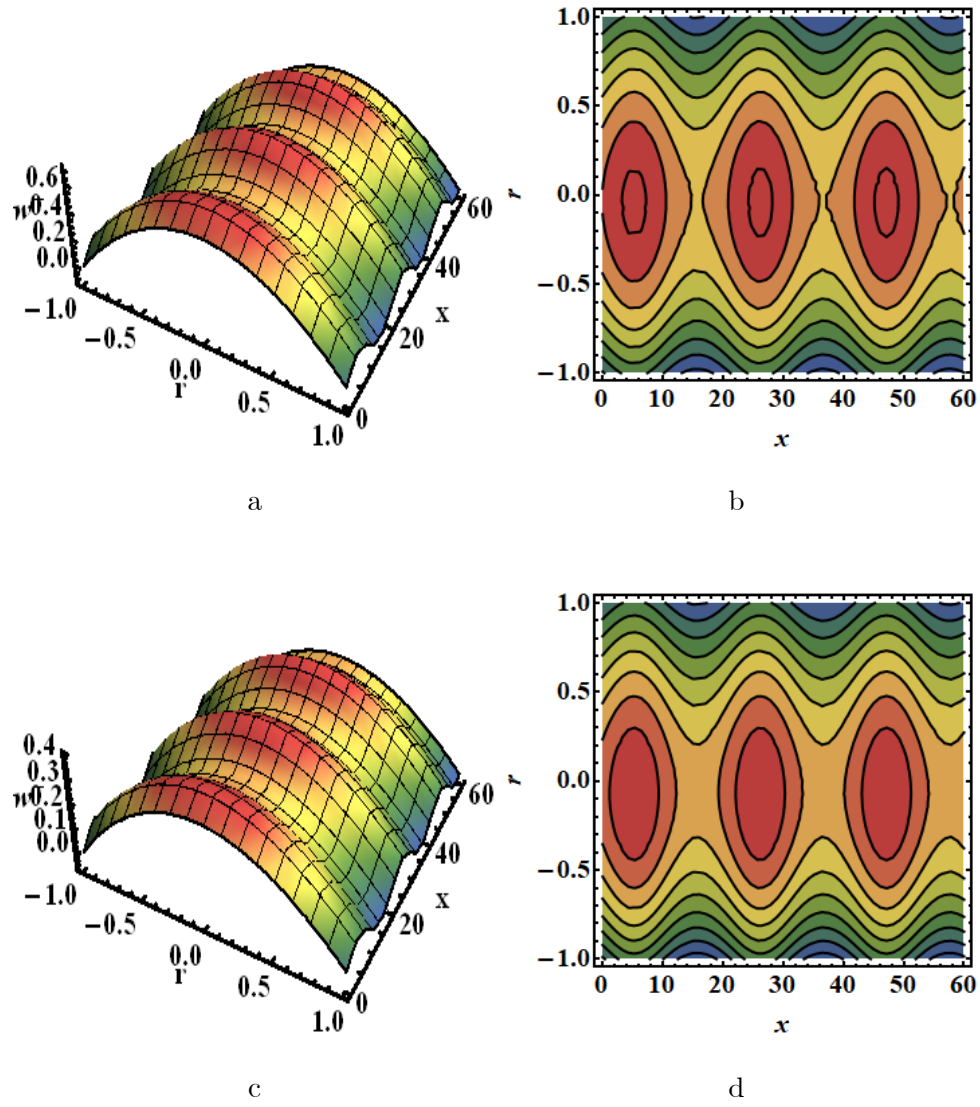


Fig. (8.4): 3D Velocity distribution and contour for $\gamma^* = 0.7$ out phase for copper (*a, b*) and silver (*c, d*).

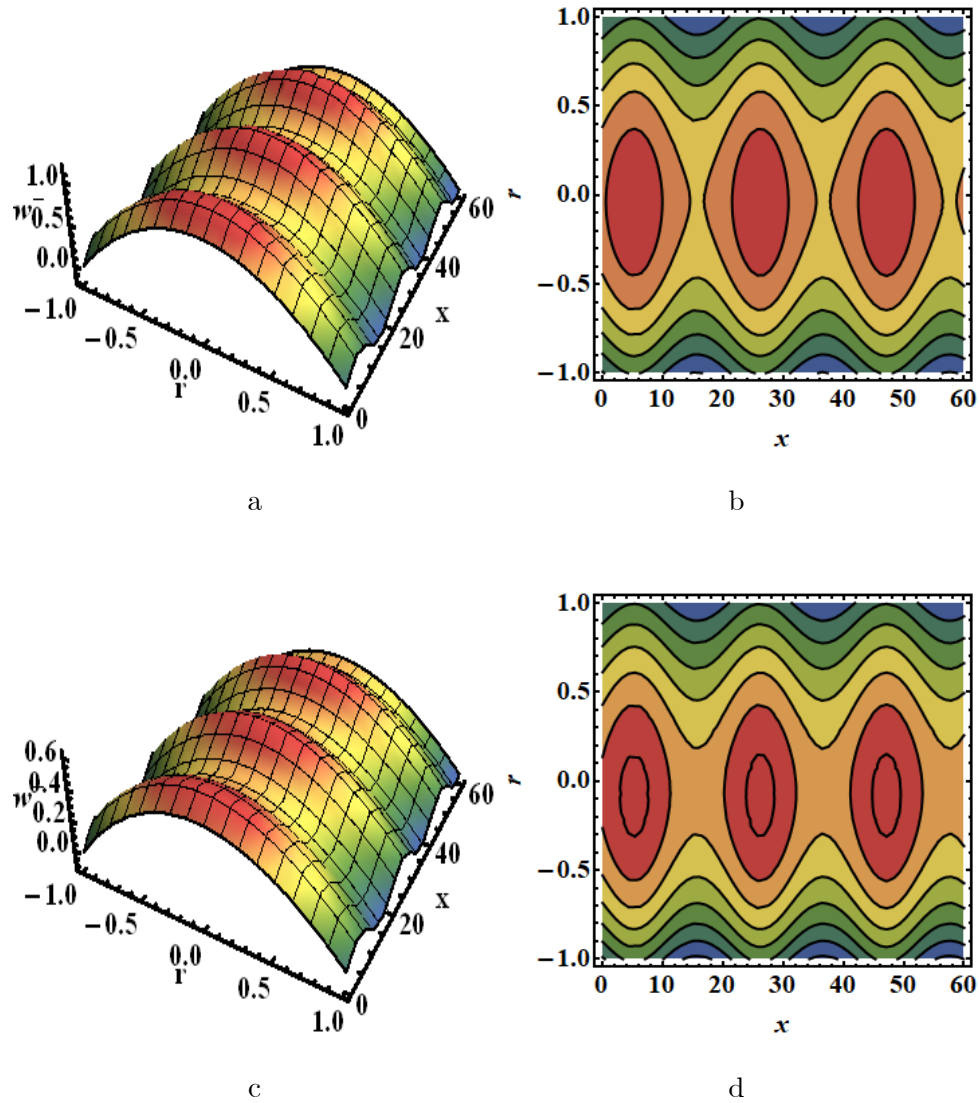


Fig. (8,5): 3D Velocity distribution and contour for $\gamma^* = 1.8$ out phase for copper (a, b) and silver (c, d).

8.5.2 Effect of wall roughness on velocity

Impact of silver and copper nanoparticles with the aid of embedded parameters on the characteristics of corrugated curved channel presented in this section through the graphs of velocity.

The 2D variations of the EMHD velocity w for various embedded parameters like Casson parameter (γ^*), Curvature parameter (k), Grashof number (Gr), Sink parameter (ϕ), Biot number (B_i) and Nanoparticle volume fraction (Φ) on velocity as exposed in Figs. 8.6 – 8.11. All these figures illustrated that the velocity profiles attains maximum value at the centre when we take $\varepsilon = 0.1$ and $\beta = 5$. Fig. (8.6) demonstrates that the velocity w increases for Casson parameter γ^* and it is elucidated that velocity plot gives giant altitude for copper as compare to silver nanoparticles by increasing γ^* . Fig. (8.7) illustrates the impact of k on the EMHD velocity by increasing k velocity profile increases and increasing effect is more prominent for silver nanoparticle. Fig. (8.8) demonstrates that w increases for various values of Grashof number as a result of decreasing in viscosity and increase in velocity is more prominent for copper nanoparticle. Figs. (8.9) shows that the velocity w increases for various observation of the ϕ and effect is more prominent for silver nanoparticles. Fig. (8.10) illustrates that the impact of B_i on the EMHD velocity and negligible results due to silver and copper nanoparticles on velocity profile. Fig. (8.11) exhibits the consequence of Φ on EMHD velocity and velocity plot declines with enlarging the value of nanoparticle volume fraction. These results are more prominent in silver nanoparticles as compare to copper nanoparticle.

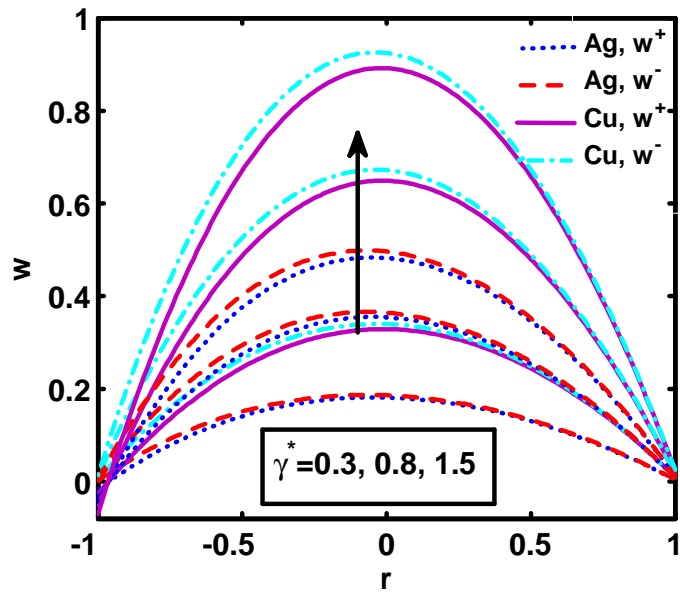


Fig. (8.6): 2D Variation of velocity for Casson parameter γ^* .

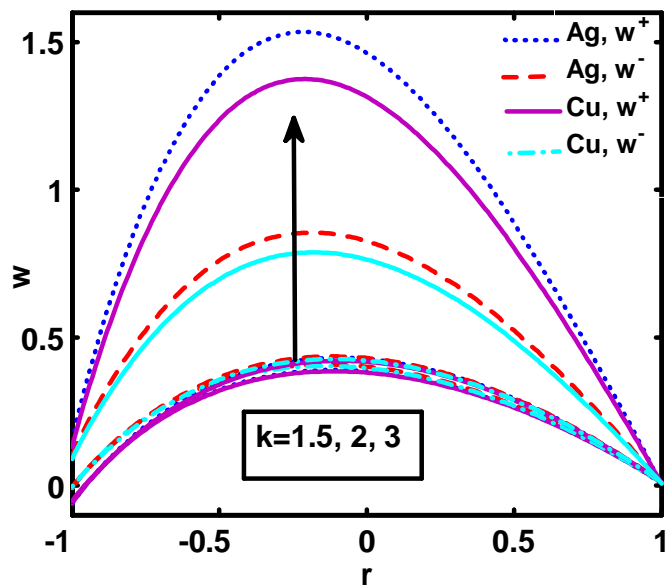


Fig. (8.7): 2D Variation of velocity for Curvature parameter k .

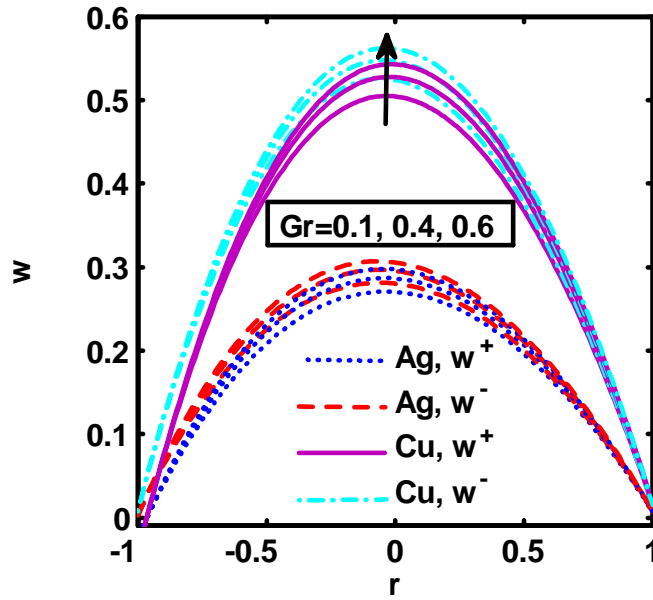


Fig. (8.8): 2D Variation of velocity for Grashof number Gr .

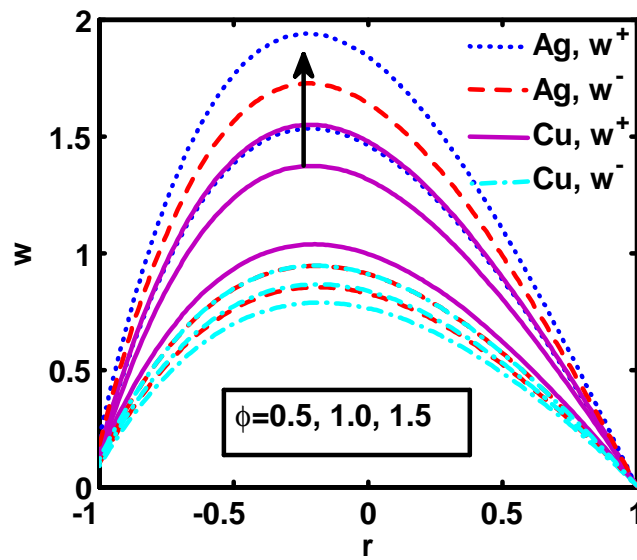


Fig. (8.9): 2D Variation of velocity for Heat source parameter ϕ .

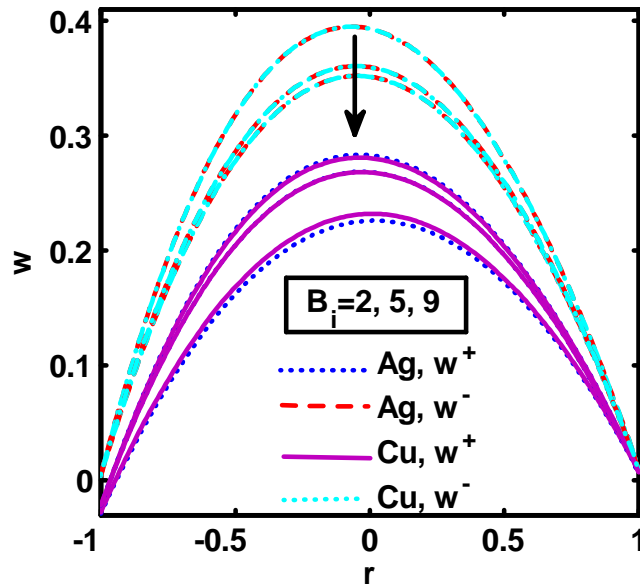


Fig. (8.10): 2D Variation of velocity for Biot number B_i .

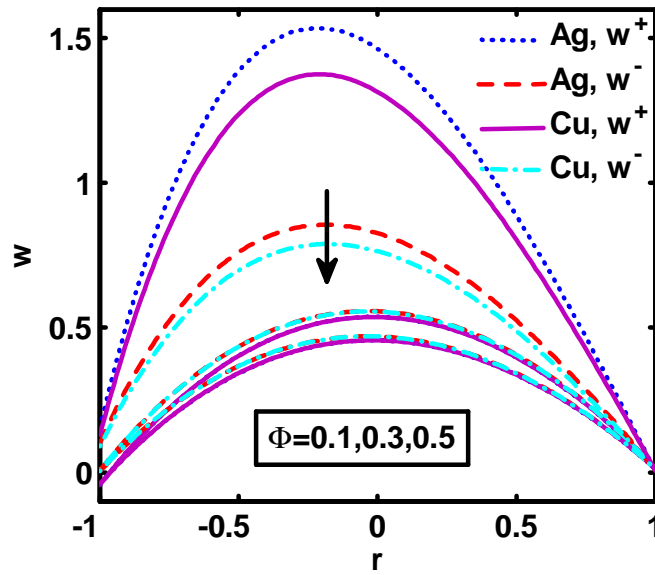


Fig. (8.11): 2D Variation of velocity for Nanoparticle volume fraction Φ .

8.5.3 Effect of wall roughness on temperature

Impact of silver and copper nanoparticles with the aid of embedded parameters on the characteristics of corrugated curved channel presented in this section through the graphs of temperature. The 2D variations of the EMHD temperature θ for various embedded parameters like Biot number (B_i), Sink parameter (ϕ) and Curvature parameter (k) on temperature as exposed in Figs. 8.12 – 8.14. Fig. (8.12) shows that profile of temperature increases when the B_i are increase and negligible effect due to silver and copper nanoparticles on temperature profile. Fig. (8.13) depicts that profile of temperature decreases in the portion $[-1, 0]$ and increases in the portion $[0, 1]$ when the heat absorption coefficient ϕ are increase. Fig. (8.14) shows that profile of temperature increases when the Curvature parameter k are increase.

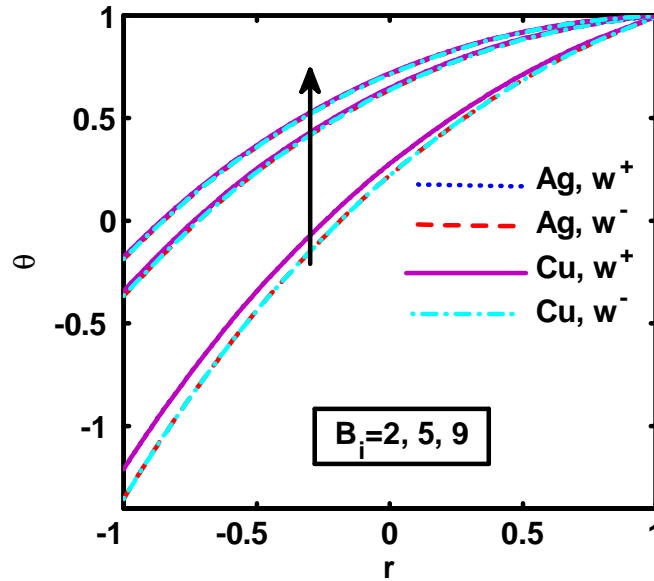


Fig. (8.12): 2D Variation of temperature for Biot number B_i .

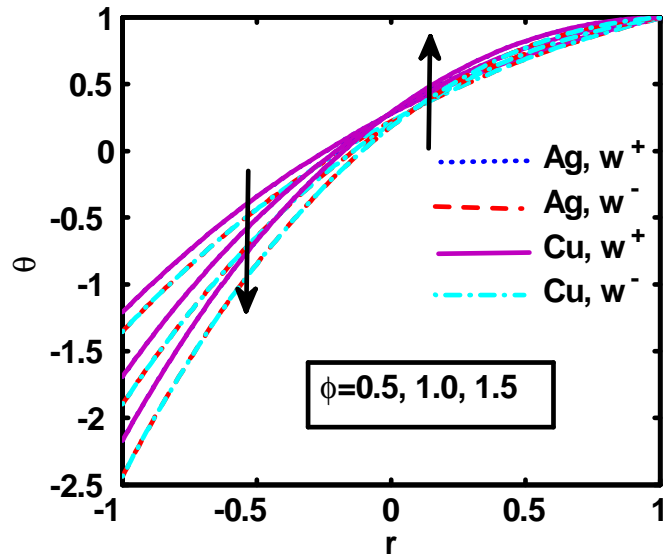


Fig. (8.13): 2D Variation of temperature for Heat source parameter ϕ .

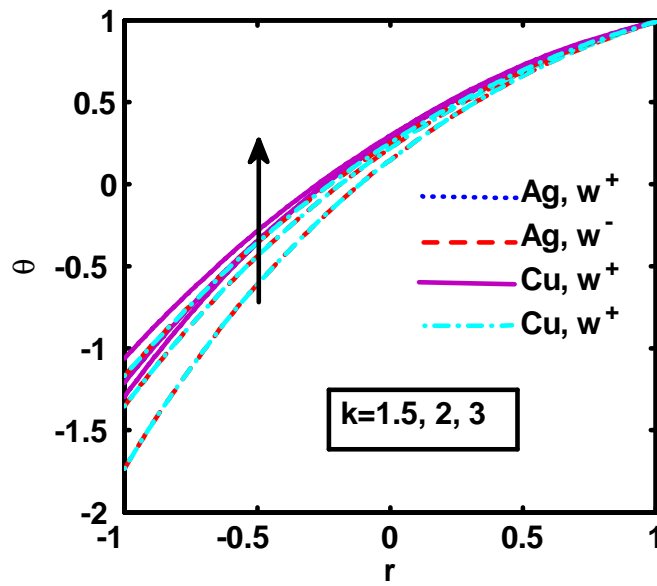


Fig. (8.14): 2D Variation of temperature for Curvature parameter k .

8.5.4 Tables Description

In this section, the impact of Nusselt number $Nu^\pm = -\frac{k_f^n}{k_f^n} \theta'(r_u)$ on EMHD flow of Casson fluid discussed in the curved channel through corrugated walls. This section expressed the behavior of Biot number B_i on the Nusselt number Nu^\pm . Table 7.2 demonstrates that the Nu^+ declines with the enlarging value of x and the Nu^+ decreases with the rise of the Biot number B_i for both the copper and silver nanoparticles. Table 7.3 shows that the Nu^- grows with the enlarging value of x and the Nu^- decreases with the rise of the Biot number B_i for both the copper and silver nanoparticles.

For Nusselt number Nu^+						
For copper nanoparticle			For silver nanoparticle			
x	$B_i = 2$	$B_i = 5$	$B_i = 7$	$B_i = 2$	$B_i = 5$	$B_i = 7$
0	7.82735	0.116966	0.0274677	7.83192	0.117007	0.0274975
0.1	7.71548	0.106945	0.0209968	7.71994	0.106984	0.0210261
0.2	7.57082	0.0971166	0.0145824	7.57517	0.0971549	0.0146112
0.3	7.39295	0.0875268	0.00825245	7.39716	0.0875641	0.00828068
0.4	7.18186	0.0782175	0.00203288	7.18593	0.0782538	0.00206063
0.5	6.93802	0.0692255	-0.00405237	6.94195	0.0692609	-0.00402508
0.6	6.66241	0.0605826	-0.00998156	6.66616	0.0606172	-0.00995472
0.7	6.35639	0.0523158	-0.0157352	6.35996	0.0523496	-0.0157088
0.8	6.02181	0.0444471	-0.021296	6.02519	0.0444802	-0.02127
0.9	5.66091	0.0369935	-0.0266491	5.66409	0.0370259	-0.0266234
1	5.27635	0.0299671	-0.0317816	5.27932	0.0299989	-0.0317563

Table (8.2): Effect of Biot number B_i on Nusselt number Nu^+ .

For Nusselt number Nu^-						
For copper nanoparticle			For silver nanoparticle			
x	$B_i = 2$	$B_i = 5$	$B_i = 7$	$B_i = 2$	$B_i = 5$	$B_i = 7$
0	4.43789	0.0516885	-0.00860913	4.44028	0.0517206	-0.00858331
0.1	4.75904	0.0527978	-0.00896355	4.76161	0.0528303	-0.00893758
0.2	5.0551	0.0541474	-0.00923036	5.05783	0.0541802	-0.00920424
0.3	5.32406	0.00557392	-0.00940574	5.32695	0.0557725	-0.00937944
0.4	5.56435	0.057572	-0.00948721	5.56738	0.0576057	-0.00946072
0.5	5.77482	0.0596412	-0.00947363	5.77798	0.596754	-0.00944694
0.6	5.95476	0.0619388	-0.00936527	5.95804	0.0619736	-0.00933836
0.7	6.1039	0.0644537	-0.00916373	6.10729	0.064489	-0.00913659
0.8	6.2224	0.0671714	-0.00887193	6.22588	0.0672074	-0.00884456
0.9	6.31082	0.0700746	-0.00849407	6.31439	0.0701113	-0.00846645
1	6.37014	0.0731433	-0.00803552	6.37378	0.0731806	-0.00800764

Table (8.2): Effect of Biot number B_i on Nusselt number Nu^- .

8.6 Deduction

The impact of nanoparticles on EMHD flow with corrugated walls in microchannel is discussed.

The main observations from this theoretical analysis is concise as follows,

- Velocity plot increases for Casson parameter γ_* and it is elucidated that velocity plot gives giant altitude for copper as compare to silver nanoparticles by enlarging γ^* .
- The velocity plot increases by enlarging k and effect is more prominent for silver nanoparticle.
- The velocity increases for Grashof number and and heat absorption coefficient.
- Temperature profile increases when the B_i are increase and negligible effect due to silver and copper nanoparticles on temperature profile.

- The profile of temperature declines in the portion $[-1, 0]$ and increases in the portion $[0, 1]$ when the heat absorption coefficient ϕ are increase.
- Temperature increases when the Curvature parameter increases.
- Nusselt number Nu^+ declines with the increasing value of x and decreases with the raise of the Biot number B_i for both the copper and silver nanoparticles.
- Nusselt number Nu^- increases with the increasing value of x and the Nusselt number Nu^- decreases with the raise of the Biot number B_i for both the copper and silver nanoparticles.

References

- [1] C.Y. Wen, C. P. Yeh, C. H. Tsai and L. M. Fu, Rapid magnetic microfluidic mixer utilizing AC electromagnetic field, *Electrophoresis*, 30 (2009) 4179.
- [2] S. Z. Qian and H. H. Bau, Magneto-hydrodynamics based microfluidics, *Mechanics Research Communications - Journal - Elsevier*, 36 (2009) 10.
- [3] J. P. Gleeson, O. M. Roche , J. West and A. Gelb, Modeling annular micromixers, *SIAM Journal on Applied Mathematics* , 64 (2004) 1294.
- [4] P. D. S. Reddy, D. Bandyopadhyay, S. W. Joo, A. Sharma and S. Qian, Parametric study on instabilities in a two-layer electromagnetohydrodynamic channel flow confined between two parallel electrodes, *Physical Review E* , 83 (2011) 036313.
- [5] S. Chakraborty and D. Paul, Microchannel flow control through a combined electromagnetohydrodynamic transport, *Journal of Physics D: Applied Physics*, 39 (2006) 5364.
- [6] R. Jhorar, Electroosmosis modulated biomechanical transport through asymmetric microfluidics channel, *Indian Journal of Physics*, 92 (2018) 1229.
- [7] P. Tso, K. Sundaravadivelu, Capillary flow between parallel plates in the presence of an electromagnetic field, *Journal of Physics D: Applied Physics*, 34 (2001) 3522.
- [8] M. Rivero and S. Cuevas, Analysis of the slip condition in magnetohydrodynamic (MHD) micropumps, *Sensors Actuators B*, 166 (2012) 884.

- [9] K. H.W.Chu, Small-Knudsen-number flow in a corrugated tube, *Meccanica*, 34 (1999) 133.
- [10] B. Tashtoush and M. Al-Odat, Magnetic field effect on heat and fluid flow over a wavy surface with a variable heat flux, *Journal of Magnetism and Magnetic Materials*, 268 (2004) 357.
- [11] P. Ligrani, D. Blanchard and B. Gale, Slip due to surface roughness for a Newtonian liquid in a viscous microscale disk pump, *Physics of Fluids*, 22 (2010) 052002.
- [12] C. O. Ng and C. Y. Wang, Darcy–Brinkman Flow Through a Corrugated Channel, *Transport Porous Media*, 85 (2010) 605.
- [13] A. E. Bergles, Some perspectives on enhanced heat-transfer—2nd generation heat-transfer technology, *Journal of Heat Transfer*, 110 (1988) 1082.
- [14] J. Szumbariski and J. M. Floryan, Transient disturbance growth in a corrugated channel, *Journal of Fluid Mechanics*, 568 (2006) 243.
- [15] H. Luo, M.G. Blyth, C. Pozrikidis, Two-layer flow in a corrugated channel, *Journal of Engineering Mathematics*, 60 (2008) 127.
- [16] D. Si and Y. Jian, Electromagnetohydrodynamic (EMHD) micropump of Jeffrey fluids through two parallel microchannels with corrugated walls, *Journal of Physics D: Applied Physics*, 48 (2015) 085501.
- [17] M. Rashid, I. Shahzadi and S. Nadeem, Corrugated walls analysis in microchannels through porous medium under Electromagnetohydrodynamic (EMHD) effects, *Results in Physics*, 9 (2018) 171.
- [18] E. A. M. Elshafei, M. M. Awad, E. El-Negiry and A.G. Ali, Heat transfer and pressure drop in corrugated channels, *Energy*, 35 (2010) 101.
- [19] A. Riaz, S. Nadeem, R. Ellahi and A. Zeeshan, Exact solution for peristaltic flow of Jeffrey fluid model in a three dimensional rectangular duct having slip at the walls, *Applied Bionics and Biomechanics* , 11 (2014) 81.

- [20] M. Akbarzadeh, S. Rashidi, N. Karimi and R. Ellahi, Convection of heat and thermodynamic irreversibilities in two-phase turbulent nanofluid flows in solar heaters by corrugated absorber plates, *Advanced Powder Technology*, 29 (2018) 2243 .
- [21] N. Phan-Thien, On the Stokes Flow of Viscous Fluids Through Corrugated Pipes, *Journal of Applied Mechanics*, 47 (1980) 961.
- [22] N. M. Bujurke and R. B. Kudenatti, MHD lubrication flow between rough rectangular plates, *Fluid Dynamics Research*, 39 (2007) 334.
- [23] M. Buren, Y. Jian and L. Chang, Electromagnetohydrodynamic flow through a microparallel channel with corrugated walls, *Journal of Physics D: Applied Physics*, 47 (2014) 425501.
- [24] Z. K. H. Chu, Slip flow in an annulus with a corrugated walls, *Journal of Physics D: Applied Physics*, 33 (2000) 627.
- [25] J. G. Smits, Piezoelectric micropump with 3 valves working peristaltically, *Sensors and Actuators A* 21 (1990) 203.
- [26] R. K. Rathy, *An Introduction to Fluid Dynamics*, Oxford and IBH Publishing Co, New Delhi, 1976.
- [27] Z. Alamri, R. Ellahi, N. Shehzad and A. Zeeshan, Convective radiative plane Poiseuille flow of nanofluid through porous medium with slip: An application of Stefan blowing, *Journal of Molecular Liquids* 273 (2019) 292.
- [28] N. S. Akbar, A. W. Butt, D. Tripathi and O. A. Beg, Physical hydrodynamic propulsion model study on creeping viscous flow through a ciliated porous tube, *Pramana - Journal of Physics*, 88 (2017) 52.
- [29] Kh.S. Mekheimer and Y. Abd elmaboud, Peristaltic flow through a porous medium in an annulus: Application of an endoscope, *Applied Mathematics and Information Sciences*, 2 (1) (2008) 103.

- [30] M. M. Bhatti, A. Zeeshan, R. Ellahi and G.C. Shit, Mathematical modeling of heat and mass transfer effects on MHD peristaltic propulsion of two-phase flow through a Darcy-Brinkman-Forchheimer Porous medium, *Advanced Powder Technology*, 29 (2018) 1189.
- [31] A. Rapits, N. Kafousias and C. Massalas, Mass transfer flow through a porous medium bounded by a vertical surface, *ZAMM - Journal of Applied Mathematics and Mechanics*, 62 (1982) 489.
- [32] Kh. S. Mekheimer and T. H. Al-Arabi, Nonlinear peristaltic transport of MHD flow through a porous medium, *International Journal of Mathematics and Mathematical Sciences*, 26 (2003) 1663.
- [33] M. F. El Sayed, Electrohydrodynamic instability of two superposed viscous streaming fluids through porous medium, *Canadian Journal of Physics*, 75 (1997) 499.
- [34] C. L. Varshney, Fluctuating flow of viscous fluid through a porous medium bounded by a porous plate, *Indian Journal of Pure and Applied Mathematics*, 10 (1979) 1558.
- [35] S. U. S. Choi and J. A. Eastman, Enhancing thermal conductivity of fluids with nanoparticles, Argonne National Lab, 1995.
- [36] N. S. Akbar, Metallic nanoparticles analysis for the peristaltic flow in an asymmetric channel with MHD, *IEEE Transactions on Nanotechnology*, 13 (2014) 357.
- [37] J. Buongiorno, Convective transport in nanofluids, *ASME Journal of Heat Transfer*, 128 (2005) 240.
- [38] Y. Xuan and W. Roetzel, Conceptions for heat transfer correlation of nanofluids, *International Journal of Heat and Mass Transfer*, 43 (2000) 3701.
- [39] K. Sadik and A. Pramuanjaroenkij, Review of convective heat transfer enhancement with nanofluids, *International Journal of Heat and Mass Transfer*, 52 (2009) 3187.
- [40] M. Sheikholeslami and Ganji, Magnetohydrodynamic flow in a permeable channel filled with nanofluid, *Scientia Iranica B*, 21 (2014) 203.

- [41] T. Hayat, T. Muhammad, S. A. Shehzad and A. Alsaedi, On magnetohydrodynamic flow of nanofluid due to a rotating disk with slip effect: a numerical study, *Computer Methods in Applied Mechanics and Engineering*, 315 (2017) 4677.
- [42] M. Sheikholeslami and S.A. Shehzad, CVFEM simulation for nanofluid migration in a porous medium using Darcy model, *International Journal of Heat and Mass Transfer*, 122 (2018) 1264.
- [43] K. Khanafer, K. Vafai and M. Lightstone, Buoyancy-driven heat transfer enhancement in a two-dimensional enclosure utilizing nanofluids, *International Journal of Heat and Mass Transfer*, 46 (2003) 3639.
- [44] M. Sheikholeslami, K. Vajravelu and M. M. Rashidi, Forced convection heat transfer in a semi annulus under the influence of a variable magnetic field, *International Journal of Heat and Mass Transfer*, 92 (2016) 339.
- [45] R. Nasrin, M. A. Alim and A. J. Chamkha, Prandtl number and aspect ratio, *International Journal of Heat and Mass Transfer*, 55 (2012) 7355.
- [46] A. Andreozzi, O. Manca, S. Nardini and D. Ricci, Forced convection enhancement in channels with transversal ribs and nanofluids, *Applied Thermal Engineering*, 98 (2016) 1044.
- [47] E.N. Maraj, N.S. Akbar, and S. Nadeem, Biological analysis of Jeffrey nanofluid in a curved channel with heat dissipation, *IEEE Transactions on NanoBioscience*, 13 (2014) 431.
- [48] Z. Iqbal, E. Azhar, Z. Mehmood and A. Kamran, Unsteady transport of MHD mixed convection inspired by thermal radiation and partial slip performance: Finite difference approach, *Thermal Science*, 23 (2019) 1875.
- [49] M. Sheikholeslami, M. Jafaryar, S. Saleem, Z. Li, A. Shafee and Yu Jiang, Nanofluid heat transfer augmentation and energy loss inside a pipe equipped with innovative turbulators, *International Journal of Heat and Mass Transfer*, 126 (2018) 156.

- [50] I. Shahzadi and S. Nadeem "Role of Inclined Magnetic Field and Copper Nanoparticles on Peristaltic Flow of Nanofluid through Inclined Annulus: Application of the Clot Model", *Communications in Theoretical Physics*, 67 (2017) 704-716.
- [51] S. Ijaz, Iqra Shahzadi, S. Nadeem, and A. Saleem, A Clot Model Examination: with Impulsion of Nanoparticles under Influence of Variable Viscosity and Slip Effects, *Communications in Theoretical Physics*, 68 (2017) 667.
- [52] A. M. Hussein, K.V. Sharma, R. A. Bakar and K. Kadirgama, A review of forced convection heat transfer enhancement and hydrodynamic characteristics of a nanofluid, *Renewable and Sustainable Energy Reviews*, 29 (2014) 734.
- [53] A. M. Hussein, R.A. Bakar, K. Kadirgama, K.V. Sharma, The effect of nanofluid volume concentration on heat transfer and friction factor inside a horizontal tube, *Journal of Nanomaterials*. 2013, article ID 859563.
- [54] J. Wang, J. Zhu, X. Zhang and Y. Chen, Heat transfer and pressure drop of nanofluids containing carbon nanotubes in laminar flows, *Experimental Thermal and Fluid Science*, 44 (2013) 721.
- [55] S. Suresh, K. P. Venkataraj, P. Selvakumar and M. Chandrasekar, Effect of Al_2O_3 - Cu/water hybrid nanofluid in heat transfer, *Experimental Thermal and Fluid Science*, 38 (2012) 65.
- [56] G. G. Momin, Experimental investigation of mixed convection with water- Al_2O_3 & hybrid nanofluid in inclined tube for laminar flow, *International Journal of Scientific and Technology Research*, 2 (2013) 195.
- [57] M. J. Nine, M. Batmunkh, J. H. Kim, H. S. Chung and H. M. Jeong, Investigation of Al_2O_3 -MWCNTs hybrid dispersion in water and their thermal characterization, *Journal of Nanoscience and Nanotechnology*, 12 (2012) 4553.
- [58] M. Batmunkh, M. R. Tanshen MR, M. J. Nine, M. Myekhlai, H. Choi, H. Chung and H. Jeong, Thermal conductivity of TiO_2 nanoparticles based aqueous nanofluids with an

addition of a modified silver particle, *Industrial and Engineering Chemistry Research*, 53 (2014) 8445.

- [59] M. H. Esfe , A. A. A. Arani, M. Rezaie, W. M. Yan and A. Karimipour, Experimental determination of thermal conductivity and dynamic viscosity of Ag-MgO/ water hybrid nanofluid, *International Communications in Heat and Mass Transfer*, 66 (2015) 189.
- [60] R. Cortell, Analysing Flow and Heat Transfer of a Viscoelastic Fluid over a Semi-Infinite Horizontal Moving Flat Plate, *International Journal of Non-Linear Mechanics*, 43 (2008) 772.
- [61] K. R. Rajagopal and A. S Gupta, On a Class of Exact Solutions to the Equations of Motion of a Second Grade Fluid, *International Journal of Engineering Science*, 1981, 19 (1981) 1009.
- [62] C. Dorier and J. Tichy, *Behaviour of a Bingham-Like Viscous Fluid in Lubrication Flows*, *Journal of Non-Newtonian Fluid Mechanics*, 45 (1992) 291.
- [63] M. E. Clark, J. M. Robertson and L. C. Cheng, Stenosis severity effects for unbalanced simple-pulsatile bifurcation flow, *Journal of biomechanics*, 16 (1983) 895.
- [64] N. Casson, C C In: Mill, editor, *Rheology of dispersed system*, Oxford: Pergamon Press, 1959.
- [65] N. T. M. Eldabe and M. G. E. Salwa, Heat transfer of MHD non-Newtonian Casson fluid flow between two rotating cylinder, *Mechanics and Mechanical Engineering*, 5 (2001) 237.
- [66] A. G. Fredrickson, *Principles and Applications of Rheology*, Prentice-Hall, Englewood Cliffs, 1964, 1377.
- [67] R. K. Dash, K. N. Metha and G. Jayaraman, Casson fluid flow in a pipe filled with a homogeneous porous medium, *International Journal of Engineering Science*, 34(1996) 1145.
- [68] S. Nadeem, R. Ul Haq and C. Lee, MHD flow of a Casson fluid over an exponentially shrinking sheet, *Scientia Iranica*, 19 (2012)1550.

- [69] K. Ramesh, Influence of heat and mass transfer on peristaltic flow of a couple stress fluid through porous medium in the presence of inclined magnetic field in an inclined asymmetric channel, *Molecular Liquids*, 219 (2016) 256.
- [70] N. A. Khan, H. Khan and S. A. Ali, Exact solutions for MHD flow of couple stress fluid with heat transfer, *Egyptian Mathematical Society*; 24 (2016) 125.
- [71] K. Kaladhar, Natural Convection Flow of couple Stress Fluid in a Vertical Channel With Hall and Joule Heating Effects, *Engineering*, 127 (2015) 1071.
- [72] G. C. Sankad and P. S. Nagathan, Influence of the Wall Properties on the Peristaltic Transport of a couple Stress Fluid with Slip Effects in Porous Medium, *Engineering*, 127 (2015) 862.
- [73] G. C. Shit and M. Roy, Hydromagnetic effect on inclined peristaltic flow of a couple stress fluid, *Alexandria Engineering Journal*, 53 (2014) 949.
- [74] B. M. Shankar, Jai Kumar and I. S. Shivakumara, Stability of natural convection in a vertical couple stress fluid layer, *International Journal of Heat and Mass Transfer*, 78 (2014) 447.
- [75] M. Devakar, D. Sreenivasu and B. Shankar, Analytical solutions of couple stress fluid flows with slip boundary conditions, *Alexandria Engineering Journal*, 53 (2014) 723.
- [76] H. Sato, T. Kawai, T. Fujita and M. Okabe, Two dimensional peristaltic flow in curved channels, *Transactions of the Japan Society of Mechanical Engineers*, 66 (2000) 679.
- [77] H. J. De Vriend, Curved-channel microchannel array plates, *Journal of Fluid Mechanics*, 107 (1981) 423.
- [78] J. V. Ramanamurthy, K. M. Prasad and V. K. Narla. Unsteady peristaltic transport in curved channels, *Physics of Fluids*, 25 (2013) 0919035 .
- [79] S. Nadeem and S. Hina, Ciliary motion phenomenon of viscous nanofluid in a curved channel with wall properties, *European Physical Journal Plus*, 131 (2016) 65.

- [80] S. Eskinazi and H. Yeh, An Investigation on Fully Developed Turbulent Flows in a Curved Channel, *Journal of the Aeronautical Sciences*, 23 (1956) 23.
- [81] S. Nadeem and E. N. Maraj, The Mathematical Analysis for Peristaltic Flow of Hyperbolic Tangent Fluid in a Curved Channel, *Communications in Theoretical Physics*, 59 (2013) 729.
- [82] S. Hina, M. Mustafa, T.Hayat and N. D. Alotaibid, On peristaltic motion of pseudo-plastic fluid in a curved channel with heat/mass transfer and wall properties, *Applied Mathematics and Computation*, 263 (2015) 378.
- [83] W. R. Dean and S Chapman, Fluid motion in a curved channel, *Proceedings of the Royal Society of London. Series A, Containing Papers of a Mathematical and Physical Character*, 121(7871928) 402.
- [84] A. Malvandi, F. Hedayati and D. D. Ganji, Thermodynamics optimization of fluid flow over an isothermal moving plate, *Journal of Alexandria Engineering*, 52 (2013) 277.
- [85] Y. D. Gao, T. N. Wong, C. Yang and K. T. Ooi , Two-fluid electroosmotic flow in microchannels, *Journal of Colloid and Interface Science*, 284 (2005) 306.
- [86] S. Nadeem, I. Raishad, N. Muhammad and M. T. Mustafa, Mathematical analysis of ferromagnetic fluid embedded in a porous medium, *Result in Physics*, 7 (2017) 2361.
- [87] M.Q. Brewster, *Thermal Radiative Transfer and Properties*, John Wiley & Sons, New York, NY, USA, 1992.